



**Non-contact 3D Surface Scanning of Traumatic Injuries for
Forensic Medicine**

Awatif Mohamed M. Shamata

A Thesis Submitted in Partial Fulfilment of the Requirements of
Teesside University for the Degree of Doctor of Philosophy

April 2019

Abstract

Non-contact three-dimensional (3D) surface scanning methods are accurate and shown to produce advanced wound documentation and analysis in forensic medicine: the structured light 3D scanning technique is one of these methods. Despite the progress with this technique, much is yet to be discovered regarding the results of using it to record traumatic injuries. The aim of this study was to assess the efficiency of this technique for recording and analysing different types of traumas, while involving living persons and considering conventional documentation methods. This assessment has been completed by achieving three research objectives, which are proposed to begin with evaluation the overall feasibility of the method on the living persons by scanning different intact body areas, then to assess the methods' capability for reconstructing different types of closed traumas from injured subjects alongside open traumas from artificial mannequins.

Methods: Live subjects who were students and staff at Teesside University were participated to scan different bare areas of extremities, torso areas, challenging surfaces (such as dark skin and hairy surfaces) and complicated anatomical areas (such as the neck and the axillary area), alongside facial scanning. This was achieved after establishing simple scanning guidelines to use within this study. Then, injured live victims from the Medico-Legal Centre in Benghazi city were included to scan a wide range of traumas, such as abrasion, bruise and stitched wounds using the Pico scan structured light 3D scanner. While simulated open wounds located on artificial mannequins, having complicated areas and depths of up to 3 to 5 cm, were also scanned in laboratory conditions using the HP structured light 3D scanner. At the same time, all of the injuries were recorded using a professional digital camera which allowed a complete comparison between the two recording methods to be completed.

Results: 3D scanning results of different intact body areas of live subjects came in the form of acceptable 3D geometric reproductions with colour-textured information. The different traumatic wounds were reconstructed three-dimensionally and the results showed detailed and intact geometry without holes or defects, combined with evident colour-textured information. The visualisation of the 3D and 2D results of the same injuries on the screen was almost identical, but some important wound features, which are useful for wound analysis, were better represented in the 3D results, for example, wound edges and colour-textured resolution. These 3D documents were observed to have extra advantages over the 2D documents. Importantly, they reflected true scales and could be manipulated from different angles while displaying 3D geometry of the wounded areas instead of 2D flat presentation. Such advantages

would be favourable during wound examination alongside measurements and for wound presentation in court. Intra-observer reliability of 3D wound measurements in all calculated dimensions were classified as good and excellent (ICC 0.998 to 1.000). No statistically significant differences were exhibited between the 3D wound measurements and the direct manual measurements. The strength of the relationship between them exhibited strong positive correlations (93.5% to 99.4%), which were statistically significant. This research provided a novel method for examining forensic injuries in three dimensions and further validated an approach for measuring wounds in 3D.

Conclusion: Based on the above, using the structured light 3D technique in forensic medicine for wound documentation and analysis is a valuable contribution and advance in the field.

Key words

3D; three dimensional; surface scanning; structured light; forensic medicine; wounds; injuries; human body.

Table of Contents

Abstract	ii
Key words	iii
List of Tables	ix
List of Figures	xi
List of Abbreviations	xvii
Acknowledgements	xviii
Publications arising from this research	xix
Chapter 1: Significance of wounds in forensic medicine	1
1.1 Introduction.....	1
1.2 Medico-legal significance of wounds in forensic medicine.....	1
1.3 Documentation and measurements of wounds in forensic medicine	3
1.4 Research question	5
1.5 Research objectives.....	6
1.6 Thesis outline and structure	6
1.7 Personal motivation behind the selection of this research	7
Chapter 2: Examination and analysis of wounds in forensic medicine	9
2.1 Introduction	9
2.2 Forensic wounds.....	9
2.2.1 Wound definition	10
2.2.2 Classification of wounds and their medico-legal significance	10
2.2.2.1 Blunt force injuries	10
2.2.2.2 Sharp force injuries	13
2.2.2.3 Projectile wounds	16
2.2.2.4 Other injuries	17
2.3 Conventional wound documentation methods and their weaknesses.....	18
2.3.1 Manual documentation	18
2.3.2 Photography.....	18
2.3.3 Problems of digital photography	23
2.3.4 Lack of wound photography guidance	28
2.4 Conventional wound measurement methods and their weaknesses	35
2.4.1 Introduction	35
2.4.2 Ruler method overview.....	36

2.4.3 Disadvantages of the ruler method	36
2.4.4 Digital method overview	37
2.4.5 Disadvantages of the digital method.....	38
2.5 Conclusion	40
Chapter 3: Non-contact 3D surface scanning: techniques and their applications in forensic medicine	41
3.1 Introduction.....	41
3.2 Non-contact 3D surface scanning techniques	41
3.2.1 Stereo-photogrammetry.....	42
3.2.2 Photogrammetry	43
3.2.3 Laser triangulation 3D surface scanning.....	44
3.2.4 Structured light 3D surface scanning	45
3.2.5 Structured light versus laser 3D surface scanning	48
3.3 Applications of non-contact 3D surface scanning techniques.....	54
3.3.1 Applications of passive 3D surface scanning	54
3.3.1.1 Computer Aided Design (CAD)-supported photogrammetry	54
3.3.1.2 Single camera photogrammetry and stereo-photogrammetry	55
3.3.1.3 Multi-camera photogrammetry	56
3.3.1.4 Modern multi-camera photogrammetry	58
3.3.2 Applications of active 3D surface scanning	59
3.3.2.1 Structured light patterns 3D surface scanning	59
3.3.2.2 Hand-held structured light 3D surface scanning	61
3.3.2.3 Laser 3D surface scanning	64
3.4 Conclusion.....	65
Chapter 4: Research Methods	68
4.1 Introduction.....	68
4.2 Pico Scan 3D surface scanner.....	70
4.2.1 The Pico Scan scanning process	70
4.2.2 Scanner post-processing.....	71
4.2.3 PicoScan3 software settings.....	72
4.2.4 Mephisto process software settings.....	73
4.2.5 Geometric calibration	74
4.2.6 Scanning principle and algorithm.....	76
4.2.6.1 Phase Measuring Profilometry (PMP).....	76
4.2.6.2 Binary-coding patterns.....	77
4.3 HP 3D surface scanner Pro S3	79
4.3.1 The HP scanner scanning process	79

4.3.2 HP scanner post-processing.....	80
4.3.3 Calibration process.....	80
4.3.4 Triangulation algorithm.....	82
4.3.5 Pattern parameter profiles.....	83
4.4 Conclusion.....	84
Chapter 5: Using structured light 3D scanning on living individuals: key considerations and best practice for forensic medicine	85
5.1 Appropriate 3D scanning technique to scan different body areas.....	85
5.2 Optimum number of scans.....	88
5.3 Elimination of environmental background noise	89
5.4 Scanning approaches to access different body areas	91
5.5 Conclusion.....	92
Chapter 6: Structured light 3D surface scanning of intact living body areas: three studies	93
6.1 3D surface scanning of upper and lower limbs and torso areas.....	95
6.1.1 Materials and Method.....	95
6.1.2 Results	97
6.1.3 Discussion.....	105
6.1.4 Conclusion	107
6.2 3D surface scanning of complicated anatomical areas	114
6.2.1 Introduction	114
6.2.2 Materials and Methods.....	115
6.2.3 Results and Discussion	115
6.2.4 Conclusion	123
6.3 3D facial scanning	124
6.3.1 Introduction	124
6.3.2 Materials and Methods.....	124
6.3.3 Results	128
6.3.4 Discussion.....	136
6.3.5 Conclusion and Recommendations.....	143
Chapter 7: Documentation of traumatic wounds in clinical forensic medicine involving structured light 3D surface scanning	145
7.1 Materials and Methods.....	145
7.2 Results.....	152
7.2.1 Comparison between 3D and 2D documentation results	152
7.2.2 Comparison between 3D and conventional wound measurements.....	161

7.3 Discussion	163
7.5 Difficulties faced with this application	168
7.5.1 Problems related to using a living body	168
7.5.2 Problems related to 3D scanning method	171
7.5.3 Problems related to improper use of the scanner	174
7.6 Assessment of torso and lower limb 3D models	179
7.7 Conclusion	182
Chapter 8: Determining the effectiveness of structured light 3D surface scanning for the assessment of open wounds.....	183
8.1 Materials and Methods.....	183
8.2 Result	197
8.2.1 Structured light 3D surface scanning of open wounds.....	197
8.2.2 Features of open wound in 3D and 2D results	198
8.2.3 Complete versus limited structured light 3D surface scanning.....	201
8.2.4 Wound measurements analysis	206
8.2.4.1 Comparison between 3D and conventional wound measurements.....	206
8.2.4.1.1 Length and width measurements.....	206
8.2.4.1.2 Surface area measurements	210
8.2.4.1.3 Depth measurements	214
8.2.4.2 Further analysis around 3D surface area measurements	215
8.2.4.3 Intra-observer reliability	219
8.3 Discussion	220
8.4 Repeatability of structured light 3D surface scanning.....	226
8.5 Conclusion	227
Chapter 9: Overall discussion	230
9.1 Structured light 3D surface scanning of intact body areas.....	230
9.2 Structured light 3D surface scanning of wounded areas	232
9.3 Structured light 3D surface scanning versus 2D digital photography.....	233
9.4 3D wound measurements versus conventional measurements.....	235
Chapter 10: Conclusion and implications of the study	237
10.1 Conclusion	237
10.2 Implications of the study.....	239
10.2.1 Contribution to knowledge	239
10.2.2 Implications for medico-legal practice.....	240
10.2.3 Implications for future research	240

References	242
Appendices	270
Appendix A: Tables.....	270
Appendix B: Figures	273
Appendix C: Ethical approvals	277
Appendix D: Research participant information sheets and consent forms.....	282

List of Tables

Table 1.1: Legal applications based on wound's duration of treatment	3
Table 2.1: Main differences between incised and lacerated wounds	15
Table 2.2: Impact of angular distortion and scale tilting on linear dimensions	24
Table 3.1: Some technical features of passive, laser and structured light 3D surface scanning	46
Table 3.2: Using structured light 3D surface scanners in forensic medicine	62
Table 3.3: Impacting factors on passive, laser and structured light 3D surface scanning	67
Table 4.1: Pico Scan verses HP structured light 3D scanner	69
Table 4.2: PicoScan3 software settings and selected options	73
Table 4.3: Vertices and triangles in 3D raw scans using different profiles	83
Table 4.4: Scanning time based on selected profile	84
Table 5.1: Different number of scans of the same view and total number of vertices in final 3D models	88
Table 5.2: Testing different screen colours for noise removal	90
Table 6.1: Position of upper limb areas during scanning	96
Table 6.2: Position of lower limb areas during scanning	96
Table 6.3: Scanned some challenging body surfaces	97
Table 6.4: Impact of breathing on raw chest scans	109
Table 6.5: Manual and 3D distance measurements between markers on chest ...	111
Table 6.6: Manual and 3D distance measurements between markers on torso ...	123
Table 6.7: Different conditions of facial scanning	126
Table 6.8: Suggested deviation values and results	127
Table 6.9: Main specifications of used computers	142

Table 7.1: Types and number of recorded injuries by Pico Scan structured light 3D scanning and digital photography	147
Table 7.2: Wound measurements of the recorded dimension using manual, 2D and 3D methods	148
Table 7.3: Results of numerical tests of normality	149
Table 7.4: Descriptive statistics of all measurements	161
Table 7.5: Spearman's correlations between manual, 2D and 3D measurements	162
Table 7.6 Differences between 3D and conventional measurement methods	166
Table 8.1: Types and number of recorded injuries on artificial mannequins	185
Table 8.2: Wound length and width dimensions using tape, 2D and 3D methods	190
Table 8.3: Wound areas using 2D and 3D methods	192
Table 8.4: Wound depths using manual and 3D methods	194
Table 8.5: Significance values of SW test of all measurements	196
Table 8.6: Scanning parameters of complete 3D surface scanning	202
Table 8.7: Scanning parameters of limited 3D surface scanning	202
Table 8.8: Descriptive statistics of length measurements	208
Table 8.9: Descriptive statistics of width measurements	208
Table 8.10: Differences between wound measurements of linear dimensions	208
Table 8.11: Significance values of Sign test between wound measurements of linear dimensions	209
Table 8.12: Descriptive statistics of area measurements	211
Table 8.13: Differences between 2D and 3D measurements of surface areas	212
Table 8.14: Descriptive statistics of area measurements of smaller wounds	213
Table 8.15: Descriptive statistics of depth measurements.....	214
Table 8.16: Differences between manual and 3D depth measurements	215
Table 8.17: Manual areas of six selected wounds against 3D and 2D areas.....	216
Table 8.18: 3D wound areas in MeshLab and Geomagic software	218
Table 8.19: 3D wound areas based on twice scanning of the same wounds.....	219
Table 8.20: Single measures of ICC	219
Table 8.21: Area measurements of regularly shaped objects.....	224

List of Figures

Figure 2.1: Forensic injuries in two categories	10
Figure 2.2: Abrasion with serous fluid	11
Figure 2.3: Bruise	12
Figure 2.4: Lacerated wound with tissue bridges	13
Figure 2.5: Incised wound.....	14
Figure 2.6: Multiple stab wounds	15
Figure 2.7: Forensic body chart	18
Figure 2.8: Digital and RUV photographs of bruise	20
Figure 2.9: Digital and IR photographs of bloody surface4.....	21
Figure 2.10: Digital and IR photographs of faint tattoo4	21
Figure 2.11: Wound photography using narrow-banded visible light.	22
Figure 2.12: Type one angular distortion and type three scale bending	23
Figure 2.13: ABFO No.2 scale specifications	26
Figure 2.14: Correct and incorrect camera position.....	30
Figure 2.15: Angular distortion (right image)	30
Figure 2.16: Traditional measurement methods and precision error.....	38
Figure 3.1: 3D surface scanning techniques used in forensic medicine	42
Figure 3.2: Stereo-photogrammetry	43
Figure 3.3: Photogrammetry	44
Figure 3.4: Laser triangulation	44
Figure 3.5: Structured light scanning and sequence of binary coding patterns	46
Figure 3.6: Structured light (left) and laser scanning (right).....	50
Figure 3.7: Vectra H1 hand-held surface scanner (VH1).....	55
Figure 3.8: Botscan photogrammetry and 3D results with artefacts	57
Figure 3.9: DI3D photogrammetry and bite mark investigated by the system.....	57
Figure 3.10: VirtoScan-on-Rails	58
Figure 3.11: ATOS II structured light 3D surface scanner	59
Figure 3.12: Virtobot system	60
Figure 3.13: Artec Eva structured light 3D surface scanner	61
Figure 3.14: Konica Minolta 3D laser scanner and model created by the scanner .	64

Figure 4.1: Pico Scan structured light 3D surface scanner.....	70
Figure 4.2: Some acquired images with light stripes, plus one coloured image.....	71
Figure 4.3: Post-processing phase using Mephisto process software	72
Figure 4.4: Workflow of the Pico Scan 3D scanner.	72
Figure 4.5: Mephisto process software settings and selected options	74
Figure 4.6: Calibration board of the Pico Scan 3D scanner.....	75
Figure 4.7: Calibration board recorded in different positions	76
Figure 4.8: Amount of checker corners detected by the scanner.....	76
Figure 4.9: HP structured light 3D surface scanner Pro S3	79
Figure 4.10: Workflow of the HP 3D scanner Pro S3	80
Figure 4.11: Successful calibration	82
Figure 4.12: Triangulation principle of structured light scanning.....	83
Figure 5.1: 3D models of abrasion resulting from ATOS II (left) and Konica Minolta 3D scanner (right)26	85
Figure 5.2: Final 3D model of wrist joint free from artefact (left) and with overlapping artefact (right)	86
Figure 5.3: Using black screen to remove unwanted points (noise)	90
Figure 6.1: Assessed different intact body areas	93
Figure 6.2: Final 3D models of forearm.....	98
Figure 6.3: Final 3D model of foot shows blurred toes area (left) and clear lateral surface of the foot (right).....	98
Figure 6.4: Final 3D model of knee joint (left), the model manipulated on the screen to show unrecorded area (right).....	99
Figure 6.5: 3D raw data of chest with horizontal lines artefact (left), the data manipulated to show distorted points highlighted in red colour (right)	99
Figure 6.6: The same data reconstructed with two different shutter speeds: 1/6 sec (left) and 1/13 sec (right).....	100
Figure 6.7: The same data in Figure 6.6 shows distorted points highlighted in red colour.....	100
Figure 6.8: 3D raw data of chest with right and left shoulder	101
Figure 6.9: Final 3D model of chest with overlapping artefacts	101
Figure 6.10: Final 3D model of chest without overlapping artefacts	101
Figure 6.11: Final 3D model of dark coloured skin of two different volunteers.....	103
Figure 6.12: Final 3D model of palm moist with water	103
Figure 6.13: Final 3D model of the hairy posterior surface of the forearm	104
Figure 6.14: Final 3D model shows silver ring has no impact on scanning.....	104

Figure 6.15: Final 3D model shows clear tattoo 104

Figure 6.16: Final 3D model shows recorded blood stain..... 104

Figure 6.17: Illumination of the anterior and lateral surface of the foot with structured light stripes 106

Figure 6.18: Two 3D raw scans of chest..... 110

Figure 6.19: 3D geometry of chest in HP 3D scan software (left) and MeshLab software (right)..... 110

Figure 6.20: Colour bar comparison result of two 3D raw scans of chest 111

Figure 6.21: Two 3D raw data of abdomen 112

Figure 6.22: 3D geometry of abdomen in HP 3D scan software (left) and MeshLab software (right)..... 112

Figure 6.23: Colour bar comparison result of two 3D raw scans of abdomen..... 113

Figure 6.24: Injuries on uneven surfaces: 114

Figure 6.25: 2D digital photograph of under-chin area (left), 3D geometry of the area resulting from scanning using 22° camera angle (right) 116

Figure 6.26: 3D geometry of the same area resulting from scanning using 25° (left) and 15° (right) camera angle 116

Figure 6.27: Life camera view of 25° (left) and 15° camera angle (right)..... 117

Figure 6.28: 2D digital photograph (first) and 3D geometry of the same area (second) 118

Figure 6.29: 2D digital photograph of axillary area 119

Figure 6.30: 3D raw scans of axillary area show unrecorded arm 119

Figure 6.31: 3D geometry of axillary area in HP 3D scan software (first) and MeshLab software (second) 120

Figure 6.32: 3D geometries of the anterior and posterior surface of the knee 121

Figure 6.33: 2D digital photograph of deformed torso 121

Figure 6.34: Fused result (3D geometry) of deformed torso..... 122

Figure 6.35: Colour bar comparison result of noisy scans (first) and their 3D model shows movement artefacts around fingers and wrist (second)..... 128

Figure 6.36: Colour bar comparison result of completely matched scans (first) and their 3D model (second)..... 128

Figure 6.37: 3D raw scans of frontal, right and left views of subject with facial hair 129

Figure 6.38: 3D geometry of subject with facial hair in HP 3D scan software (left) and MeshLab software (right) 130

Figure 6.39: Colour bar comparison result of subject with facial hair 130

Figure 6.40: 3D raw scans of shaved face without colour-textured information 131

Figure 6.41: 3D geometry of shaved face 132

Figure 6.42: Colour bar comparison result of shaved face 132

Figure 6.43: 3D noisy raw scans without colour-textured information..... 133

Figure 6.44: 3D geometry (fused result of noisy facial scans) 133

Figure 6.45: 3D geometry from different views..... 134

Figure 6.46: 3D geometry and colour-textured result of dark skin face..... 135

Figure 6.47: Colour bar comparison result of dark skin face 135

Figure 6.48: 3D raw facial scans without colour-textured information shows glasses artefacts..... 136

Figure 6.49: Vectra XT 3D facial scanning (left) and 3dMDface system (right)..... 137

Figure 6.50: 3D raw facial scan with vertical ridges..... 140

Figure 6.51: Facial scanning with eyeglasses using botscan (left) and structured light scanner (right) 141

Figure 6.52: Left scan with correct aperture and right scan with the smallest aperture (Alienwaire computer)..... 142

Figure 6.53: Left scan with correct aperture and right scan with the smallest aperture (HP computer) 143

Figure 7.1: 3D document (first) and 2D document (second) of small ordinary contused wound with moderate swelling 153

Figure 7.2: 3D document (first) and 2D document (second) of longitudinal brush abrasion..... 154

Figure 7.3: 3D and 2D documents of two healed bite marks 156

Figure 7.4: 3D document (first) and 2D document (second) of bruise on the posterior aspect of the right arm 158

Figure 7.5: 3D document (first) and 2D document (second) of stitched defence cut wound..... 159

Figure 7.6: 3D document (left) and 2D document (right) of stitched cut wound on the anterior aspect of the left arm 160

Figure 7.7: 3D document (left) and 2D document (right) of stitched cut wound on the postero-lateral aspect of the left arm..... 160

Figure 7.8: Manual, 2D and 3D wound measurements of the recorded dimension 161

Figure 7.9: Scatterplot matrix of manual, 2D and 3D measurements 162

Figure 7.10: Two sets of 3D measurements of the same wound dimensions by the same observer 163

Figure 7.11: Two sets of 2D measurements of the same wound dimensions by the same observer 163

Figure 7.12: Changing the posture during 3D acquisition..... 169

Figure 7.13: Final 3D model of leg with overlapping artefact..... 169

Figure 7.14: 3D raw data of abdomen..... 171

Figure 7.15: Final 3D model of abdomen 171

Figure 7.16: 3D result (left) and 2D result (right) of small stitched stab wounds ... 173

Figure 7.17: Illumination of unwanted area 174

Figure 7.18: 3D result (first) with inconsistent degree of skin colour and 2D result (second) 175

Figure 7.19: Overexposed 3D result 176

Figure 7.20: Underexposed 3D result 177

Figure 7.21: Out of focus 3D result 178

Figure 7.22: C2C comparison between two 3D raw data of the anterior aspect of the left shoulder (first) and its histogram (second) 180

Figure 7.23: C2C comparison between two 3D raw data of the upper lateral aspect of the left leg (first) and its histogram (second) 181

Figure 8.1: Structured light scanning of Mannequin A using the HP scanner 185

Figure 8.2: Mannequin wrapped with light pattern and filled the camera view 186

Figure 8.3: Limited 3D surface scanning to the injury 186

Figure 8.4: Different recorded views of complete 3D surface scanning 187

Figure 8.5: 3D result of STL and OBJ file format 192

Figure 8.6: 3D depth measurement using HP scanner (left) and Konica Minolta scanner (right) 193

Figure 8.7: Detailed geometry and colour texture of stage-4 pressure injury 197

Figure 8.8: Detailed geometry and colour texture of unstageable pressure injury and stage-3 pressure injury 197

Figure 8.9: 3D and 2D results of deep tissue pressure injury 198

Figure 8.10: 3D and 2D results of long surgical wound 199

Figure 8.11: 3D and 2D results of explosion injury at the top of the head 199

Figure 8.12: 3D result of mannequin B shows undermined area 200

Figure 8.13: 3D and 2D results of stage-3 pressure injury 201

Figure 8.14: 3D and 2D results of cut wound on the dorsal aspect of the hand 201

Figure 8.15: Detailed geometry and colour-textured information of the complete 3D surface scanning of the head 203

Figure 8.16: Complete 3D surface scanning of Mannequin A 204

Figure 8.17: Complete 3D surface scanning of Leg and foot 205

Figure 8.18: 3D result of limited scanning of cut wound (left), the wound magnified to show detailed geometry (right) 206

Figure 8.19: Wound length measurements in cm 207

Figure 8.20: Wound width measurements in cm 207

Figure 8.21: Correlation between direct manual and 3D measurements (in cm). . 210

Figure 8.22: Wound area measurements in seq. cm 211

Figure 8.23: Area measurements of smaller wounds in seq. cm 213

Figure 8.24: Wound depth measurements in cm 214

Figure 8.25: Correlation between direct manual and 3D measurements (in cm). . 215

Figure 8.26: Segmented wounds in CloudCompare software 217

Figure 8.27: 3D result of toes area of leg and foot mannequin 221

Figure 8.28: 3D models of the same object resulting from different scanning (left),
C2M comparison result of these models (right)..... 227

List of Abbreviations

ABFO	American Board of Forensic Odontology
APS-C	Advanced Photo System type-C
ATOS	Advanced Topometric Sensor
CAD	Computer Aided Design
CD	Compact Disk
CT	Computer Tomography
C2C	Cloud to Cloud
C2M	Cloud to Mesh
DI3D	Dimensional Imaging 3D
DSLR	Digital Single Lens Reflex
DVD	Digital Versatile Disc
FFLM	Faculty of Forensic and Legal Medicine
FMMS	Forensic Medicine for Medical Students
FPHG	Forensic 3D/ computer aided design (CAD)-supported photogrammetry
ICP	Iterative Closest Point
ISO	International Standards Organization
JPG	Joint Photographic Expertise Group
LASER	Light Amplification by Stimulated Emission of Radiation
LCD	Liquid Crystal Display
MAVIS	Measurements of Area and Volume Instruments System
MLC	Medico-Legal Centre
MRI	Magnetic Resonance Imaging
OBJ	Object File
PLY	Polygon File
PMP	Phase Measuring Profilometry
PNG	Portable Network Graphics
PVC	Polyvinylchloride
RMS	Root Mean Square
SARC	Sexual Assault Referral Centres
SPSS	Statistical Package for Social Sciences
STL	Stereolithographic File
SW	Shapiro-Wilk
TIFF	Tagged Image File Format
WORM	Write Once and Read Many
2D	Two Dimensional
3D	Three Dimensional

Acknowledgements

First and foremost, to the most precious man of my heart, my father, Mr. Mohamed Shamata, who has always stood behind me, and encouraged me from my childhood to seek knowledge and without his support, I wouldn't have been able to reach this stage.

Similar profound acknowledgements to my great supervision team at Teesside University Prof. Tim Thompson and Dr. Helen Tidy. Special thanks go to Prof. Tim Thompson not only for his continuous academic support and guidance during my PhD study, but also for giving me an opportunity to conduct my project in 3D surface scanning technology.

I would like to extend my sincere thanks to:

Dr. David Errickson who introduced structured light 3D technique to me while it was totally new knowledge. Additionally, the topic of this thesis is one of Dr. Errickson's recommendations.

Dr. Sabah Al-Qamati, and Mr. Gaith Al-Fakhari who welcomed me in 2017 to Benghazi Medico-Legal Centre (MLC) where I conducted a part of my PhD work. I am also grateful to my other colleagues in the MLC and my nephew, Ahmed Atia El-Masmari, for their support throughout my application process.

All volunteers for their participation in this study.

It would have been impossible for me to achieve this without the relentless support of my family and my mother's prayers for me.

Thank you all,

Publications arising from this research

Shamata, A. and Thompson, TJU. (2018-a) 'Using structured light three-dimensional surface scanning on living individuals: key considerations and best practice for forensic medicine', *Journal of Forensic and Legal Medicine*, 55, pp. 58-64. DOI: [10.1016/j.jflm.2018.02.017](https://doi.org/10.1016/j.jflm.2018.02.017).

Shamata, A. and Thompson, TJU. (2018-b) 'Documentation and analysis of traumatic injuries in clinical forensic medicine involving structured light three-dimensional surface scanning versus photography', *Journal of Forensic and Legal Medicine*, 58, pp. 93-100. DOI: [10.1016/j.jflm.2018.05.004](https://doi.org/10.1016/j.jflm.2018.05.004).

Shamata, A. and Thompson, TJU. (2019) 'Determining the effectiveness of non-contact three-dimensional surface scanning for the assessment of open wounds', *Journal of Forensic Sciences*. DOI: [10.1111/1556-4029.14205](https://doi.org/10.1111/1556-4029.14205).

Chapter 1: Significance of wounds in forensic medicine

1.1 Introduction

Forensic medicine combines medicine with legal procedures by analysing the medical circumstances of victims of criminals or unfortunate events while providing a report for the prosecution. This domain includes clinical forensic medicine and forensic pathology. In Libya, forensic pathology covers suicide, homicide, road traffic accidents and any suspicious deaths. After the Arab Spring, the examinations in this area have been extended to include skeletal remains, firearm deaths from military clashes, and deaths due to suicide bombing or accidental shootings. On the other hand, clinical forensic medicine includes medico-legal examination of different types of wounds, such as road traffic accident injuries, wounds due to blows from blunt or sharp instruments, injuries due to firearms, injuries from occupational accidents, and evidence of domestic abuse; however, child abuse cases are rarely seen in Libya. Clinical forensic medicine also includes age estimation for those not in civil registry since birth, determination of the eligibility of elderly people, and virginity and sexual assault examinations. However, the most crowded area in clinical forensic medicine is the examination of wounded victims. Each wound has important medico-legal significance and therefore requires careful examination, documentation and measurement. However, in some situations, the medico-legal examination of the wounds can be negatively influenced by unclear wound features alongside their inaccurate measurements and documentation. In the next sections (1.2 and 1.3), the medico-legal significance of the wounds is briefly defined and the traditional wound documentation and measurements are then outlined.

1.2 Medico-legal significance of wounds in forensic medicine

The examination of wounds in medico-legal centres is an important issue. Any findings during wound examinations have medical meaning, while any statement in a forensic medical report has legal importance.

Medico-legal examination of wounds is based on the interpretation of the wounds and their features to find the medico-legal significance. For example, epidermal tags of abrasions can be used to know the direction of the impact (Saukko and Knight, 2004). Moreover, the mechanism of the impact is clarified through the type of abrasion. Tangential abrasion is caused by tangential impact, whereas crush abrasion, such as a bite mark or ligature mark is caused by direct vertical impact (Jones and Karch, 2003; Saukko and Knight, 2004). If bruises have different ages then this means that

the assault probably took place at different times. Additionally, the causative object could be known from the shape of the bruise. The most well-known bruise shape that can be correlated with the causative object is a tram-line bruise (Saukko and Knight, 2004; Payne-James, Crane and Hinchliffe, 2005). Furthermore, when bruises are located around the genital areas, sexual assault is possible (Crane, 2009). The examination of wound edges, margins and angles are important for analysing the difference between the incised and lacerated wounds; especially when they have mixed features of cut and laceration: which can happen in many situations (see [2.2.2.2.1](#)). Firearm injuries on upper or lower limbs can also be seen and examined in clinical forensic medicine. The type of weapon is the most important concern that the prosecution needs to know. In order to decide whether the weapon is rifled or non-rifled, careful examination of the inlet and area around the inlet is required. Estimation of the direction and the range of the firing are also possible and can be explained through the careful examination of inlet.

Therefore, wound analysis in forensic medicine is an important issue. However, in some cases, the wound examination is difficult due to, for example, the smaller wound size, the healing process of the wounds and the overlapping between two different types of wounds. In these situations, visual examination or current recording methods are insufficient. Wound interpretations, and their medico-legal significance in forensic medicine, including presentation of some challenging situations, are reviewed in detail in Chapter 2.

The outcome of the medico-legal examination is to write the medico-legal report which includes, for instance; the type and location of the injuries, the wound dimensions, an expected causative tool alongside the expected duration of the treatment and whether the injury will cause permanent infirmity or not. The report also includes notes about wound complications, the history of hospital admissions and history of surgical interventions (if they had happened). Prosecutors consider every written statement in the report while relying on all the written medical findings as well as the final medical decision to categorise the assault into a minor crime or criminal offence. If any significant medical information is missed, the assault could be mistakenly classified as minor.

In Libyan law, according to the wound's duration of treatment, the harm is legally classified as simple, moderate or dangerous. Table 1.1 shows some legal applications based on wound's duration of treatment; however, in dangerous harm, other conditions are taken into account, such as permanent infirmity, facial deformity, or abortion forced upon a pregnant woman.

Finally, it has to be said that the medico-legal reports are not only useful to protect the victim's rights, but it is also useful to help or acquit the accused: if he is an innocent case.

Table 1.1: Legal applications based on wound's duration of treatment

Duration of treatment	Legal classification	Type of crime	Legal judgement
1 to 40 days	Simple harm	Minor crime	Jail for not more than one year, or financial penalty of not more than 50 dinars.
> 40 days	Moderate harm	Minor crime	Prison for not more than two years, or financial penalty of not more than 100 dinars.
Other conditions	Dangerous harm	Criminal offences	Prison for not more than five years.

1.3 Documentation and measurements of wounds in forensic medicine

Forensic wound documentation is an essential task in clinical forensic setting, such recordings serve many functions including sources of wound interpretation by examiners, evidences for written medico-legal reports and sources of wound measurements. They are also used to match patterned injuries to suspected causative instruments. Ultimately such recordings may be used to represent the injuries (which may have since healed) in court (Shamata and Thompson, 2018-b). Although the digital photography is a common method for wound documentation, it can be easily affected by certain factors, such as distance and lighting condition. Very close-up distance causes 3D objects to appear out of focus, proximity effect (Verhoff et al., 2012). The lighting condition is also a serious factor, not easy to control during the photography (Green and Schulman, 2010; Casas, Castaneda and Treuillet, 2011; Chang et al., 2011; Marsh, 2011; Pavlovcic et al., 2011; Shaw and Bell, 2011). Digital photographs can also be featured distortions, noise and technical errors. Such distortions have been categorised by Evans et al. (2014) into four types: angular distortion and other three types of scale distortions. Noise is a random signal, destroys some parts of image information. Many different types of the noise can occur during the imaging steps, and they are very difficult to remove. The noise originates from different sources, such as Charge Coupled Devices (CCD), inaccurate cameras and misaligned lenses (Boyat and Joshi, 2015). Examples include, photon noise, electronic noise, impulse noise, periodic noise, quantization noise and coloured noise (Boyat and Joshi, 2015; Verme and Ali, 2013). The technical errors may result from improper camera adjustment of the aperture, shutter speed and white balance which

can cause wrong exposure or distorted colour (Green and Schulman, 2010). The main deficiencies of digital photography and their impacts on the wound analysis are reviewed in detail in [2.3.3](#).

Forensic wound measurements are important descriptions in the medico-legal reports, particularly for injured live victims. They are a record of wound severity and the degree of the force used. In addition, the overlay matching depends on the accurate measurements (Payne-James, 2012). In clinical forensic medicine, a ruler and measurement method that relies on digital photographs are commonly used methods. However, both methods have serious disadvantages which can limit their accuracy. The ruler method has been shown to overestimate wound areas (Majeske, 1992; Wysocki, 1996; Chulhyun and Richard, 2008; Rogers et al., 2010; Chang, Dearman and Greenwood, 2011; Shaw and Bell, 2011), while the digital method could underestimate the wound areas (Rennert et al., 2009; Treuillet, Albouy and Lucas, 2009; Chang, Dearman and Greenwood, 2011). Both methods are contact methods and have risk of infection. The main shortages of the ruler and digital wound measurement methods are reviewed in detail in [2.4.3](#) and [2.4.5](#).

In the light of the above information, the conventional methods of the wound documentation and measurements are not adequate. Accordingly, there are recommendations to record forensic injuries using non-contact 3D surface scanning methods (Thali, Braun and Dirnhofer, 2003-a; Sansoni et al., 2009-a; De Sainte Croix et al., 2016). These methods are known to be accurate methods (Thali, Braun and Dirnhofer, 2003-a; Sansoni et al., 2009-a; Ishii, 2012; Sivanandan and Liscio, 2017; Villa, 2017-a) which generate high-resolution 3D models reflecting actual-sizes. These techniques compute 3D coordinates (x, y, z) of surface points (Geng, 2011) and create 3D models instead of 2D images. There are passive and active 3D surface scanning methods. The passive scanning relies on taking a series of photographs (Salvi et al., 2010), while the active scanning is based on projection of a laser beam or structured light patterns (Errickson, Thompson and Rankin, 2014). Such techniques were originally developed for industrial applications, such as the aerospace (John Tzou, Artner and Pona, 2014) and automobile industry (Thali, Braun and Dirnhofer, 2003-a). They were also developed for reverse engineering (Salvi, Pages and Batlle, 2004). But they have been increasingly used in many other areas, such as medicine, plastic surgery, facial recognition, archaeology, heritage, crime scene and forensic science, as well as forensic medicine. However, the use of these techniques in forensic medicine is currently mostly for the purpose of research, rather than practice. Urbanova, Hejna and Jurda (2015, p. 82) stated that “forensic post-

mortem examination is concerned neither Photogrammetry nor 3D scanning has been fully integrated into regular workflow". Passive, laser and structured light 3D surface scanning techniques have been used to scan injuries or full body, to match patterned injuries with suspected causative instruments and to merge external 3D data of the injury with internal MRI or CT data of the same injury. However, most of this research focused on introducing the different types of 3D techniques in forensic medicine rather than analysis of 3D results of forensic findings. These 3D techniques and their applications in forensic medicine are reviewed in Chapter 3.

From this researcher's point of view, structured light 3D surface scanning is the most convenient method for scanning traumatic injuries on living subjects and dead bodies. It relies on projection of highly designed light patterns with coding strategy that allows accurate correspondence between the projected image and the captured image. It is a fast 3D scanning method and has no significant safety concerns. However, most of the studies that have been achieved using structured light scanning are based on the ATOS (Advanced Topometric Sensor) structured light scanner, which is demanding to use; its application can be difficult while time-consuming (Urbanova, Hejna and Jurda, 2015; Villa, 2017-a). Although structured light method was introduced into forensic medicine since 1998 (Subke, 2000), there has been a clear deficiency in forensic literature review about applying the structured light technique to recording traumas of living persons, while there is no written standard procedure to scan injured live subjects. The same deficiency has been observed in the validation of 3D wound measurements based on this method, particularly depth and surface area. Moreover, no study has yet compared wound results from 2D digital photography with results using the structured light 3D method. Therefore, the study was aimed at assessing the efficiency of the structured light technique in recording and analysing different traumatic wounds while involving living subjects and considering conventional recording methods.

1.4 Research question

This research was focused on recording wounds using structured light 3D surface scanning in order to answer the following question:

Can the above-mentioned method be used to reconstruct and analyse the different types of traumatic injuries in forensic medicine?

To answer this question, the research objectives, in 1.5, were established.

1.5 Research objectives

1. To evaluate the ability of structured light 3D surface scanning for recording different intact uninjured body areas of living subjects in order to consider the overall feasibility of the method on the human body.
2. To assess the method's capability for reconstructing traumas from living subjects in a clinical forensic medicine.
3. To evaluate the possibility of using structured light 3D surface scanning for digitizing open injuries containing complicated areas and depths.

1.6 Thesis outline and structure

The thesis comprises ten chapters, which are as follows:

Chapter 1 is the overall introduction to the research topic. It clarifies that forensic wound examination, documentation and measurements have legal applications; on the other hand, the chapter shows how these forensic tasks could be affected by some challenging situations and by the shortcomings of the current recording methods. Thus, this chapter is followed by Chapters 2 and 3. Chapter 2 provides details about the current issues while Chapter 3 introduces the promising alternative solution.

Chapter 2 presents the current challenges surrounding traumatic wound examination alongside wound recording and measurements. It introduces different traumatic injuries and their medico-legal significance while including explanations of some difficult situations related to the wound interpretation. This chapter also reviews conventional wound recording and measuring methods and shows how their serious limitations can negatively affect the wound analysis.

Following the above, Chapter 3 introduces more accurate and powerful recording methods, non-contact 3D surface scanning methods, which can be used as an alternative to the current recording technique in order to improve the wound analysis and documentation. This also reviews the literature surrounding the applications of these techniques in forensic medicine and shows how these applications have developed the subject field. However, the limitations of each application are identified and the gaps that exist are also highlighted.

Next, Chapter 4 looks at research methods. This demonstrates the two structured light 3D surface scanners that were selected and used in the research. Separately, the chapter presents the calibration process, scanning and post-processing of each

scanner. These scanners were used in this study to reconstruct and analyse the different types of the traumatic injuries in order to answer the main research question. Following this, Chapter 5 is focused on methodological pilot studies to investigate 3D surface scanning related to living bodies and develop a series of simple scanning principles. These principles included using an appropriate 3D scanning technique to scan different body areas, scanning approaches to access different body areas, optimum numbers of scan for each scanned area and the elimination of background noise from the scans. A research paper has been published in Journal of Forensic and Legal Medicine demonstrating these simple scanning guidelines.

For Chapters 6, 7 and 8, the actual experimentations and applications of structured light 3D surface scanning are presented to address the research objectives. Each application sets out the material and methods, results and discussion. Chapter 6 aims to achieve the first objective of the research. It presents and discusses the results of applying structured light scanning to the different intact body areas of living persons, in order to evaluate the overall feasibility of the research method on the human body. Then, Chapter 7 intends to achieve the second objective of the research, while the work in Chapter 8 addresses the third objective of the research. Both of these present and discuss the results of applying structured light 3D scanning to traumatic wounds on living bodies and open wounds on artificial mannequins in comparison to results of conventional methods. A research paper and a technical note have been generated from these chapters, demonstrating how structured light 3D surface scanning is efficient for reconstructing traumas from living subjects in a medico-legal centre, and able to reconstruct extensive traumas having complicated areas and depths in laboratory conditions.

The final two chapters are Chapters 9 and 10. The former is an overall discussion focusing on the main results of the three important experimental applications of Chapters 6, 7 and 8 and clarifies their implications; while the latter, Chapter 10, draws conclusions and implications of the study alongside identifying scopes for future works.

1.7 Personal motivation behind the selection of this research

When I attended an autopsy on my first day in the mortuary, in 2004, it was a terrifying experience. This autopsy had been carried out on two Libyan men to establish the cause of death. In order to achieve this, their scalps had been pulled into anterior and posterior directions to allow the top of the skull to be saw-cut, followed by the removal of the brain. The subcutaneous tissue of the chest, abdomen and pelvis had been

dissected and then the rib cage had been opened, which had allowed the removal of the main organs. Personally, I found this process very distressing. Additionally, in some nations, such as my own country Libya, autopsies are carried out with little control, while facing difficulties such as a lack of equipment and poor facilities. Since my first autopsy, I have considered how to improve the procedure with an alternative method and found that internal 3D documentation, Virtual Autopsy (Virtopsy), is a solution. Therefore, I decided to carry out external 3D documentation (3D surface scanning) on external injuries, which are a common issue in the field. By undergoing this experience in surface scanning, I hope then to work within Virtopsy and one day combine both skills to use in my own country.

Chapter 2: Examination and analysis of wounds in forensic medicine

2.1 Introduction

Examination of wounds in forensic medicine is intended to find the medico-legal significance of the examined injuries. Each traumatic wound has important features which can be connected to this medico-legal significance. For example, the shape of the inlet of the firearm wounds or the small skin tag of the abrasions can be linked to the direction of the impacts. The shape of the edges of the cut and lacerated wounds can be linked to the causative tools. Wound feature interpretation can be used afterwards to answer questions in court, or to write the medico-legal reports that are important for categorising assaults into minor crime or criminal offences. Therefore, it is important for forensic specialists, who are examining and documenting the injuries, to ensure that they have recorded the injuries clearly and covered all fine details. However, in some cases the critical wound features are not clear, either because of the smaller wound sizes, the healing process or the overlapping between two different types of the wounds. Moreover, the technique of the current recording methods, such as digital photography, suffers from some major disadvantages which impact the accuracy and resolution of the wound recording, and subsequently they impact the accuracy of the wound analysis. Additionally, the current wound measurement methods are contact methods, have risk of infection and have been shown to over or underestimate the wound measurements.

Therefore, this chapter begins by introducing the wounds and their significance in forensic medicine while including explanations of some difficult situations related to wound examination. Then, it reviews the conventional methods of recording and measuring wounds and exposes the main disadvantages of each method.

2.2 Forensic wounds

This section introduces forensic wounds and accounts for their medico-legal importance in the field. Some complicated wound situations related to the wound examination are included to clarify why the examination and recording of these wounds requires more powerful methods other than the conventional ones. The section is presented under two main headings: wound definition and classification of wounds and their medico-legal significance.

2.2.1 Wound definition

A wound is a disruption of the tissue continuity caused by an external mechanical force, whereas the definition of an injury can have a wider meaning, and include not only damage produced by mechanical force, but also produced by heat, cold, chemicals, electricity and radiation (Pounder, 1993). Saukko and Knight (2004, p.136) stated that injuries or wounds can be defined as “damage to any part of the body due to the application of mechanical force”. Applying this latter description, in this study, ‘wound and injury’ have been used as alternatives for each other.

2.2.2 Classification of wounds and their medico-legal significance

Wounds are medico-legally classified into: blunt force injuries, sharp force injuries, projectile injuries and other injuries. The blunt and sharp force injuries and projectile injuries are mechanical traumas, caused by the transfer of energy from an external moving object to the tissues, whereas other injuries are non-kinetic injuries, caused by physical or chemical agents. Figure 2.1 shows forensic injuries in two main categories.

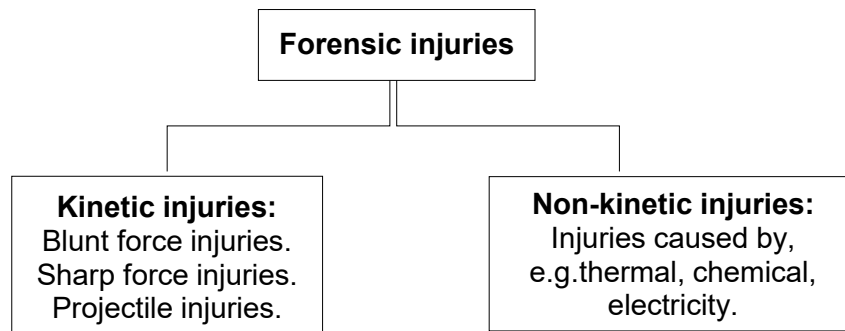


Figure 2.1: Forensic injuries in two categories

2.2.2.1 Blunt force injuries

These injuries are resulting from forceful contact between a blunt object and the body (Pounder, 1993); they include abrasions, contusions (bruises) and lacerations (Jones and Karch, 2003).

2.2.2.1.1 Abrasion

This is the most superficial injury, and it usually involves only the epidermal layer; for that reason, there is no bleeding. However, when the dermal papillae is included, it will present serous fluid (Figure 2.2) or slight blood (Jones and Karch, 2003; Saukko

and Knight, 2004; Payne-James, Crane and Hinchliffe, 2005). An abrasion is basically caused by a tangential or vertical impact. A tangential abrasion can reflect the direction of the impact through a skin tag at the end of the injury, whereas a patterned abrasion, that caused by a vertical impact, can match the shape of the causative tool. Common examples of patterned abrasions are bite marks, ligature marks (Jones and Karch, 2003; Saukko and Knight, 2004), a footwear mark that is caused by forceful kicking (Johnson, Lyall, Johnson, 2015), and the muzzle imprint of contact shooting. Finger nail abrasions can be short curved marks or linear scratches (Saukko and knight, 2004). They have medico-legal significance in sexual attacks and strangulation.



Figure 2.2: Abrasion with serous fluid

In the practical field, interpretation and diagnosis of this type of wound is straightforward; however, there are some difficult situations that make the wound analysis challenging. Determining the direction of the impact is difficult when the small epidermal tag cannot be clearly observed. Ohshima (2000) claimed that a binocular operation microscope should be used to observe any small tag closely. However, it is rarely available due to the cost and training needs and is suitable only for post-mortem cases. Thali et al. (2003-a) applied ATOS II structured light 3D scanning to record a small skin tag and they found that the small tag could be seen clearly in the 3D results.

Moreover, matching the patterned abrasion with a suspected causative tool to find enough that corresponds is difficult to achieve accurately by traditional methods of matching, such as an overlay technique and the direct insertion of a weapon into the wound. The direct matching of the suspected weapon into the patterned injury or plastic casting of the injury leads to loss of or cover fine details (Thali et al., 2003-d). On the other hand, matching between 3D models of the injuries and the causative tools has been tested and found better than the traditional matching by photography (Thali, Braun and Dirnhofer, 2003-a; Sansoni et al., 2009-a). Matching based on forensic 3D computer-aided design (CAD)-supported photogrammetry (FPHG) (Thali et al., 2000; Thali et al., 2003-c; Thali et al., 2003-d) has been used and has already been established in Swiss courts (Thali et al., 2005).

2.2.2.1.2 Bruise

A bruise is discoloration of the intact skin (Figure 2.3). The injury lies under the intact epidermis, caused by a blunt force which leads to the rupture of blood vessels and the leaking of blood into the surrounding tissue under the pressure of circulation. However, bruising is not limited to the skin; it can take place anywhere inside the body (Jones and Karch, 2003; Saukko and Knight, 2004; Crane, 2009). Saukko and Knight (2004) stated that the word bruise describes an injury that happens in the subcutaneous tissues and is visible through the skin, whereas contusion means the injury occurs anywhere inside the body, such as in a mesentery, in a muscle or the spleen. Pounder (1993) suggested that bruise, contusion and ecchymosis all are synonyms for each other. However, using '*bruise*' to describe the injury that is visible through the skin is more reasonable.

The characteristic feature of the bruise is the colour change which appears when the haemoglobin breaks down into coloured products, to gradually fade away (Jones and Karch, 2003; Saukko and Knight, 2004). The colour change can be used to estimate the age of the bruise, and consequently the time of the assault. However, it should not be used as an accurate calendar as it is a variable process (Saukko and Knight, 2004; Sharma et al., 2011).



Figure 2.3: Bruise

Although the diagnosis of the bruise is a simple task, the bruise could be presented in some states that make the diagnosis or interpretation difficult, for example, almost healed bruises are difficult to confirm by visual examination and difficult to identify in digital photographs. Special photography, such as cross-polarized photography, can be useful in this situation (Baker, Marsh and Quinones, 2013). In other cases, a bruise on dark skin might be hidden without the obvious swelling or hematoma underneath. According to Pounder (1993), UV photography may enhance bruises on dark skin. However, according to Baker, Marsh and Quinones (2013), IR photography is more useful since the IR bypasses the melanin of the epidermal layer and penetrates deeper. Another example, the post-mortem bruise is generally small and requires

great force to be generated (Jones and Karch, 2003). Any peri-or post-mortem bruises that are located on dependent parts of the body can overlap with hypostasis or anti-mortem bruises.

2.2.2.1.3 Laceration

Laceration is caused by considerable blunt force which leads to a tearing of the full thickness of the skin by compressing the skin between the force and the underlying bone (Figure 2.4) (Jones and Karch, 2003; Saukko and Knight, 2004; Payne-James, Crane and Hinchliffe, 2005; Crane, 2009; Sharma et al., 2011). Any tissue can be lacerated; for example, bone fractures or ruptures of the Achilles tendon are lacerations (Pounder, 1993). However, skin laceration is the most common and most frequently seen. A scalp laceration is the best example of skin laceration (Jones and Karch, 2003; Saukko and Knight, 2004; Crane, 2009). Characteristic features of this trauma are tissue bridges (nerves and fibrous bands), irregular edges, and abraded or contused margins (Jones and Karch, 2003; Saukko and Knight, 2004; Payne-James, Crane and Hinchliffe, 2005; Crane, 2009). The inside of the laceration is also important, and often contains a source of trace evidence that may link the injury to the causative object (Payne-James, Crane and Hinchliffe, 2005).



Figure 2.4: Lacerated wound with tissue bridges¹

2.2.2.2 Sharp force injuries

These injuries are caused by sharp-edged or sharp-pointed objects. Incised wounds (cuts) and stab wounds are the main types of these injuries (Pounder, 1993). Self-inflicted and defence wounds can be included in this group of injuries

¹ (Isaac, 2014).

2.2.2.2.1 Incised wound

An incised wound is a clean cut of the skin and underlying tissues caused by a sharp-edged object, such as a knife, broken glass or razor, so that the key features of this wound are well-defined edges and a clean margin (Figure 2.5). There is always complete sharpness of tissues within the depth of the wound (Jones and Karch, 2003; Saukko and Knight, 2004; Crane, 2009).



Figure 2.5: Incised wound

Although laceration and incised wounds have some clear characteristic features (Table 2.1), overlapping between these wounds can take place in some cases. Wounds which are caused by heavy sharp instruments, such as a chopper, meat-cleaver or machete, may have mixed features of incised and lacerated wounds (Payne-James, Crane and Hinchliffe, 2005), i.e. the injuries are incised wounds with abrasion and/or bruising on the wound margin (Pounder, 1993). Additionally, sharp instrument injuries in certain areas, such as the axillary region, the scrotum or the abdominal wall, are usually similar to lacerated wounds as these areas have redundant skin. Also, an irregular jagged sharp instrument, such as the edge of a broken glass, can cause irregularly edged wounds anywhere. Furthermore, lacerated wounds on the scalp usually simulate incised wounds as the scalp is stretched over the skull (Saukko and Knight, 2004; Payne-James, Crane and Hinchliffe, 2005). These situations need careful examination of the wound edges, margins, angles and tissue bridging to define the type of wound and the causative instrument. The examination is usually conducted by the naked eye or a hand-held magnifying lens while taking photographs.

Table 2.1: Main differences between incised and lacerated wounds

	Incised wounds	Lacerated wounds
Shape	Linear or elliptical often deeper at starting end	Any shape
Edges and angles	Clean edges with acute angles	Ragged with no angles
Margin	No abrasions and bruises on the margin	Surrounded by abrasions or bruises
Base	Sharply and cleanly cut No bridging of tissues	Compressed with bridging of tissues across the edges. May contain foreign bodies
Surrounding hairs	Sharply and cleanly cut	Crushed or irregularly cut
Bleeding	Profuse bleeding due to cutting of blood vessels	Minimal bleeding due to crushing and retraction of blood vessels except in the scalp
Liability to sepsis	Less liable to sepsis due to washing of contaminations by profuse bleeding	Great liability to sepsis due to severe tissue destruction with minimal bleeding
Healing	Rapid healing with thin scar	Delayed healing with thick scar

2.2.2.2.2 Stab wound

This is a penetrating injury (Pounder, 1993). It has depth rather than length and width (Figure 2.6) (Saukko and Knight, 2004; Payne-James, Crane and Hinchliffe, 2005; Sharma et al., 2011). Any weapon with a point or tip can cause a stab wound. The commonest weapon is a knife (Jones and Karch, 2003; Payne-James, Crane and Hinchliffe, 2005). A stab wound can be subdivided into puncture, perforating and penetrating wounds.

Figure 2.6: Multiple stab wounds²

2.2.2.2.3 Self-inflicted wounds

They are also known as fabricated injuries. They are usually superficial incised wounds (Bhullar and Aggarwal, 2007), parallel to each other, directed towards the

² (Koronfel, 2014).

centre of the body, and on approachable parts, such as the anterior aspect of the wrist, forearm or the lateral aspect of the upper arm (Payne-James, Crane and Hinchliffe, 2005; Crane, 2009; Saukko and Pollak, 2013). They are usually created by a person on his own body to implicate his opponent (Thompson, 2008) or are seen among prisoners, soldiers or drug addicts (Saukko and Pollak, 2013). Although these injuries have key features and clear criteria to be diagnosed, they might create doubt or a difficult situation in decision-making.

2.2.2.2.4 Defence wounds

These wounds can be of any type (Saukko and Knight, 2004; Payne-James, Crane and Hinchliffe, 2005; Crane, 2009); however, they are commonly sharp force injuries. They occur when the victim attempts to protect himself. They are normally seen on the forearm, arm or palmar surface of the hands (Payne-James, Crane and Hinchliffe, 2005; Mohite et al., 2013).

2.2.2.3 Projectile wounds

These are caused by smooth-bore weapons (shotguns) or rifled weapons (rifles, hand guns, air rifles and military weapons). These wounds also include injuries caused by rubber and plastic bullets, and humane killer gun bullets, and arrows from bows and crossbows (Jones and Karch, 2003). Projectile wounds are usually recognizable, unique (Sharma et al., 2011), and typically have two characteristic features: (1) loss of the tissue substance and (2) the presence of inlet and, usually, exit wounds.

The severity of any injury (tissue damage) is based on a bullet's velocity (Stefanopoulos et al., 2014), the nature of the projectile, the material of the projectile, the distance and angle of the firing, and the part of the body involved (Yetiser and Kahramanyol, 1998; Saukko and Knight, 2004; Sonkhya, Singhal and Srivastava, 2005; Sharma et al., 2011). This means that in some situations, identification of firearm injuries could be hindered by difficulties (Sharma et al., 2011). For example, the extensive tissue damage of a high velocity rifled bullet can overlap with injuries produced by high-speed bomb fragments or expanding bullets. Another problem may arise when a bullet leaves the tissue sideways rather than nose first as it causes an exit wound like an incised wound. Additionally, when a bullet strikes the body tangentially from a long distance, it leads to a superficial injury that may simulate an abrasion or an abraded bruise.

2.2.2.4 Other injuries

Other injuries are non-kinetic injuries caused by non-physical forces, such as thermal, chemical agents and electricity (Jones and Karch, 2003). These forces damage the body surface by direct application, which is usually unintentional, and therefore they do not have major medico-legal significance. Burns and electrical injuries are common examples of these traumas.

2.3 Conventional wound documentation methods and their weaknesses

The main objective of forensic wound documentation is a legal purpose. So far, manual and digital photography have been the main methods of documentation. Both methods are reviewed here, and the main disadvantages and problems are highlighted.

2.3.1 Manual documentation

Forensic documentation by hand has been used foremost. Currently, recording by hand is a suitable means of preserving the most important evidence when other methods are not available (Buck et al., 2009). Written descriptions or notes are two types of manual documentation (Payne-James, 2003; Payne-James, Crane and Hinchliffe, 2005). Drawing on a forensic body chart (Figure 2.7) is another type of manual documentation (Payne-James, 2003; Sherpherd, 2003; Payne-James, Crane and Hinchliffe, 2005; Riviello, 2010). Although photographic documentation is superior to manual, the FFLM (2017) suggested that body diagrams can still play a part by helping with logging the descriptions of the injuries. Also, they are useful when an image of an injury cannot be acquired through photography due to pain and tenderness.

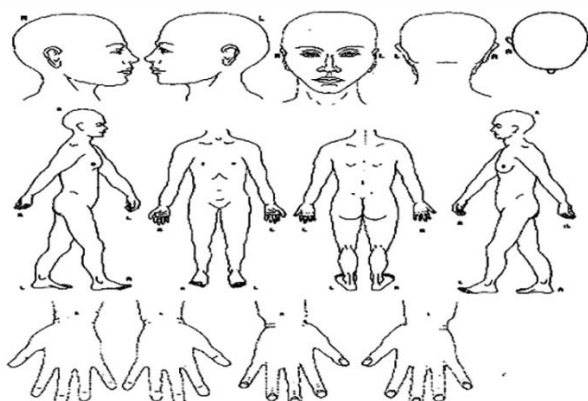


Figure 2.7: Forensic body chart³

2.3.2 Photography

Photography has been used the most in the forensic domain as a recording tool since 1900. It has been used to capture important findings during autopsy (Walz et al., 1983, cited in Buck et al., 2009, p. 51), and injuries ranging from a slight redness to gunshot wounds (Spraggs, 2007). Although photography plays a significant role in

³ (Payne-James and Crane, 2005).

the forensic field in documenting the different types of evidence, there are debates around using photography in some situations (Thompson, 2008). For example, there are still restrictions around the imaging injuries in sensitive areas, especially injuries of adult victims of sexual assault (Brennan, 2006). Moreover, not all relevant photographs are accepted for submission to court. If the photographs are of severe injuries which could negatively impact the jury or if the benefit of viewing these images is minimal, they may be rejected (Douglas et al., 1997). Furthermore, concern has been raised regarding simple photograph manipulation (Thompson, 2008; Karpoor and Arlikatti, 2012); nearly anyone can produce alterations in an image with basic software if the photograph is digital in nature.

Having said this, photography is still valuable and still the method of choice, and a photographic document serves some useful functions, including:

- Being a source of injury interpretation made by an examiner.
- Evidence for a written medico-legal report.
- A means of presenting injuries or autopsy findings in court.
- A resource for research or in a teaching context.

Nowadays, digital photography per se has become a standard recording method. It has many advantages over film photography. The main advantages are the improvement of the photograph quality, and the ability of the computer software to adjust the photographs (Karpoor and Arlikatti, 2012; Rajshekar, Kruger, Tennant, 2012). Moreover, digital photographs can be used as an electronic source of wound measurements (wound dimensions/ wound areas), or to match a patterned skin injury to a suspected causative instrument, or to send for second opinions.

Some specific types of photography have been used in forensic medicine to capture unclear injuries that are not visible to the naked-eye or not evident in ordinary digital photographic images (Saukko and Knight, 2004). Reflected ultraviolet (RUV) photography, reflected infrared (IR) photography and cross-polarized photography are examples of these types of photography and they are explained below.

2.3.2.1 Cross-polarized photography

In this type of photography, the light passes through two (or more) linear polarizing filters at 90° to each other before reaching the sensor (Marsh, 2011). One linear polarizing sheet is placed over the light source (the camera-flash unit); this filter is oriented either vertically or horizontally. Another linear polarizing filter is placed over the camera-lens oriented at 90° to the flash filter (Hanlon, 2017; Meek, 2017). The flash filter orients unpolarised light to polarized waves which allows it to penetrate the

surface several nanometres deeper than ordinary light (Hanlon, 2017). This increases the colour saturation (Constant, 2000; Marsh, 2011), i.e. enhances the contrast and the colour of the bruise (Baker, Marsh and Quinones, 2013; Trefan et al., 2018), burns, bite-marks and strangulation marks (Marsh, 2011). It also removes the white glare and reflections (Constant, 2000; Marsh, 2011; Vecellio and Bryant, 2017) that are caused by oil or sweat of skin (Baker, Marsh and Quinones, 2013).

2.3.2.2 Reflective Ultraviolet (RUV) photography

This photography requires a strong UV light source (320-390 nm), and a filter over the lens to allow only the UV light to reach the film, which should have a sensitivity to the UV spectrum (Karpoor and Arlikatti, 2012). Today, film cameras are no longer used (Marsh, 2011), and digital cameras are available which can impede the UV and IR rays in order to capture the image only using visible light. This means that special digital cameras are required to obtain RUV photography (Marsh, 2011).

The difference in skin colour, tone and pigmentation, which may appear trivial in the results of ordinary photography, may become evident in the results of RUV photography. This photography has been used to enhance images of nearly-healed traumas (Marsh, 2011), such as a healed bruise (Figure 2.8) (Klinge and Reiter, 2008). However, Baker, Marsh and Quinones (2013) stated that RUV photography is insufficient at recording a healed bruise unless it is a shallow bruise, dark in colour and on pale (unpigmented) skin. This is could be due to the fact that the UV light penetrates only a few microns into the skin, making it useful only to define injuries associated with the skin and no thing deeper (Karpoor and Arlikatti, 2012). Moreover, when the skin is pigmented, the melanin effectively absorbs this light (Tetley, 2005).

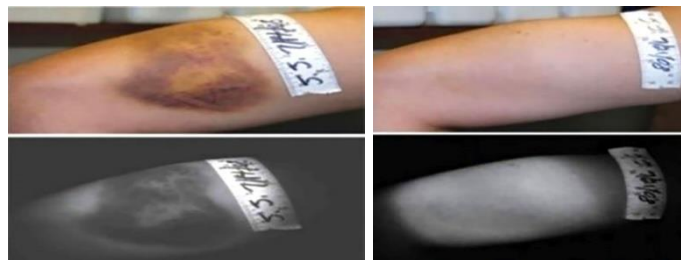


Figure 2.8: Digital and RUV photographs of bruise⁴
The photographs captured after 88 hrs (left) and 280 hrs (right)

⁴ (Klinge and Reiter, 2008).

2.3.2.3 Infrared (IR) photography

This is also done using infrared film cameras or suitable digital cameras. IR light penetrates deeper tissue that lies beneath the epidermis and dermis, penetrating the skin by up to 3 mm (Klinge and Reiter, 2008; Marsh, 2011; Karpoor and Arlikatti, 2012). Thus, IR photography can be useful in the following situations:

- Capturing injuries below the surface of the skin (Karpoor and Arlikatti, 2012).
- Vanishing the bloody surface to obtain a clearer photograph (Figure 2.9 right).
- It can be used to more easily expose tattoos in a victim with advanced stages of decomposition (Figure 2.10 right).

This type of photography is not significant in the documentation of healed bruise on pale skin (Klinge and Reiter, 2008; Rowan, 2010; Baker, Marsh and Quinones, 2013), but it is valuable to enhance showing bruises on dark skin because it bypasses the melanin of the epidermal layer (Baker, Marsh and Quinones, 2013).



Figure 2.9: Digital and IR photographs of bloody surface⁴



Figure 2.10: Digital and IR photographs of faint tattoo⁴

Narrow-banded visible light sources have also been investigated to expose injuries that are not seen by the naked eye. The injuries are illuminated and examined directly under light (Limmen et al., 2012) or captured by a digital camera with a coloured lens (coloured filter) (Hettrick and Hardigan, 2017). Figure 2.11 (left) shows no clear trauma in digital photograph, whereas Figure 2.11 (right) displays that when photograph is recorded by 475 nm blue wavelength with yellow lens, the trauma is clearly visualized.

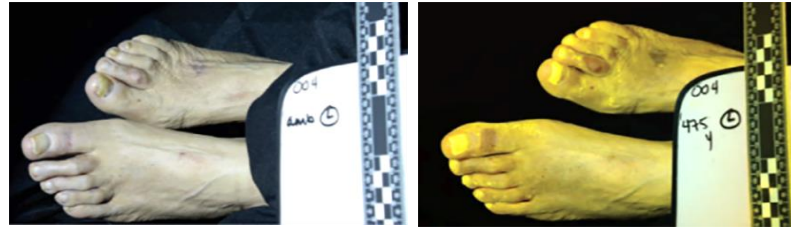


Figure 2.11: Wound photography using narrow-banded visible light⁵.

2.3.2.4 Close-up photography using close-up lens

A close-up lens is a lower power magnifying lens; it is also called a supplementary lens or Diopter. It is screwed over a primary lens of a DSLR (Digital Single Lens Reflex) camera, allowing it to focus a little closely than normal. It has different optical powers from +1 to +10: the higher the number, the greater the amount of magnification. Using a close-up lens with a digital camera is the simplest way to have slightly greater magnification. It allows the primary lens to focus more closely as this lens reduces the minimum focusing distance of the camera's lens; a photographer can move closer to an object until the lens obtains its focus. However, there are some drawbacks related to this lens, which are summarised in the following points:

- It is not good optically unless the two-element is used.
- It suffers from edge distortion.
- It has a lower value with a shorter focal length.
- It is not normally colour-corrected.
- It does not have an anti-flare coating.

In addition, close-up work can face other problems, such as light loss, lens flare, vignetting⁶ and diffraction (Constant, 2000).

⁵ (Hettrick and Hardigan, 2017).

⁶Vignetting: it is underexposure (darkening) around the corners of the image in a circular pattern. It is caused by interference of a filter or an adaptor ring where these objects block the light in front the lens

2.3.3 Problems of digital photography

Although digital photography is a fast, simple method (Verhoff, et al., 2012) and plays an important role in wound documentation, it can obtain serious weaknesses in its results, such as distortion and noise. Additionally, it is associated with problems regarding inaccuracy of photographic scale and lack of depth information. Moreover, photography can be negatively impacted by some factors such as lighting conditions, distance and technical errors. All these disadvantages are discussed below.

2.3.3.1 Distortion

Digital images are vulnerable to have some kinds of distortion (Wang et al., 2004). Evans et al. (2014) categorised the distortions into four types:

Type one: angular distortion, which happens when using an improper angle of acquisition (Figure 2.12 left).

Type two: it takes place when the scale is not placed on the skin on the same plane as the injury.

Type three: scale bending occurs resulting from applying too much pressure to the scale (Figure 2.12 right).

Type four: scale tilting.

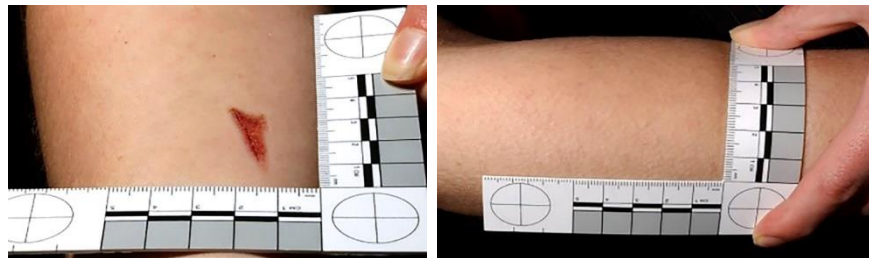


Figure 2.12: Type one angular distortion and type three scale bending⁷

Type one distortion has an impact on the appearance and estimation of the actual wound area (Chang, Dearman and Greenwood, 2011; Foltynski et al., 2015); however, it is not stated in the literature review if the linear measurements are impacted by angular distortion or not. Type two and three distortions most likely have an impact on the appearance and measurement of the wounds. If the scale is not on the same injury plane, being too close to the camera and too far from the skin, the injury will appear smaller (FFLM, 2017). From the researcher's point of view, type four distortion (scale tilting) has no impact on the wound measurements if the photograph is acquired from the correct angle.

⁷ (FMMS, 2015-b).

A simple test was done to confirm this; it was also done to see the impact of angular distortion on linear dimensions. A line of 100 mm length was drawn on a sheet of paper and photographed with a scale. The drawn line was captured from a correct angle and an incorrect angle. It was also captured from the correct angle with slight and severe scale tilting. Table 2.1 shows the length measurements that were taken from the captured photographs using Image J software. Then, the percentage of error formula was applied.

It was noted that (1) the angular distortion had an impact on the linear dimensions as the error increased 10 times when the camera was in the wrong position, and (2) scale tilting in the photograph taken from the correct angle had no significant effect on the measurements.

Table 2.2: Impact of angular distortion and scale tilting on linear dimensions

Camera position	Length measurements (in mm)				Percentage of error
	1 st	2 nd	3 th	Average	
Correct angle	100.201	100.644	101.533	100.792	0.8 %
Incorrect angle	110.898	110.373	110.373	110.548	10.5%
Correct angle & little scale tilting	100.590	100.358	100.357	100.435	0.4%
Correct angle & sever scale tilting	101.040	101.041	101.273	101.118	1%

To know if the photo has angular distortion before taking the wound measurement, the following can be considered (Rajshekar, Kruger, Tennant, 2012):

- Any circular reference in the scale must be rounded, not oval.
- A grid projection with L-shaped scale should be used (Ferrucci et al., 2016).

There are other different types of distortions which can have a clear impact on the image view. These are optical and perspective distortions. Optical distortions are caused by the lens's optical design. There are three types of optical distortions: barrel distortion, pincushion distortion and mustache distortion. Perspective distortion is caused by the camera position in relation to the subject. If the subject is very close to the camera, it can appear larger or distorted (Mansurov, 2017).

2.3.3.2 Noise

Noise is an arbitrary signal which destroys some image information. Different types of noise can occur during the imaging steps, and they are difficult to delete. Noise originates from different sources, such as using an inaccurate camera, a misaligned lens or a faulty memory location (Boyat and Joshi, 2015). According to Verme and Ali

(2013), the noise can result from the effects of basic physics, such as the photon nature of light or the thermal energy of the heat inside the sensor. Examples of these noise are photon noise (Poisson noise), electronic noise (Gaussian noise), impulse noise, periodic noise, quantization noise, speckle noise and coloured noise (Patidar and Srivastava, 2010; Verme and Ali, 2013; Boyat and Joshi, 2015). Photon noise appears when the number of photons detected by the sensor are not enough to deliver detectable statistical information (Patidar and Srivastava, 2010), whereas impulse noise arises from sudden and acute changes of the image signal (Verme and Ali, 2013). Impulse noise produces black and white dots in the image (Patidar and Srivastava, 2010; Verme and Ali, 2013); because of this it is called salt and paper noise (Verme and Ali, 2013; Boyat and Joshi, 2015). Therefore, different kinds of noise produce different effects in the digital images.

2.3.3.3 Inaccuracy of photographic scales

A photographic scale (ABFO No.2) is commonly used in forensic photography as a standard reference scale. The ABFO (American Board of Forensic Odontology) has published specifications for their ABFO No.2 scale (Hyzer and Krauss, 1988). These specifications are summarised in the following points and shown in Figure 2.13:

- The overall accuracy of the scale is ± 0.1 mm.
- Internal and external diameters of the three circles are 19.75 and 23.00 mm respectively.
- The error in placement of the three circles is within 0.25% of the nominal 80-mm separation between their centres.
- The legs (sides) are equally perpendicular to ± 2 min of arc.

Despite this standardisation, Ferrucci et al. (2016) assessed the scales of four companies and found that more than half of the tested scales were outside of these specifications in terms of the perpendicularity of the two legs. Moreover, centre to centre distances and internal and external diameters a lack of adherence to specifications. A four- years re-assessment shows slight variations in the length of the scale and the centre-to-centre distance. However, the perpendicularity shows significant change, and therefore they claimed that “a review of commercially available photo scales shows a lack of consistency in quality and accuracy”.

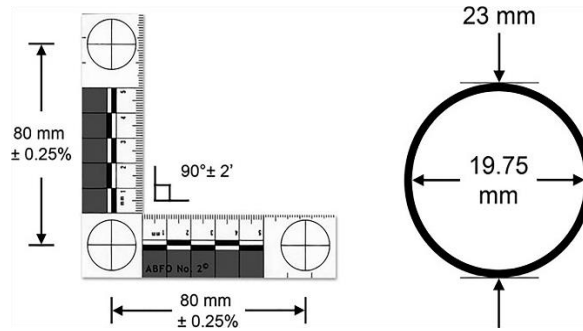


Figure 2.13: ABFO No.2 scale specifications⁸

2.3.3.4 Lack of depth information

Digital photography creates flat photographs having two axes (x & y) and therefore it reduces the 3D injury to 2D level, lacking information on wound depth (Krouskop, Baker and Wilson, 2002; Thali, Brauna and Dirnhofera, 2003-a; Casas, Castaneda and Treuillet, 2011). This constraint limits the examiner's ability to understand the complexity of the 3D entities (Geng, 2011).

2.3.3.5 Unreliable method for nearly healed trauma

Old or almost healed injuries are not clearly visible to the human eye, and they cannot be clearly enough detected by standard digital photography. For that reason, RUV, IR and cross-polarized photography are used to enhance showing these traumas. However, the RUV and IR photography are not significant in healed bruise documentation. Moreover, the results of reflected UV photography are variable, based on several factors, such as skin tone (Marsh, 2011). All ranges of UV light are harmful for the human skin and eye (Limmen et al., 2012). IR photographs appear fuzzy or out of focus because the camera lens is focused on the surface, and the resulting image is 3 mm away from the surface (Curtis and Katie, 2008; Karpoor and Arlikatti, 2012). Finally, RUV and IR photography require suitable cameras. This is because normal digital cameras cannot capture images with the UV spectrum (Marsh, 2011).

2.3.3.6 Impact of lighting conditions

During the photography, the lighting conditions are not easy to control (Green and Schulman, 2010; Casas, Castaneda and Treuillet, 2011; Chang, Dearman and Greenwood, 2011; Marsh, 2011; Shaw and Bell, 2011; Pavlovic et al., 2015). For

⁸ (Ferrucci et al., 2016).

example, Marsh (2011) stated that office lighting causes a colour cast on any object captured. Furthermore, photography near windows or near a bright light can cause the subject to appear darker (Patient Focused, 2018). The lighting conditions may be the room light which, in turn, could be darker light, brighter light, side light or light through the window. The proper selection of an exposure triangle is important in solving this situation. However, the proper selection of an exposure triangle requires good expertise and experience.

The pop-up flash of the camera has also some problems. For example, it fires the light in one direction (Zuckerman, 2013). This might cause harsh direct illumination in the image (Green and Schulman, 2010; Zuckerman, 2013), a red-eye effect (Zuckerman, 2013), or washed-out photographs (washed out colours and details) if the camera is too close to the target (Spraggs, 2007; Green and Schulman, 2010). Moreover, it is effective only over a short distance as it is small and has limited power (Zuckerman, 2013).

2.3.3.7 Impact of distance

The distance between the subject and camera is another difficulty related to using photography (Lane and Harrell, 2008). Close-up photography at very close distances causes three dimensional objects to appear out of focus (proximity effect) (Spraggs, 2007; Verhoff et al., 2012).

2.3.3.8 Technical errors

Technical errors may result from the improper selection of camera settings, such as aperture size, shutter speed, ISO and white balance that subsequently can cause over exposure, under exposure or inaccurate colour (Green and Schulman, 2010; Michienzi et al., 2018).

Finally, according to Evans et al. (2014), image errors are easily made even by the most experienced and knowledgeable practitioner. This is because photography requires many considerations and it is easily affected by several factors; therefore, no guarantees can be given. According to Constant (2000, p. 4), "Digital photography can take an hour or more to get a single shot just right". According to Errickson, Thompson and Rankin (2014), photographers may accidentally impose their own errors in the photographs. Conversely, non-contact 3D surface scanning techniques are available with accurate algorithms and their 3D outcomes are more reliable than 2D digital photographs. However, 3D techniques still lag behind conventional methods

(Blais, 2004), especially in forensic medicine, where such techniques are still at a research stage.

2.3.4 Lack of wound photography guidance

Forensic wound photography has no specific protocols. This is possibly due to the following three reasons:

1. Injuries photography requirements vary from one injury to another. For example, black eye photography is different from bite mark photography (Marsh, 2011).
2. The photographer can be a medical doctor, police officer or a forensic specialist. Each one captures the wound from different viewpoints; i.e. each captures the injuries for different reasons. In addition, they record the injuries with different levels of photography experience. According to Marsh, (2011, p.160), "In the UK and many other countries, police photographers, unlike medical photographers, are generally not trained to a set national standard".
3. Resources and regulations of the workplace vary from one area to another, and possibly from country to country. However, the basic points of forensic injuries photography, such as placing a scale around the wound and setting good lighting conditions, are the same everywhere.

Some injuries protocols have been published to cover certain injuries or to target certain aspects. Evans et al. (2014) have published photography guidelines for patterned injuries. Bloemen et al. (2012) have published photography protocols for injuries in the elderly. Marsh (2011) has published general knowledge about injuries photography without detailed instructions. The FFLM (2017) has proposed injuries photography guidelines for professionals who works in Sexual Assault Referral Centres (SARC) and police custody. Spraggs (2012) has published some injuries photography guidelines for police officers. These different protocols have shown that there are similarities between injuries photography in a clinical setting and in a forensic setting. Also, some basic photographic procedures that are used in crime scenes photography can be used in injuries photography (Spraggs, 2012). Therefore, the author's recommendations regarding injuries photography in different disciplines are reviewed and discussed in the next section. The recommendations are concerned with using the appropriate camera and suitable lenses, choosing a camera setting, using a photographic scale, setting up the lighting, background and examination room, deciding on the number of photographs required, the position of the injured person, the file format and form of photo storage.

2.3.4.1 Camera

A digital single lens reflex (DSLR) camera has been recommended for forensic injuries photography (Spraggs, 2007; Marsh, 2011; FFLM, 2017). This is because the sensor is larger, resulting in better image quality (Verhoff, et al., 2012); it has a changeable lens system (FFLM, 2017); and the DSLR has more advanced settings and features, such as an LCD screen and macro settings (Spraggs, 2012; FFLM, 2017).

The outcomes are preferable when using a camera with more than 3 megapixels (Darlene et al., 2007): “Any digital camera with four mega pixel capacity should be quite enough for documentation purposes” (Ozkalipci and Volpellier, 2010, p.50).

2.3.4.2 Lens

A standard prime lens rather than a zoom lens is advised to capture the injuries at the same focal length (Marsh, 2011; Evans et al., 2014); however, Spraggs (2007) recommended a zoom lens to obtain a longer focal length. The longer focal length allows better flash exposure. It also mitigates against washed-out results; washed-out photographs are a result of the camera being too close to the injury. Also, the longer focal length generates an image with less optical distortion.

2.3.4.3 Camera setting

An automatic setting is usually the choice; however, it is better to use manual settings (Spraggs, 2007) since these allows for better adjustments. Any harsh illumination caused by the pop-up flash can be avoided by increasing the ISO or any undesirable lighting conditions can be resolve by adjusting the exposure settings manually. On the other hand, the macro-setting (flower icon) allows the camera to take better close-up images (Spraggs, 2007; Sperring and Baker, 2014).

2.3.4.4 Camera position

Injury photography should be taken while the camera is in the proper position (Figure 2.14 left); the sensor plane (the camera body) must be parallel to the wound plane (Green and Schulman, 2010; Evans et al., 2014; Sperring and Baker, 2014). In other words, the lens's optical axes should be perpendicular to the wound plane (Thali et al., 2003-d; Bloemen et al., 2012; Foltynski et al., 2015). During the documentation of any evidence, this consideration is important with regard to generating an image free from angular distortion (Figure 2.15), to estimating the actual size of the wound, and to obtaining accurate wound measurements.

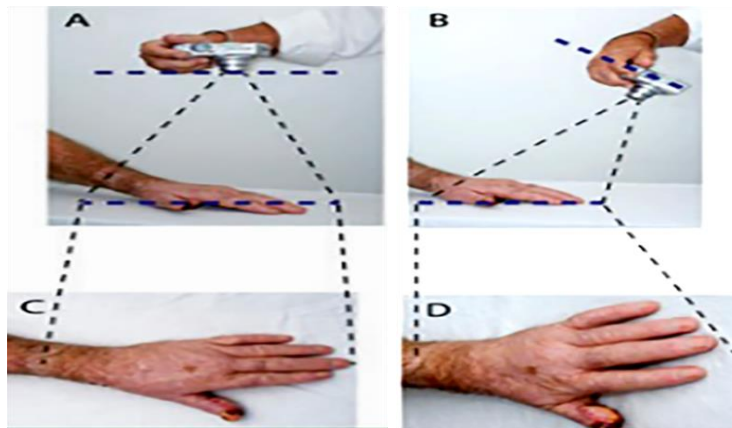


Figure 2.14: Correct and incorrect camera position⁹



Figure 2.15: Angular distortion (right image)¹⁰

2.3.4.5 Photographic scale

Firstly, there are different types of scales, including straight, L-shaped, and Y-shaped scales, as well as disposable and adhesive scales (FFLM, 2017). A scale is used in wound photography for four reasons:

1. It is used to estimate the size of the wound (Marsh, 2011).

⁹ (Sperring and Baker, 2014).

¹⁰ (FFLM, 2017).

2. It is an important factor for the admissibility the evidence in court (Evans et al., 2014).
3. It assists in contrast and colour correction (Marsh, 2011).
4. It is used to calibrate the software and take digital wound measurements.

The following points should be considered when using a scale:

1. A rigid scale is the choice (LeMay, 2002; Evans et al., 2014). The use of adhesive scales should be avoided (Evans et al., 2014) because they can bend with the body's surface curvature and cause distortion. Also, they are reflective scales. Plastic rulers are also not recommended as they create hotspots when illuminated with a flash (Marsh, 2011).
2. The scale should have a matte finish to reduce reflection (LeMay, 2002; Marsh, 2011; Evan et al., 2014).
3. It should be flat and thin. If a thick scale is used, any injury will appear smaller than its actual size, when the photo is enlarged (LeMay, 2002).
4. It should be placed on the skin, on the same level as the injury (LeMay, 2002; Spraggs, 2007; Evans et al., 2014; FMMS, 2015-b; FFLM, 2017). If the scale is too close to the camera and too far from the skin, the injury will appear smaller than actual size (FFLM, 2017).
5. It should be placed close to the injury, but not too close (Bloemen et al., 2012; FFLM, 2017).
6. Avoid applying any pressure on the scale to avoid scale bending (Bloemen et al., 2012; Evans et al., 2014; FMMS, 2015-b). Tilting the scale should also be avoided (Evans et al., 2014).
7. It should be cleaned after each use (FFLM, 2017).

According to Evans et al. (2014), an ABFO No. 2 scale (rigid L-shaped) and a longer straight scale can be used for larger patterned skin injuries. According to Marsh (2011), a small L-shaped scale can be used in close-up photography, and the longer straight scale be employed in general photography. Although, the ABFO No. 2 scale is specifically designed and used for bite marks, it can also be used with other types of skin injuries and many different types of evidence in the crime scene (LeMay, 2002; Ferrucci et al., 2016).

Selection of the scale is based on: (1) the anatomy of the wounded area; for example, the L-shaped scale is difficult to use for an injury on the side of the nose (Patient

Focused, 2018); and (2) the types of wound, if the injury has length dimension, the straight scale can be used, but if the wound has area, the L-shaped scale is better. When the ABFO L-shaped scale is used, the three circles of the scale should be included in the camera view to identify any angular distortion (Evans et al., 2014), and two axes of the scale should be parallel to the imaging plane (FMMS, 2015-b). Despite this guideline, it should be borne in mind that according to Ferrucci et al. (2016, p. 509), “a review of commercially available photo scales shows a lack of consistency in quality and accuracy” and Evans et al. (2014, p.5) stated that “the measurements on scales are not consistent among the various brands”.

2.3.4.6 Lighting

The lighting includes both the flash light and the room light. A pop-up flash is not recommended for injuries photography. This is because the light that emerges from the flash is narrowly directed, producing a harsh direct illumination in the photograph (Marsh, 2011). Dual mounted flashguns are recommended to produce smooth illumination (Marsh, 2011; Evans et al., 2014). On the other hand, it is much more difficult to control the room light. It requires proper selection of an exposure triangle alongside considering the colour cast of the light and white balance setting.

2.3.4.7 Background and the examination room

The background should be either a wall, portable screen (Marsh, 2011; FFLM, 2017), or background sheeting that is stored and rolled rather than folded (FFLM, 2017). A bright coloured background should be avoided since this can reflect colour casts onto any object close to it (Marsh, 2011); thus, a neutral colour is preferred (Spraggs, 2007).

Medical examination rooms are usually cluttered locations. The room will usually contain medical cabinets, chairs, posters, desks and computers; these can provide clutter in the wound photographs. Moving potential clutter or moving the subject away from it are simple ways of improving the photographs (FFLM, 2017).

2.3.4.8 Number of photographs required

According to Bloemen et al. (2012), each injury should be captured four times: two distance photographs and two close-up photographs, both with and without a scale. However, FFLM (2017) recommended three photographs: one distance and two close-up photographs. The distance photographs are taken to capture the wound with any anatomical landmarks while the close-up photographs are focused on the wound

itself. Any close-up image should include the injury and the scale; both are required to fill the image (Spraggs, 2007; Evans et al., 2014). In order to record these photographs, the photographer can either adjust the focal length of the camera (shorter and longer), or can move closer or farther away from the injury (Sivanandan and Liscio, 2017). In addition, supplementary close-up lenses with optical powers from +1 to +10 can be mounted over the primary camera lens to obtain the close-up images.

Injuries on a curved area should be acquired many times from different angles: at least three angles. The scale should be moved in each view in order to be on the same focal plane (Evans et al., 2014).

2.3.4.9 Participant position

Bloemen et al. (2012) recommended variable positions based on the injured body region. However, the injured victim can sit or stand in a position that he finds comfortable to avoid unnecessary stress to the victim and to avoid unnatural photography production (Marsh, 2011).

2.3.4.10 File format

According to Marsh (2011) and Evans et al. (2014), a RAW file format is recommended for capturing photographs of the forensic injuries. The next recommended file format is the TIFF (Tagged Image File Format). The JPEG (Joint Photographic Expertise Group) is not recommended for forensic injuries (Evans et al., 2014; Marsh, 2011). However, the FFLM (2017) stated that the images can be stored in different formats, and that the JPEG is the commonest file type. The file format is not related to the admission of the evidence; quality is the only issue (Cohen and MacLennan-Brown, 2007).

Each file format has advantages and disadvantages. RAW files are difficult to access (Marsh, 2011; FFLM, 2017); Adobe Photoshop or other special software are required to open these files (Evans et al., 2014) and convert them to a readable format. Conversely, the JPEG format is readable by most viewing software (FFLM, 2017). A RAW file has more colour information. It has 16-bit colour depth that provides a range of 65,536 colours on each channel (Marsh, 2011); therefore, it can be subject to greater adjustments (e.g. brightness, contrast and level) without any significant photograph degradation or the removal of important details (Marsh, 2011; Evans et al., 2014). A JPEG has 8-bit colour depth, which gives only 256 colours (Marsh, 2011). The data of a JPEG file is compressed to varying degrees; it can be corrupted

with repeated usage or further compression (Marsh, 2011; FFLM, 2017). It compresses when it is captured, processed and resaved (Evans et al., 2014). A RAW file size can be increased once it has been processed (Marsh, 2011).

2.3.4.11 Storage

The perfect data storage is the main concern of the examiner. The following points are general principles concerning data storage (Cohen and Maclennan-Brown, 2007; FFLM, 2017):

1. The photographs should be stored in a secure media that is WORM (write once and read many), such as a hard drive, CD or DVD.
2. The original photograph should remain intact and be called a '*master copy*'. Any copy of the master copy should be made as soon as possible and should be called a '*working copy*'.
3. Any corrections made to a photograph, such as cropping or enhancement, should be made on the working copy.
4. Once the photographs have been stored in the secure media, they cannot be altered.
5. The file should be marked with the patient's number rather than the patient's name.
6. An audit trail of access must be available.

The enhanced working copy and the master copy must be stored and submitted together. Any alterations or corrections must be explained.

2.4 Conventional wound measurement methods and their weaknesses

2.4.1 Introduction

The purpose of wound measurement differs from one discipline to another. In a clinical setting, chronic wound measurements are essential in order to follow the healing process and to evaluate the impact of any treatment (Plassmann and Jones, 1998; Langemo et al., 2008; Plassmann and Peters, 2001; Roger et al., 2010; Sikka et al., 2012; Savage and Jeffery, 2013). In forensic medicine, wound measurements are important descriptions in the medico-legal report, particularly for wounded live victims in clinical forensic medicine. They indicate the degree of force and the wound severity. In addition, any required overlay matching between an injury and a suspected weapon is based on accurate measurements (Riviello, 2010; Payne-James, 2012). If the location of an injury is required, it is described metrically by measuring a distance between the injury and a fixed anatomical point (Slot, Larsen and Lynnerup, 2014). Finally, wound measurements are not fixed; they might be re-measured if the second opinion is requested by a criminal defence lawyer or a judge. There are many different wound measurement methods, but the most practical method is by using a ruler to measure the length and width dimensions. The ruler method is an internationally accepted standard method (Savage and Jeffery, 2013). Other measurement methods include the wound tracing method, which involves tracing the wound onto transparent sheet, and the digital measurement method that is based on digital photographs. In the forensic setting, the ruler is most commonly used, as well as the digital method.

In clinical forensic medicine, the injured victims are live victims; they have already obtained medical intervention and the open wounds have already been stitched. Therefore, the maximum length dimension is usually the main measurement of the stitched wounds. Abrasions, bruises and abraded bruises usually have areas; thus, the areas of these wounds are measured by multiplying the greatest length and width measurements taken by a ruler, or by outlining the border of the wound in a digital image. Wound volume is another measurement task. It is important in a clinical setting to follow the progress of wound healing. This is because wounds tend to heal from the base (Jones and Plassmann, 1995), but in the clinical forensic context, the volume is not an issue. However, the depth is important in some situations in forensic pathology (i.e. with injured corpse). The depth of a stab wound in post-mortem cases is significant and should be measured in addition to the length. This is because these dimensions can be matched with a suspected instrument; the length and width of a

blade can be estimated from the depth and length of the stab wound. The depth measurement in post-mortem cases is mostly conducted by introducing a metal probe to the wound. However, this way of depth measurement is not acceptable for two reasons: it may produce additional destruction to the tissue (Denton, Segovia and Filkins, 2006) and it exhibits a lack of respect to the dead body.

In the following section, the ruler and digital measurement methods are described with main advantages and disadvantages.

2.4.2 Ruler method overview

This is simple, inexpensive and easy to use (Majeske, 1991; Goldman and Salcido, 2002; Haghpanah et al., 2006; Langemo et al., 2008; Chang, Dearman and Greenwood, 2011; Wendelken et al., 2011). It is executed by measuring the greatest linear wound dimensions (the longest length and the widest width) with a ruler or a tape measure. The wound area based on this method is calculated by multiplying the two dimensions (Thawer et al., 2002; Haghpanah et al., 2006; Rogers et al., 2010; Foltynski et al., 2015). These two dimensions are perpendicular to each other (Goldman and Salcido, 2002; Chang, Dearman and Greenwood, 2011). There are four ruler techniques which can be used in order to measure the maximum length and width of a wound (Diane et al., 2008; Langemo et al., 2008):

- The longest length head-to-toe orientation and widest width side-to-side, perpendicular to the length.
- The longest length head-to-toe orientation and widest width side-to-side at any angle to one another.
- The longest length and widest width perpendicular to one another, regardless of head-to-toe orientation.
- The longest length and widest width at any angle, regardless of head-to-toe orientation.

2.4.3 Disadvantages of the ruler method

Although it is a commonly used method, it has some drawbacks, which are:

1. It is a subjective method, and limited by inter-observer variability (Haghpanah et al., 2006; Roger et al., 2010; Shah, Wollak and Shah, 2015). Determining the greatest wound dimensions can vary from one examiner to another (Mayrovitz, Smith and Ingram, 1998), especially if the wound is irregular.
2. Reproducibility of the method is clearly influenced by movement and the changing of the subject position (Plassmann and Jones, 1998).

3. It over or underestimates the wound area. Assessing the measurement of a wound area by multiplying its length and width assumes that the wound shape is rectangular or square (Majeske, 1992; Wysocki, 1996; Chulhyun and Richard, 2008; Treuillet, Albouy and Lucas, 2009; Rogers et al., 2010; Chang, Dearman and Greenwood, 2011); it overestimates the actual area of the wound by up to 10% - 44% or more (Goldman and Salcido, 2002; Keast et al., 2004; Diane et al., 2008; Langemo et al., 2008; Rogers et al., 2010; Shetty, Lamba and Gupta, 2012). Greater overestimation arises when the injuries are larger and more irregularly shaped (Langemo et al., 2008). Length x width x 0.785 is another formula (the ellipse formula) suggested for the measurements of a wound area (Plassmann, 1995; Fette, 2006; Treuillet, Albouy and Lucas, 2009; Shaw and Bell, 2011; Sprigle, Nemeth and Gajjala, 2012); however, the results based on the application of this formula are still unreliable (Bowling et al., 2009). It is accurate for smaller wounds but underestimates larger or irregular wounds (Thomas and Wysocki, 1990). According to Foltynski et al. (2013), using the elliptical method (length x width (perpendicular to each other) x 3.1416/ 4) to measure areas of irregularly shaped wounds overestimates the areas by up to 33%, and its use is not recommended in fields where the wound areas are an important measurement.
4. The method is uncertain in terms of accuracy when determining the area (Majeske, 1992; Goldman and Salcido, 2002; Haghpanah et al., 2006; Roger et al., 2010; Shetty et al., 2012).
5. There are no permanent records. If the wound has healed or a corpse is not available, the measurements cannot be re-assessed for a second opinion.
6. It is a contact method and thus poses a risk of infection (Wysocki, 1996; Plassmann and Peters, 2001; Keast et al., 2004).

2.4.4 Digital method overview

This method is conducted by capturing a digital photograph of the wound with a scale; the photo is then loaded into the software to take the measurements (Treuillet, Albouy and Lucas, 2009; Casas, Castaneda and Treuillet, 2011; Chang, Dearman and Greenwood, 2011; Foltynski et al., 2015). The wound area, as well as the wound linear dimensions (length and width), can be obtained digitally. Different software is used for this, such as Image-J software (Chang, Dearman and Greenwood, 2011; Shetty et al., 2012; Shah, Wollak, and Shah 2015), VeV MD system (Haghpanah et al., 2006; Wendelken et al., 2011), Pictzar Digital Planimetry Program Software (Wendelken et al., 2011) and AWAMS (Casas, Castaneda and Treuillet, 2011).

The method is considered accurate and reliable (Rajbhandari et al., 1999; Thawer et al., 2002; Chang, Dearman and Greenwood, 2011; Shaw and Bell, 2011) (Figure 2.16). Moreover, it provides permanent wound records, including wound appearance and colour (Chang, Dearman and Greenwood, 2011).

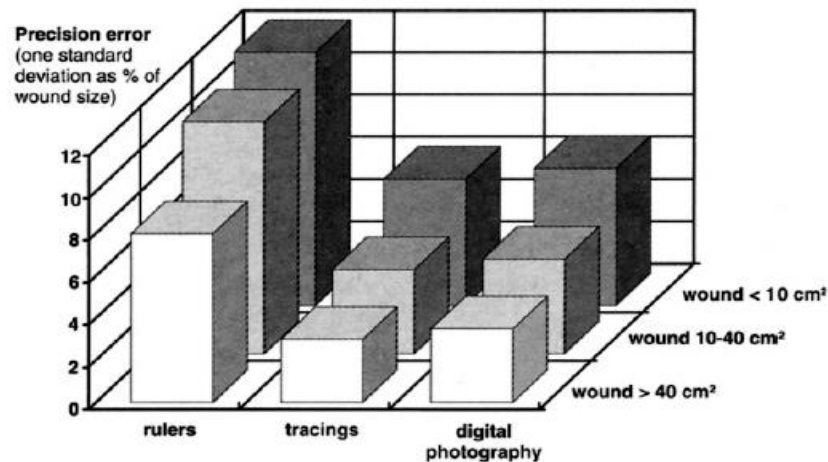


Figure 2.16: Traditional measurement methods and precision error¹¹

2.4.5 Disadvantages of the digital method

This measurement method has some significant drawbacks which consequently impacts on its accuracy (Bianco and Williams, 2002). These include:

1. The outline of the wound border used to calculate the area is subjective, having an involved human intervention (Wysocki, 1996; Plassmann and Jones, 1998; Treuillet, Albouy and Lucas, 2009; Chang, Casas, Castaneda and Treuillet, 2011; Dearman and Greenwood, 2011).
2. The wound border can be obscured (Chang, Dearman and Greenwood, 2011) by a scale, blood, or an associated injury.
3. It can under or overestimate the wound area. To obtain the actual site, size and shape of the wound, the image should be captured from the correct angle (Thali et al., 2003-d; Diane et al., 2006; Casas, Castaneda and Treuillet, 2011; Wendelken et al., 2011; Foltynski et al., 2015). A slight change of the angle can have an influence on the photograph view, resulting in underestimation of the wound area by up to 10%-34.8% (Palmer, Ring and Ledgard, 1989; Rennert et al., 2009; Treuillet, Albouy and Lucas, 2009). The greater the change in the angle, the greater the measurement error (Foltynski et al., 2015).

¹¹ (Plassmann and Peters, 2001).

An improper angle can also have an impact on the scale. The scale can appear larger or smaller according to its position in the photo (below or above the object). If the scale appears smaller, the area has possibly been overestimated (Foltynski et al., 2015).

In reality, acquiring the image from the exact recommended angle is unlikely to be achieved because the camera is hand-held and the injuries could be anywhere on the body (Foltynski et al., 2015).

4. Capturing three-dimensional injuries in two dimensional photographs reduces the injuries to the 2D level (Krouskop, Baker and Wilson, 2002; Thali et al., 2003-a; Casas, Castaneda and Treuillet, 2011; Chang, Dearman and Greenwood, 2011; Malian and Azizi, 2005); therefore, the depth and the volume of the injuries cannot be obtained digitally (Eriksson et al., 1979; Boersma, et al., 2000; Bianco and Williams, 2002; Shetty et al., 2012) and have to be collected manually (Treuillet, Albouy and Lucas, 2009).

5. The plain photograph measurement method does not consider the normal surface curvature of the body and therefore they are biased when the wounds are located on curved surfaces (Palmer, Ring and Ledgard, 1989; Plassmann and Jones, 1998; Little et al., 2009; Treuillet, Albouy and Lucas, 2009; Bianco and Williams, 2002; Casas, Castaneda and Treuillet, 2011).

6. Circumferential wounds are another source of error for this measurement method. These wounds need to be captured by more than one image (Palmer, Ring and Ledgard, 1989; Wysocki, 1996). Even if the wound is fully captured, the measurements will not be accurate as the optical methods neglect the normal surface curvature of the body (Plassmann and Jones, 1998).

7. Researchers consider the digital measurement method as contactless, and so there is no risk of infection (Palmer, Ring and Ledgard, 1989; Krouskop, Baker and Wilson, 2002; Chang, Dearman and Greenwood, 2011; Pavlovic et al., 2015). However, it has an element of direct contact when the scale is placed by the injury. Therefore, neither of the currently applied methods are satisfactory (Bryant et al., 2001; Keast et al., 2004; Fette, 2006). Each method has its advantages and serious disadvantages, and neither measurement method is perfect (Plassmann and Peters, 2001).

Finally, “no measurement method is completely objective, because, at some point, human judgment is involved in acquiring the measurements. There is no absolute measurement, only the best approximation” (Wysocki, 1996, p. 88).

2.5 Conclusion

Within forensic medicine, each wound has important medico-legal significance and, therefore, each wound requires careful examination, documentation and measurements. However, in some cases, the examiner could face some difficulties due to, for example, the healing process or the size of the wound which make its examination a challenging task. Moreover, to date, traumas are commonly documented by digital photography, which is an approved method since the results are clear and in colour, are permanently recorded, and can be saved digitally or used in distance assessment. Ultraviolet, infrared and cross-polarized photography are sometimes used to record unclear or nearly healed traumas. From a negative perspective, the outcomes of this method are flat 2D photographs which reduce 3D wounds to the 2D level. Moreover, it is not just enough to record important forensic issues since the method has serious disadvantages which cannot be ignored, and which can produce errors or doubts ([2.3.3](#)) in the results that are later needed for legal purposes.

The ruler and digital wound measurement methods are the main methods used to record wound dimensions; however, they are subjective methods, involve contact with the wound area, carry the risk of infection, and can lead to over or under-estimation of the actual wound sizes ([2.4.3](#) and [2.4.5](#)).

There are varieties of more precise active and passive non-contact 3D surface scanning methods which could be adapted as methods for wound recording and wound measurements, in combination with conventional methods or used as an alternative. These methods are used in clinical settings to record chronic wounds and to take measurements. When compared to measurements collected through conventional methods, the measurements of these techniques have been found to be accurate and reproducible, particularly measurements based on the structured light technique (Ozturk et al., 1996; Plassmann and Jones, 1998; Shah, Wollak and Shah, 2015). Unfortunately, in the forensic setting, there is a shortfall in the use of these techniques for traumatic wound documentation and measurement. Therefore, Chapter 3 introduces these techniques and their application to forensic medicine.

Chapter 3: Non-contact 3D surface scanning: techniques and their applications in forensic medicine

3.1 Introduction

As explained in Chapter 2, there are some difficult situations related to the wounds that make its interpretation challenging. It was also explained how the current recording and measuring methods could negatively affect the wound documents and measurements. On the other hand, there are 3D surface scanning methods which can be used to address these problems alongside improving the wound interpretation and recording. This is because the 3D outcomes of these methods provide a higher level of accuracy and resolution. Therefore, Chapter 3 reviews the literature surrounding the application of these methods in forensic medicine.

Firstly, the chapter introduces different types of 3D surface scanning methods from a technical viewpoint. Then it explores the applications of these techniques in forensic medicine, with the emphasis placed on forensic injuries. This shows how these applications have developed the field. However, identifying the limitations of each application and the gaps that exist in these applications are also exposed.

3.2 Non-contact 3D surface scanning techniques

Non-contact 3D surface scanning techniques are used to extract 3D models of solid objects by computing the 3D coordinates of the object's surface points without physical contact with it (Geng, 2011). The 3D surface scanning process has two main steps: (1) generation of 3D geometry; and (2) the application of colour-textured information over the geometry (Lane and Harrell, 2008; Al-Khatib, 2010). The 3D optical techniques are conducted by active and passive scanning methods (Sansoni, Trebeschi and Docchio, 2009-b). The active scanning methods emit light, such as laser or white light, whereas the passive scanning methods are photo-based techniques (Sadlo et al., 2005; Abdul-Rani et al., 2011; Kalisperakis et al., 2011; Weinmann et al., 2011; Errickson, Thompson and Rankin, 2014).

Popular methods of passive and active 3D surface scanning (Figure 3.1) including stereo-photogrammetry, photogrammetry, laser triangulation and structured light scanning are presented in this section (3.2).

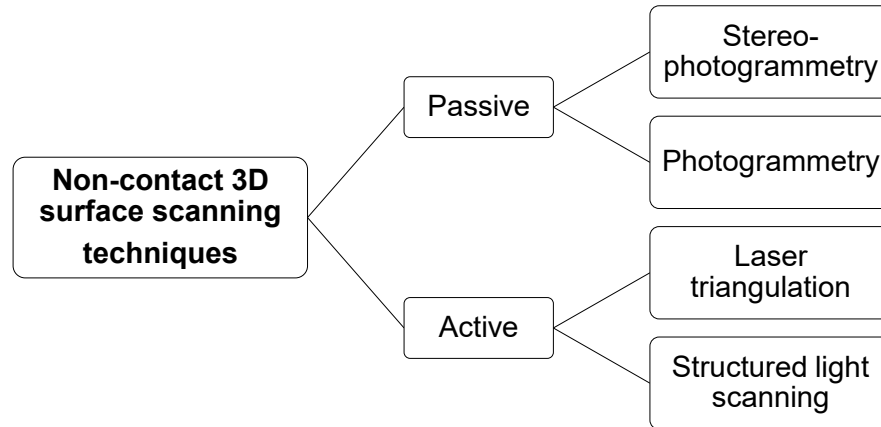


Figure 3.1: 3D surface scanning techniques used in forensic medicine

3.2.1 Stereo-photogrammetry

This is a passive scanning technique based on taking two images of an object using two high-quality calibrated cameras (Figure 3.2). Correspondence between the same points in the two images is obtained by sophisticated stereo triangulation algorithms. The algorithms identify and match unique surface points (features) between the two images, triangulate their 3D position, and generate a point cloud. Once the 3D geometry has been created, the software maps the colour-texture information onto the geometry (Eriksson et al., 1979; Salvi, Pages and Batlle, 2004; Lane and Harrell, 2008; John Tzou et al., 2014). Stereo-photogrammetry is best defined by Adams and Spirakis (1997, p. 17) as being “concerned with obtaining precise three-dimensional (x, y, z) coordinates of common discrete points appearing on a pair of images”.

There are two types of stereo-photogrammetry: passive and active. The passive is based on natural features on the surface of the objects, whereas the active is based on the projection of unstructured light patterns to give the algorithms more information (Lane and Harrell, 2008), and to reduce the correspondence problem (John Tzou et al., 2014). However, the correspondence problem might take place even if the passive projection technique is used (Tehrani, Saghaeian and Mohajerani, 2008), or epipolar geometry¹² is taken into account (Salvi, Pages and Batlle, 2004). Despite recent advances, the technique is still suffering from basic limitations (Lohry, Chen and Zhang, 2014).

¹²The epipolar geometry is reducing the searching area from the whole 2D image plane to 1D line (epipolar line) which means that the corresponding points will be found only on the epipolar line.

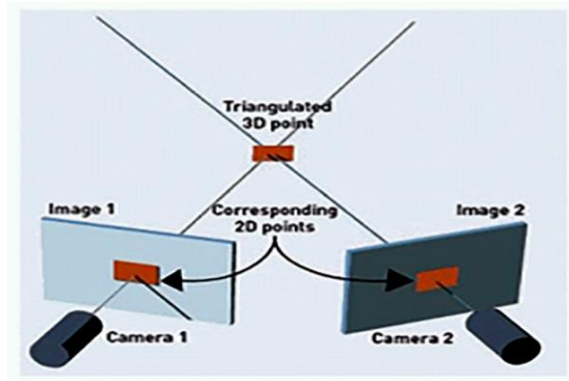


Figure 3.2: Stereo-photogrammetry¹³

3.2.2 Photogrammetry

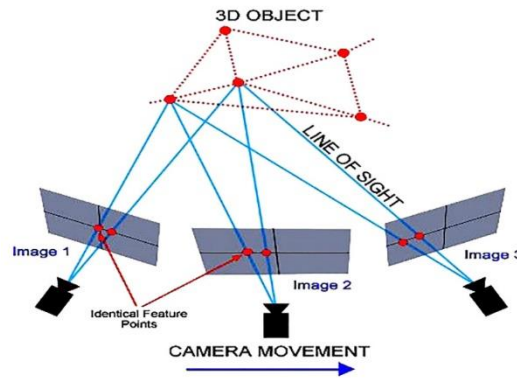
Photogrammetry is a passive scanning technique which relies on a series of overlapping photographs of an object's surface that are captured from different angles by a single calibrated camera under pre-set lighting conditions. Photogrammetry requires only a digital camera and photogrammetric software (Thali et al., 2005; Sansoni, Trebeschi and Docchio, 2009-b; Buck et al., 2013; Slot, Larsen and Lynnerup, 2014). Multiple-camera photogrammetry can also be used (D'Apuzzo and Gruen, 2009; De Sainte Croix et al., 2016; Leipner, 2016).

The software uses sophisticated matching algorithms to determine corresponding points in the different images, forwards rays intersection (Figure 3.3), computes their 3D coordinates and produces a point cloud (D'Apuzzo and Gruen, 2009). In the absence of natural reference points, artificial markers, such as reflective markers (Clemson University, 2018) and pen-markers, are used (Bruschweiler et al, 2003; Thali et al., 2003-c). Alternatively, points of light may be projected onto the surface (Bruschweiler et al., 2003; Thali et al., 2000; Malian and Azizi, 2005). In addition to the reference markers, an established reference distance within the area is also required (Bruschweiler et al., 2003; Buck et al., 2013). In some work, the photogrammetry has been achieved without placing reference marks (Urbanova, Hejna and Jurda, 2015; Leipner, 2016; Villa, 2017-a; Villa et al., 2017-b). This means that some types of matching algorithms do not require these markers.

According to Luhmann et al. (2006), photogrammetry is called so based on:

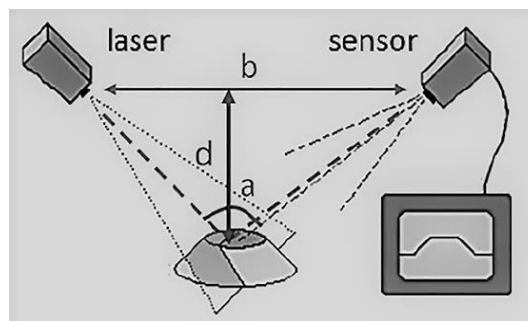
- The camera position and object distance: close-range photogrammetry and macro-photogrammetry.
- The number of images: stereo-photogrammetry.
- The method of recording and processing.

¹³(Solberg et al., 2016).

Figure 3.3: Photogrammetry¹⁴

3.2.3 Laser triangulation 3D surface scanning

This is an active short-range scanning technique based on the projection of a single wavelength laser light (a spot, a single line, or a series of parallel lines) onto an object's surface. The laser line is deformed by the shape of the object and reflected into a sensor (in a specific position). The angle and the distance between the laser source and the sensor are known. The angle of reflection can be calculated from the position of the spot image on the pixels of the sensor; then, the position of the surface point can be detected by using the triangulation principle. Figure 3.4 shows the scheme of the laser triangulation method. The resulting data is a set of points (a point cloud) (Jecic and Drvar, 2003; Lane and Harrel, 2008; Archaeology data service, 2009; D'Apuzzo and Gruen, 2009; Sansoni et al., 2009-a; Malhotra, Gupta and Kant, 2011). In 3D laser scanning, only a safe laser is used (D'Apuzzo and Gruen, 2009). There are another two types of laser scanning, these being time of flight (TOF) and phase shift. They are suitable for scanning larger objects from greater distances (Archaeology data service, 2009; Sansoni et al., 2009-a; Georgopoulos, Ioannidis and Valanis, 2010).

Figure 3.4: Laser triangulation¹⁵

¹⁴ (Clemson University, 2018).

¹⁵ (D'Apuzzo and Gruen, 2009).

3.2.4 Structured light 3D surface scanning

This is an active scanning technique based on projection encoded structured light patterns from a projector onto an object's surface. It is deformed by the shape of the object, while a digital camera captures the images of the object with the deformed light pattern (Figure 3.5 left) (Yalla and Hassebrook, 2005; Wang et al., 2007; Lane and Harrel, 2008; Georgopoulos, Ioannidis and Valanis, 2010; Geng, 2011; Kalisperakis et al., 2011; Akca, 2012; John Tzou et al., 2014; Pandey and Cather, 2016). Sometimes complex scanning systems with multiple cameras and projectors are used (D'Apuzzo and Gruen, 2009). The 3D data is then obtained by analysing the deformation of the captured patterns (deformed patterns) with respect to the projected patterns (Batlle, Mouaddib and Salvi, 1998; Salvi et al., 2010; Buchon-Moragues et al., 2016). This scanning method uses various principles and algorithms (Zhang and Huang, 2006; Geng, 2011).

The structured light technique is used to overcome the correspondence problem of the passive scanning techniques as one of the cameras of the passive method is replaced by the projector that emits the encoded light patterns (Batlle, Mouaddib and Salvi, 1998; Salvi, Pages and Batlle, 2004; Yalla and Hassebrook, 2005; Wang et al., 2007; Salvi et al., 2010; Lohry, Chen and Zhang, 2014). There are different coding strategies of structured light (Salvi, Pages and Batlle, 2004; Sadlo et al., 2005; Salvi et al., 2010; Geng, 2011; Ishii, 2012); this means that the light patterns can be codified in different ways (Buchon-Moragues et al., 2016). The selection of the coding strategy is based on the application, the software and the properties of the scanned object. A binary coding system is most often used (Figure 3.5 right) (D'Apuzzo and Gruen, 2009).

This technique allows accurate and robust acquisition (Sadlo et al., 2005), and is "able to achieve information of very high density and very high accuracy" (Georogopoulos, Ioannidis and Valania, 2010, p. 250). Based on this, it has been widely used in a variety of fields (Yalla and Hassebrook, 2005; Wang et al., 2007; Buchon-Moragues et al., 2016), such as medical applications (Abdul-Rani et al., 2011), culture heritage (Akca, 2012), archaeology (McPherron, Gernat and Hublin, 2009), underwater reconstruction (Bruno et al., 2011), and forensic sciences (Errickson, Thompson and Rankin, 2015; Errickson et al., 2017; Thompson and Norris, 2018).

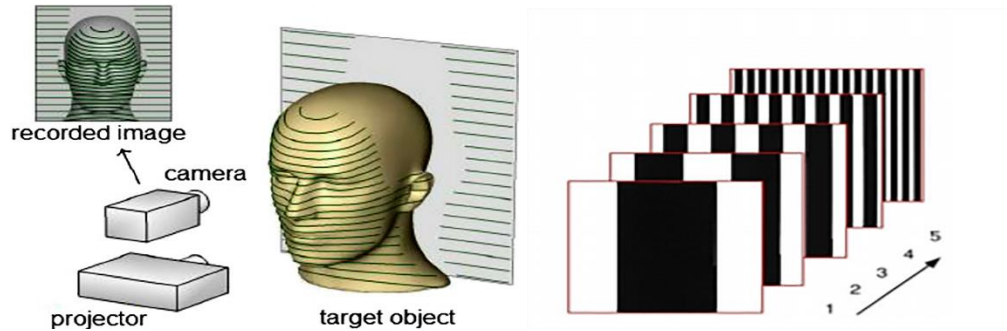


Figure 3.5: Structured light scanning¹⁶ and sequence of binary coding patterns¹⁷

In conclusion, passive and structured light techniques should find the correspondence between the image(s) points before obtaining the 3D data. The passive 3D surface scanning technique matches the same points in two images, or multiple images, whereas in the structured light 3D surface scanning method, one camera is replaced by a light projector to project encoded structured light, and therefore the correspondence is achieved between the projected image and the recorded image with a high level of accuracy. The laser 3D surface scanning method is a little different as it is based on the projection and reflection of an accurately focussed single wavelength, and the depth of the point/ points is calculated by applying the triangulation principle.

Some technical features of each technique are summarised in Table 3.1.

Table 3.1: Some technical features of passive, laser and structured light 3D surface scanning

Feature	Structured light scanner	Laser scanner	Passive scanning
Calibration	Required	Required	Required
Recording technique	Projection of coded structured light	Projection of laser beam	Capturing photographs
Correspondence problem	No correspondence problem	No correspondence problem	Possible problem
Accuracy	Accurate	Accurate	Less accurate
Resolution	Based on the number of projected patterns & camera resolution	Based on the number of collected points	Based on the number of matched points

¹⁶ (Stella, 2017).

¹⁷ (D'Apuzzo and Gruen, 2009).

Scanning time	Fast	Slow	Slow
Reference markers	Based on the scanner type (software)	Not required	Based on matching algorithm
Colour-textured results	Based on the scanner type (software)	Usually textured less 3D results	Textured 3D results
Cost	High	High	Less cost
Safety concerns	Safe	Below class 2M is safe	Safe
Training requirements	Required	Required	Easy to use

3.2.5 Structured light versus laser 3D surface scanning

Although both structured light and laser scanning are active techniques, there are some technical points which differentiate them. Accuracy, resolution, object motion, measurement speed, safety issue, outdoors performance and using reference marks are different technical features for each technique, and all are discussed below.

3.2.5.1 Accuracy

The accuracy of the results is based mostly on the technique. From a researcher's point of view, the scanning results of the structured light scanners have a high level of accuracy because the structured light system projects intricately designed light patterns with a coding strategy; the correspondence between the projected image and the captured image is accurately delineated (Salvi, Pages and Batlle, 2004; Yalla and Hassebrook, 2005; Wang et al., 2007; Salvi et al., 2010; Weinmann et al., 2011; Lohry, Chen and Zhang, 2014). Moreover, the structured light scanning technique uses various principles and algorithms to calculate the 3D coordinates of the object surface points (Zhang and Huang, 2006; Geng, 2011); these algorithms are accurate and robust, such as the Phase Measuring Profilometry (PMP) principle (Wang et al., 2007; Lohry, Chen and Zhang, 2014; Pico Scan user guide). Nevertheless, the results of the laser 3D surface scanning are also accurate. According to Patil, Kothari and Bhurchandi (2015), these results are more accurate than from the structured light technique as a directional laser source, using a single wavelength, is used. Moreover, Sansoni et al. (2009-a) claimed that the accuracy level of the laser 3D surface scanning technology makes it appropriate for measurement applications and quality control in industrial production.

The accuracy of the results is also based on the accuracy of the scanner; each scanner has an accuracy rate according to its application in the market. For example, the accuracy of the ATOS II (structured light scanner) is 0.005 mm (Jecic and Drvar, 2003), and the accuracy of the Konica Minolta (laser scanner) is up to 0.10 mm in TELE mode, short-range configuration (Konica Minolta, 2002).

The calibration process plays an important role in obtaining accurate scanning and accurate results, and both scanners are subject to accurate calibration.

3.2.5.2 Resolution

The resolution of the structured light scanning result is based on the number of projected light patterns (Wang et al., 2007). Better quality results are obtained by the projection of more structured light patterns (Zhang and Huang, 2006). However, the

resolution of the camera should be considered. The laser scanner projects a laser spot or stripe onto the object's surface, then the sensor captures the reflection of the laser as one point or many points. The resolution of the laser scanning result is based on the number of calculated points. The most laser scanners can scan to a rate of 2000 to 500000 points/sec (Corsarca, Jocea and Savu, 2009), whereas the resolution of results from the ATOS II structured light scanning is up to 1.3 million object points (Thali, Braun and Dirnhofer, 2003-a).

The resolution of the results is also based on other factors which could reduce it, such as acquired noise in the data and the properties of the scanned object (Klaas, 2012), in addition to the scan volume (Ebert et al., 2016).

3.2.5.3 Acquisition time and object motion

Slow measurement is the main limitation of the 3D laser scanners (Al-Khatib, 2010; Patil, Kothari and Bhurchandi, 2015). The scanner emits a laser beam to the surface of the scanned object (Figure 3.6 right), moves slowly across the surface, and then reflects it back to a sensor. During this scanning time, most laser scanners require the scanned object to be motionless (Urbanova, Hejna and Jurda, 2015). Therefore, motion, breathing and muscle activity have clear impacts on the laser scanning (Kovacs et al., 2006-a; Corsarca, Jocea and Savu, 2009; Treuillet, Albouy and Lucas, 2009) and could lead to distortion of the collected image points (Corsarca, Jocea and Savu, 2009; Treuillet, Albouy and Lucas, 2009). Because of this natural motion, it is not preferable to scan the human body (Malian and Azizi, 2005; Urbanova, Hejna and Jurda, 2015). In a forensic setting, the 3D laser scanners are superior for use in the following situations:

1. To scan crime scenes: the scanner sends the laser light to the crime scene while rotating with vertical and horizontal angles to cover the entire scene. The light reflected back to the scanner sensor in order to compute the 3D point cloud of the crime scene. They have already been used by police since 2004 for the recording of crime scenes and accidents (Buck et al., 2013).
2. To scan skeletal remains (Sholts et al., 2011), traumas on dead bodies (Sansoni et al., 2009-a) or full-body surface scanning of cadavers (Davy-Jow, Less and Russell, 2013).
3. To scan forensic evidence, such as a dental cast to match with a bite mark (Thali et al., 2003-c), or a suspected weapon to match with a lesion, and find the correspondence between both (Sansoni et al., 2009-a).

Conversely, fast scanning is one of the main advantages of structured light scanners. They can record multiple points or entire views (an entire surface) instead of one point at a time (Figure 3.6 left) and reduce the distortion problem that results from motion (Georgopoulos, Ioannidis and Valanis, 2010; Ishii, 2012). This advantage is a major difference between the laser and structured light scanning techniques (Blais, 2004; D'Apuzzo and Gruen, 2009). Some 3D structured light systems have been developed to scan deformable objects (e.g. facial expressions) in real time (Zhang and Huang, 2006; Patil, Kothari and Bhurchandi, 2015).

However, Leipner et al. (2016) observed that regardless of the type of 3D scanning system, the main challenging factor in recording a living person is the question of movement.

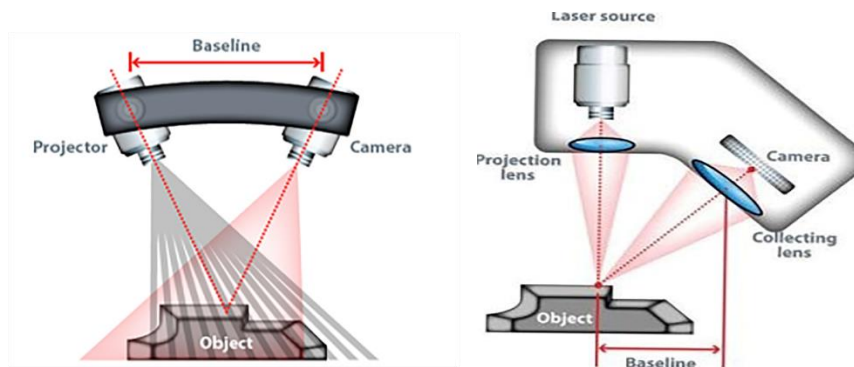


Figure 3.6: Structured light (left) and laser scanning (right)¹⁸

3.2.5.4 Safety issue

There is a concern about the safety of laser scanning (Kovacs et al., 2006-a; Archaeology Data Service, 2009), so much so that there is a need to use protective equipment and take special precautions when operating it (Jones and Rioux, 1997; Al-Khatib, 2010). The safety issue of the laser is caused by its ability to stay in focus, i.e. it is able to focus light energy and intensity onto very small space (Tong, 2011). Laser systems are intended for human scanning are available; however, these systems need to be assessed for Eye-Safe and certified below Class 2M (Tong, 2011). The Konica Minolta VI-910 3D laser scanner has two ISO certifications: ISO 9001 and 14001. It also has an FDA Laser Class 1 certification (Konica Minolta, 2002). For that reason, the Konica Minolta 3D laser scanner is used for facial scanning (Kovacs et al., 2006-a; Sansoni et al., 2009-a). On the other hand, the

¹⁸ (Perreault, 2016).

structured light scanning method has no safety issues (Pastorius, 2015); this advantage makes it an active area of research for the scanning of live subjects.

3.2.5.5 Outdoors Performance

3D laser scanners can be operated efficiently outdoors (Carew and Errickson, 2019) since they are monochromatic, highly directional, more coherent and stay in focus (Bereldin et al., 2000; Patil, Kothari and Bhurchandi, 2015). Moreover, a narrow bandwidth optical filter can be placed in front of the imager (Pastorius, 2015). However, using the filter can cause unreliable scanning (Georgopoulos, Ioannidis and Valanis, 2010). Because the laser scanner performs well outdoors, it can be used to scan cadavers at a crime scene before the handling the body and the disturbance of the corpse's posture (Sansoni et al., 2009-a). However, it should be mentioned that the slit laser scanners that project a laser line (a complete profile of points) are clearly impacted by strong ambient light, even if the optical filter is used. This is because the laser power is spread along the emitted line and the signal to noise ratio is reduced (Blais, 2004). On the other hand, structured light scanning is dramatically affected by the ambient light (Abate et al., 2007; Georgopoulos, Ioannidis and Valanis, 2010) as this is white light, having a visible spectrum. In many situations, the structured light competes with stronger ambient light and, because of the limited range of the camera sensors, the signal intensity of the structured light can be extremely low in the captured images, resulting in poor 3D reconstructed results (Klaas, 2012; Gupta, Yin and Nayar, 2013). Therefore, it is preferable to use such scanners indoors (in a darkroom) (Buck et al., 2018). Then, if there is an element of the light inside the scanning room, it will not be an issue (Tong, 2011; Pastorius, 2015). However, it is better to conduct structured light scanning in controlled lighting conditions (Georgopoulos, Ioannidis and Valanis, 2010).

3.2.5.6 Reference markers

Some structured light scanners, such as the ATOS II structured light 3D scanner, require reference markers because the software uses these markers to define the object coordinate system, and to merge the colour photograph with the 3D geometry of the object (e.g. injury) (Thali, Braun and Dirnhofer, 2003-a). The Pico Scan 3D structured light scanner does not require these reference markers (Shamata and Thompson, 2018-b). Laser scanners also do not require markers on the scanned surface.

3.2.5.7 Colour-textured information

Colour-texture information over a 3D geometry is an important feature regarding 3D injuries imaging. Laser scanning does not usually record any colour-texture information; its 3D results are colourless (Sivanandan and Liscio, 2017). However, the 3D geometry results can be superimposed with a colour photograph (Sansoni et al., 2009-a). However, it should be noted that some 3D laser scanners have two sensors, one sensor to capture the reflected profile and the second sensor to capture the colour-texture (Pavlovic et al., 2015). Structured light 3D surface scanners, such as the ATOS scanners, use a colour photograph or photographs that are captured during photogrammetry or use a photogrammetry TRITOP system for the automatic colour-texture mapping of their 3D surface data (Thali, Braun and Dirnhofer, 2003-a; Thali et al., 2005; Buck et al., 2013; Campana et al., 2016; Ebert et al., 2016; Buck et al., 2018). Other structured light 3D surface scanners, such as the Pico Scan, are able to record the colour information instantaneously during the acquisition process (Shamata and Thompson, 2018-b; Thompson and Norris, 2018).

3.2.5.8 Human skin

Skin should not be an obstruction to structured light scanning as the scanning is based on white light. In comparison, skin colour is potentially problematic for laser scanning. This scanning technique barely digitises dark coloured surfaces as the laser is a monochromatic light, one which is absorbed by dark- coloured surface (Errickson, Thompson, Rankin, 2015), leaving the reflected signal weak (Cosarca, Jocea and Savu, 2009). In addition, the quality of the laser scanning results may be restricted by the reflectivity of the red laser beam on the skin (Treuillet, Albouy, and Lucas, 2009).

3.2.5.9 Cost

Structured light and laser scanners are both expensive; in addition, they require powerful computers, storage space and sometimes an additional software. The cost is the main limitation of these 3D systems (Komar, Davy-Jow and Decker, 2012; Ebert et al., 2016; Buck et al., 2018). However, the valuable benefits of offered by 3D results, such as the accuracy and the resolution, outweigh the cost. Ebert et al. (2016, p. 6) stated that “technological developments may reduce the cost of surface scanning equipment while maintaining a high scanning accuracy”.

Some studies have been focused on generating low-cost 3D systems (Bouguet and Perona, 1998; Rocchini et al., 2001; Winkelbach, Molkenstruck and Wahl, 2006).

However, before introducing evidence to the court which has been generated by non-commercial or homemade 3D scanners, it is necessary to make sure that there is no legal block by using such systems (Komar, Davy-Jow and Decker, 2012).

3.2.5.10 Proper training

Structured light and laser scanners both require proper training as the incorrect use of these scanners can produce artefacts in the 3D results (Komar, Davy-Jow and Decker, 2012; Sivanandan and Liscio, 2017; Buck et al., 2018). Such training need not be long-term; operators just require a good understanding of the calibration process and software settings.

3.3 Applications of non-contact 3D surface scanning techniques

In Section 3.2, the passive and active non-contact 3D surface scanning techniques used in forensic medicine are presented from a technical side. The following review explores the application of these techniques in forensic medicine, with a focus on traumatic injuries. The strengths and weaknesses of each application are also highlighted in order to show the most convenient technique for recording traumatic injuries.

3.3.1 Applications of passive 3D surface scanning

In forensic medicine, passive 3D technology has been applied. Some applications have used forensic 3D/computer-aided design (CAD)-supported photogrammetry to record pattern injuries and match the results with suspected causative instruments. Other studies have used single or multiple camera photogrammetry, or stereo-photogrammetry, to record skin injuries or for full body surface scanning. Some work has been done to merge 3D coloured photogrammetric data of a recorded surface with 3D gray-scale radiological internal data to obtain full body documentation (Thali et al., 2003-b; Villa et al., 2017-b); however, this kind of application is outside the scope of this project and not defined within the chapter.

3.3.1.1 Computer Aided Design (CAD)-supported photogrammetry

Forensic 3D/ computer aided design (CAD)-supported photogrammetry (FPHG) is mainly used to record and match patterned injuries with possible causative tools. It is a combination of photogrammetry and 3D/CAD software. The method requires capturing the injury and the causative tool in two series of photographs using a metric camera. The causative tool can be scanned with a Dr. PICZA 3D scanner if there is a need to increase the point's density. The method also requires two computer programs: (1) the RolleiMetric, multiple image evaluation system, required to produce the 3D models of the injury and the object; and (2) the 3D/CAD software, which uses the 3D models to create graphic true-to-object volume models, and to match them against each other (i.e. the injury and the suspected causative instrument).

Bruschweiler et al. (2003) presented the guidelines of the procedure which some researchers have used to match a patterned bruise with a car tire, a bite mark with a suspected dentation and a skin injury patterned with the muzzle of an air gun (Thali et al., 2000; Thali et al., 2003-c; Thali et al., 2003-d). They found that it is a fast, simple, non-invasive and non-contact method. They also cited that the matching of

the injury with even complex instruments can be achieved in the virtual space. The method has been validated in courts in Switzerland (Thali et al., 2005).

However, it has some drawbacks, as illustrated in the following points:

1. It requires placing reference markers on and around the wound which are used later for object assessment, to make it well-defined by the software. However, using the markers might cause evidence artefact or image occlusion.
2. The resolution of the photogrammetry is relatively low. The technique cannot obtain the same level of detail and accuracy that can be obtained by active 3D surface scanners (Bruschweiler et al., 2003; Casas, Castaneda and Treuillet, 2011; Lohry, Chen and Zhang, 2014). For that reason, the suspected causative instruments could be scanned with the Dr. Picza 3D scanner (Bruschweiler et al., 2003; Thali et al., 2003-c).
3. This technique is suitable only for small objects (Thali et al., 2005).

3.3.1.2 Single camera photogrammetry and stereo-photogrammetry

Both methods have been tested to assess their applicability in forensic medicine (Urbanova, Hejna and Jurda, 2015). The photogrammetry and Vectra H1 hand-held surface scanner (stereo-photogrammetry) (Figure 3.7) were applied to a living person and two post-mortem forensic cases for full-body surface scanning. Also, internal body cavities were assessed during the autopsy. Generally, the procedures were easy to conduct, posing no risk to the living subject. Placing markers around the area of interest was not required. Also, both methods were able to produce colour-textured geometry. However, the methods faced some significant limitations, as illustrated in the following points:



Figure 3.7: Vectra H1 hand-held surface scanner (VH1)¹⁹

¹⁹ (Urbanova, Hejna and Jurda, 2015).

1. Movement of living person, despite trying to maintain the same standing position, in addition to involuntary movements of thoracic and diaphragmatic breathing, lead to the production of a set of images which failed to generate an adequate 3D model.
2. Both methods posed difficulties in scanning areas covered in hair, such as the pubic and axillary areas.
3. The documentation of deep cavities during the autopsy was problematic as the camera could not see or access the cavities; additionally, the surfaces were moist, which caused a gap in the results.
4. The methods demand more time when they document the full surface of the body. Manual alignment of VH1 scans can only be achieved in 10 hrs. Final processing requires a computer with RAM of at least 32 or 64 GB.

Single camera photogrammetry was also applied to record the external injuries from the cadavers. The different types of forensic injuries were recorded, and their 3D wound measurements (linear dimensions) validated by comparing to the manual measurements. However, the researcher encountered some limitations. For example, surfaces covered in hair or areas covered with water was found to require special care; blurred edges of a bruise was not clearly captured; and the positions of some wounds were difficult to access such as axillary areas (Villa, 2017-a).

Buck et al. (2018) compared some results of single camera photogrammetry with results from structured light scanning and found that the geometry of a skin lesion, the face, and the sole of a shoe produced by the photogrammetry were less detailed; however, their results with colour-texture were good. Edwards and Rogers (2018) demonstrated that photogrammetry requires more effort and knowledge to produce high-detailed results, for example, it could require using a high quality digital camera, and optimal lighting condition.

3.3.1.3 Multi-camera photogrammetry

The Botscan multi-camera system of photogrammetry is composed of sixty-four cameras, fixed in a cylindrical chamber (Figure 3.8 left). The system has been used to scan a full live person in the standing position (Leipner et al., 2016). The method does not require placing markers on the body as its software works without references, and it is not affected by movement. According to the authors, this system is better than either single camera photogrammetry or surface scanners as it does not require a longer scanning time. However, the system has some drawbacks (Figure 3.8 right) summarised in the following points:

1. The cameras have been set in the chamber at a limited height (2.5 m), and the cameras on the top are not perfectly located, resulting in unsatisfying results at the top of the final 3D model.
2. It is unable to generate a model with smooth edges in some areas, such as the area between the chest and arm, or the area between the legs.
3. It has been shown that eyeglasses cause artefacts (occlusion) in the final model.
4. It has also been shown that there is variation in mesh quality due to inadequate colour information in pixels, especially if the clothes are too bright or too dark.

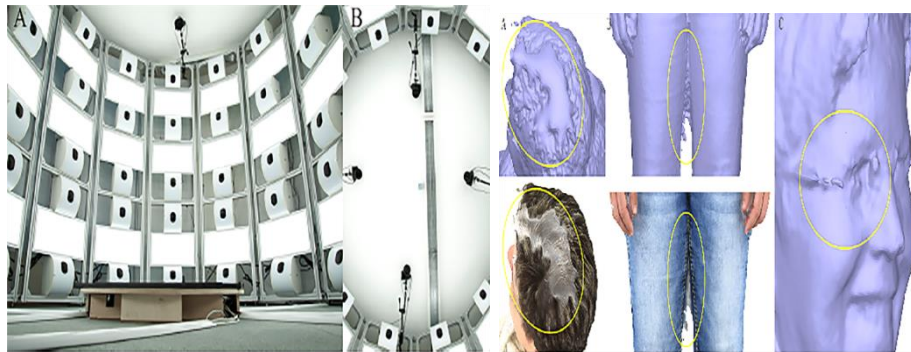


Figure 3.8: Botscan photogrammetry and 3D results with artefacts²⁰

Stereo-photogrammetry (DI3D) is another example of multi-camera photogrammetry; it uses six cameras (Figure 3.9 left). The system has been applied to 10 living volunteers to investigate bite marks on forearms (Figure 3.8 right). Researchers noted that the 3D outcomes of this system had some edge distortion. Also, placing a scale around the area might cause reflection and error. They suggested using more cameras to overcome edge distortion; however, this problem had no great impact on the results since the area of the interest is in the centre of the forearm (De Sainte Croix et al., 2016).

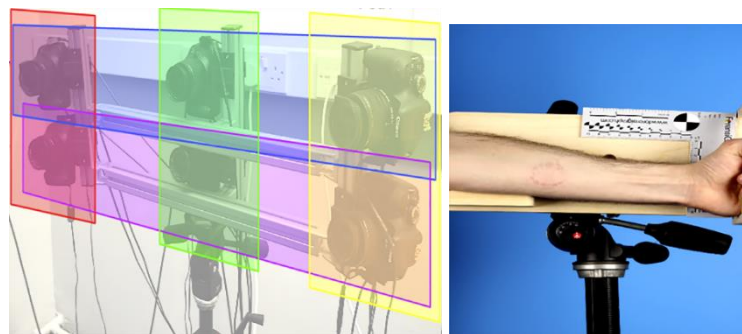


Figure 3.9: DI3D photogrammetry and bite mark investigated by the system²¹

²⁰ (Leipner et al., 2016).

²¹ (De Sainte Croix et al., 2016).

3.3.1.4 Modern multi-camera photogrammetry

The VirtoScan-on-Rail is a movable multi-camera system photogrammetry. It was designed in February 2018 in the autopsy room at Zurich University (Kottner et al., 2019). It has been built to be automated, easy to use and allow forensic examiners who have no experience in 3D technique to use it. The system contains three important units: the linear motion and lifting unit; the image capturing unit; and an operating unit. The image capturing unit is composed of 10 Canon DSLR cameras which are arranged with an arched form (Figure 3.10). The system does not require reference marks on the body, but requires reference scales.

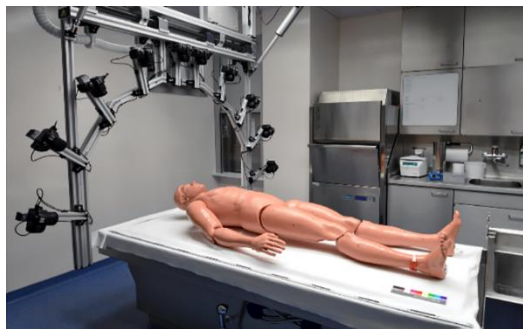


Figure 3.10: VirtoScan-on-Rails²²

It has been used for one side of the body surface scanning of injured cadavers and to scan some organs during autopsy. It was fast method and according to authors, it will be a solution for full-body surface scanning in autopsy rooms. However, the system is still need some improvements, such as

1. Using more professional cameras.
2. Using lenses with auto-focus to improve blurred images caused by the focus issue.
3. Increase the number of the cameras and angles to obtain more detail photographs and to record occluded areas.
4. Using wide angle camera lenses to capture larger bodies.

Finally, all methods of passive scanning can be negatively affected by the environmental light (Leipner et al., 2016). Strong light may cause glare and reduce the number of details (Lane and Harrell, 2008).

²² (Kottner et al., 2019).

3.3.2 Applications of active 3D surface scanning

Active 3D surface scanning includes structured light and laser scanning. Structured light 3D surface scanners, such as Streifenlichttopometrie, have been used in forensic medicine since 1998, in Germany (Subke et al., 2000). The ATOS structured light 3D surface scanner has been used in the Institute of Forensic Medicine, Switzerland, since 2003. Structured light 3D scanners are available as portable scanners that project light patterns or hand-held scanners. Both types of scanners have been used in forensic medicine. Laser scanning has also been applied to scan some injuries on deceased cases within forensic medicine.

3.3.2.1 Structured light patterns 3D surface scanning

The advanced Topometric Sensor structured light scanner (ATOS II) (Figure 3.11) is a fast system with a high level of accuracy and resolution. It has been assessed in a study recording forensic injuries (Thali, Braun and Dirnhofer, 2003-a). Only two smaller injuries were scanned: a small epidermal abrasion with a skin tag and a skull fracture and the suspected instrument. Both injuries were documented in real life size and shaped 3D models. Additionally, the 3D model of the skull fracture was matched against its causative tool in a 3D CAD programme. It should be noted that this scanner needs reference markers on the surface object to define the object coordinate system, and to merge the colour photograph over the 3D geometry.

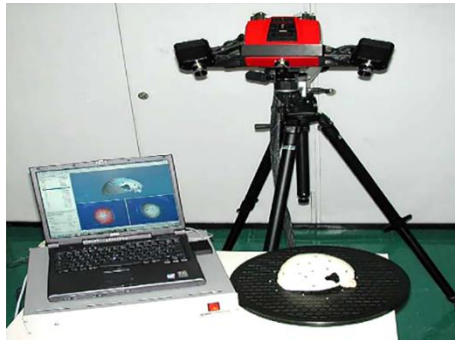


Figure 3.11: ATOS II structured light 3D surface scanner²³

A similar system was used in combination with photogrammetry using a TRITOP software (TRITOP/ATOS II system) to obtain 3D TRITOP/ATOS coloured and high-resolution surface data of a larger object so that a full-body surface or complete vehicle could be documented. Although, it has been used for a larger scale scan, fine details or smaller injuries can also be recorded by this system (Thali et al., 2005; Buck

²³ (Thali, Braun and Dirnhofer, 2003-a).

et al., 2013). This combination technique is necessary for automatic colour-texture mapping of full-body scanning (Buck et al., 2018).

The ATOS Compact Scan 5M structured light scanner is a part of the second version of a Virtobot system (Figure 3.12). It has been used to obtain a complete scan of the surface of deceased bodies (Ebert et al., 2016); however, only 5 % of the submitted cases to the Institute of Forensic Medicine for medico-legal investigation are scanned by this system. The main two issues faced during the surface scanning obtained from this system are (1) the scanner documents only a limited area, and (2) the resolution depended on the scan volume (a larger scan volume reduces the scan resolution). These issues have been resolved by using multiple scans and fusion. Fusing several scans requires distinctive marks used to manoeuvre overlapping scans. Photogrammetry technique is used before the ATOS scanner to calculate the 3D position of the markers; the scanner then relies on the previously established 3D coordinate system. Photographs of the photogrammetry method are also used for the colour texturing of the 3D geometries of the scanned bodies.

An ATOS III Rev. 02 was used in the same work to scan suspected causative instruments and injuries on living subjects. The scanning of the injury was limited to 2-3 scans to avoid the effect of movement. No photogrammetry was required with this scanner; only reference marks were applied, and digital photographs were taken for texturing.

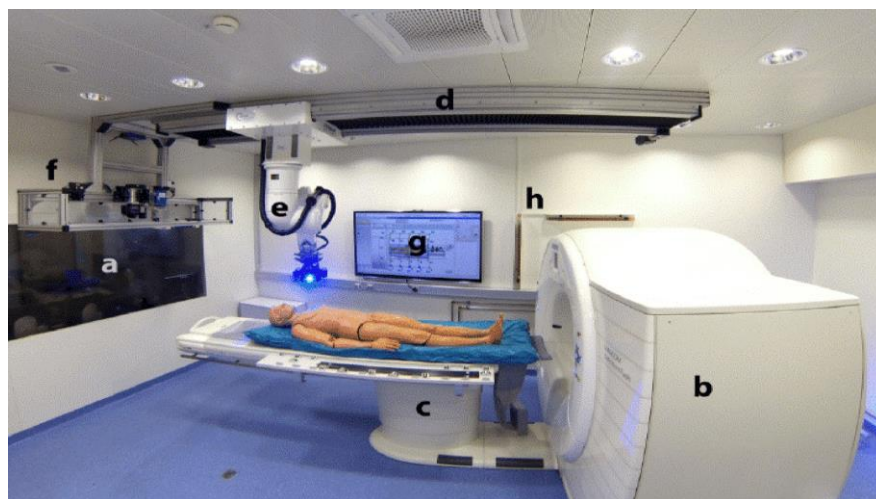


Figure 3.12: Virtobot system
(CT, structured light scanner and digital camera)²⁴

²⁴ (Breitbeck et al., 2013).

Although the ATOS structured light scanning system has been actively used in forensic medicine since 2003, it is a demanding scanner. It needs reference marks to be attached to the body surface; moreover, it requires colour-texture photographs to be applied over its geometric results. According to Urbanova, Hejan and Jurda (2015, p. 78), “ATOS scanners required more controlled conditions while producing high resolution surface data of various volume”, and Villa (2017 a) stated that preparation of the body for scanning by the ATOS is time consuming. Additionally, the initial cost of this scanning system is high (Ebert et al., 2016; Buck et al., 2018).

3.3.2.2 Hand-held structured light 3D surface scanning

The Artec Eva structured light 3D scanner (Figure 3.13) was tested on a live volunteer to scan eleven temporary tattoos having length and width (Sivanandan and Liscio, 2017). In addition, in this study, the Artec Eva successfully scanned a bullet trajectory setup; the resulting 3D data could be examined and manipulated from various angles. There are other aspect of this system to note. It has been shown that (1) the effect of breathing was minimally noted in the 3D models of the living volunteer; (2) a computer with a high processing power is recommended in order to reduce documentation time; and (3) the cost is still the main limitation when considering active 3D surface scanners. The cost of the Artec Eva is about €13,700 (Artec3D, 2018). Furthermore, there is concern about the resolution of the hand-held structured light 3D results (Ebert et al., 2016; Buck et al., 2018), particularly when the Artec Space Spider and CREAFORM GOScan 50 scanner have been compared to structured light patterns scanner (Buck et al., 2018).



Figure 3.13: Artec Eva structured light 3D surface scanner²⁵

²⁵ (Sivanandan and Liscio, 2017).

Table 3.2 below shows the research that have been involved regarding the use of structured light 3D surface scanners in forensic medicine to record traumas or subject full-bodies.

Table 3.2: Using structured light 3D surface scanners in forensic medicine

No.	Title	Authors	Year	Region
1.	Streifenlichttopometric (SLT): A new method for the 3D photorealistic forensic documentation in colour.	Subke et al.	2000	Germany
2.	Optical 3D surface digitizing in forensic medicine: 3D documentation of skin and bone injuries.	Thali et al.	2003	Switzerland
3.	VIRTOPSY- Scientific documentation, reconstruction and animation in forensic: individual and real 3D data based geometric approach including optical body/object surface and radiological CT/MRI scanning.	Thali et al.	2005	Switzerland
4.	Accident or homicide-Virtual crime scene reconstruction using 3D methods	Buck et al.	2013	Switzerland
5.	Virtobot- A robot system for optical 3D scanning in forensic medicine.	Breitbeck et al.	2013	Switzerland
6.	Aspect of 3D surface scanner performance for post-mortem skin documentation in forensic medicine using rigid benchmark objects.	Schweitzer et al.	2013	Switzerland
7.	Forensic 3D surface documentation at institute of forensic medicine in Zurich-workflow and communication pipeline.	Ebert et al.	2016	Switzerland
8.	Assessing Structured Light 3D Scanning using Artec Eva for Injury Documentation during Autopsy.	Sivanandan & Liscio	2017	Canada
9.	Using structured light three-dimensional surface scanning on living individuals: Key considerations and best practice for forensic medicine.	Shamata & Thompson	2018	UK
10.	Documentation and analysis of traumatic injuries in clinical forensic medicine involving structured light three-dimensional surface scanning versus photography	Shamata & Thompson	2018	UK
11.	Validation and evaluation of measuring methods for the 3D documentation of external injuries in the field of forensic medicine	Buck et al.	2018	Germany

As can be seen, the technique is limited to use in some forensic institutes (Campana et al., 2016; Ebert et al., 2016) due to the cost, work load and insufficient research supplies. Therefore, it has not been completely integrated into routine forensic work everywhere (Urbanova, Hejna and Jurda, 2015).

Some of the research displayed above in Table 3.2, such as the research no.3 and research no.4 merged structured light 3D surface scanning with internal documentation. The Gom TRITOP/ATOS II system, Magnetic Resonance Imaging (MRI) and Computed Tomographic (CT) are the systems most used to combine external and internal 3D techniques to attain full 3D data of analysed trauma.

Research no. 9 and research no.10 in Table 3.2 were generated from this thesis.

3.3.2.3 Laser 3D surface scanning

Sansoni et al. (2009-a) employed the Konica Minolta VI-910 3D laser scanner (Figure 3.13 left) to scan three post-mortem findings: abrasions on the thigh, lacerated wounds on the forehead (Figure 3.14 right) and their suspected causative tool (a metallic rod), and several cut marks on the femur. The 3D results were superimposed with the colour-texture information. The 3D matching between the injury and its instrument was achieved. Some analysis of the measurements was conducted around all the reconstructed injuries. It concluded that a 3D wound examination could produce information about the severity, speed and the direction of the attack. It could also help determining whether the instrument was the causative tool or not.

According to Komar, Davy-Jow and Decker (2012), laser 3D surface scanning could be considered for application in post-mortem examination, particularly in those cases that involve patterned injuries, such as bite-marks, ligature marks or tool marks. The method could also be used to scan the surface texture of some organs during the autopsy, such as a cirrhotic liver, since digital photography cannot record such pathology clearly.



Figure 3.14: Konica Minolta 3D laser scanner and model created by the scanner²⁶

²⁶ (Sansoni et al., 2009-a).

3.4 Conclusion

From the reviewed literature in this chapter, it is clear that the use of the 3D surface scanning methods in forensic medicine is currently mostly for research purposes, rather than practical applications, and most of this research focused on introducing the 3D techniques rather than the analysis of 3D results of forensic findings, for example, traumatic wounds.

It is also clear that passive 3D techniques, as well as laser 3D surface scanning, have some limitations that make them unsuitable as the method of choice to scan forensic wounds.

The passive methods cannot obtain the same level of accuracy and point density compared to the active 3D scanners (Bruschweiler et al., 2003; Casas, Castaneda and Treuillet, 2011; Lohry, Chen and Zhang, 2014). Finding the correspondence between the photographs is difficult (Malian and Azizi, 2005; Tehrani, Saghaeian and Mohajerani, 2008). The lighting conditions may have an impact on the photo-matching (Casas, Castaneda and Treuillet, 2011; John Tzou, Artner, Pona, 2014; Kottner et al., 2019). Moreover, the 3D passive technology is affected by motion and the breathing process of living subjects, especially when single camera photogrammetry is used for full-body surface scanning (Slot, Larsen, Lynnerup, 2014; Urbanova, Hejna and Jurda, 2015). Using multiple camera photogrammetry to record the injuries is not practical since it cannot access injuries on certain areas of the body (Leipner et al., 2016; Michienzi et al., 2018). Areas of the body that are covered by hair or that are wet cannot be recorded totally accurately using passive 3D methods (Malian and Azizi, 2005; Urbanova, Hejna and Jurda, 2015; Villa, 2017-a). Despite recent advances, these methods are still suffering from the basic limitations (Lohry, Chen and Zhang, 2014) that have been highlighted before. Therefore, passive 3D scanning is not the perfect choice for the reconstruction of injuries in living and deceased cases. Laser 3D scanners are clearly challenged by the effects of motion (Kovacs et al., 2006-a; Corsarca, Jocea and Savu, 2009; Treuillet, Albouy and Lucas, 2009); they require the objects to be motionless for a longer period of time during scanning. Also, there is a concern about the safety of the laser (Kovacs et al., 2006-a; Archaeology Data Service, 2009) and its effect on the retina (Tong, 2011). Although there are laser systems designed for human scanning, these systems need to be assessed for Eye-Safe and certified below Class 2M (Tong, 2011). Furthermore, laser 3D scanning barely digitises the dark surfaces (Errickson, Thompson and Rankin, 2015) as the light is absorbed by the dark colours.

Structured light 3D surface scanners are actively used in many areas (Yalla and Hassebrook, 2005; Wang et al., 2007; Buchon-Moragues et al., 2016). Their popularity is underlined by rapid image acquisition and the accuracy of the 3D surface geometry. Coded structured light overcomes the correspondence problem of the passive 3D methods (Batlle, Mouaddib and Salvi, 1998; Salvi, Pages and Batlle, 2004; Yalla and Hassebrook, 2005; Wang et al., 2007; Salvi et al., 2010; Lohry, Chen and Zhang, 2014) by giving specific code-words to every point on the object's surface. The coding strategy plays an important role in producing accurate 3D results. In addition, there are a wide variety of coding strategies (Salvi, Pages and Batlle, 2004; Salvi et al., 2010; Geng, 2011). Although all 3D non-contact measurement methods prefer an object to be static, moving objects can be scanned by the structured light technique as it is able to measure almost the entire field of view at once within seconds (Georgopoulos, Ioannidis and Valanis, 2010). Also, structured light methods have no safety issues and are risk-free for live subjects. These advantages (accuracy, high resolution, fast measurement, full-view measurement, safety and availability of a wide variety of patterns) make it a scanner of choice for this research. However, there still remain two concerns. Firstly, it is impacted by the lighting conditions; it cannot be used outdoors (Klaas, 2012; Gupta, Yin and Nayar, 2013). Secondly, there are issues over the cost (Ebert et al., 2016; Buck et al., 2018), but the greater advantages of its 3D results, such as accuracy and high resolution compensate for that.

Table 3.3 summarises some impacting factors on passive and active 3D surface scanning techniques.

Table 3.3: Impacting factors on passive, laser and structured light 3D surface scanning

Impacting factors	Structured light scanner	Laser scanner	Passive scanning
Lighting conditions	Impacted by lighting	Not impacted by lighting	Impacted by lighting
Movements	Impacted by movements	Impacted by movements	Impacted by movements
Breathing	Impacted by breathing	Impacted by breathing	Impacted by breathing
Hairy surface	It can scan fine to moderate hairy surfaces	Impacted by hair
Moist surfaces	It can scan moist surfaces	Impacted by moist areas
Dark (black) skin	It can scan dark skin	It is hardly digitized dark surface	It can record dark skin
Reflective materials	Impacted by reflective materials	Impacted by reflective materials	Impacted by reflective materials

Finally, most of the studies that used structured light scanning are based on the ATOS (Advanced Topometric Sensor) structured light scanner which is an expensive scanner and demanding to use. Additionally, there has been a clear deficiency in the forensic literature review about applying the structured light technique to recording traumas of living persons, and there is no written standard procedure to scan injured live subjects. The same deficiency has been observed in the validation of 3D wound measurements based on this method, particularly depth and surface areas. Moreover, no study has yet compared wound results from 2D digital photography with those using the structured light 3D method.

Chapter 4: Research Methods

4.1 Introduction

According to the literature review in Chapter 3, the common structured light 3D surface scanners that have been used in forensic medicine were the ATOS scanners. For example, the ATOS II; TRITOP/ATOS II; ATOS Compact Scan 5M and ATOS III Rev.02 were used in forensic medicine (Thali, Braun and Dirnhofer, 2003-a; Thali et al., 2003-b; Thali et al., 2005; Elbert et al., 2016; Buck, et al., 2018). They all have dual cameras alongside project structured light patterns-stripes and therefore this means they are accurate scanners and produce high resolution results. However, applying these scanners can be difficult and time-consuming (Urbanova, Hejna and Jurda, 2015; Villa, 2017-a). This is because they require reference marks to be attached to the surface of the body before scanning and the software uses these markers to define the object coordinate system in the particular object ranges. It also uses the markers to merge an additional colour photograph to the geometry of the 3D result (Thali, Braun and Dirnhofer, 2003-a). Some types of ATOS scanners rely on coded reference markers, TRITOP software and photogrammetry to fuse separate scans (Thali et al., 2003-b; Thali et al., 2005; Elbert et al., 2016; Buck, et al., 2018). Moreover, they are expensive scanners costing up to € 50.000 (Elbert et al., 2016; Buck, et al., 2018).

Hand-held structured light scanners have also been used in two researches within forensic medicine; Artec Eva 3D scanner (Sivanandan and Liscio, 2017) and Artec Space Spider and Creaform Go Scan 3D scanner (Buck et al., 2018). They also have high point accuracy and high resolution. However, the geometries of these scanners are less detailed than the geometries of the stripe-light scanners. Additionally, these scanners are also expensive, for example, costing between € 15.000 to 30.000 (Buck, et al., 2018).

Some other structured light scanners are available in the market, such as the EinScan Pro, Pico Scan and HP 3D Scan Pro. According to their manufacturers, they are accurate scanners, and therefore can be used effectively for 3D scanning. The EinScan is a hand-held scanner and is more expensive than the Pico and HP versions. These latter scanners are light pattern-stripe scanners and their costs are affordable. Table 4.1 summarises the main features of both scanners. They are inexpensive, accurate, have high level of resolution and therefore they have been used as core devices in this research to answer the research question, which is: *can*

the structured light 3D surface scanning be used to reconstruct and analyse the different types of traumatic injuries in forensic medicine?

Accordingly, this chapter presents these two structured light 3D surface scanners. It includes the details of the main parts of the scanners, their procedures and post-processing alongside the calibration process of both.

Table 4.1: Pico Scan verses HP structured light 3D scanner

Scanner features	Pico scan scanner	HP scanner
Accuracy	0.1 mm	0.05 mm
Point to point distance	0.16 mm	According to fusion resolution
Type of camera	Canon ESO 1100 D	CAM-4-M full HD camera
Number of cameras	One camera	One camera
Position of camera	Vertically aligned on the projector	On the left side of the projector
Camera resolution	698 x 644 pixels	1920 x1200 pixels
Type of projector	LCD (Pico) Projector	LCD (Acer) projector
Projector resolution	800 x 600 pixels	1280 x 800 pixels
Measuring range (scanned area)	Corresponding to calibration board size (25 x18 cm)	Corresponding to calibration board size (up to 35 cm)
Working range	Around 40 to 50 cm	Around 85 cm
Underlying algorithm	Phase Measuring Profilometry (PMP)	Triangulation algorithm.
Calibration time	Up to 8 min	Around 44 sec
Acquisition time	18-20 sec	15-30 sec
Raw data	3D point Cloud	3D mesh
Software	(1) PicoScan3 software. (2) Mephisto process software.	HP 3D scan software Pro
User-friendly software	Many settings, but easy to use	Few settings, easy to use
Colour-textured data	Captured spontaneous	Captured spontaneous
References markers	Not required	Not required
Outputs file formats	PLY, STL, OBJ, ASCII.	OBJ, STL, PLY.
Computer requirements	32 bit-Windows 4GB RAM Nvidia or ATI graphic card	64 bit-Windows 8 GB system memory 3D graphic card
Easy to learn	Easy	Easy
Portability	Portable	Portable
Cost	£1995.00	£2679.25

4.2 Pico Scan 3D surface scanner

The Pico Scan 3D surface scanner is a structured light scanner, consisting of a Pico LCD projector and a Canon EOS 1100D camera which are vertically aligned and connected to PicoScan3 software to process the acquired information (Figure 4.1).



Figure 4.1: Pico Scan structured light 3D surface scanner

The scanner has been used previously in some forensic work and found to be effective. It has been used to scan footwear impression and human skeletal remains (Errickson, Thompson and Rankin, 2015; Errickson et al., 2017; Thompson and Norris, 2018). It has also been used in non-forensic work (Pandy and Cather, 2016).

4.2.1 The Pico Scan scanning process

The scanning process was conducted to reconstruct the raw 3D data of the interested surface of the body area. It was performed in a dark room; the scale was not required during the scanning. In each scan, the projector emitted encoded structured light patterns toward the interested surface; the light illuminated an area corresponding to the size of the calibration board (25×18 cm). The light deformed by the shape of the surface. Simultaneously, the camera captured 14 images of the illuminated surface, plus one colour-textured mapping image (Figure 4.2). According to Gorthi and Rastogi (2010), this image (the colour-textured image) is an additional image captured by the method without projection of patterns; this is then mapped onto the geometry. It should be noted that the ATOS structured light 3D surface scanners require a separate colour photograph and reference markers attached to the body surface to merge the colour photograph with the geometry (Thali et al., 2003-a), or require photogrammetry using the TRITOP system (Thali et al., 2005; Buck et al., 2013; Campana et al., 2016; Ebert et al., 2016) both of which are time-consuming steps (Urbanova, Hejna and Jurda, 2015; Villa, 2017-a).

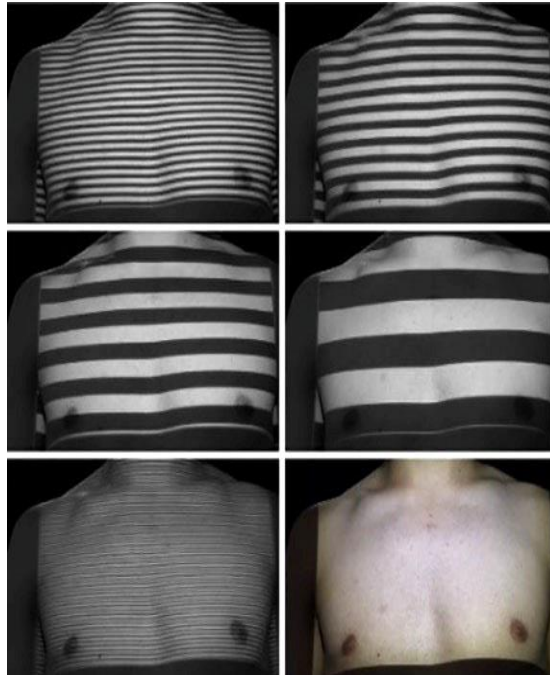


Figure 4.2: Some acquired images with light stripes, plus one coloured image

The output of scanning phase was the raw 3D data (point cloud) which was resulting from processing the 14 images by the PicoScan3 software.

The software had many settings, including processing and reconstruction settings. The appropriate options were selected before scanning. These settings are described later in the section 4.2.3. A Phase Measuring Profilometry (PMP) principle was used by the system to compute the 3D coordinates of the surface points. The strategy of this principle is explained later in the section 4.2.6.1.

The scanning procedure was followed by the post-processing phase to post-process all the raw 3D data and obtain a final 3D model.

4.2.2 Scanner post-processing

All reconstructed raw 3D data were opened in a separate Mephisto process software programme. This was done for the complete processing of all the raw data (Figure 4.3), i.e. the removal of noise from all the data, the integration of all data into the main data, and the alignment and final processing.



Figure 4.3: Post-processing phase using Mephisto process software

The result of the final processing was a 3D model of the scanned surface of the body area (geometry with colour-textured information). The right options were selected from a range of settings before the post-processing. These settings are shown later in the section (4.2.4). Exportation of the final 3D model was done in ‘Ply’ file format. The final 3D model was presented in a wireframe or flat mode in 3D MeshLab software for visualization and assessment. Figure 4.4 shows the overall working scheme of the Pico Scan 3D scanner.

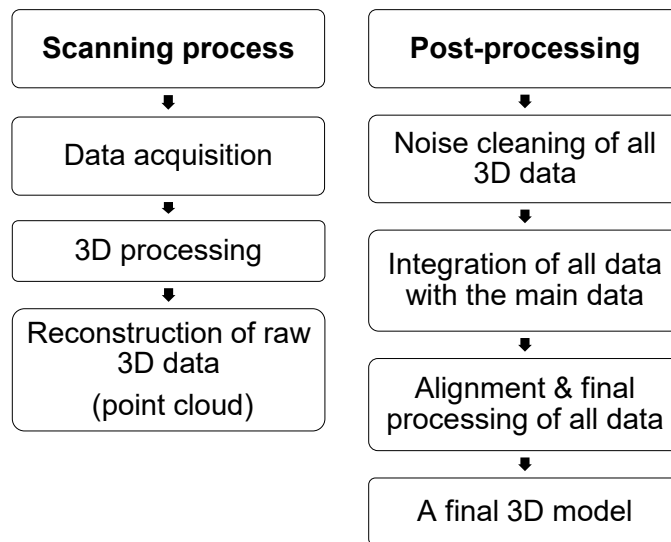


Figure 4.4: Workflow of the Pico Scan 3D scanner.

4.2.3 PicoScan3 software settings

The software comprised of processing settings, reconstruction settings and other settings. Table 4.2 displays all the settings and options that were selected before the scanning process. The options were decided upon following most of them having

been tested. For example, some intensity threshold options (0, 5, 10, 20, 25, 30) were tested while the calibration board was scanned. The results showed that the intensity thresholds of 20 and 25 were excellent because the board was reconstructed clearly, without any background noise. When the intensity threshold was reduced to 10 or less, the board was reconstructed with considerable background noise. However, the background noise formation was also related to the larger opening of the aperture and slower shutter speed. The intensity threshold beyond 25 produced a result (board) with a destroyed border.

Table 4.2: PicoScan3 software settings and selected options

Processing settings		
Settings	Available options	Selected options
Intensity threshold	0-250	0 /10 / 25
Signal strength	0.00-1	0.20
Signal uncertainty	0.00-1	0.80
Smoothing region	0-40	3
Denoise region	0-40	3
Diffusion steps	6
Dilation steps	6
Erosion steps	6
Reconstruction settings		
Subsample step	1
Min. distance	0 mm.	100 mm
Max. distance	700 mm
Invalidate boundaries	...px.	1
Min. vertices/patch		10.000.000
Max. angle deviation	0-180	80
Max. internal angle	0-180	130
Max. aspect ratio	0-30	4
Texture settings		
Brightness	0.01-5	1
RBG ratios
Visualization settings		
Colour mode	High resolution texture.	
Draw mode	Points.	

4.2.4 Mephisto process software settings

The software included some settings about the geometry, colour-texture and smoothing of the final 3D model. Figure 4.5 displays all the settings and selected options. When the low sampling resolution of the shape was selected, the final 3D result was generated with no clear shape (geometry) and details. The number of vertices and faces were low (vertices were 915 points and faces were 1752 triangles). Whereas when the high sampling resolution was selected, the typical resolution of the final 3D model was produced. The vertices of this example were 293167 and the

faces were 586255. The same was observed with the sampling resolution of the texture stitching, and therefore the high sampling resolution was the best selection since it made the colour texture information of the result clear. In terms of the smoothing setting, the low smoothing value produced a 3D model with rough boundaries; for that reason, high smoothing was selected.

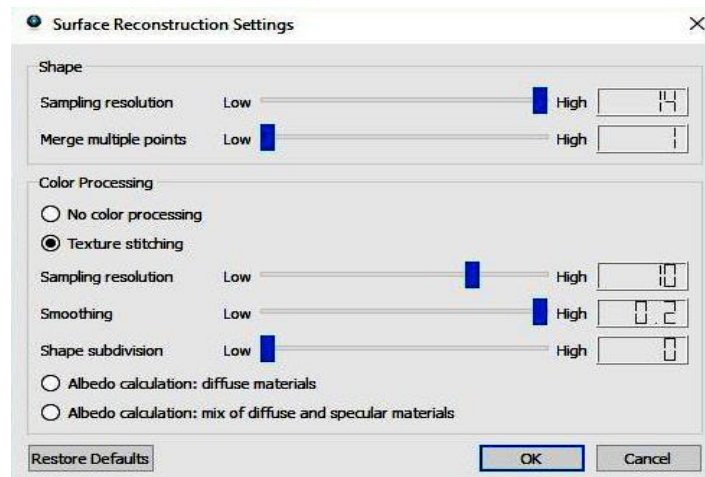


Figure 4.5: Mephisto process software settings and selected options

4.2.5 Geometric calibration

Calibration of the scanning system is the key step to obtaining accurate 3D reconstruction (Chen et al., 2009). The significance of the calibration process increases with structured light 3D scanning. The calibration process in other applications may not be an issue, but in forensic applications it is an important consideration since the methods that are not known error rate will not be accepted in the court-room (Errickson, Thompson and Rankin, 2015). Therefore, the Pico Scan 3D scanning was preceded by geometric calibration to ensure the accuracy of the scanner.

The Pico Scan geometric calibration was intended to estimate the intrinsic and extrinsic information of the camera and projector. This information concerned focal length, lenses distortions of the camera and projector, and the position of the camera and projector relative to each other. The Pico Scan system uses (1) a known structure and size flat calibration board having printed colour checker patterns and (2) a robust calibration algorithm (Pandy and Cather, 2016; Pico Scan user guide). The camera calibration was achieved by detecting the corners of the printed checker patterns in different calibration board positions. Using known constraints, the software defined the 3D positions of the calibration board and estimate the properties and distortion of

the camera lens. The projector calibration was achieved in the same way (Pico Scan user guide).

Therefore, the calibration process was conducted using the standard sized calibration board (21x15 squares of 11 mm²: 25x18 cm) (Figure 4.6). The board was placed in front of the scanner, the focus pattern was projected onto the board and the image of the board filled the camera field of view. The projected pattern and the camera were focused on the same point (the centre of the board). The distance at which the projector and the camera were in focus, being around 470 mm, was maintained. The ISO, aperture and shutter speed were selected. When the calibration began, the projector emitted its own black and white patterns into the board. Eight to ten calibration board images were captured in different positions (Figure 4.7). In each position, the scanner acquired two images: one for the camera and one for the projector. These calibration images were represented as icons with numbers in a spreadsheet, the number indicated the amount of checker corners detected by the system (Figure 4.8) (Pandy and Cather, 2016; Pico Scan user guide). The accuracy of the calibration process was expressed as Root Mean Square (RMS) errors. The RMS errors presented the differences between the estimated position of where the corners should be and the actual observed corners in the images expressed in subpixel values. The results were good as the RMS values of the camera, projector and the system were within 0.2 to 0.5 RMS errors (Pico Scan user guide). If the results had been out of this range, the scanning outcome would have been distorted (Errickson, 2015).



Figure 4.6: Calibration board of the Pico Scan 3D scanner



Figure 4.7: Calibration board recorded in different positions

	System	Projector	Camera
1	<input checked="" type="checkbox"/>	70	142
2	<input checked="" type="checkbox"/>	73	156
3	<input checked="" type="checkbox"/>	67	157
4	<input checked="" type="checkbox"/>	72	186
5	<input checked="" type="checkbox"/>	71	211
6	<input checked="" type="checkbox"/>	71	210

Figure 4.8: Amount of checker corners detected by the scanner

4.2.6 Scanning principle and algorithm

Structured 3D surface scanning uses various principles and algorithms to calculate the 3D coordinates of the object surface points (Zhang and Huang, 2006; Geng, 2011). The Pico scan 3D scanner used Phase Measuring Profilometry (PMP) in addition to the binary coding patterns.

4.2.6.1 Phase Measuring Profilometry (PMP)

This is one of the most robust and precise methods among all the structured light scanning principles (Wang et al., 2007; Lohry, Chen and Zhang, 2014). It is accomplished by using a sine wave pattern with a known frequency. It involves phase

shifted patterns, usually three patterns in number. The 3D geometry of the object distorts these projected patterns for each shift and leads to phase deviation in the patterns observed by the camera. Subsequently, the 3D coordinates of the surface points are computed with sub-pixel accuracy by measuring the phase deviation for each pixel (Pico Scan user guide; Pandey and Cather, 2016).

The Pico Scan 3D scanner uses binary code patterns in combination with the phase shift to resolve the π ambiguity problem of the phase shifting method. The binary code patterns provide a unique code for each pixel in the image to cope with the π ambiguity (Pico Scan user guide). The strategy of binary-coding patterns is explained in Section 4.2.6.2. At this point, the PMP technique can be generally summarised in the following points:

- A sinusoidal pattern is projected onto the object several times.
- The projected pattern is distorted by the object's geometry.
- The sinusoidal signal phase is changed.
- The phase change of each pixel is measured and used to reconstruct the object shape.

The main advantages which make the PMP superior to other techniques are:

1. High 3D measurement accuracy. It allows accurate sub-pixel correspondence between the camera and the projector (Wang et al., 2007; Lohry, Chen and Zhang, 2014; Pico Scan user guide).
2. High spatial resolution results. It can obtain pixel-by-pixel 3D shape measurement (Gorthi and Rastogi, 2010; Lohry, Chen and Zhang, 2014).
3. High-speed 3D measurement. The whole scanned area can be captured and processed at once (Zhang and Huang, 2006; Wang et al., 2007; Lohry, Chen and Zhang, 2014).
4. It is resistant to ambient light effects. It analyses the phase information of the structured light patterns instead of directly utilizing intensity (Lohry, Chen and Zhang, 2014).
5. It has a lower sensitivity to reflective surfaces (Lohry, Chen and Zhang, 2014).
6. It is an adjustable method, can be adapted to scan nearly all types of materials and surfaces (Pico Scan user guide).

4.2.6.2 Binary-coding patterns

In addition to the phase shifting method, the Pico Scan 3D scanner uses additional patterns (binary coding patterns) to resolve the π ambiguity problem of the phase shifting method. The binary code patterns technique is a sequence of binary patterns

of black and white stripes. The stripes are coded as 0 and 1. Zero corresponds to black illumination and 1 corresponds to light illumination. The number of patterns (N) can code 2^N stripes. Every point on the object's surface is identified by a unique sequence of black and white stripes and a unique numbered code word is obtained. The length of the code word is equal to 2^N (Salvi, Pages and Batlle, 2004; Salvi et al., 2010; Geng, 2011). Although this technique provides accurate and reliable results, the maximum resolution cannot be achieved (Salvi, Pages and Batlle, 2004; Zhang and Huang, 2006; Lohry, Chen and Zhang, 2014). However, in combination with the phase shifting method, the maximum resolution is obtained since the phase shifting technique projects the patterns periodically, many times, shifting it each time; thus, the resolution of the measurement is increased (Salvi, Pages and Batlle, 2004). Therefore, in this research, the phase measuring profilometry principle and binary-coding patterns technique were used by the Pico Scan to compute the 3D coordinates of the surface points (point cloud).

4.3 HP 3D surface scanner Pro S3

This is a structured light scanner. It has two main parts: an LCD video projector (Acer K 132) and an HP 3D HD Camera Pro (Figure 4.9), both are connected to the HP 3D scan software Pro V.5.3.0 to process the acquired information. The camera is mounted on the left side of the projector; in this position, the scanner can scan an area of up to 350 mm. The range of the camera angle is from 10-30°. The ideal angle is 22°; however, 20° to 25° are also recommended (3D Printer Superstore, 2015).

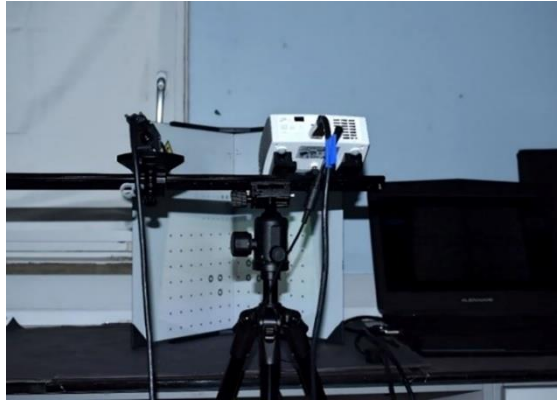


Figure 4.9: HP structured light 3D surface scanner Pro S3

4.3.1 The HP scanner scanning process

The scanning process began with background scanning to remove the background noise from the raw scans. The background data was stored and automatically removed from the actual raw scans (Lievendag, 2017). The manual scan sequence was then selected. Once the scanning was activated, the projector emitted light patterns. The camera then acquired an image with deformed light and the HP 3D scan Pro V. 5.3.0 software processed the acquired information and reconstructed the raw 3D data (in the form of mesh data). Therefore, the output of each scan was the raw 3D mesh data. The 3D algorithm of the system was based on the triangulation geometric principle. The strategy of this principle is explained in 4.3.4. The acquisition speed was based mainly on the selected profile of pattern parameters and the scanning time of each pattern parameter profile. The differences between these profiles were tested and are presented in 4.3.5. The scanning software had some settings with recommended values; these were: smooth average (0), outlier removal (0.1) and quality check (0.5). Other available options were all tested on a static object, and the results confirmed that the recommended values were the best. The scanning was conducted in a dark room; the scale was not required during the scanning. The scanning process was followed by the post-processing of all raw 3D scans to obtain a final 3D model.

4.3.2 HP scanner post-processing

All raw 3D data were post-processed using the same software (HP 3D scan software Pro V.5.3.0 software). The post-processing involved three stages: cleaning, alignment, and the fusion of all the raw 3D scans. Polygon selection cleaning was employed to clean the data. Free alignment was used and followed by global fine registration. Finally, the scans (raw data) were fused. The fusion setting had many resolution and sharpness options, all of which were tried. The resolution options ranged from 250-4000; the higher values took a longer fusion time. Moreover, Edwards and Rogers (2018) stated that (1) crashes of software is experienced when larger data are processed, and (2) retaining larger data may retain more artefacts. The sharpness had positive and negative options (from -3 to +5), the positive values made the noise more noticeable in the result while the negative values made the result smoother. Therefore, the data were mostly fused with resolution 1000; default sharpness; and closed holes 0%. The output was a final 3D model having a geometry and colour-textured information. The exportation was done in OBJ file format. The model was presented in 3D MeshLab and Geomagic Studio 2014 software for visualization and for measuring. Scanning and post-processing of the HP 3D surface scanner Pro S3 are summarised in Figure 4.10 below.

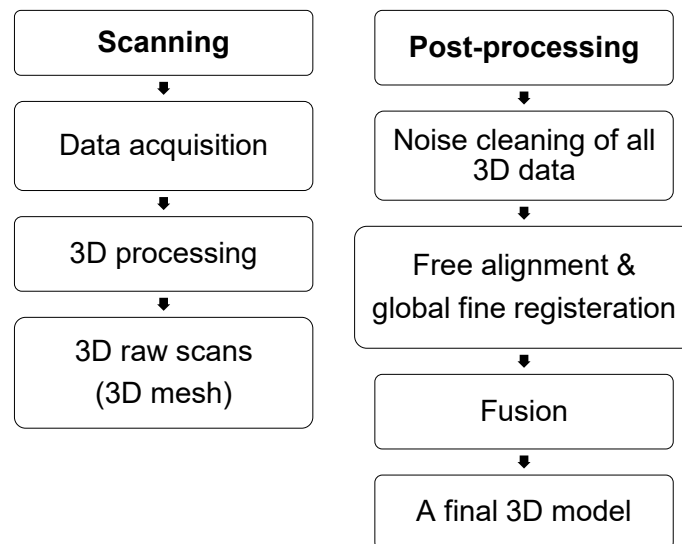


Figure 4.10: Workflow of the HP 3D scanner Pro S3

4.3.3 Calibration process

The scanning was preceded by a calibration process. This was conducted by using an HP 3D calibration panel pro, with a 90-degree corner. It was placed squarely to allow the software to determine the basis, angles, and other calibration parameters, such as the camera and projector parameters (Buchon-Moragues et al., 2016). The

panel had four different calibration pattern scales: 240, 120, 60 and 30 mm. The selected scale needed to be larger than the object. The calibration was conducted by placing the panel in front of the scanner. The projected pattern was set to the selected scale, and six rings and 15 calibration points of the calibration pattern had to be displayed in the camera view. A successful calibration was deemed to have taken place if a checkerboard pattern was projected onto the panel and the square corners of this projected pattern fell exactly onto the points of the calibration pattern (Figure 4.11). During the calibration, the software measured the position, angle, focal length and lens distortion of the camera. Then the software measured the same for the projector. The calibration file can be used many times if the scanner remains unchanged (Buchon-Moragues et al., 2016). It was possible to move, rotate, and tilt the scanner as a whole, but if the camera or the projector were moved separately, this led to the loss of the measured parameters and the calibration had to be repeated. Before calibration, the interested object had to be placed in front of the scanner to complete some important steps:

1. Set the camera angle.
2. Set the basis by moving the camera towards or away from the projector until the camera could see the object. The object was then displayed in the centre of the camera view (the basis is a distance between the projector and camera).
3. Obtain the proper distance between the object and the scanner, which was mainly based on the object size. The distance was kept the same during the calibration and scanning.
4. Focus the projected pattern on the scanned object,
5. Focus the camera lens onto the scanned object.
6. Adjust the aperture while the projector brightness was set to 255 lumens (maximum value).

The shutter speed of the camera was recommended to be 1/60 sec to compensate the frame rate of the projector.

Having completed these steps, the object was removed, and the calibration panel was placed at the same distance as the object had been. The calibration took about 44 seconds, but this time did not include distance measurement, camera adjustment and projector focus.

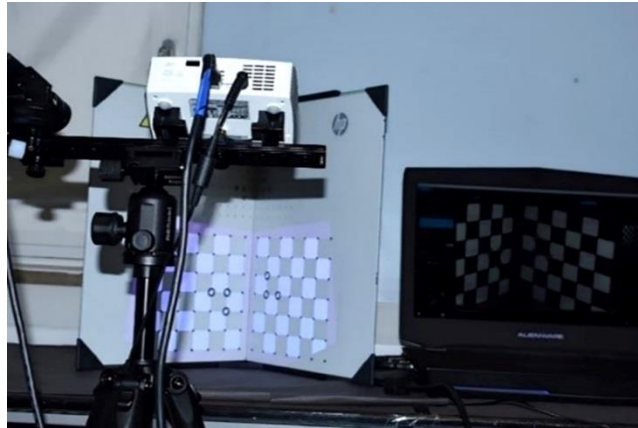


Figure 4.11: Successful calibration

4.3.4 Triangulation algorithm

Structured-light 3D surface scanning extracts the 3D surface geometry of the scanned object from the information obtained from the deformation of the projected patterns (Geng, 2011). The geometric principles of the structured light scanning are based on a projection of the sequences of the binary patterns to the scanned object, and an analysis of the deformation of these reflected patterns (Buchon-Moragues et al., 2016). A projector is used to emit the structured light patterns, and the camera is used to acquire a 2D image of the object with the deformed patterns (Geng, 2011). Figure 5.12 shows the scheme of the structured light scanning (Buchon-Moragues et al., 2016), with the geometric triangulation created between the projected image (projected patterns), the object and the captured image (deformed patterns). In order to measure the deformation, three basics should be determined in the calibration process: the basis, the angle of the camera and projector (α & β), and the coordinates of the centre of the projector and camera. Then the geometric structure is defined using all of these following parameters:

1. The coordinates of the centre of the camera (x_c, y_c, z_c) and projector (x_p, y_p, z_p).
2. The coordinates of the points of the projected and captured (deformed) images (x_{pi}, y_{pi} and x_{ci}, y_{ci})
3. The focal lengths of the camera and projector (f_c, f_p).
4. The rotations for the orientation of the camera ($\kappa_c, \phi_c, \omega_c$) and projector ($\kappa_p, \phi_p, \omega_p$).
5. The terrain coordinates of each point of the measured object (X_i, Y_i, Z_i).

Put simply, (r_i), that is shown in Figure 4.12, is a deformation value which is obtained by a simple comparison between a projected stripe and a deformed stripe (coordinate

differences). This value is called the parallax and represents the depth of each point (Z).

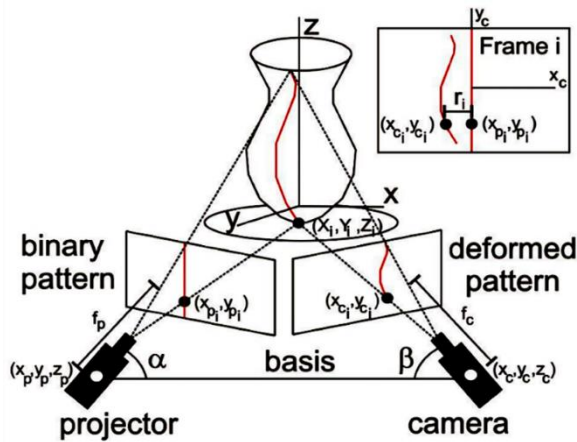


Figure 4.12: Triangulation principle of structured light scanning²⁷

4.3.5 Pattern parameter profiles

The scanners have four profiles: quality (66 patterns), default (35 patterns), speed (25 patterns) and custom (66 patterns). In order to realize the difference between these profiles, the same test object was scanned with the four different profiles. The test object was an anterior view of the palm, which was rested on the scanning table facing the scanner. The calibration pattern scale of 120 mm was used. The view was scanned once in the same position with each profile. Table 4.3 shows the 3D raw scans of each tested profile after cleaning the scans of noise, the number of vertices in the 3D raw scan of each tested profile, all at around 500.000 points. By visual inspection of the 3D raw scans of all the profiles (without colour-texture), there was no noticeable difference. The total number of acquired vertices were almost the same with each profile.

Table 4.3: Vertices and triangles in 3D raw scans using different profiles

Profile	Vertices	Triangles	Vertex spacing
Quality profile	541,648	1,070,410	0.21 mm
Default profile	547,853	1,086,407	0.21 mm
Speed profile	539,553	1,066,986	0.23 mm
Custom profile	533,177	1,050,810	0.21 mm

In addition, the pattern parameters profiles were also tested to measure the scanning time of each profile. The anterior view of different objects with different sizes were

²⁷(Buchon-Moragues et al., 2016).

tested. The objects were scanned while the time was recorded. The results are presented in Table 4.4.

Table 4.4: Scanning time based on selected profile

Pattern parameter profiles	Scanning time
Quality profile	≈30 sec
Default profile	18-19 sec
Speed profile	≈15 sec
Custom profile	≈31 sec

4.4 Conclusion

The Pico Scan and HP 3D scanners are relatively inexpensive 3D scanners in comparison to some structured light 3D scanners used in the literature review, such as the ATOS or Artec Eva 3D scanner. The Pico and HP versions had fast scanning times, between 15 to 20 sec/scan and did not require preparation before scanning, for example, their software did not need reference markers to be placed on the skin. They also did not require extra software to merge an additional colour photograph to their 3D results as the colour-textured information was captured spontaneously during the scanning process. Both scanners were preceded by a geometric calibration process to calculate the intrinsic and extrinsic parametrises of the scanners which were used to reconstruct accurate 3D data. However, reconstruction of the data in the Pico Scan relied on the PMP principle, while the HP needed the 3D triangulation geometry. Both scanners emitted highly designed light patterns with coding strategy that allowed accurate correspondence between the projected image and the captured image, which subsequently allowed accurate 3D reconstruction. Application of both scanners was a controlled process, this is because; (1) the scanning was conducted in a dark room which meant that the scanning was not affected by lighting conditions and the projected structured light was not competing with an ambient light; (2) the exposure values (shutter speed, ISO and brightness) were within the recommended range; and (3) the scanning distance was defined: both scanners utilised similar working and measuring ranges.

Based on the above, it can be said that they are easy to use and applicable scanners for routine work, while also having high levels of resolution and accuracy. Therefore, two affordable structured light 3D surface scanners: the Pico Scan and HP 3D scanner were selected to conduct this research and to answer the research question.

Chapter 5: Using structured light 3D scanning on living individuals: key considerations and best practice for forensic medicine

Although structured light 3D surface scanning is the method of choice to scan living individuals as it is a safe, accurate and fast method, there are no written standard procedures to scan injured areas of living victims. Therefore, this chapter contains preliminary studies that investigate some 3D scanning issues related to the living subjects in order to develop a series of scanning principles. The Pico Scan 3D scanner and the live test subjects were used, and the following concerns were investigated and discussed separately as following:

- 5.1 Appropriate 3D scanning technique to scan different body areas
- 5.2 Optimum number of scans
- 5.3 Elimination of environmental background noise
- 5.4 Scanning approaches to access different body areas

5.1 Appropriate 3D scanning technique to scan different body areas

The technique which can be used to scan a body area was the primary issue. A decision had to be made whether the area will be reconstructed by using 360° scanning (complete scanning over the entire area) or scanning only one surface (surface of interest) in the stationary manner.

In previous studies, the injury is reconstructed by scanning only an injured surface (Figure 5.1) (Thali et al., 2000; Thali, Braun and Dirnhofer, 2003-a; Thali et al., 2003-c; Thali et al., 2003-d; De Sainte et al., 2006; Sansoni et al., 2009-a; Villa, 2017-a). However, to decide the scanning technique in this work, a foot (foot, ankle and lower leg) was scanned in two ways: 360°-scanning and scanning only one surface in the static manner.

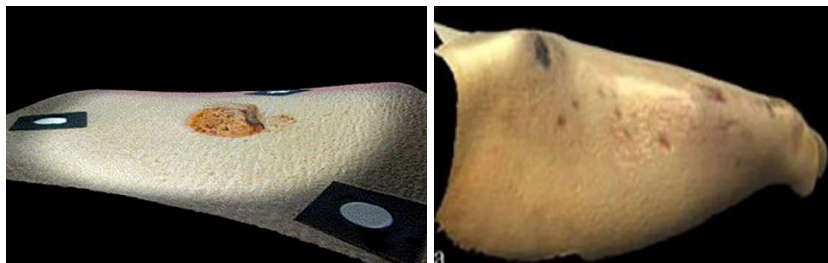


Figure 5.1: 3D models of abrasion resulting from ATOS II (left)²⁸ and Konica Minolta 3D scanner (right)²⁶

²⁸ (Thali, Braun and Dirnhofer 2013-a).

The scanning process in both trials were undertaken with the same experimental conditions and with the same scanner parameters. Fixing the object and moving the scanner around the object is not practical to scan the area of live body. Therefore, 360°-foot scanning was done by asking the volunteer to turn the foot from one view to another in a constant circular manner. The outcome of 360°-foot scanning was multiple raw 3D data which were integrated and post-processed together after noise cleaning. A final 3D model was visualized in the wireframe mode of the MeshLab software however, overlapping shadow impaired the quality of the final 3D image. Whereas scanning only one surface (one view) in the unchangeable manner produced limited data and mitigated the unwanted shadow. The final 3D model was of good quality and provided clear visualization.

The different areas of the upper limb were difficult to be accessed by the scanner when attempting to scan them in the 360°. Therefore, the wrist joint was scanned from at least two different views: anterior and anterolateral surfaces. Also, the area was scanned from one view only in unchangeable manner.

The result generated from scanning only one view (one surface) in the stable manner was free from artefact and had clear visualization (Figure 5.2 left). Whereas, the final 3D model resulting from scanning the anterior and antero-lateral surfaces had poor quality due to the overlapping artefact (Figure 5.2 right).

The poor quality of the final 3D model was explained by physiological means of the muscle activity. Turning from one view to another required muscle contraction and relaxation and this caused change in the muscle contours. Therefore, calculation of 3D coordinates of some previously measured points in the first view will not be in the same 3D position in the new view, this consequently resulting in some points lose their alignment and overlapping shadow (artefact). Conversely, scanning a view in the stable manner produced good results free from artefact.



Figure 5.2: Final 3D model of wrist joint free from artefact (left) and with overlapping artefact (right)

In addition to the muscle activity, there were some other technical issues that affected the scanning process when the complete scanning was attempted, these issues were:

1. Scanning the area in 360°-required prolonged scanning time of approximately 20 minutes. The prolonged time is unwanted as the participant will move and will add extra motion artefact to the results. Minimizing the scanning time is recommended to reduce the artefacts and increase the quality of the results (Kovacs et al., 2006-a; Villa, 2017-a). Moreover, because the method will be applied to the injured participants, it will not be accepted to expose the wounds for extended period.
2. Scanning the area in 360°-generated many raw 3D data, around thirty-four data. These data demanded time for manual noise cleaning, integration and final processing.
3. Combining the different scans required drawing reference markers, during which time it was preferable to avoid touching the subject area.

In light of the above, scanning only one surface (surface of interest) of the body area in the stable manner was recommended as a standard 3D scanning technique since this technique eliminate the negative impact of the muscle activity and provided better image acquisition when compared to the complete 360°scanning technique.

5.2 Optimum number of scans

Because of absence standard number of scans of the interested surface and number of data points in each scan, the optimal number of the scans had to be determined. Ebert et al. (2016) stated that number of the scans per wound is limited to two or three to avoid the negative effect of the motion which make the fusion of the scans difficult. Sansoni et al. (2009-a) cited that three scans are used to obtain forehead lacerated injuries.

To decide how many scans should be obtained by the Pico Scan in this work, the following test was performed. An anterior surface of the wrist joint was scanned with 2, 3, 4, 5 and 6 scans respectively (Table 5.1). The volunteer was able to maintain stability during these scan's number. Presentation of the final 3D models resulting from post-processing of each set of the scans in the wireframe mode in the MeshLab software demonstrated that the results were similar to each other, all provided acceptable looking. However, when the wireframe 3D results inspected more closely on the screen, differences were noticeable between them based on the number of the scans. The wireframe 3D models resulting from post-processing more than three scans remained clear after zooming in, whereas the 3D models resulting from post-processing two or three scans lost their clarity upon closer inspection. This consideration was important since the presentation of forensic evidence in the courtroom usually requires on screen magnification and manipulation to display crucial findings. Therefore, the number of the scans of the relevant view was decided to be more than three scans for wireframe mode presentation.

Flat mode was another mode of presentation in the MeshLab software; however, the flat mode visualization required only two scans.

It is expected that in a practical setting, some raw 3D data of the live subjects will be easily affected by movement and will not be post-processed. This means that some extra raw data should be considered.

Table 5.1: Different number of scans of the same view and total number of vertices in final 3D models

Number of scans	Total number of vertices after alignment	Total number of vertices pots-processing
2 scans	232,281	117,887
3 scans	347,839	288,339
4 scans	463,873	285,231
5 scans	579,295	416,873
6 scans	693,899	435,967

5.3 Elimination of environmental background noise

The minimum and maximum distance were determined in the PicoScan3 software setting before the scanning process. The Pico Scan 3D scanner scanned the object between these distances. However, the camera of the scanner was still able to capture any object in the camera's field of view beyond the maximum distance and generated noise (background noise) with the raw 3D data. This means that the object within this distance was reconstructed by the scanner as raw 3D data and the object beyond the maximum distance was captured by the camera as unwanted data (noise). The formation of the noise was related to the aperture of the camera and the intensity threshold of the light. When the aperture was larger (lower f/stop value) and the intensity threshold of the light was low, the background noise was acquired clearly. Moreover, slow shutter speed was another cause to record the background noise even when the intensity threshold was high. Although the noise could be removed manually before the final post-processing, it was preferable to eliminate or reduce them from outset. This is because the camera sensor had limited range and acquiring noise during the scanning process will reduce the possibility of capturing more relevant data.

It is well known that dark surfaces (black) tend to absorb most of the light while the white surfaces reflect most of the light (Corsarca, Jocea and Savu, 2009). Therefore, a black screen was tested and placed behind the scanned area (behind the volunteer) to eliminate the background noise formation with the acquired data. The anterior aspect of the wrist joint was scanned twice, i.e., with and without the black screen. In each test, the area was scanned five times. The scanning was initiated under the same circumstances and using the same scanner parameters, such as the same calibration process and the same reconstruction and processing settings. The total number of the removed unwanted points (noise) from all five-row 3D data in the first test without using the black screen was 669,397 points. Whereas the total number of the removed unwanted points (noise) in the second test with using the screen was 120,654 points (Figure 5.3). The eliminated noise was the background noise, the remaining noise (120,654 points) was other noise. The wanted area was rested on a stand; therefore, it was extremely difficult to scan the wanted view without scanning the platform. So that, few remaining noise were generated from the stand and removed manually.

Therefore, using the black screen was strongly recommended during the scanning process to eliminate the background noise formation and preserve the acquired (raw)

data, and this result was similar to a previous publication in the literature review (Errickson, Thompson and Rankin, 2015).

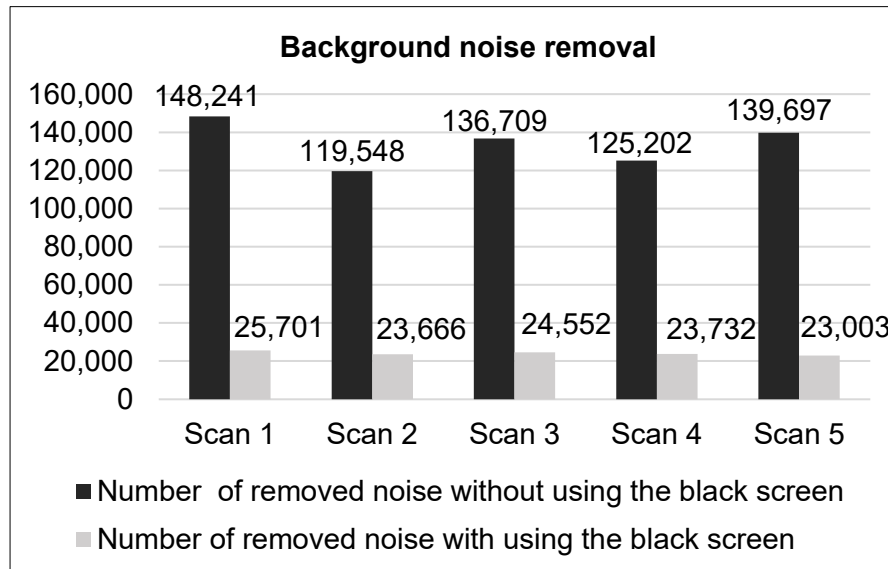


Figure 5.3: Using black screen to remove unwanted points (noise)

Before using the black screen to eliminate the background noise, the white screen and no screen were compared to the black screen. A calibration board was scanned three times (without scree, with white screen as well as with black screen) under the same circumstances. Table 5.2 display the differences between using these screens. It was obvious that using the black screen was appreciated in the background noise elimination.

Table 5.2: Testing different screen colours for noise removal

Scanning of calibration board	No. of vertices	No. of vertices after noise cleaning	Removed noise
Without screen	319,328	242,851	76,477
With white screen.	387,951	242,828	145,123
With black screen	242,813	242,661	152

5.4 Scanning approaches to access different body areas

The active 3D surface scanners are originally designed to scan static industrial objects (Thali, Braun and Dirnhofer, 2003-a; Kovacs et al., 2006-a; Kovacs et al., 2006-b; John Tzou, Artner and Pona, 2014; Ebert et al., 2015); therefore, to enable the scanner access the different areas of the body, three different approaches were suggested and aimed to make the area 1) easily accessible and 2) facing the scanner in the parallel way. During these approaches, participants were aware to maintain the same position.

Scanning approach no.1

It was proposed to access the different areas of the upper limb. The Pico Scan system was fixed on the tripod at height about 110 cm, the volunteers were in the standing position. The wanted surface of the area was rested on the ordinary stand matching the height of the scanner and faced the scanner.

Scanning approach no.2

It was proposed to access the different areas of the lower limb (foot, ankle and lower 2/3 of the leg). The Pico Scan system was fixed on the tripod at a height about 22 cm, the volunteers were in the standing position. The wanted surface of the area was faced the scanner. The upper third of the leg, knee joint and lower third of the thigh were accessed by facing the scanner while the tripod at height about 55 cm.

Scanning approach no.3

It was proposed to access the torso areas. The Pico Scan system and the volunteers were in the same condition of the approach no.1. The area (the chest or abdomen) was faced the scanner, then the scanner level was adjusted to the chest or abdominal level.

5.5 Conclusion

This work analysed the main 3D scanning issues using live test subjects and the Pico Scan structured light 3D scanner to set up some scanning principles. The guidelines were concluded based on the results illustrated above. These guidelines were summarised as following:

1. Scanning an interested surface of the body area in the stationary manner was more efficient when compared to the complete 360°-scanning. This is because the particular surface scanning technique eliminated the negative impact of the muscle activity and provided better image acquisition; therefore, it was used as a standard 3D scanning technique to scan intact and injured surfaces of different areas of the living subjects in Chapters 6 and 7.
2. More than three scans were ideal to obtain optimum wireframe mode representation of the wanted view.
3. Placing the black screen behind the scanned area (participant) was highly recommended to eliminate the background noise formation and preserve the acquired 3D data.
4. Three simple approaches were suggested to access the different body areas.

Chapter 6: Structured light 3D surface scanning of intact living body areas: three studies

Active 3D surface scanning methods were originally designed for industrial applications (Kovacs et al., 2006-a; Kovacs et al., 2006-b; Elbert et al., 2016), such as the aerospace (John Tzou, Artner and Pona, 2014), the automobile industry (Thali, Braun, and Dirnhofer, 2003-a) and reverse engineering (Salvi, Pages and Battle, 2004). This means that the technique should be investigated first on the human bodies, which are completely different from industrial static objects (Kovacs et al., 2006-b). Therefore, it was applied to living subjects without traumas to assess the overall method towards the human body and to achieve the first objective of the research, which is: *to evaluate the ability of structured light 3D surface scanning for recording different intact uninjured body areas of living subjects in order to consider the overall feasibility of the method on the human body.*

The assessment was done by scanning (1) different intact areas of upper limb, lower limb, torso, and challenging surfaces, (2) some complicated anatomical areas, and (3) facial scanning. Figure 6.1 shows different intact body areas that have been scanned and assessed using structured light 3D surface scanning.

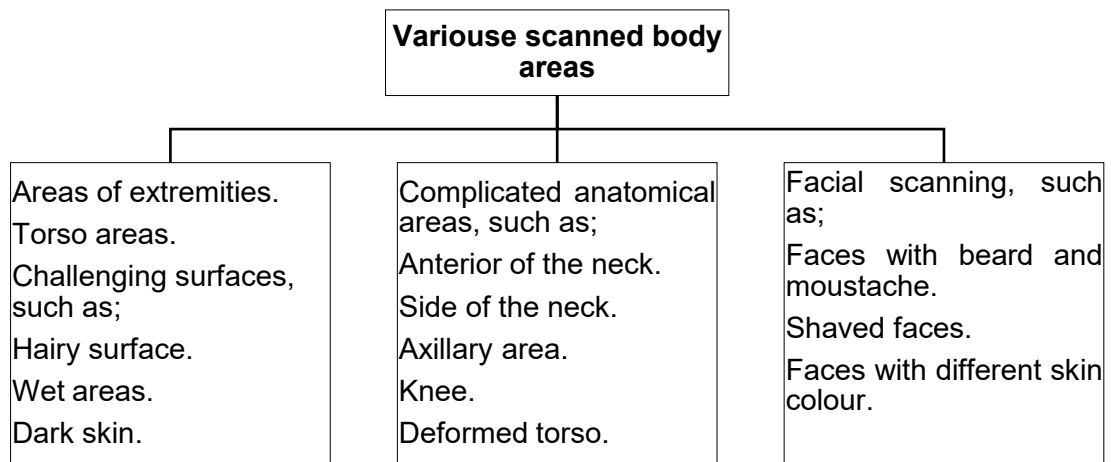


Figure 6.1: Assessed different intact body areas

The results of these areas were evaluated visually by using some suggested criteria. If the raw 3D data fulfilled these, then the data was accepted and underwent post-processing to generate the final 3D model. These criteria are:

1. The reconstructed raw 3D data are more suitable when they are free from noise (environmental background noise).
2. The reconstructed raw 3D data should be free from distorted points which had been generated from the scanned area and caused by motion.
3. The reconstructed raw 3D data should be free from any type of artefact.
4. The vertices of the reconstructed raw 3D data should be manipulated as a single cohesive entity in the Mephisto process software.
5. All reconstructed raw 3D data should have the same level of emitted light.
6. The reconstructed data are better when they have evident colour-textured information.

Therefore, the chapter covers the following three studies and each study has methodology, results, discussion, and conclusion:

- 6.1 3D surface scanning of upper and lower limbs and torso areas, and challenging surfaces
- 6.2 3D surface scanning of complicated anatomical areas
- 6.3 3D facial scanning

6.1 3D surface scanning of upper and lower limbs and torso areas

This application was achieved in two main categories: (1) scanning different bare areas of the upper limb, lower limb, and torso. (2) Scanning more challenging body surfaces, such as dark skin, hairy and moist surfaces.

6.1.1 Materials and Method

6.1.1.1 Ethical considerations

Ethical approval was obtained from Teesside University Research Ethics Committee. A participant information sheet was prepared and approved, that had information about the work, scanning procedure, the possible risk, confidentiality, and right of withdrawal.

6.1.1.2 Work place

The work was done in the M8.03 Laboratory at Teesside University. The laboratory was prepared to be suitable for 3D surface scanning.

6.1.1.3 Volunteers

Participants were students and staff at Teesside University with different nationalities. The volunteers read the participant information sheet and received a brief verbal demonstration about the process. Informed consent was obtained from all participants, then the subject chose an area of the body to be scanned. Removal of jewellery, watches, and clothing that covered the desired area was required before scanning. During the scanning, the participants were required to remain motionless.

6.1.1.4 Method

The Pico scan, structured light, 3D surface scanner was used. A full description of this scanner and its scanning process is demonstrated in [4.2](#). The 3D scanning principles that suggested in [5.5](#) were followed in this work. Therefore, scanning an interested surface of the body area in the stationary manner was used as a standard technique and > 3 scans were taken. A black screen was placed behind the volunteer to eliminate the background noise and preserve the acquired data. Three different suggested approaches were followed to access different areas of the body. Any source of light was eliminated to keep only the scanner light. When the scanning completed, the data were anonymised and stored on a password-protected university computer.

6.1.1.5 Application of the method

Pico Scan 3D surface scanning was applied to scan the body in two main forms:

6.1.1.5.1 Scanning different bare areas of upper limb, lower limb and torso

Different bare areas of upper limb, lower limb, and torso were scanned. The three different approaches suggested in [5.4](#) were followed to allow the scanner access to these areas. Scanning approach no. 1 and no. 2 were followed to access the different areas of the upper and lower limb, whereas scanning approach no. 3 was followed to access the torso. The 3D scanning results of each area were assessed visually. Table 6.1 shows the scanning position of the different areas of the upper limb and the number of testing, whereas Table 6.2 shows the scanning position of the different areas of the lower limb and the number of testing.

Table 6.1: Position of upper limb areas during scanning

Interested area	Position of the area to easily illuminated by the light and acquired by the camera	No. of test
Hand (Palm and dorsum)	Facing the camera & the projector	5 times
Wrist joint (anterior and posterior surface)	Facing the camera & the projector	13 times
Forearm (anterior and posterior surface)	Facing the camera & the projector	14 times
Elbow joint (anterior surface)	In the extension position, and facing the camera & the projector	4 times
Elbow joint (posterior)	In the flexion position (90-degree), or in extension position, and facing the camera & the projector	7 times
Arm (medial & lateral aspect)	In the flexion position (90-degree), and facing the camera & the projector	8 times

Table 6.2: Position of lower limb areas during scanning

Interested area	Position of the area to easily illuminated by the light and acquired by the camera	No. of test
Anterior surface of the foot, and anterior aspect of the ankle joint	Facing the camera & the projector	6 times
Lateral surface of the foot, lateral aspect of the ankle joint and lower $\frac{2}{3}$ of the leg	Facing the camera & the projector	11 times
Medial surface of the foot, medial aspect of ankle joint and lower $\frac{2}{3}$ of the leg	Facing the camera & the projector	3 times

6.1.1.5.2 Scanning more challenging body surfaces

Hairy skin; wet or moist surfaces; dark coloured skin; and highly reflective personal items or shiny jewellery are known to be difficult surfaces that are not easy to scan by passive and active scanning methods. These issues were tested by the Pico Scan 3D scanner. The hairy skin areas were tested by scanning hairy posterior aspect of forearms. Wet palm with water and wet a researcher wrist with her own blood were tried. Black coloured skins, areas with shiny jewellery and areas with tattoo were assessed. Table 6.3 shows the scanned surfaces and number of testing.

Table 6.3: Scanned some challenging body surfaces

Area	No. of test
Hairy skin	5 times
Wet surface	3 times
Dark (black) skin	3 times
Areas with jewellery	2 times
Areas with tattoo	2 times

6.1.2 Results

The scanning outcome of each area was a 3D model. The model had geometry and acceptable colour-textured information. Each model resulted from post-processing about six raw 3D data and the model exported and saved in a Ply file. The models had various numbers of vertices and faces and different size of Ply files, which based on anatomical details and the size of the scanned area. The 3D models were visualized in wireframe mode in the MeshLab software.

N.B. All following figures of final 3D models were snapped from wireframe mode in the MeshLab software, whereas the figures of raw 3D data were snapped from the Mephisto process software.

6.1.2.1 Different bare areas of the upper limb

The scanning process of the different areas of the upper limb was achieved without limitations. The raw 3D data sets of the different areas of the upper limb fulfilled the scanning criteria; thus, the 3D data sets of various areas underwent post-processing to obtain the final 3D models (Figure 6.2). The good scanning achievement of these areas was due to good stabilisation and full illumination of the upper limb areas.



Figure 6.2: Final 3D models of forearm

6.1.2.2 Different bare areas of the lower limb

Scanning the different areas of the lower limb was also well-achieved other than the anterior surface of the foot. The scanning result of this area showed blurry visualisation of the toes area in the 3D MeshLab software (Figure 6.3 left). The scanning process was repeated many times and the results were the same. However, the scanning results of medial and lateral surfaces of the foot had acceptable visualisation (Figure 6.3 right).

Moreover, the final scanning result of the anterior surface of the knee joint of one in four of the volunteers showed unrecorded area antero-medially in the 3D MeshLab presentation, indicated with arrows in Figure 6.4. This area represents a concaved area between the convexity of the knee joint and the upper part of the leg. It was re-scanned with some turning to illuminate it with more light and to acquire it without a hole in the scanned image.

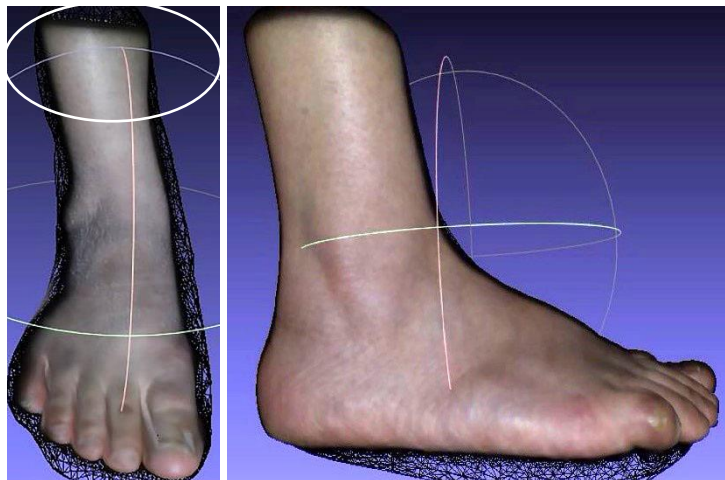


Figure 6.3: Final 3D model of foot shows blurred toes area (left) and clear lateral surface of the foot (right)

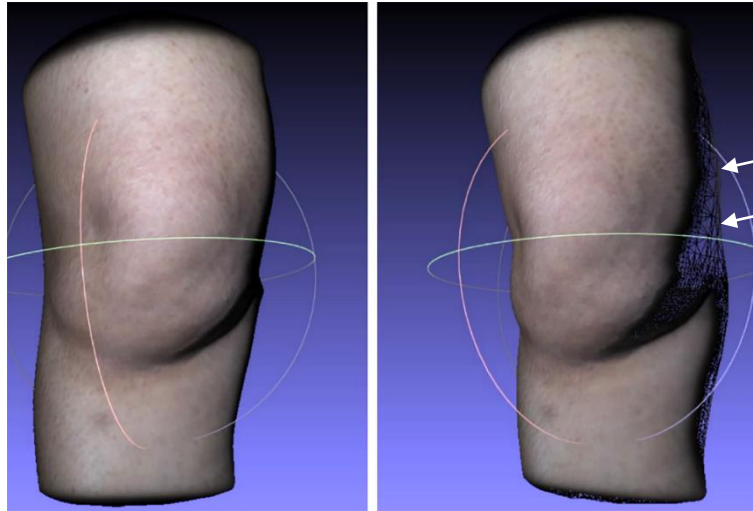


Figure 6.4: Final 3D model of knee joint (left), the model manipulated on the screen to show unrecorded area (right)

6.1.2.3 Torso areas

Torso scanning was not achieved properly. The raw 3D data sets did not fulfil the scanning criteria. The data had two types of torso artefacts: (1) multiple fine horizontal lines (lines had no data) and (2) distorted points. Chest scanning was repeated eight times with four different volunteers, and all data sets had the same types of torso artefacts. Figure 6.5 displays the torso artefacts in one volunteer.

N.B. Torso scanning was done while the volunteers were in a standing position and holding their breath was not requested.

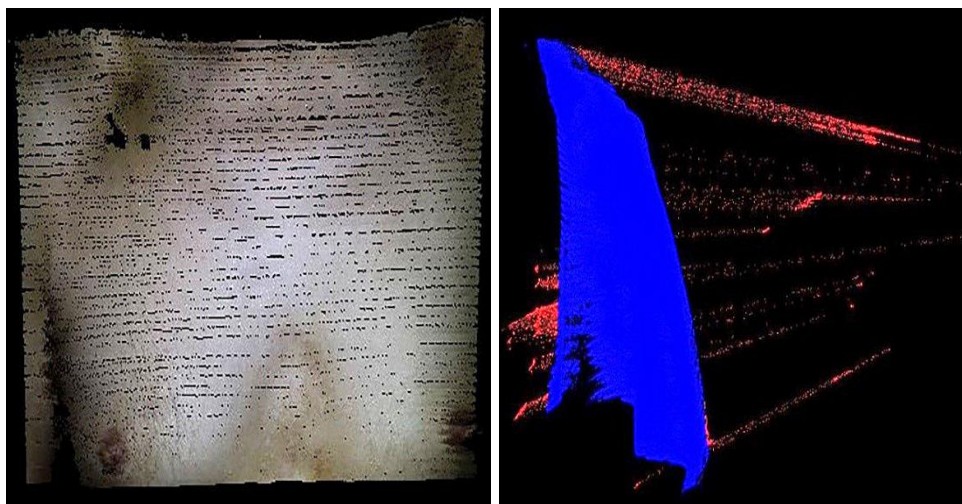


Figure 6.5: 3D raw data of chest with horizontal lines artefact (left), the data manipulated to show distorted points highlighted in red colour (right)

The shutter speed recommended by the Pico Scan user guide to be within 0'6 – 1/10 of a second. However, a chest was tested twice, once with the shutter speed within

the recommended range ($1/6$), and another with a speed of $1/13$ to capture the chest more quickly and reduce artefacts formation. Results showed that with using faster speed, the artefacts were reduced, (Figure 6.6 and Figure 6.7), but data were darker.

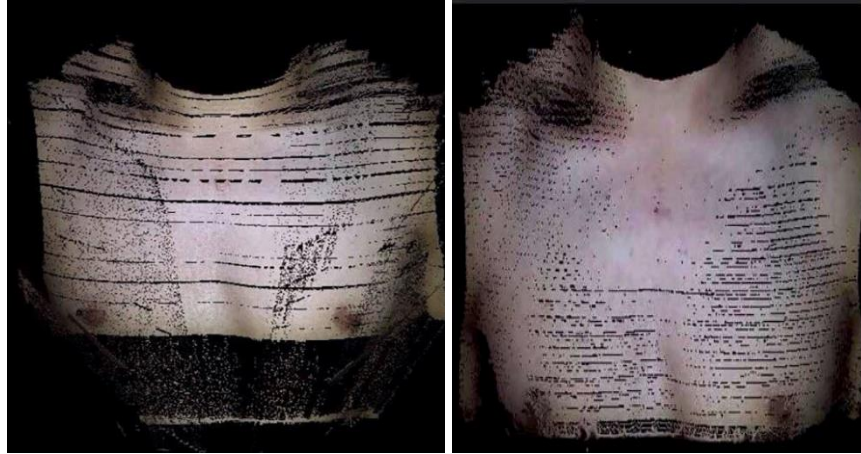


Figure 6.6: The same data reconstructed with two different shutter speeds: $1/6$ sec (left) and $1/13$ sec (right)

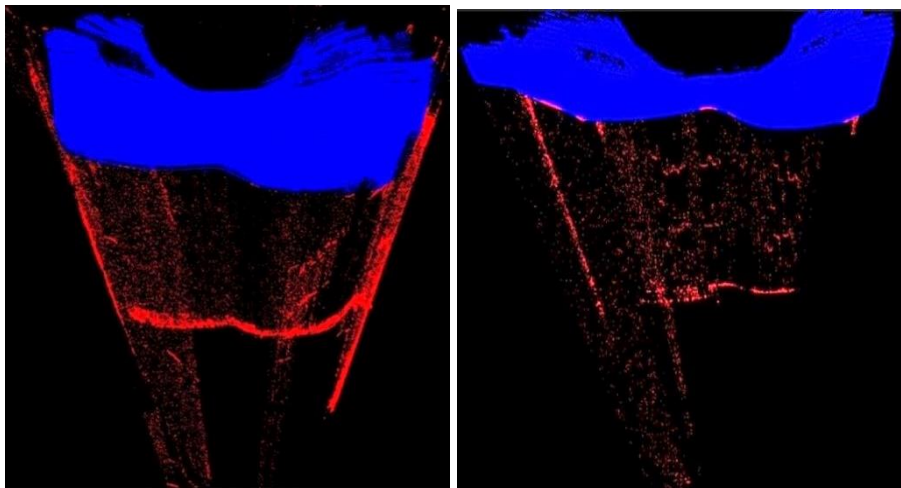


Figure 6.7: The same data in Figure 6.6 shows distorted points highlighted in red colour

In addition, another chest scanning was conducted to acquire the chest along with right and left shoulder. The volunteer was asked to keep as quite as possible, the chest scan was acquired, and then the volunteer moved twice, one step to the right side to expose the left shoulder to the scanner, and the same was done to the right shoulder. The final 3D model resulting from post-processing of all 3D sets (Figure 6.8) had overlapping artefacts between the chest, and right and left shoulder (Figure 6.9). The same test repeated with moving the scanner to the right and left shoulders rather than moving the volunteer. This way, it was possible to integrate and post-process

the 3D data sets of the chest with the right and left shoulder sets without overlapping artefacts. The final 3D model had an acceptable presentation (Figure 6.10).

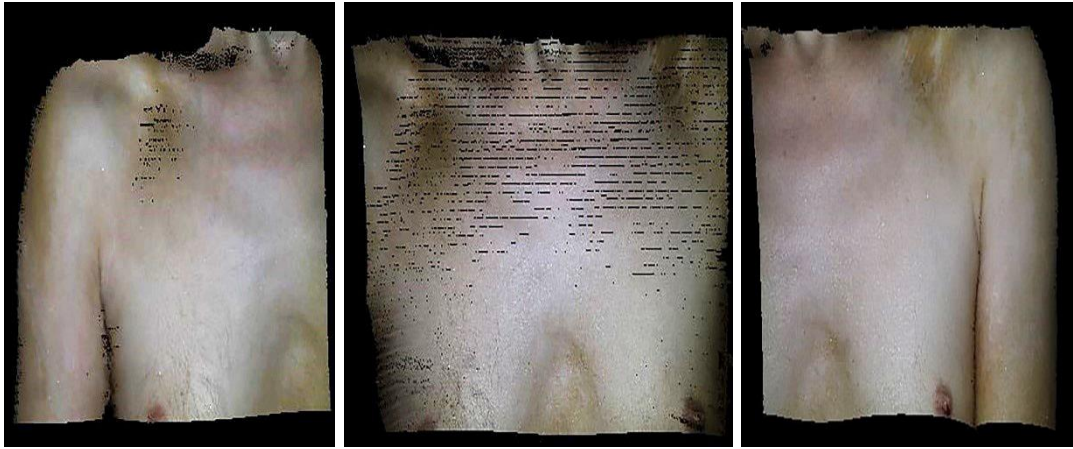


Figure 6.8: 3D raw data of chest with right and left shoulder

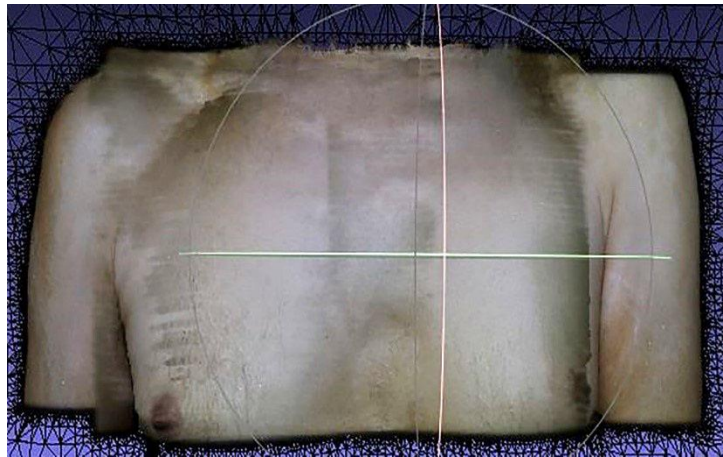


Figure 6.9: Final 3D model of chest with overlapping artefacts

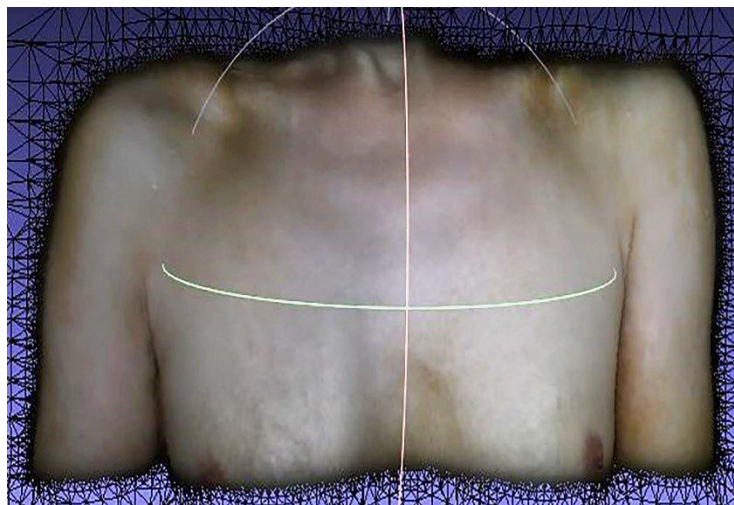


Figure 6.10: Final 3D model of chest without overlapping artefacts

The scanning results of the abdomen had the same scenario as the chest scanning. The area was scanned three times with two different volunteers. The raw 3D data sets had the same types of torso artefacts.

6.1.2.4 More challenging body surfaces

Scanning of dark skin, hairy areas, wet areas and areas with tattoo and jewellery were tested by the Pico Scan 3D surface scanner.

The nationality of the volunteers was different, and included Indian, Egyptian, Palestinian, Libyan, British, American, and Nigerian. Therefore, different degrees of skin colour were recorded and assessed. However, when dark skin was scanned, the intensity threshold had to be decreased to 10, 5, or even zero to have good result with clear boundaries (Figure 6.11); moreover, the clarity of the result increased by increasing the aperture size (f-stop) of the camera and reducing the shutter speed particularly when the scanned area had no distinctive features. However, a slow speed such as 1/4 should be avoided to avoid a prolonged acquisition time.

Wet areas with water were recorded (Figure 6.12). Areas of posterior aspect of hairy forearms were scanned, and the final 3D models were acceptable (Figure 6.13). Figure 6.14 shows the final 3D model of the posterior aspect of the hand with a silver ring. The scanner recorded the ring without any kind of artefacts. Whereas scanning an area with a stainless-steel watch shows that raw 3D data had distorted points generated from the watch because the item was shiny and reflective. A body area with a tattoo was scanned and acquired easily (Figure 6.15). A researcher wrist joint with her own blood was scanned, the final 3D results were generated with good quality (Figure 6.16). Furthermore, the concavity area was observed during the torso scanning, as one of the chest volunteers had an obvious concavity area in the centre of the chest. It was fully illuminated by the light and acquired easily by the scanner.

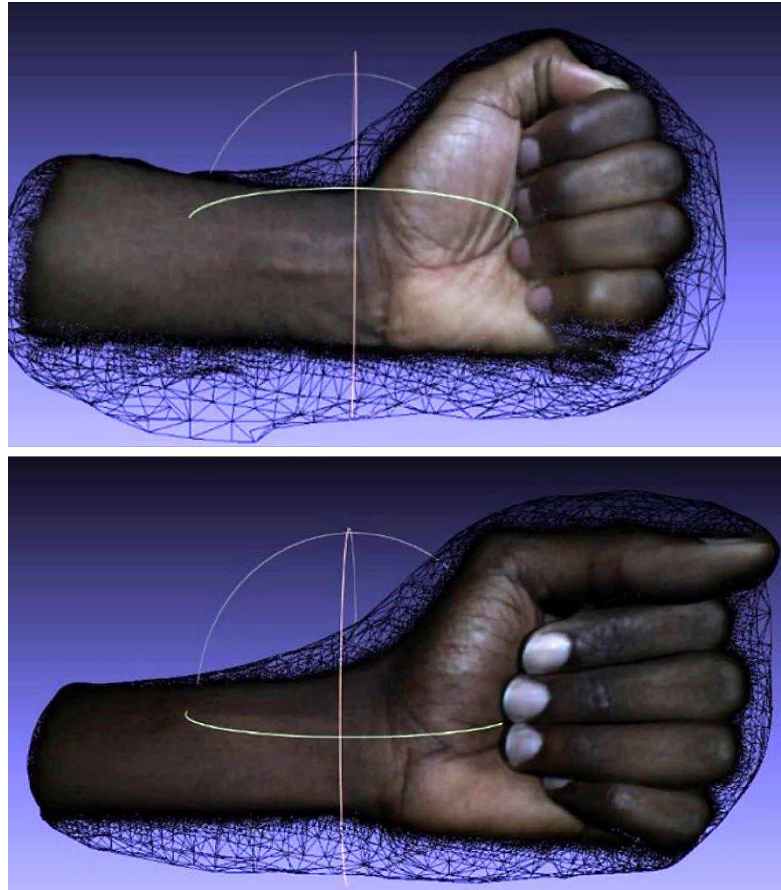


Figure 6.11: Final 3D model of dark coloured skin of two different volunteers
(Intensity threshold zero and aperture f/8)

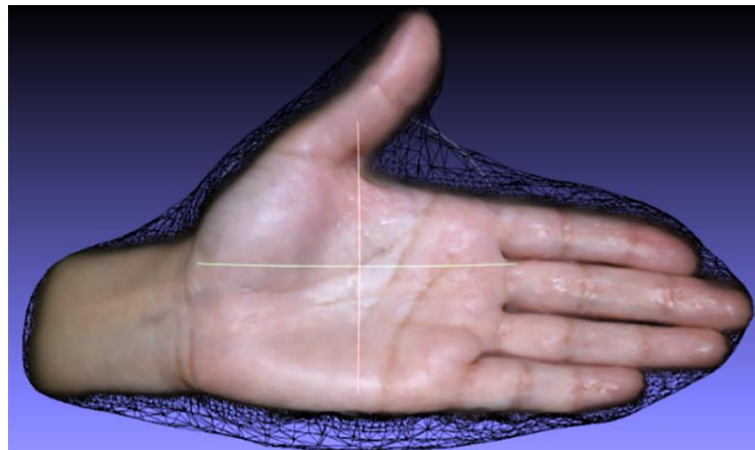


Figure 6.12: Final 3D model of palm moist with water

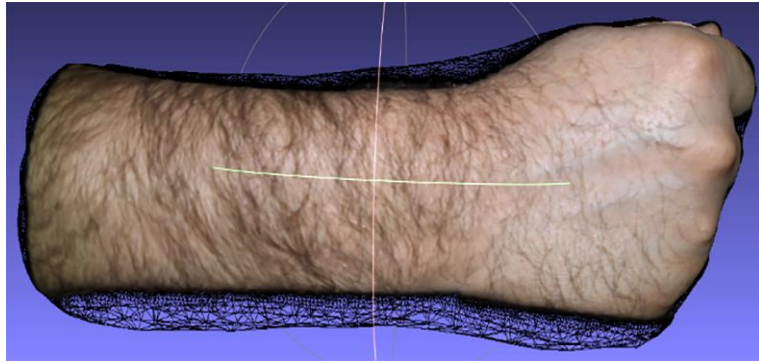


Figure 6.13: Final 3D model of the hairy posterior surface of the forearm

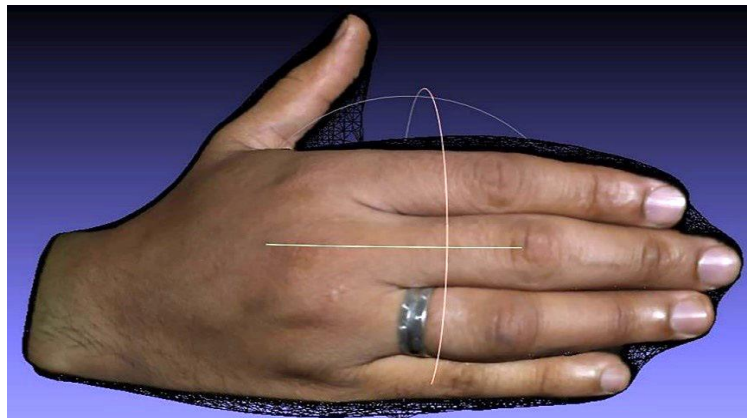


Figure 6.14: Final 3D model shows silver ring has no impact on scanning

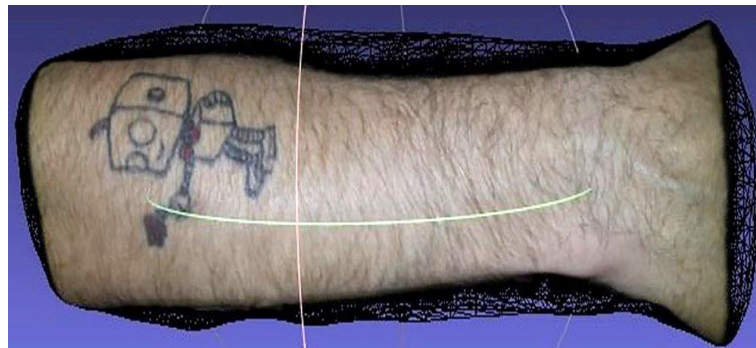


Figure 6.15: Final 3D model shows clear tattoo



Figure 6.16: Final 3D model shows recorded blood stain

6.1.3 Discussion

The scanning results were acceptable 3D models, with geometry and colour-textured information that was recorded instantaneously. These results had a high level of accuracy because of (1) the geometric calibration process, (2) the projection of encoded structured light patterns and (3) the accuracy of the underlying PMP 3D algorithm.

Some areas are well-known to be more challenging areas and that are difficult to record by passive 3D surface scanning systems. Single camera photogrammetry produces a distorted geometry of hairy surfaces, and VH1 (Stereo-Photogrammetry) produces holes or open boundaries in the results of these surfaces because its algorithm skips the hairy area to avoid producing inaccurate results. The same findings (distorted geometry or gaps) are obtained when the systems are tried to scan moist surfaces, such as dissected tissues or an area covered with body fluid (Urbanova, Hejna and Jurda, 2015). Villa (2017-a) cited that acquiring the hairy areas by single camera photogrammetry requires special care, and wet areas with water can cause error in photo orientation because water drops are not fixed points and reflecting surfaces. Difficulty to record wound with a moist surface is also observed by some other authors when they have used passive recording methods (Boersma et al., 2000; Bowling et al., 2011). According to Joun Tzou et al., (2014), Canfield Vectra, DI3D, 3Dmd and Crisalix 3D (Stereo-Photogrammetry) and Axisthree structured light scanners all have limitations in scanning hairy and shiny areas. Moreover, the material of the interested object plays an important role in the structured light scanning. Highly reflective materials or shiny objects and highly absorbed material are difficult to scan properly (Georgopoulos, Ioannidis and Valanis, 2010; Ebert et al., 2015). Furthermore, 3D laser scanning is not able to record black coloured surfaces, as they absorb the laser, so no data will be collected since the laser absorbed by dark surfaces (Errickson, Thompson and Rankin, 2015). On the other hand, the Pico Scan, structured light, 3D surface scanner overcame the above-mentioned limitations. (1) It produced 3D models of hairy surfaces of the body areas; however, it should be mentioned that areas with coarse hair such as a scalp should be tried. According to Lane and Harrell (2007), no 3D surface scanner is validated to accurately scan the hair volume, but some software can approximate the data to generate hair geometry. (2) The Pico Scan 3D scanner recorded wet areas with water and blood stains and generated good 3D results. This means that the structured light scanner will not be impacted by the blood or body fluid. (3) It was also able to scan dark (black skin);

however, this required a little adjustment in the processing settings mainly the intensity threshold. (4) Shiny jewellery was scanned to a certain extent.

Some scanning results revealed some minor defects. The scanning results of the anterior surface of the foot showed blurred visualisation of the toes area. This is because the surface of this area faced upward rather than fully facing the scanner and was not fully illuminated by the emitted light. In this situation, a professional hand-held scanner is a solution. It can easily access and scan unreachable sites. Whereas scanning results of the medial and lateral surfaces of the foot had good visualisation as these surfaces faced and received the projected light equally (Figure 6.17).

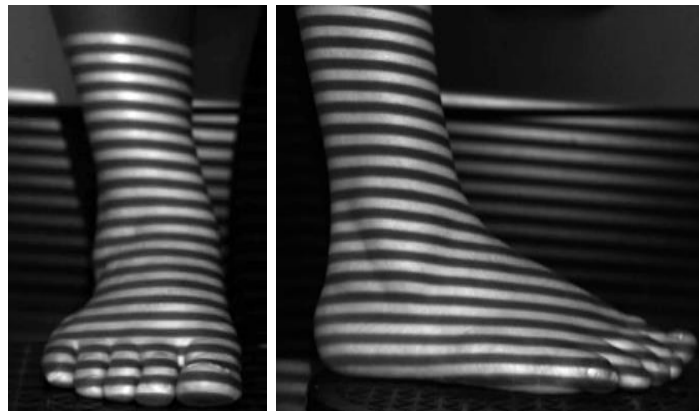


Figure 6.17: Illumination of the anterior and lateral surface of the foot with structured light stripes

The scanning results of the torso (with the volunteers in the standing position) were not satisfactory. All raw 3D data had the same type of torso artefacts: horizontal lines and distorted points. The distorted points were explained mostly by the movement of the volunteer despite trying to remain still during the scanning. The number of distorted points in the data was correlated to the amount of movement. Whereas the horizontal lines were explained by thoracic and diaphragmatic breathing. Although, the PMP principle of the Pico Scan 3D scanner was characterised by high-speed 3D measurement, the reconstructed 3D data were affected by the breathing. Asking the participants to stop breathing during the acquisition time would control the breathing artefacts, but the participants were not asked to hold their breath as the scanning time was about 20 sec/scan. Urbanova, Hejna and Jurda (2015) found that scanning the full-body surface of a volunteer in the standing position by two types of the passive 3D methods (VH1scanner and photogrammetry) was unsuccessful because of the movement of the volunteer and the breathing effect, whereas scanning the body in the lying position is influenced mostly by the breathing. According to Jones and Rioux (1997), regardless of the type of 3D surface scanning method, the main difficulty in recoding the live subjects is the breathing and movement, which may have effects on the accuracy of the 3D results (Slot, Larsen and Lynnerup, 2014). To eliminate the effect of movement, De Sainte Croix et al. (2016) asked the volunteers to place their forearms within a mechanical device (arm board) to obtain resting position and captured bite-marks on anterior surface of the forearms by the DI3D method.

6.1.4 Conclusion

The method was able to scan the body areas and provide good-quality 3D models with geometry and colour-texture. The scanner was able to create 3D models of different bare areas of the upper and lower limbs. The results also showed that the scanner easily represented moist surfaces and hairy and dark skin, which were the more challenging areas when using different 3D surface scanning techniques in previous publications. On the other hand, the scanner was not perfectly able to generate satisfactory scanning results of the torso areas when the volunteers were scanned in the standing position and holding their breath was not requested; therefore, the torso was assessed again in Section 6.1.5 with a faster structured light scanner.

6.1.5 Torso 3D surface scanning using the HP 3D scanner

The torso was the most difficult area to scan by the Pico Scan 3D surface scanner. Scanning this area was impacted by the movement and breathing. The participants were not asked to hold their breath because the scanning time of the Pico Scan was around 20 sec/scan; in addition, they were in the standing position. In the following work, the torso areas are scanned again with the HP, structured light, 3D surface scanner, which was faster (15 sec/scan), so it was requested that the volunteer hold their breath while the sitting position.

6.1.5.1 Materials and Methods

The HP, structured light, 3D scanner was used for scanning. A full description of this scanner and its scanning process is demonstrated in [4.3](#). Two volunteers participated in the chest and abdominal scanning.

In the chest scan, the volunteer was happy to repeat the scanning five times on different occasions. This was done to try different concepts: to try different camera angles (recommended and not recommended angles); to scan the chest in two divided areas; to scan the chest from the right to left shoulder in one recording; and to scan the chest with the abdomen. The effect of the breathing on raw scans was observed during these five trials (Table 6.4). The results of one of these five scanning are displayed below. The volunteer was in the sitting position with his back against the wall to keep him more stable. It was requested the volunteer hold his breath because the scanner has a faster acquisition time. Three markers were stuck to the middle of the chest to measure distances between them manually and three-dimensionally and to calculate differences between them. This was done for simple assessment of the 3D chest scanning result using the HP scanner. It was suggested that a difference up to or less than 5 mm was not significant.

In abdominal scanning, a different volunteer participated and was scanned in the standing position to make the abdomen more visualised. He was also requested to hold his breath and he was happy to do so. A 240-calibration scale was used to calibrate the scanner and the camera angle was set to 20°.

The processing computer of the scanning was an HP computer with an HD graphic card. Production of the colour-texture information by this computer was not perfect and for that reason, areas were additionally captured by a Nikon D3400 digital camera to display the colour. Two 3D raw scans were used for fusion to obtain the 3D model. The fusion resolution, sharpness and close holes were 1000, 1, and 0% respectively. Before the fusion, the two selected raw data were compared using the colour bar

comparison of the HP 3D scan V.5.3.0 software to assess both scans for any variation. One scan was used as a reference and another was used as a test. The tolerance value was 0.5 mm, and the comparison was run after alignment and global fine registration and before fusion.

Table 6.4: Impact of breathing on raw chest scans

	Total number of scans	Camera angle	Number of scans impacted by breathing
1 st chest scanning	13 scans	20°	1 of the 13 scans
2 nd chest scanning	13 scans	20°	2 of the 13 scans
	9 scans	15°	0 of the 9 scans
3 rd chest scanning	4 scans	22°	0 of the 4 scans
	8 scans	15°	0 of the 8 scans
4 th chest scanning	2 scans	20°	0 of the 2 scans
	6 scans	15°	0 of the 6 scans
5 th chest scanning	5 scans	25°	0 of the 5 scans
	10 scans	22°	3 of the 10 scans
	14 scans	15°	0 of the 14 scans

6.1.5.2 Results

6.1.5.2.1 Results of chest scanning

Results of third scanning of the chest from right to left shoulder are presented below. The 3D raw data of the chest were four scans, all of them having no breathing artefacts. Only two raw scans (Figure 6.18) were used for fusion to attain the final model, which was acceptable final model (Figure 6.19). The result of the colour bar comparison of the two selected raw data was almost zero mm deviation (Figure 6.20), this means that both chest raw scans were free from variations and artefacts and were completely matched. Moreover, two distances between the markers were measured manually by the tape and three-dimensionally using the 3D result. The difference between them was small, around 2 mm (Table 6.5).

On the other hand, as can be seen in figures bellow, the left margin of the raw chest scans was not recorded completely (the area is indicated with arrows in Figure 6.18). This defect was related to the angle of the camera. When the camera was set to the recommended angles, it was looking to the right side of the scanned area more than the left side. To improve the left border of the scanning results, the following were tried:

1. The chest was scanned in two halves (right and left half) by moving the scanner. The central area of the chest was an overlapping area in each half, but no improvement was noted in the result.

2. The same as no. 1 was repeated with a smaller camera angle (15°) and slight turning to the right side. The result (left border of the raw scans) showed some improvement.

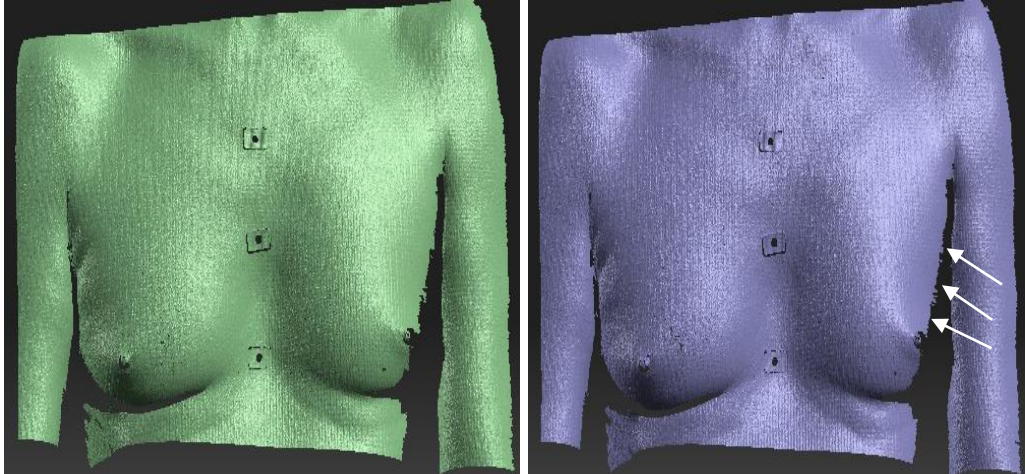


Figure 6.18: Two 3D raw scans of chest

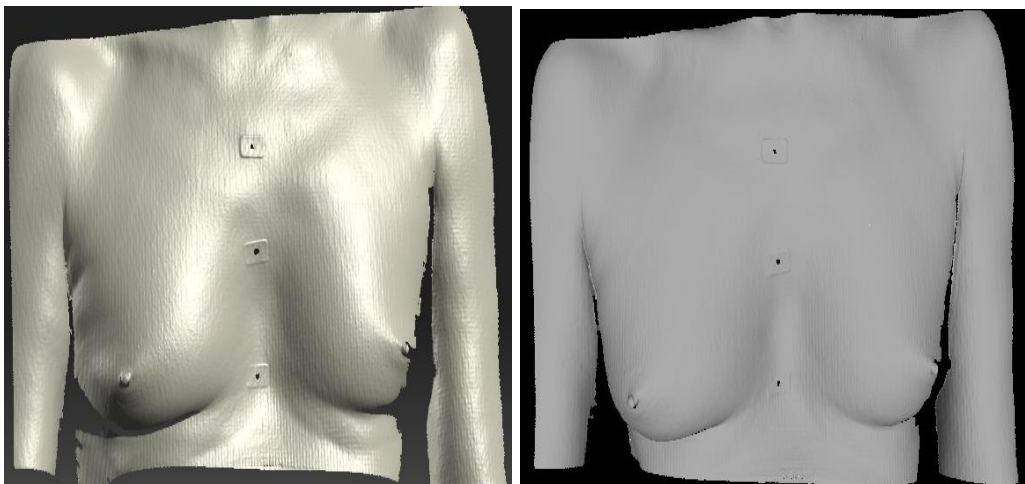


Figure 6.19: 3D geometry of chest in HP 3D scan software (left) and MeshLab software (right)

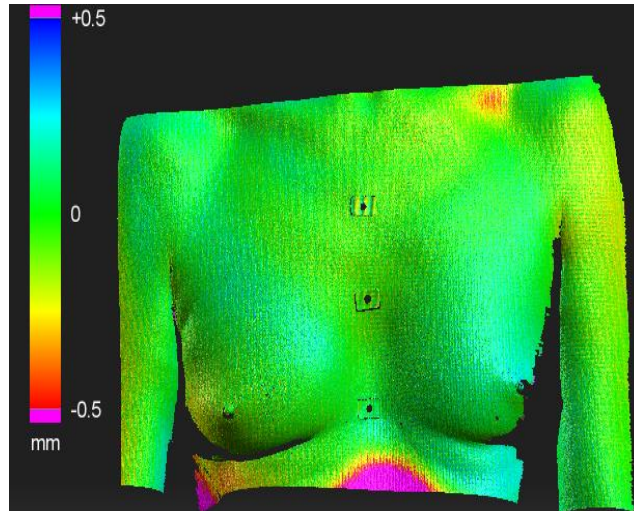


Figure 6.20: Colour bar comparison result of two 3D raw scans of chest
(Around 0 mm deviation)

Table 6.5: Manual and 3D distance measurements between markers on chest

Distance (mm)	Manual	3D in MeshLab	Difference
1 st distance	60	57.78	2.22
2 nd distance	70	67.96	2.04

6.1.5.2.2 Results of abdominal area scanning

Two raw scans (Figure 6.21) were used for fusion to obtain the final 3D model (Figure 6.22), one of them had breathing artefacts (indicated with oval shape in Figure 6.21). The volunteer was able to tolerate the first scan (first 15 sec) but he was not able to continue holding his breath for the second scan. The process was repeated about four times, and in each case the first scan recorded adequately but the second was affected by breathing. The left border of each raw scan was also not recorded properly (indicated with arrows in Figure 6.21), with the reason being as mentioned above. The result of the colour bar comparison of two raw scans was almost 0 mm deviation (Figure 6.23), except that the areas impacted by breathing were not matched with a reference scan.

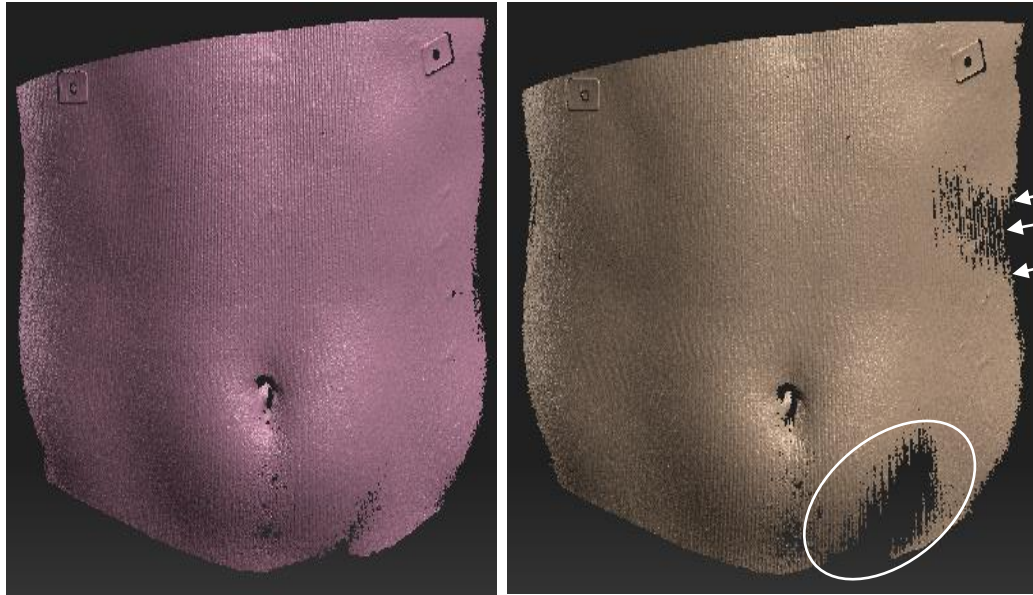


Figure 6.21: Two 3D raw data of abdomen
Left scan without artefact and right scan affected by breathing

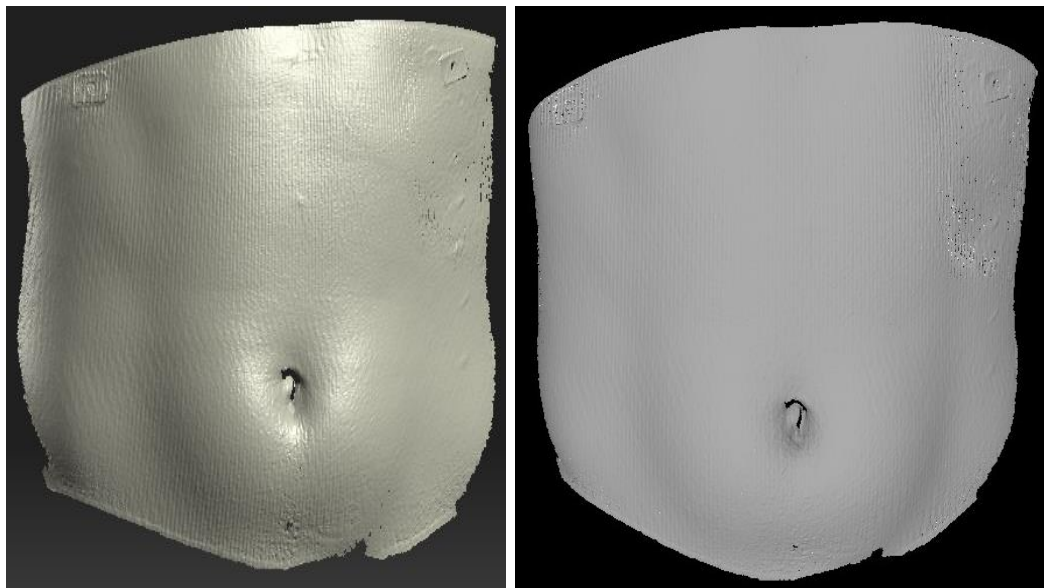


Figure 6.22: 3D geometry of abdomen in HP 3D scan software (left) and MeshLab software (right)

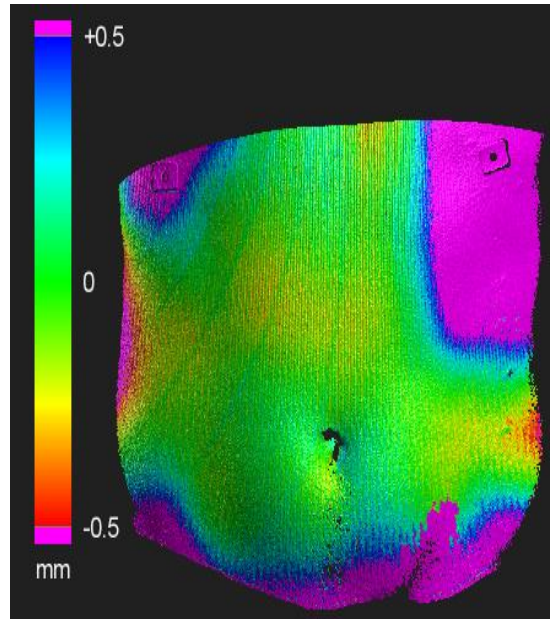


Figure 6.23: Colour bar comparison result of two 3D raw scans of abdomen

6.1.5.3 Conclusion

Torso area scanning was improved by a faster acquisition time, a sitting position, and breath-holding. However, holding their breath is not be easy and tolerable for everyone. Using a scanner that is more resistant to the breathing process (a faster scanner) is a solution that will guarantee more accurate outcomes.

6.2 3D surface scanning of complicated anatomical areas

6.2.1 Introduction

Each part of the human body is different and has amazing shape, and features. Some areas have flat, curved, or depressed surfaces. Some areas are obscured, and others are exposed and obvious. Injuries could be located anywhere, and those located on obscured areas are a little difficult to reach and record properly by ordinary digital photography, single camera photogrammetry (Villa, 2017-a; Michienzi et al., 2018) or multi-camera photogrammetry (Kottner et al., 2019). Examples include axillary area, the areas behind the ears, and the under-chin area. Also, the photographic scale cannot be placed exactly on the same injury plane (Patient Focused, 2018) when the areas have uneven surfaces (curved, or depressed surfaces). Examples of these areas are the under-chin again, the side of the neck (Figure 6. 24 left), axillary areas, and the knee joint, or any uneven aspect. It is well-known that when the scale is not placed on the same injury plane, type 2 scale distortion is obtained in 2D photographs (Evans et al., 2014), which subsequently causes wound measurement errors. Additionally, the nose is an area where the scale can obstruct the surrounding landmarks (Patient Focused, 2018), especially if Y-shape or L-shape scales are used (Figure 6. 24 right). These areas are considered complicated areas to record by digital camera or photogrammetry and thus were worth to testing by structured light 3D surface scanner to assess whether or not the 3D scanning could cope with these difficult areas.



Figure 6.24: Injuries on uneven surfaces²⁹.

²⁹ (Patient Focused, 2018).

6.2.2 Materials and Methods

The HP 3D surface scanner Pro S3 was used to scan some complicated anatomical areas. The calibration was done before each scanning. The pattern parameter profile was speed profile (15 sec/scan), the final model was fusion of two raw 3D scans, the resolution of the fusion was 1000, the sharpness value was based on the quality of the scans, but was mostly the default value, and close holes was 0%. An HP laptop with HD graphic card was used. However, an Alienware computer with a powerful graphic card (GeForce GTX (1070) was also used with some cases. The volunteer scanning position was mainly the sitting position; however, supine and prone positions were also used for some areas. Under-chin and anterior of the neck, side of the neck, axillary area (underarm), anterior and posterior aspect of the knee alongside the deformed torso were scanned, assessed and discussed separately.

6.2.3 Results and Discussion

6.2.3.1 Under-chin and anterior of the neck

To make the area fully exposed to the 3D scanning system, it was scanned in hyperextension while the volunteer was in the setting position and was aware to maintain stability during the acquisition time. The camera was set to 22°. Figure 6.25 left shows 2D digital photograph of the area.

The scanning result showed that the left border of the scanned area was not fully recorded (Figure 6.25 right). The scanning was repeated in a different day with the same participant and different participant, but the results were the same. The scanning was also repeated with different attempts: (1) the scanner was moved little to the left to ensure full recording of this side, and then moved to the right while the volunteer remained stable; however, the result was not improved. (2) The camera was changed to larger angle (25°) with new calibration process, but the result was a little exaggerated (Figure 6.26 left). Whereas, when the camera was set to a smaller angle (15°), the result was improved, particularly when a little turning was applied towards the right-side to improve the desired view (Figure 6.26 right).

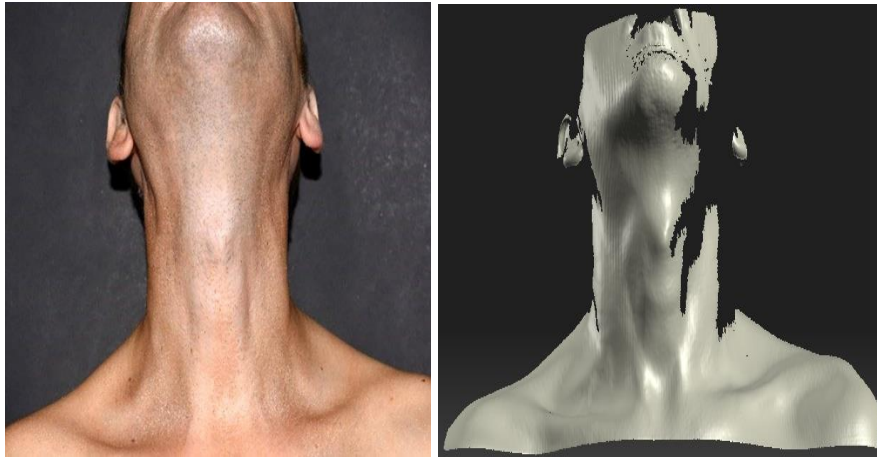


Figure 6.25: 2D digital photograph of under-chin area (left), 3D geometry of the area resulting from scanning using 22° camera angle (right)

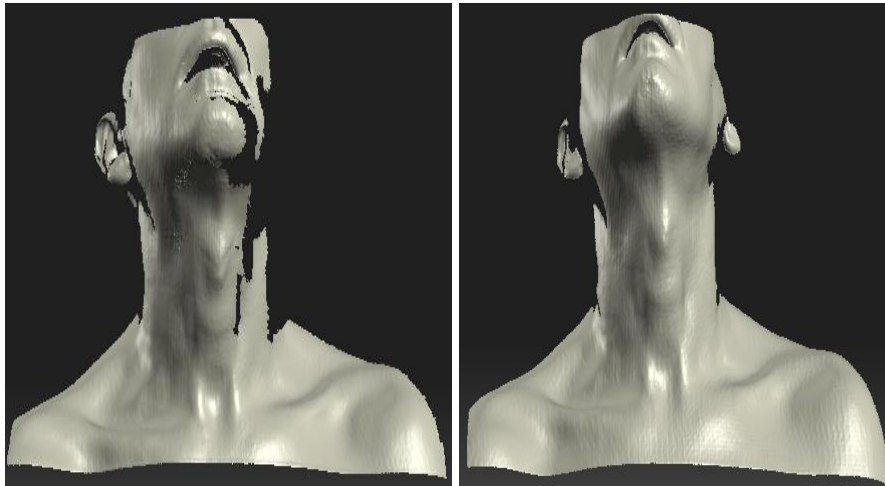


Figure 6.26: 3D geometry of the same area resulting from scanning using 25° (left) and 15° (right) camera angle

The HP 3D scanner Pro S3 is based on the triangulation principle, which is designed to essentially scan static objects in 360°. The object is rotated manually or using an automatic turn-table, that it is scanned from all different views and no view will be missed. Moreover, dual cameras were usually used to compensate each other and record both sides of each view equally. The only reason for not-recording the left side of the under-chin area and the anterior of the neck was the angle of the single camera. The camera was single and mounted on the left side of the projector. The ideal camera angle was 22-25°. It was clear that when the camera was set to these values, it seemed to be looking to the right side more than the left side. In addition, the anatomical shape of the area made the situation worse. The area was not a flat surface, it is formed from two sides. The left side was concealed behind the central neck structure. According to Lau (2012), occlusion problems wherein certain surfaces

may not be visible to the camera and the projector are typical problems with 3D surface scanning systems based on the triangulation principle. Figure 6.27 shows the scanned area with light pattern; the images were snapped from the live camera view while the camera was set to different angles (15° and 25°). The camera with 25° was looking to right side more than the left, whereas a smaller angle (15°) allowed the camera to almost see both sides of the scanned area. However, according to the user guide of the scanner, a smaller camera angle can introduce noise and create inaccurate results. Thus, a 3D scanner with dual cameras might be helpful to solve this situation.

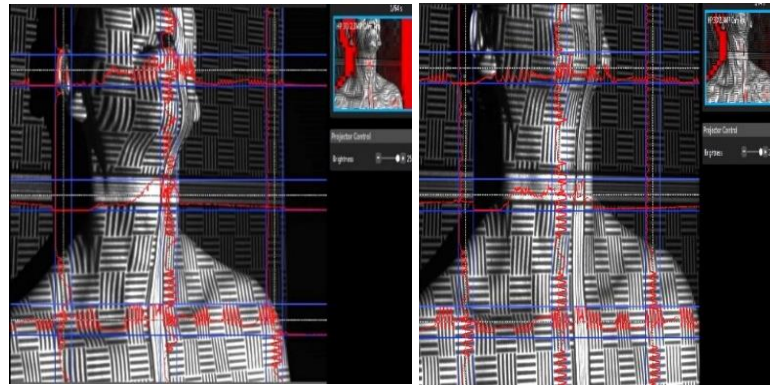


Figure 6.27: Live camera view of 25° (left) and 15° camera angle (right)

6.2.3.2 Side of the neck

The scanning was applied to two different volunteers using different camera angle scanning. It was done while the volunteers were in the sitting position. The scanning process had no limitation. The scanner simply recorded the side of the neck as the area was flat and seen by the camera. Figure 6.28 (first image) shows a 2D digital photograph of the area, and Figure 6.28 (second image) shows the 3D geometry of the same area recorded by scanning using 15° camera angle.



Figure 6.28: 2D digital photograph (first) and 3D geometry of the same area (second)

N.B. The sharpness value for the fusion was -3 for all above displayed results because the shaved areas were rough in the raw scans. When the default sharpness value or positive values were selected, the roughness was noticeable in the final fused result.

6.2.3.3 Axillary area

The volunteer was in the sitting position with his back against the wall, the arm elevated, the forearm at about 30° angle and the hand placed on the back of the head. This way, the desired area was facing the light and the camera. Figure 6.29 is the 2D digital photograph of the area. Although the scanned area was perfectly illuminated by the light and fully seen by the camera, the 3D scans were not perfect around the arm, the unrecorded area is indicated with arrows in Figure 6.30, possibly because of the motion effect of the arm in the elevated position or the flicking muscle movement in that position. However, when the scanning was repeated in the supine position, the volunteer felt more relaxed and the area was fully recorded (Figure 6.31).

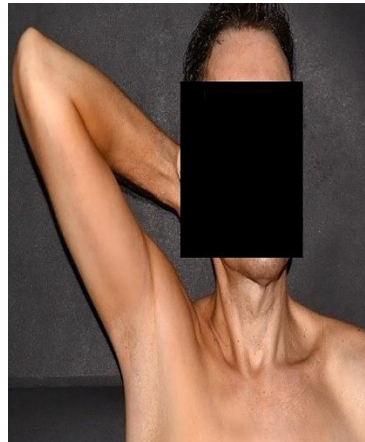


Figure 6.29: 2D digital photograph of axillary area



Figure 6.30: 3D raw scans of axillary area show unrecorded arm

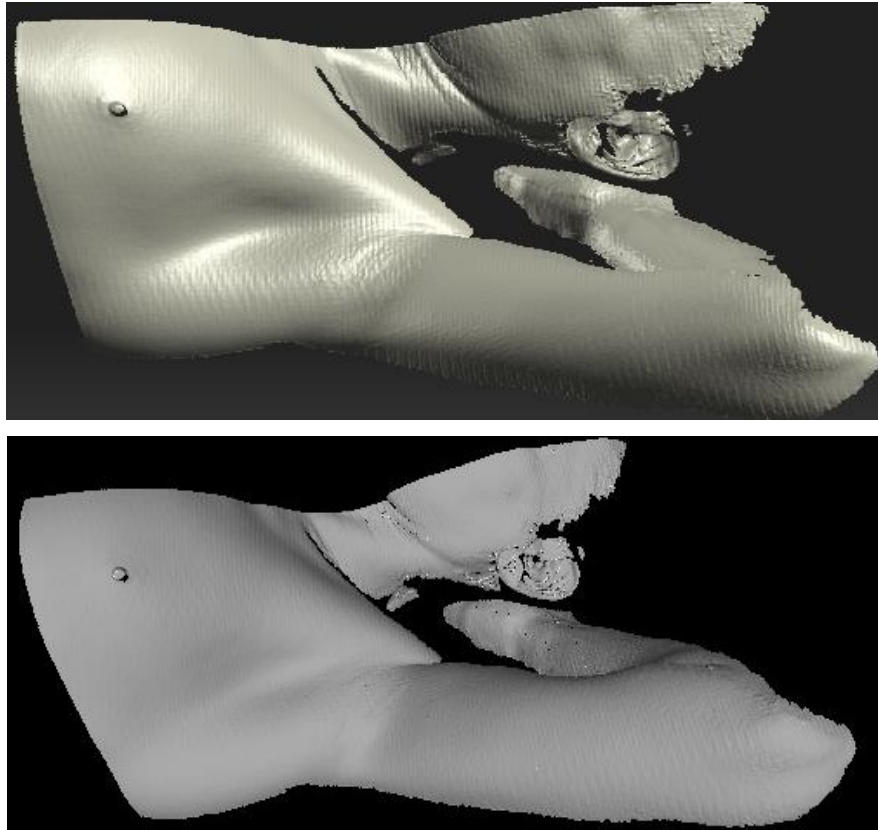


Figure 6.31: 3D geometry of axillary area in HP 3D scan software (first) and MeshLab software (second)

6.2.3.4 Anterior and posterior aspect of the knee

The anterior and back of the knee joints were scanned in the prone and supine position. These positions were expected to be better than the sitting position for the knee joint scanning. The camera was set to the typical angle (20°). The backs of the areas were easily recorded as they are almost flat surface, but the left borders were not perfectly recorded, which are indicated with arrows in Figure 6.32. As explained previously, this is related to the angle of the single camera. The scanning results of the anterior surface of the knees were almost the same with some exaggeration because the anatomical shape of the antero-medial surface was more concaved. When the result was repeated with a smaller camera angle around 18° , the result was slightly improved, but as mentioned in 6.2.3.1, the smaller angle was not the typical angle.

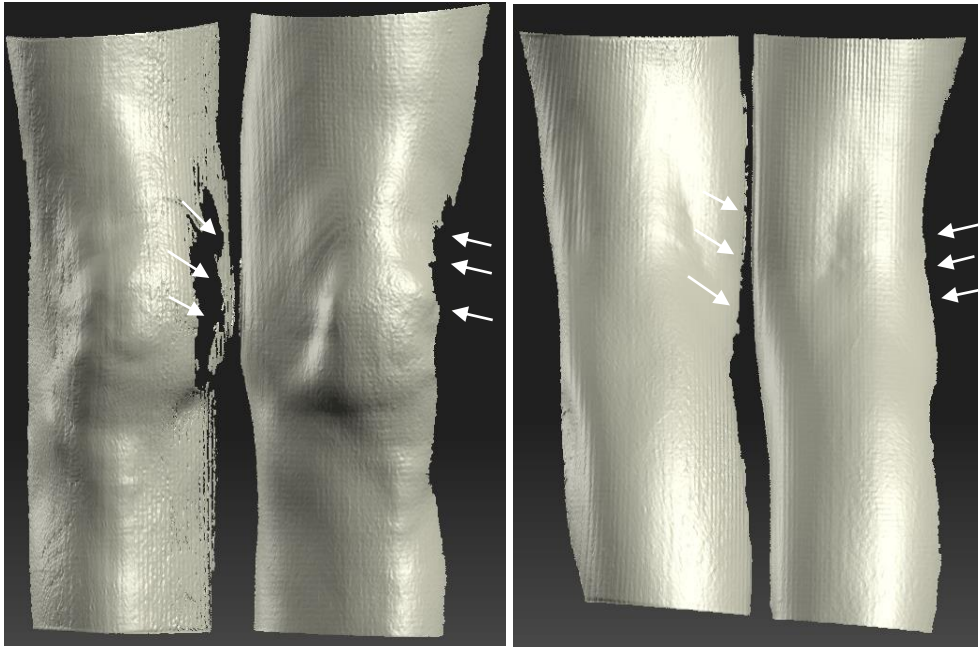


Figure 6.32: 3D geometries of the anterior and posterior surface of the knee

6.2.3.5 Deformed torso

The volunteer had an asymmetrical shaped torso and deformed surfaces. He had an elevated left shoulder, a scaphoid shape on both sides of the abdomen (Figure 6.33), and prominence in the upper left side back. It was interesting to scan the whole torso together to see if the scanner could represent the deformed surfaces in clear view. The volunteer was happy to participate and scan his torso.



Figure 6.33: 2D digital photograph of deformed torso

Chest and abdominal areas were scanned separately with the volunteer in the standing position. In this case, the standing position was the best to obtain a clear view, particularly the abdominal view. The scanning was done while the camera was set to 15° to improve the results from 22° angle. Moreover, the scanning was done with slight turning to the right side. Markers under breasts were recorded in both scans (chest and abdominal scans) to use in the alignment step. Other markers were stuck on the midway of the chest and abdominal areas to use in distance measurements manually and three- dimensionally, and to find the difference between them and was suggested that a difference up to or less than 5 mm was not significant. The measurements were taken to assess the precision of the 3D result. The result (Figure 6.34) was composed of acceptable chest and abdominal scans. The differences between the manual and 3D measurements were small and not significant (Table 6.6).

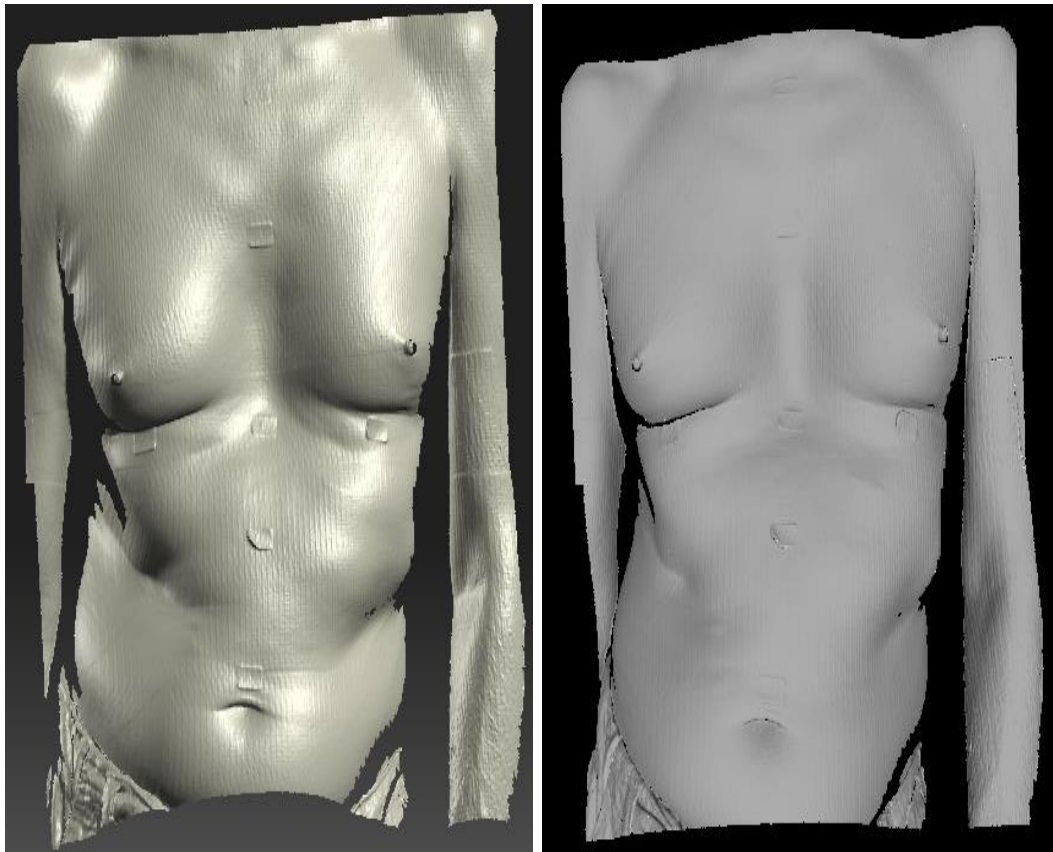


Figure 6.34: Fused result (3D geometry) of deformed torso

Table 6.6: Manual and 3D distance measurements between markers on torso

Measurements (mm)	Manual	3D mesh	Difference
1 st distance	80	76.50	3.50
2 nd distance	100	101.53	1.53
3 rd distance	70	65.44	4.56
4 th distance	70	74.09	4.09

Each measurement was taken three times and average values were used

6.2.4 Conclusion

Some complicated anatomical areas are considered difficult areas for the digital camera to record as they are obscured and difficult for the camera to see, or the scale is improperly placed in these areas. These areas were tested in this work by a 3D scanning system using a structured light scanner and they were easily accessed and scanned by the system; moreover, scale was not required during 3D acquisition time which is one of main advantages of the 3D system. Some areas, such as axillary area and knee joint, were scanned in the supine or prone position. The 3D system easily managed to scan areas in these positions and the participant felt more relaxed and stable in supine or prone positions. In general, the 3D scanning results were satisfactory, but the left side of most scanned areas was not fully recorded due to the angle of the single camera of the system. It is suggested a structured light system with dual camera be used to improve the left side recording of these areas; however, the unrecorded margin will have no influence on the findings because it only affects the boundaries of the 3D results.

6.3 3D facial scanning

6.3.1 Introduction

Facial 3D surface scanning has been achieved for many purposes. It has been used to overcome some deficiencies of 2D facial recognition related to illumination, head position, expression, ageing, and occlusions (Abate et al., 2007; Naeem, Qureshi and Azam, 2015; Patil, Kothari and Bhurchandi, 2015). In addition to the subjectivity of the method when it is based on anatomical distinguishing of the face (Goos, Alberink and Ruifrok, 2006). Urbanova (2016) cited that facial image identification should be based on scientific principles. On the other hand, 3D face recognition is more accurate, robust, provides face geometry, local and global curvatures and becoming faster and cheaper (Abate et al., 2007). Moreover, any 2D photo view, such as right, left, right or left oblique, and so on can be generated from the 3D model with no need to reposition the subject in front the camera (Lane and Williams. 2007). Some 3D face recognition research has focused on addressing occlusion and facial expression (Patil, Kothari and Bhurchandi, 2015). Several studies of face 3D surface scanning have been conducted to assess the slight facial abnormalities of some diseases such as Fabry disease (Cox-Brinkman et al., 2007) or the impact of asthma or mouth breathing on the facial shape (AL Ali et al., 2014; AL Ali et al., 2015). Face scanning has also been investigated to assess the facial plastic surgery outcome (Aung, Ngim and Lee, 1995; Kovacs et al., 2006-a; Kovacs et al., 2006-b). In these mentioned publications, the scanning is conducted mostly by applying laser or passive 3D surface scanning techniques.

In this section, faces of live subjects were scanned by single camera-structured light 3D surface scanner to assess the overall facial scanning results. Raw 3D scans and fused results were assessed visually. The impact of facial hair, different skin colours, skin texture, movement, and the impact of some technical factors, such as single camera scanner, scanning time, and processing computer are considered in assessment of the results.

6.3.2 Materials and Methods

The work was ethically approved by the ethical committee of Teesside University. The procedure was explained verbally to the participants, and they read more information about the work prior to signing a consent form. The participants were students and researchers at Teesside University.

6.3.2.1 3D Surface scanner

The scanning was conducted by the HP 3D scanner Pro S3 of single camera. The speed profile was selected (15 sec). Kovacs et al. (2006-a) cited that it is essential to scan the face with a fast speed as the face cannot be completely immobilised. The used computer to process the acquired information was an Alienware computer. The impact of the used computers was discussed later.

6.3.2.2 Subject position

Because the head is easily affected by breathing, face scanning was done while the volunteer was in the sitting position, with the occipital area of the head and the back of the torso resting on the wall (if the head was not held still, the scanner was not able to record the view). Since the occipital area of the head rested on the wall, the imaginary Frankfort horizontal line was deviated around $+10^\circ$ or less. The volunteers were asked to keep their head in the same position and their face in a neutral facial expression and remain as stable as possible. Blinking, swallowing, and deep breathing were advised to be avoided during the recording time. Volunteers were also asked to keep their eyes closed as the light was a little irritating.

6.3.2.3 Face scanning technique

The scanning started with the frontal view of the face, and the face was then subsequently turned to the right and left view. The turning was done manually by the operator while the head was in the same position and the turning was done gently. The turn angle to each view was around 30° - 40° to obtain an overlapping area with the frontal view. In each face scanning, scanning the frontal, right and left views was done more than once to select the better scans. The final 3D model resulted from the fusion of a scan of each view (frontal, right, and left view). The fusion resolution was 1000 and the sharpness value was mostly the default value. The model was exported in OBJ file format without closing holes (the close holes was 0%). Visualization was done in the flat mode of the MeshLab software. Table 6.7 shows numbers of facial scanning with different conditions.

Table 6.7: Different conditions of facial scanning

	Facial scanning	No.
Gender	Male	7
	Female	2
Skin colour	Light skin	4
	Brown skin	3
	Dark skin	2
Hair distribution	Beard & moustache	3
	Shaved	2
	Scanty beard & moustache	2
Eyeglasses	Medical eyeglasses	2
	Sunglasses	0
	Piercing	0
Total no. of testing		9

N.B. The manual face-turning technique that described above was proposed to be convenient to achieve facial scanning in this study because the HP scanner of this research had a single camera mounted on the left side of the projector, also the participants were sitting on an ordinary chair not rotating chair.

6.3.2.4 Colour bar comparison of HP 3D scan software Pro V.5.3.0

Before fusing the best selected raw scans (frontal, right and left scans), they were compared using the colour bar comparison of the HP 3D scan software Pro V.5.3.0. This was done to assess the raw scans for any deviation or artefacts. The frontal scan was used as a reference and other scans were used as test scans separately, and the overlapping area between the reference and each test scan was assessed by this comparison. The comparison was done after the alignment and global fine registration, and before the fusion while the tolerance value was 0.5 mm. The comparison was based on the calculation of signed distance in the overlapping area between two 3D entities from the test to the reference, and the results were represented in colour. To simplify the interpretation of the coloured results, deviation values were suggested according to these colours in the scale (Table 6.8). The green colour in the overlapping area between the reference and test scans was supposed to have zero deviation (completely matched). Green to sky and green to yellow were suggested to be -0.1 and +0.1mm (no deviation). Sky and yellow colours were suggested to be next lowest deviation (-0.2 and +0.2 mm) and mildly deviated, etc.

Table 6.8: Suggested deviation values and results

Colour in compared areas	Suggested deviation value	Suggested result
Green	0 mm	Completely matched
Green to sky	+ 0.1 mm	No deviation
Sky colour	+ 0.2 mm	Mild deviation
Sky to blue	+ 0.3 mm	Moderate deviation
Blue	+ 0.4 mm	Sever deviation
Magenta (reference colour)	+ 0.5 mm	Not matched
Colour in compared areas	Deviation value	Suggested result
Green	0 mm	Completely matched
Green to yellow	- 0.1 mm	No deviation
Yellow	- 0.2 mm	Mild deviation
Yellow to red	- 0.3 mm	Moderate deviation
Red	- 0.4 mm	Sever deviation
Magenta (reference colour)	- 0.5 mm	Not matched

However, a quick assessment was done to be sure of the colour result interpretation. The assessment aimed to scan (1) an unsteady area to obtain movement artefacts in the 3D raw data and (2) a completely at rest area. Two scans of each test were fused with resolution 4000 and sharpness 3. Before fusion, two 3D raw scans of each area were compared in this colour bar comparison, with the result shown below (Figure 6.35 and Figure 6.36). It was clear that the two raw 3D data of the second example were complete matched and the deviation was 0 mm as two raw data had no artefacts.

N.B. The comparison in these examples assessed the complete area of the test scan because the reference and test scans completely overlapped, but in the face scans, the comparison was run only in the overlapping area between the test and reference scans.

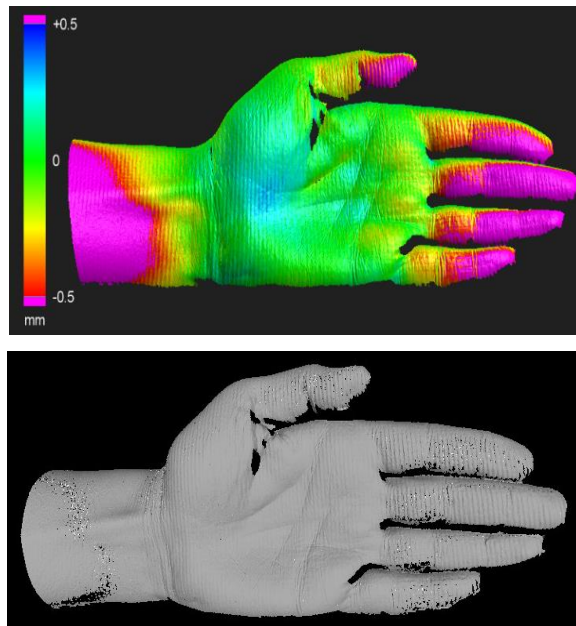


Figure 6.35: Colour bar comparison result of noisy scans (first) and their 3D model shows movement artefacts around fingers and wrist (second)

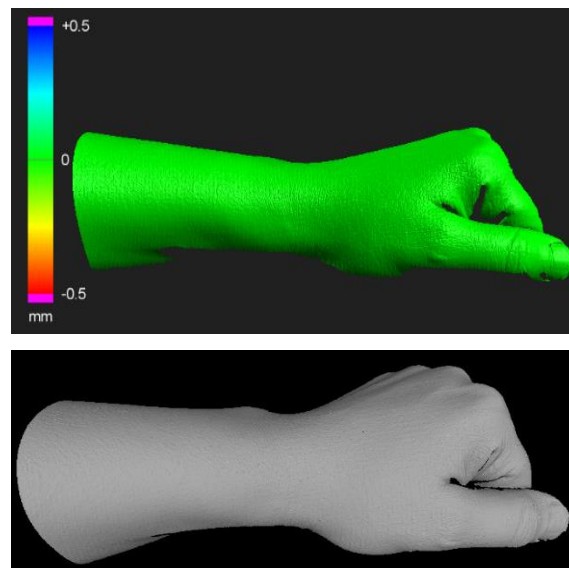


Figure 6.36: Colour bar comparison result of completely matched scans (first) and their 3D model (second)

6.3.3 Results

6.3.3.1 3D surface scanning of subject with facial hair

The scanning results of this face show:

1. Hair-bearing areas (anterior scalp hair, eyebrows, eyelashes, moustache, and beard) were not recorded in raw 3D scans (Figure 6.37).

2. Both sides of the nose (in the frontal view scan) were not recorded, as these areas were not fully facing the light and camera. However, they were recorded in the right and left face scans (Figure 6.37).
3. Movement artefacts (vertical ridges) in the raw 3D scans were noted in one of the six scans. They appeared when the scans were magnified on the screen without colour-texture.
4. The fused result of the frontal, right, and left scans still having un-recording hair-bearing areas (Figure 6.38). However, when the close holes was raised from 0 to 10%, the holes were closed, but the result was not accepted when it was displayed in geometry without colour-texture.
5. Deviation in overlapping area between the reference and right scan was around +0.4 and -0.2 mm, and between the reference and left scan was around +0.1 and -0.2 mm (Figure 6.39).

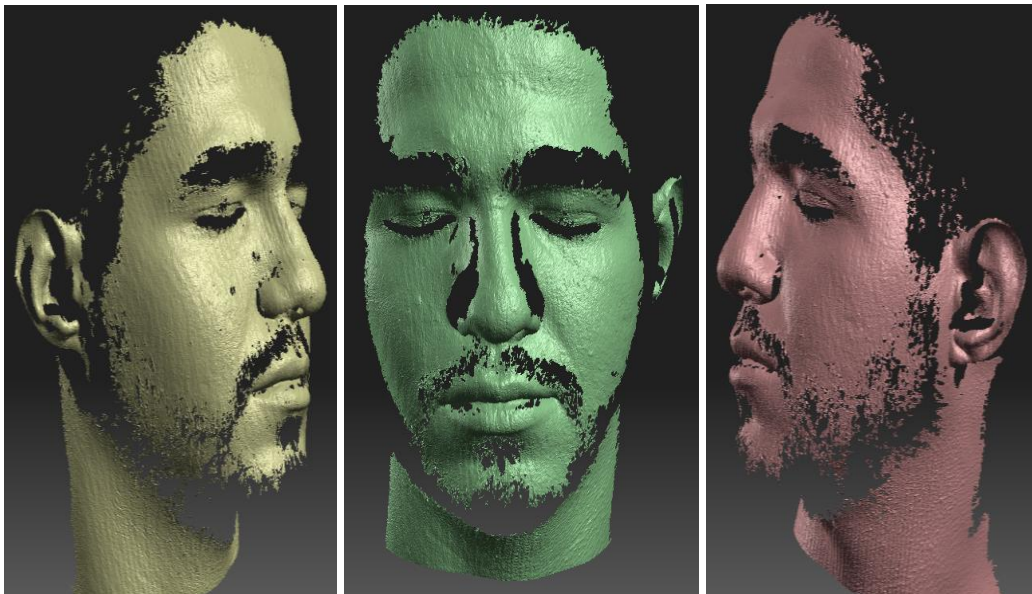


Figure 6.37: 3D raw scans of frontal, right and left views of subject with facial hair
(Raw scans without colour-textured information)



Figure 6.38: 3D geometry of subject with facial hair in HP 3D scan software (left) and MeshLab software (right)

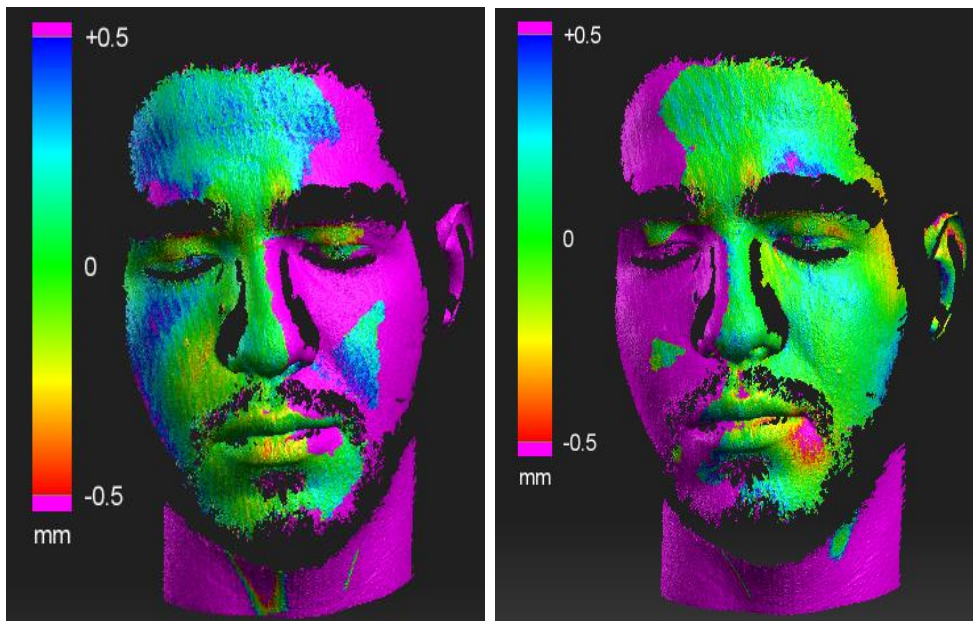


Figure 6.39: Colour bar comparison result of subject with facial hair
(Mild to severe deviation)

6.3.3.2 3D surface scanning of shaved faces

A volunteer was asked to shave his face a day before scanning. The scanning result of this face was the most satisfactory one, possibly because the volunteer was the most obedient and had smoother skin texture. The following were noted, when the raw 3D scans were inspected without colour-texture:

1. The scans were smooth as he had already smoother texture (Figure 6.40).
2. Eyebrows were recorded partially, as they were sparse.
3. The scans had movement artefacts (fine vertical ridges) in only 3 of the 14 scans. When the scanning was repeated (using a different processing computer), one scan out of nine had fine vertical ridges.
4. Left side of the nose and left ear in the frontal view were not recorded. In addition, the left margin of the left face view was not fully recorded (Figure 6.40), but this was improved by turning more to the right side. Note that the same distribution of unrecorded areas of this volunteer was observed with all cases of facial scanning. Figure 6.41 shows the fused result of the three raw scans (frontal, right, and left scans). The colour bar comparison results (deviation) in the overlapping area between the reference and each test scans were around 0.1 mm (Figure 6.42).

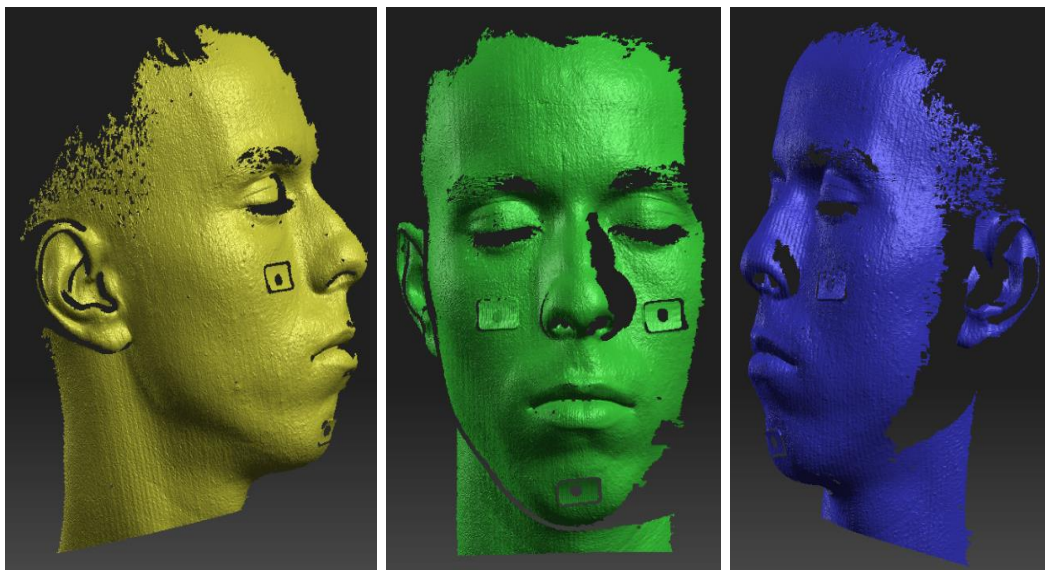


Figure 6.40: 3D raw scans of shaved face without colour-textured information

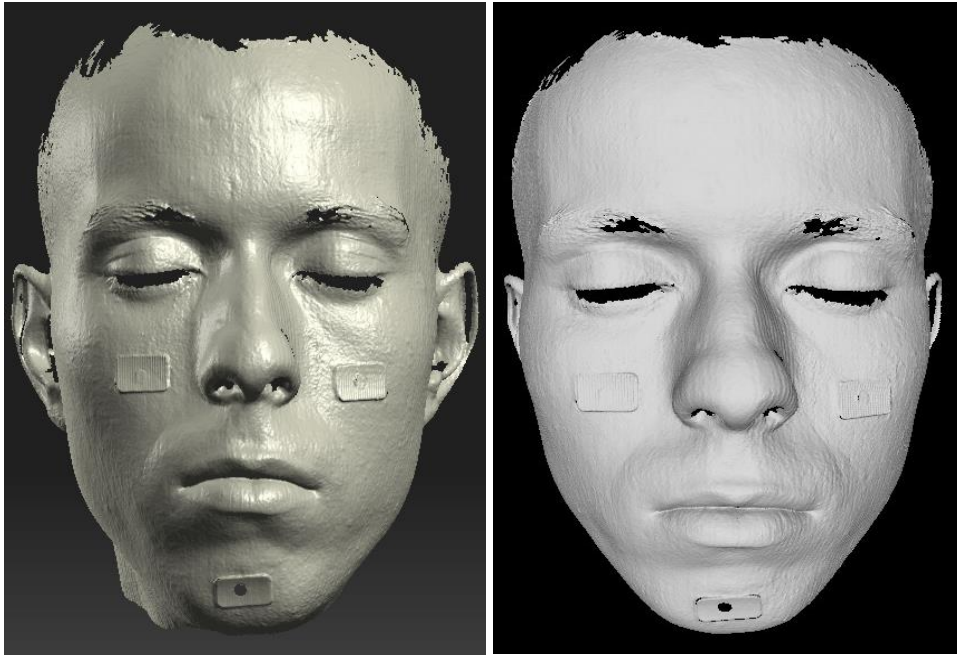
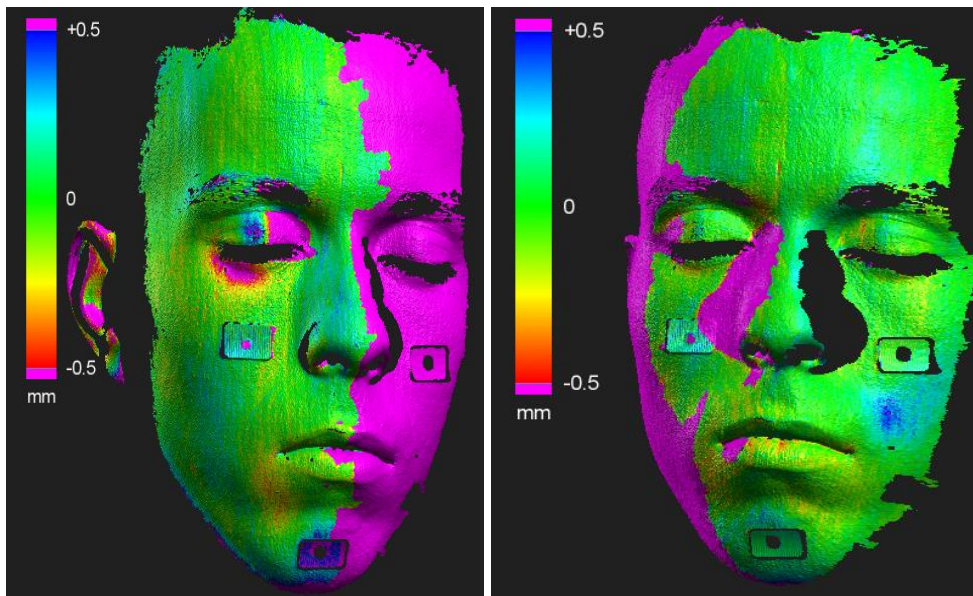


Figure 6.41: 3D geometry of shaved face

Figure 6.42: Colour bar comparison result of shaved face
(Deviation around 0.1 mm)

Another participant with shaved face was scanned. However, the shaving was done days before scanning. Moreover, it was noted that the volunteer had intermittent involuntary movement around his lips. Also, he sometimes felt a muscle tic. Most of his raw 3D scans (Figure 6.43) were noisy when they were inspected without colour-texture. They had rough surfaces that could be associated with rough skin texture or subject movement. There were also clear vertical ridges when the raw scans were zoomed in. The selected scans were fused with negative sharpness (-3) to obtain

smoother fused result, but the noise around the mouth and the vertical ridges around the nose were still obvious in the final result, they are indicated with arrows in Figure 6.44.

The raw scans had the same unrecorded areas as in previous results. In addition, small holes in the right and left temples were seen, they are indicated with arrows in Figure 6.43; however, fusing all views together abolished these holes, and repeated scanning with more side turning also eliminated these holes from the results (Figure 6.45).



Figure 6.43: 3D noisy raw scans without colour-textured information

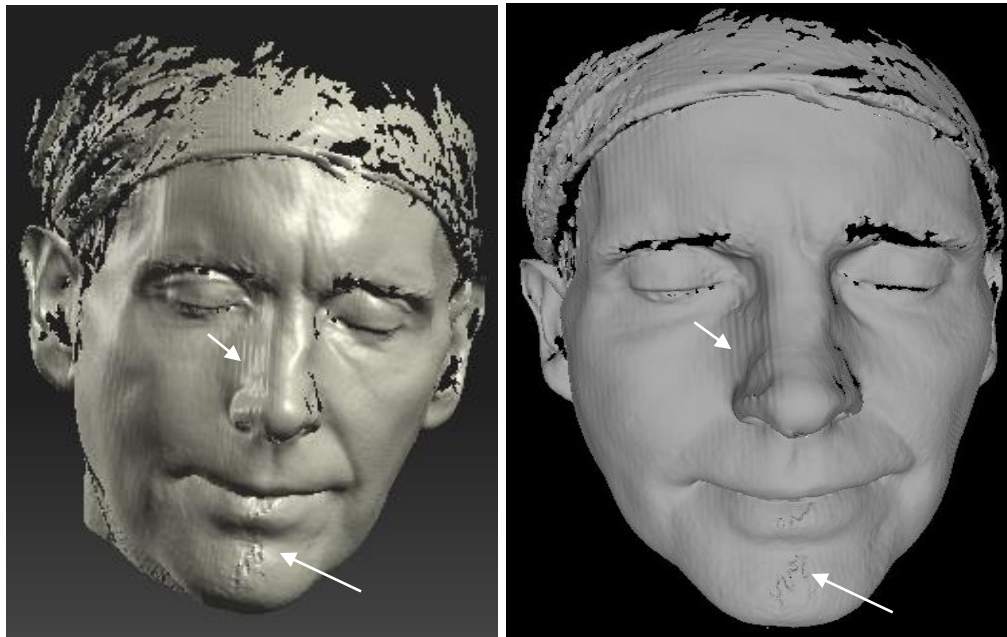


Figure 6.44: 3D geometry (fused result of noisy facial scans)

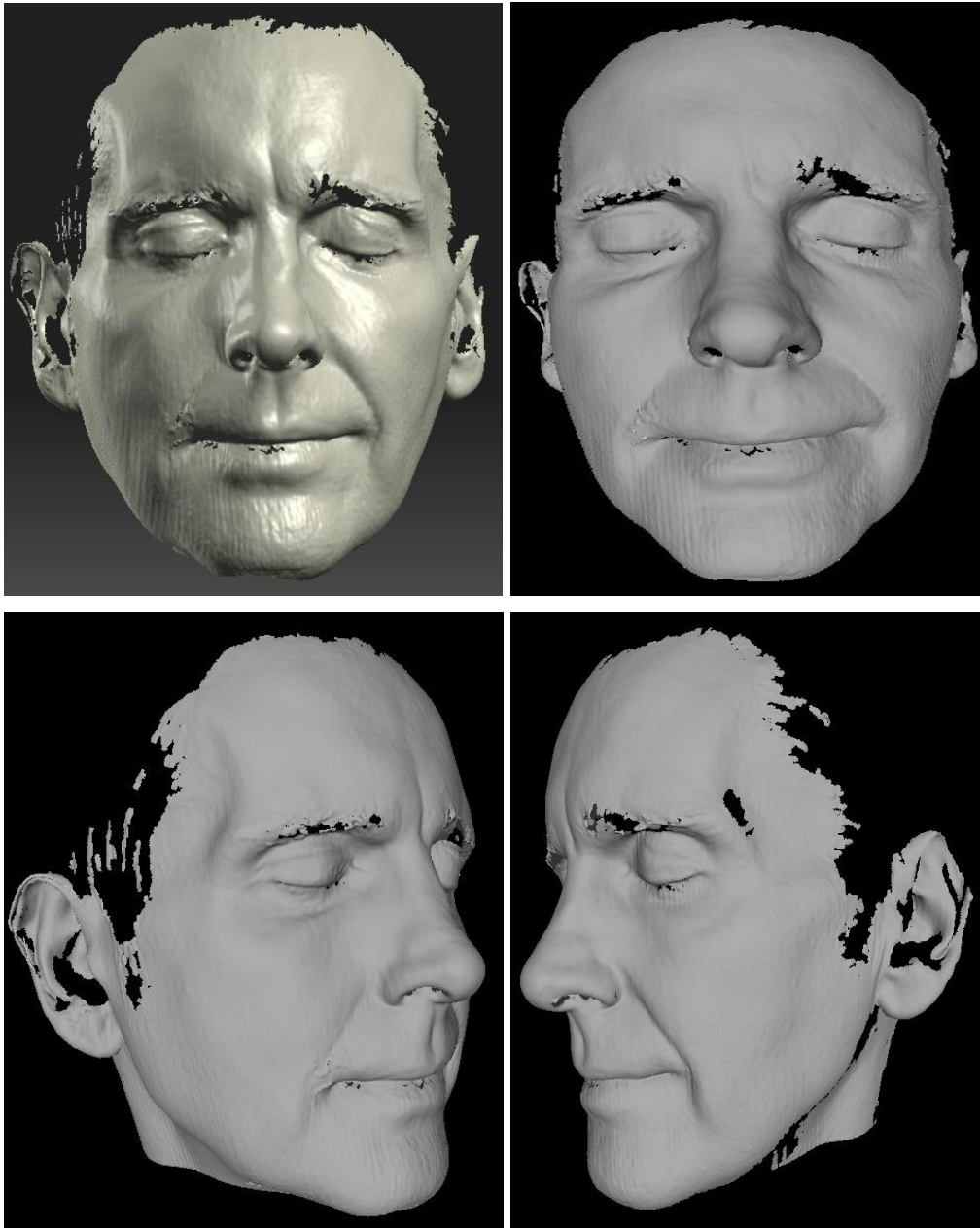


Figure 6.45: 3D geometry from different views

6.3.3.3 3D surface scanning of male dark skin faces

Two volunteers were participated to scan dark (black) skin. The aperture was adjusted to almost the maximum to allow the camera to see the dark skin with more illumination, and the shutter speed and brightness were kept to the recommended values (1/60 sec and 255 lumens). The dark skin clearly reproduced in the raw 3D scans. These scans had the same unrecorded areas as in previous results and some scans had fine vertical ridges. However, the best scans were selected for fusion. The fused result of one volunteer is shown in Figure 6.46. The colour bar comparison result of the same subject is displayed in Figure 6.47, the deviation was around +0.1

mm between the reference and each test scan (no deviation). Whereas the colour bar comparison result of the second subject showed deviation around 0.3 mm between the reference and each test scan (moderate deviation).

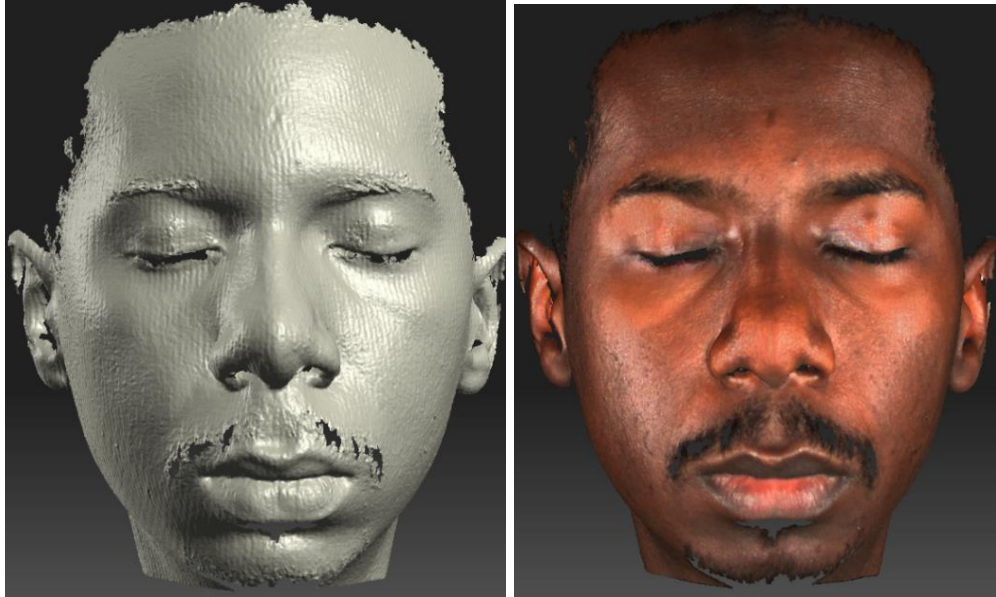


Figure 6.46: 3D geometry and colour-textured result of dark skin face

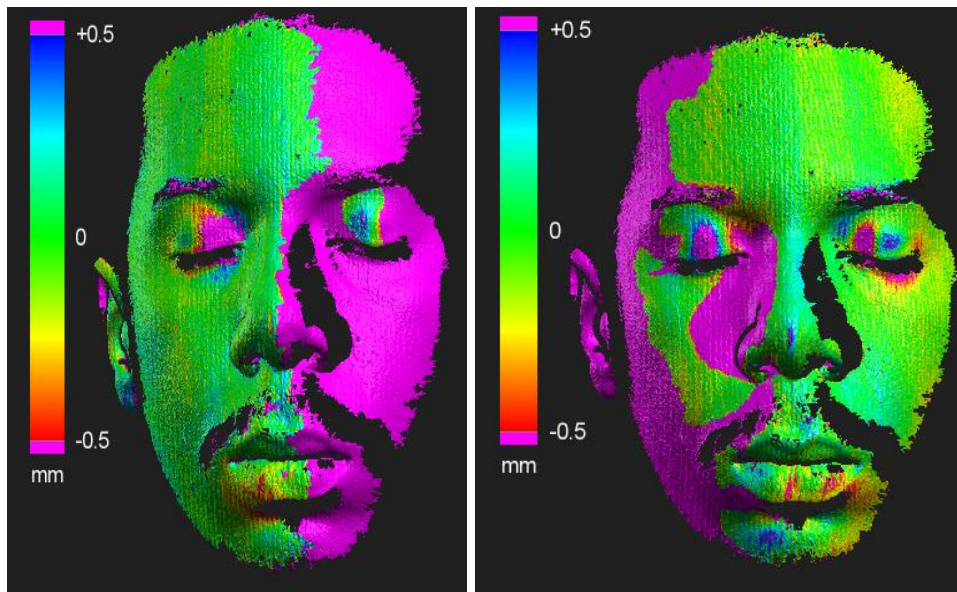


Figure 6.47: Colour bar comparison result of dark skin face
(Deviation around 0.1 mm)

6.3.3.4 3D surface scanning of female brown skin faces

Two female volunteers with brown skin were scanned. This colour was also clearly reproduced. The raw scans of the first participant had vertical ridges in four of the nine scans, and she was more cooperative. The raw scans of the second participant had vertical ridges in 8 of the 14 scans, as the participant was restless and felt

uncomfortable breathing during the recording time. The raw 3D scans had similar unrecorded areas as in previous results; however, the best scans were selected for fusion. Regarding the colour bar comparison result, the first case, the deviation in overlapping area between the reference and each test scan was around 0 mm. In the second case, the deviation was around +0.4 mm between the reference and right scan and around 0.3 mm between the reference and left scan (moderate to severe deviation).

N.B. Figures of female facial 3D scanning are not shown.

6.3.3.5 3D surface scanning of bespectacled faces

Two participants were scanned with and without eyeglasses. The scanning results showed that the lens rim, bridge and areas behind the temples of both sides were not recorded (see arrows in Figure 6.48). Shadow behind the lens rim was inspected in the raw scans and in the final result with colour texture. Mild to severe vertical ridges were seen in three of nine scans. The results of the second volunteer had the same findings; however, all scans (11 scans) were rough because of his skin texture and fine movement.

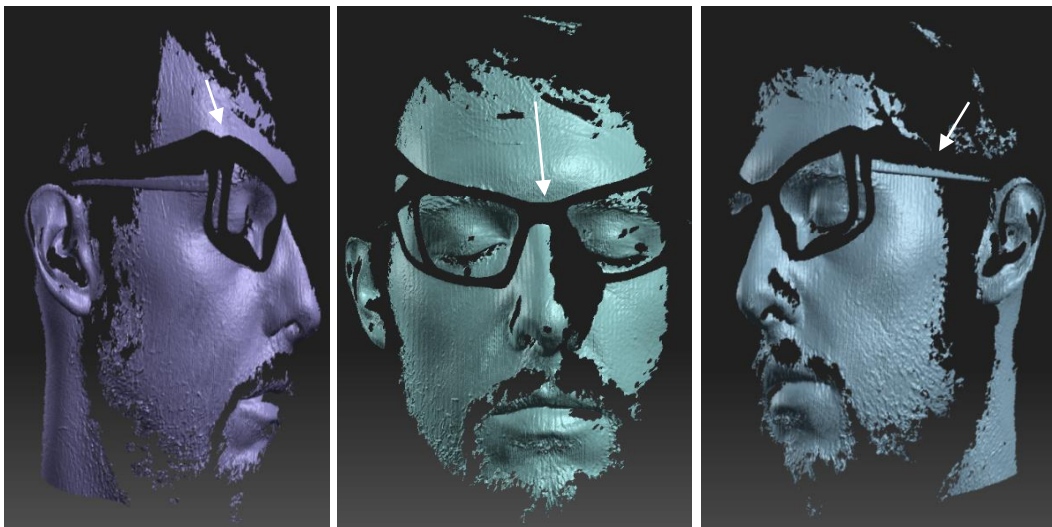


Figure 6.48: 3D raw facial scans without colour-textured information shows glasses artefacts

6.3.4 Discussion

6.3.4.1 Evaluation of fused results

In previous publications, the face scanning was done using 3D surface scanning methods that were designed for the face (Figure 6.49), such as Vectra 3D facial scanner (Urbanova, 2016) and 3dMD face scanner, (Goodwin, Evison and Schofield, 2010; Aynechi et al., 2011; Ort et al., 2012). Minolta laser scanner was used for facial

scanning while participants sitting on a rotatory chair (Kovacs et al., 2006-a). 3D methods that can be easily manipulated to scan the face, such as single camera-photogrammetry (Buck et al., 2018) has also been used.



Figure 6.49: Vectra XT 3D facial scanning (left) and 3dMDface system (right)³⁰

However, in this application, the face was scanned by the single camera structured light scanner that was not specifically designed for face scanning. As a result, a manual face-turning technique was used. Although the face was turned manually to the right and left view, the final fused result of the frontal, right and left view was coherent and homogenous and had no overlapping artefact because (1) the volunteers kept their heads in the same position; (2) the volunteers kept their facial expression neutral; (3) the turning was done while the head was held in the same position; (4) facial muscles are small and overlap with each other, which means that when the face was turned, the facial muscles were turned as one mass, with no change in their contours. Therefore, the fused results were visually accepted. Moreover, details of the face geometry were also satisfactory. According to Buck et al. (2018), the details of the face geometry resulting from a structured light scanner based on light patterns are better than those of the Artec 3D Space Sider hand-held structured light scanner and single camera photogrammetry.

Additionally, the facial 3D scans were evaluated using 3D scan deviation analysis. The colour bar comparison of the software (HP 3D Scan Pro 5.3.0) was used to assess the raw 3D scans for any deviation (6.3.2.4). The frontal view was used as a reference scan. The comparison result in the overlapping area between the reference and test scans (right or left views) was interpreted on the basis of the colour of the result. For example, a green colour represented zero deviation in the overlapping

³⁰ (Aynechi et al., 2011).

area (completely matched scans). The next value was around +0.1 to -0.1 mm (no deviation between scans), which was represented by green to sky and green to yellow. In the investigated scans, the results of the colour bar comparison were around 0 and 0.1 mm. However, 0.2, 0.3 and 0.4 mm deviations were also obtained when the volunteers were restless during scanning. This means that the deviations in overlapping areas were related to the movement of the volunteers during scanning.

6.3.4.2 Defects of raw data

Although the fused results were visually accepted and had no overlapping artefacts, some defects were noted in raw 3D scans, such as unrecorded facial hair-bearing areas, improper recording of the left sides of the scans and movement artefacts in some scans. All defects are discussed in the following section:

6.3.4.2.1 Unrecorded facial hair-bearing areas

The scanner had difficulty recording hair-bearing areas, such as eyebrows, moustache and beard. The scanner's algorithm seemed to skip or ignore the hairy surfaces. However, in some cases, sparse eyebrows were partially recorded. This means that recording of the hairy areas is based on the density of the hair. The structured light patterns scanner (the ATOS system from GOM), hand-held scanner (the Space Spider from Artec 3D), and photogrammetry based on Photoscan have difficulty capturing scalp hair and facial hair, particularly when the hair is denser (Buck et al., 2018). Moreover, the Vectra H1 does not generate a mesh in hairy areas and produces holes instead (Urbanova, Hejna and Jurda, 2015). Therefore, when the area of interest is a face or hairy surface, it is better if it is shaved before scanning (Ebert et al., 2015; Villa, 2017-a).

6.3.4.2.2 Improper recording of the left sides

The left side of the nose and left ear in the frontal view were unrecorded. The left border of the left view was not fully recorded. This failure was caused by a technical reason related to the angle of the single camera. The range of recommended angles was 20°-25° (3D Printer Superstore, 2015). When the camera angle was set within the recommended range, the camera looked to the right side of the object more than the left side and therefore the scanner recorded the right-side areas more than the left side areas. This was explained in depth in [6.2.3.1](#). However, the left border of the left view could be improved by turning more to the right or using a dual-camera

scanner. Also, the unrecorded left side of the nose and left ear in the frontal view was abolished by fusing all scans together (frontal, right and left scans).

6.3.4.2.3 Roughness

This was noted with two volunteers, when the raw scans were inspected without colour-texture. It could be related to skin texture or to movements as both volunteers were moving. Fusing all scans together almost abolished the roughness of the raw scans, particularly if a negative sharpness value was used in the fusion step.

6.3.4.2.4 Vertical ridges

There were obvious ridges in some raw 3D scans when the scans were magnified on the screen. In some cases, they were fine ridges, and in the two following situations, they were clearly noted when:

1. The quality profile was tested on the first volunteer, the raw 3D scans were clearly affected by the movement and vertical ridges were obtained (Figure 6.50 left). This is because the scanning time of the quality profile was longer than the speed profile (it was around 30 sec x 3 including the time needed to turn the face to right and left view).
2. One of the volunteers had intermittent involuntary movements and another volunteer was restless and felt uncomfortable breathing during the scanning. The speed profile was used with both volunteers (Figure 6.50 right).

Goodwin, Evison and Schofield (2010, p. 16) obtained localised ridges in two different types of mannequin heads, one PVC and the other polystyrene. They cited that the ridges are “due to a lighting bias or the particular sensitivity of a lightweight object to subtle unevenness in the platform surface”. However, in this application, the ridges were clearly related to the subject’s movement or breathing, and selection of scans that were free from these ridges addressed this problem.

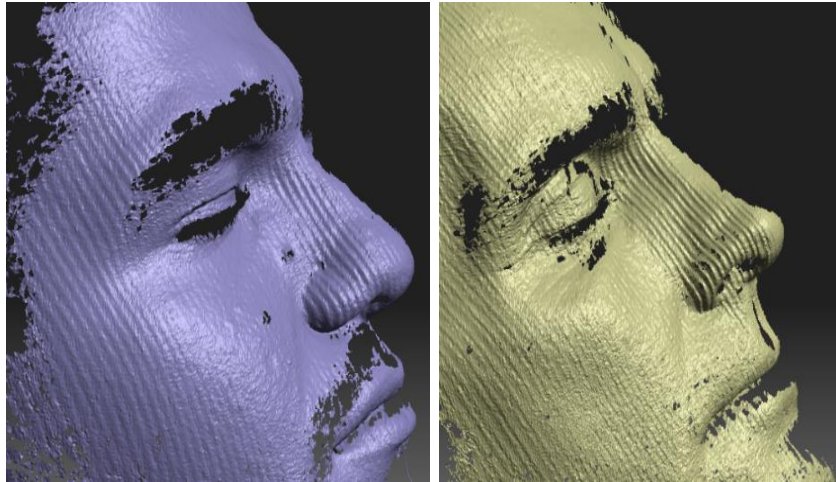


Figure 6.50: 3D raw facial scan with vertical ridges

6.3.4.3 Impact of scanning time

The speed profile was selected to conduct the face scanning as it was the shortest scanning profile. The total scanning time was 15 sec (scanning time) x 3 (number of scans) + turning time (time was needed to turn the face to right and left view). The volunteers were mostly able to keep still and tolerate this time. But, when the quality profile was tested, it consumed more time, it was about 30 sec x 3 + turning time and the subject could move during this prolonged time. As explained above, the quality profile was associated with movement artefact (vertical ridges). Moving the scanner instead of turning the face was tried, with the face kept in the same position and the scanner moving to right and left view, it was noted that the total recording time was extended. This is because after recording the frontal view the scanner was moved to the right or left view, as each time the scanner had to be moved and placed in the correct distance. Kovacs et al. (2016-a) stated that the greatest challenge in face scanning is minimising movement artefacts. They investigated three experimental techniques with different scanning times and analysed the precision of the results of each technique. In the first technique, 30° right and left face scanning was done with a one-camera laser scanner. The participant sat on a rotary chair and was manually rotated. The scanning time of this setting was 2.5 sec x 2 and the overall examination time was 45 sec. In the second technique, the participant sat on a computer-guided rotatory chair and a 360° head model was generated with a scanning time of 1.5 sec x 6 and overall examination time of 90 sec. In the third technique, two scanners were connected, and 30° right and left face scanning was done in sequence. The scanning time was 2.5 sec x 2 and the overall examination time was <10 sec. They found that the results of the last experimental setting were more precise because the overall examination time was reduced and repositioning of the test subject was avoided.

6.3.4.4 Impact of glasses

Lens glasses did not introduce artefacts in the scanning result as glass is a transparent surface and most of the light passes through. The lens rim and bridge were not recorded. Face areas behind eyeglass parts were not recorded as the areas were hidden behind. Leipner et al. (2016) scanned a face with glasses by botscan (multi-camera photogrammetry) and found that the eye-area in the result is partially occluded because of the shadowing; accordingly, they advised removing the glasses before the scanning to minimise artefacts (Figure 6.51 left). However, there was no occlusion was shown in the case of structured light scanning in this study (Figure 6.51 right). When the face is scanned to record injuries, the glasses are not required, but when the face is scanned for other purposes such as recognition, the glasses may be needed, and the scanning will need special care.

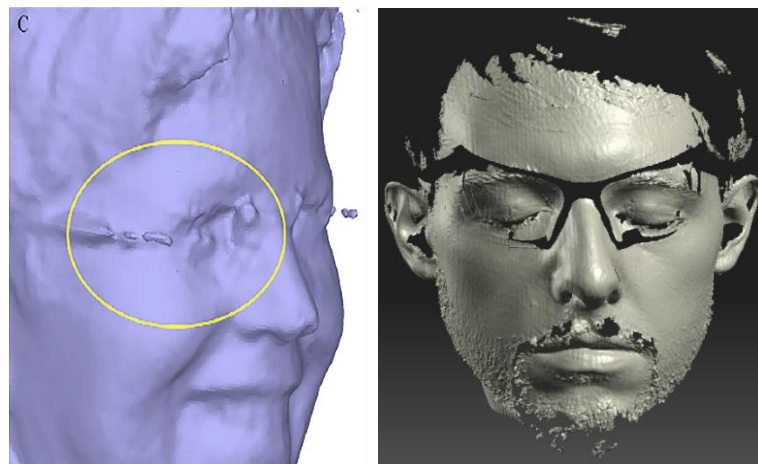


Figure 6.51: Facial scanning with eyeglasses using botscan (left) and structured light scanner (right)

6.3.4.5 Impact of processing computer

Using the HP computer with HD graphic card was not convenient for the scanner's software so displaying the result in colour-texture was not perfect; it was wrapped by horizontal stripes, whereas processing the information on an Alienware computer (GeForce GTX card, 770) eliminated these lines. However, the quality of the raw scans or fused result from each computer without colour-texture was the same.

6.3.4.6 Impact of skin colour

It was noted that production of the colour-textured information of light skin faces was not completely satisfactory. However, the colour-textured information of brown and dark skin faces was much better than that of light skin faces. When the correct aperture was used with light skin faces, the colour-textured information was orange-tinted.

To display this problem, two different scanning were run on the same light skin face by two different processing computers, computer-1 was the Alienwaire, and computer-2 was the HP, the main specifications of both computers are shown in Table 6.9.

Table 6.9: Main specifications of used computers

Computer	Type	Processor	Ram	Graphic card	Total graphic memory
Computer-1	Alienware	I 7	16 GB	GeForce GTX (770)	11227 MB
Computer-2	HP	I 7	16 GB	GeForce GTX (1050)	9929 MB

With each computer, the scanning was done three times or more and with the correct aperture³¹, which was reduced to different levels.

Figures 6.52 and 6.53 show the scanning results in the computer-1 and computer-2. Orang-tint colour-textured information was clearer when the scanning was operated in the computer-2; additionally, the results of computer-2 were warped with stripes which were mostly related to the graphic card.



Figure 6.52: Left scan with correct aperture and right scan with the smallest aperture (Alienwaire computer)

³¹The correct aperture produced a sharp image in the camera view which created a sharp object and projected pattern with no overexposed areas alongside well-controlled sinewaves. According to the scanner instruction, the well-controlled sinewaves almost reaches the blue lines in the live image.



Figure 6.53: Left scan with correct aperture and right scan with the smallest aperture (HP computer)

Exposure of the scanner was controlled by shutter speed, light brightness and aperture. The shutter speed ranged from 1/60 sec to 1/5 sec, seven shutter speed options were available. It was recommended to use 1/60 sec (3D Printer Superstore, 2015; HP customer support-instructions, 2018). It was also recommended to use a light brightness of 255 lumens (3D Printer Superstore, 2015). The aperture was the only setting that could be changed until the correct exposure was obtained. It was obvious that the unsatisfactory colour-textured of the light skin faces was associated with scanner exposure boundaries, in addition to the direct projection of the white light to the skin. However, this area will require additional analysis to study in depth the interaction of the structured white light and the different colour of the human skin. Melanocytes in the superficial layers alongside the absorption and scattering of the structured light in the skin could have a role in explaining these results.

6.3.5 Conclusion and Recommendations

Face scanning was possible with the HP structured light 3D surface scanner and with manual face-turning technique. Although some defects were obtained in the raw scans, most of them were abolished in the final fused results, such as roughness of the raw scans and the unrecorded left side in the frontal view or left margin in the left view. Assessment of the facial scanning using the 3D scans deviation analysis was good. The deviation values in overlapping areas between the reference and test scans were around 0 or 0.1 mm, if the volunteers were quiet during scanning. However, 3D facial landmarks measurements are required to consider and compare to the direct manual measurements for more validation of the same technique.

Suggestions that may be valuable to try instead of using the manual face turning technique include the following:

1. Using an ordinary office rotary chair with a head support.
2. Using a special chair connected to an automatic turning table and attached to an apparatus that supports the head in two areas, top and under chin. However, Kovacs et al. (2006-a) found that external fixation of the head is unlikely to be accepted by the volunteers and suggested projecting a grid as an alternative solution that can help to guarantee the correct position. Also, they concluded that acceleration and deceleration of the computer-guided rotatory table have an impact and cause motion artefacts.
3. Using a dual-camera scanner, with two cameras on both sides of the projector.

Chapter 7: Documentation of traumatic wounds in clinical forensic medicine involving structured light 3D surface scanning

The study in this chapter is executed to achieve the second objective of the research, which is: *to assess the method's capability for reconstructing traumas from living subjects in clinical forensic medicine*. Therefore, the 3D structured light scanner was transported to the Medico-Legal Centre for testing with live injured volunteers. The 3D results of the structured light scanning were evaluated in comparison to 2D results of digital photography; the comparison was based on a subjective visual assessment of both documents. Additionally, the 3D wound length measurements were compared to conventional measurements (ruler and 2D measurements) to determine whether there were any significant differences. A technical comparison between the 3D surface scanning method and digital photography was also discussed.

Therefore, this chapter first, provides materials and methods, results, discussion and a conclusion of this application. Later, it presents difficulties associated with this application and how these are addressed or, alternatively solutions are suggested. This is followed by a presentation of the results of the assessment of the 3D models of the most difficult body areas using wound measurements comparison, and 3D data deviation analysis.

7.1 Materials and Methods

7.1.1 Setting of the study

The work was conducted in the Centre of Clinical Forensic Medicine in Benghazi, Libya during April and May 2017. It was performed during medico-legal examination. All required equipment was available in the work room, e.g. a ruler, tape measure, disinfecting solution, a rigid photographic scale, a chair, digital camera, a Pico Scan structured light 3D surface scanner, participant information sheets and informed consent forms.

7.1.2 Participants

The volunteers were injured live victims who had been referred to the centre for medico-legal examination. Selection of the participants was based on the following criteria:

- Age: ≥ 18 years.
- Gender: males and females.
- Participants had no pain.

- Participants could walk and stand.

Those who were requested to participate obtained brief oral information about the project, read the participant information sheet and signed the informed consent form.

7.1.3 Injuries

The selection of injuries was based on the following criteria:

- Injuries located on upper and lower limbs, and torso.
- Injuries that had no active bleeding.
- Injuries that had no signs of infection.

A range of traumatic forensic injuries (blunt and sharp force injuries and firearm injuries) were involved. All data were anonymous.

7.1.4 Data collection

The data collection was gathered according to following categories:

- History taking and wound examination.
- Wound documentation.
- Wound measurements.

7.1.4.1 History taking and wound examination

The history was achieved by asking the participants some questions (see data collection sheet in [Table A.1](#) in Appendix A). Two questions were helpful throughout the examination and during the 3D wound interpretation on the screen. These questions were about the time of the violence and the type of the causative instrument. Wound examination data were obtained by inspection and writing notes about: wound type; wound site; wound dimensions (length and width or length only); and type of causative instrument from a researcher's point of view.

7.1.4.2 Wound documentation

Wound documentation was done using the Pico Scan structured light 3D surface scanner and Nikon D70 digital camera with a close-up lens + 4. The scanner has been described in detail in [4.2](#). The scanning principles that were suggested in [5.5](#) were followed in order to scan the injuries of the living cases. The wound digital photography was done considering basic photographic practice. The scanning principles and photography considerations are presented in 7.1.6.

The 3D and 2D documentation results were compared based on a subjective visual assessment. Fifty-seven wounded live victims participated. Fifty were males and seven were females. The different types of traumatic injuries were recorded by both methods (Table 7.1).

Table 7.1: Types and number of recorded injuries by Pico Scan structured light 3D scanning and digital photography

Blunt force injuries	Sharp force injuries	Firearm injuries	Unclassified injuries	Swelling
16 abrasions	11 stitched cut wounds	7 (3 recent and 4 old)	2	1
9 bruises	6 superficial incised wounds			
2 abraded bruises	3 stitched stab wounds with surgical intervention			
2 contused wounds with swelling				

Note that four wounds of firearm injuries were old because some wounded victims asked to come again for re-assessment after a healing period. All cut and stab wounds were stitched because the victims had already obtained medical intervention before they sought the medico-legal examination.

7.1.4.3 Wound measurements

Wound measurements were taken to compare the 3D measurements to traditional measurements. Plassmann and Peters (2001, p. 25) stated that “for a measurement to be of any value it must be possible to compare it with other measurements”.

Almost all recorded injuries in this work were closed. Thus, the recorded injuries that had length dimension, such as superficial incised wounds, stitched cut wounds, longitudinal abrasions and scratches were used for wound measurement comparisons. Twenty injuries were selected, and the measurements were taken manually and digitally.

The manual measurements were taken during the medico-legal examination using a ruler in mm or tape measure. The digital wound measurements were taken from 2D photographs and 3D models and called 2D and 3D measurements. The 2D measurements were taken after uploading the scaled photographs into Image J

software; this is free and open source software (<http://rsbweb.nih.gov/ij/download.html>). A scale was used to calibrate the software. A line selection tool was selected from the toolbar, and a 10 mm line was drawn on the scale. The set scale was selected, and 10 mm was used as the known distance. The straight-line tool was selected again to measure the longest length of the wounds by measuring the distance between two points. The 3D measurements were taken after importing the 3D model into the 3D MeshLab software, using a measuring tool to measure a distance between two points. This is also free and open source software (<http://www.meshlab.net/#download>). All measurements were taken from the same starting point of the recorded dimensions. All measurements are displayed in Table 7.2; they ranged from 10 to 85 mm.

N.B. The manual measurements were taken during the medico-legal examination, while the digital measurements were taken later on computer screen.

Table 7.2: Wound measurements of the recorded dimension using manual, 2D and 3D methods

Wound	Manual measurements	2D measurements	3D measurements
Wound 1	10	10.14	12.04
Wound 2	15	14.31	14.59
Wound 3	15	18.73	17.44
Wound 4	15	15.01	14.75
Wound 5	17	19.27	19.47
Wound 6	18	18.81	18.97
Wound 7	19	16.27	17.47
Wound 8	20	16.24	17.03
Wound 9	30	29.16	29.39
Wound 10	40	40.43	37.34
Wound 11	40	33.26	29.25
Wound 12	42	42.32	42.97
Wound 13	45	49.68	49.32
Wound 14	55	51.89	51.9
Wound 15	60	58.97	59.66
Wound 16	71	73.61	71.22
Wound 17	79	72.85	76.51
Wound 18	80	68.22	66.92
Wound 19	80	83.93	80.15
Wound 20	85	82.83	82.90

7.1.5 Measurement analysis

The statistical analysis was achieved using IBM SPSS Statistics 23 software. Excel 2016 was used to create bar charts of the measurements.

The measurements were statistically analysed by the Friedman test to determine whether there was a statistically significant difference between the traditional wound measurements and 3D measurements. The Friedman test was used instead of One-way repeated measures ANOVA test because the collected data were not normally distributed. Assumption of the normality of the ruler, 2D and 3D measurements was considered using visual methods and numerical tests. The histograms had no approximated shapes of normal curves, but the box plots and Q-Q plots were visually normal. However, the visual methods of assessing the normal distribution are heled to be unreliable (Ghasemi and Zahediasl, 2012). Also, they may not be helpful when the sample size is small, fewer than 50 (Kim, 2013). The numerical methods of assessing the normality test, such as Shapiro-Wilk test and Z-test using Skewness and kurtosis were applied. The Shapiro-Wilk sig. value was < 0.05 in three groups, which means the data significantly deviated from the norm, whereas the Z- values were somewhere between -1.96 to $+1.96$ (Table 7.3). Therefore, the decision was taken to change the parametric test (One-way repeated measures ANOVA) into a nonparametric test (Friedman test).

Spearman's Rank-Order Correlation Coefficient was considered to determine the strength of a relation between the measurements of the three methods. According to Bland and Altman (2010), the product-moment correlation coefficient (r) measures the strength of a relation between variables (each two variables).

The Intra-class Correlation Coefficient (ICC) test was used to assess intra-observer reliability of the 2D and 3D measurement methods. According to Koo and Li (2016), the ICC is a desirable reliability index. Two-way mixed model and absolute agreement were selected. The test (ICC) compared two sets each of the 3D and 2D wound measurements that were taken from the same wounds on two different occasions (two weeks apart) by one observer.

Table 7.3: Results of numerical tests of normality

Measurements	Sample size	Shapiro-Wilk Sig.	Z-Skewness	Z-Kurtosis
Manual	20	0.017	0.8	0.3
2D	20	0.028	0.8	1.3
3D	20	0.016	0.9	1.3

7.1.6 Wound documentation protocols

According to Plassman and Peters (2001, p. 25), “measurements without protocols are not only useless but can be dangerous”. Therefore, wound documentations by the 3D surface scanning and digital photography were done by following some rules.

7.1.6.1 3D scanning principles

The scanning principles that suggested in [5.5](#) were followed as guidelines to scan injuries of living subjects. Briefly, they involved the following rules:

1. Scanning only the injured surface in the stationary manner was used as a standard 3D scanning technique.
2. The number of scans measured was more than three. The final number of post-processed scans was based on a desirable mode of presentation in MeshLab software. For example, the flat mode required only two data set, whereas the wireframe mode needed more than three.
3. Although placing a black screen behind the scanned area (behind the subject) was highly recommended to eliminate the background noise and preserve the acquired raw 3D data, it was not used in this application. This is because the scanning was conducted in a complete dark room, and the data were free from background noise.
4. Three different suggested scanning approaches were followed with some adjustments. Scanning approach no. 1 was applied to access different injured areas of the upper limbs. It was applied as it is and was useful. Scanning approach no. 2 was applied to access different injured areas of the lower limbs. However, some participants preferred to raise the foot or leg up on the chair rather than allow the scanner to be moved up or down. Injuries on the thigh were scanned while the participant in sitting position. Scanning approach no. 3 was applied to access the chest, abdomen and back. The volunteers were scanned in the sitting position rather than in the standing position. This is because chest scanning in the standing position was confirmed to be unsatisfactory in [6.1.2.3](#).
5. The room light was switched off during the calibration and 3D scanning; there was no source of natural light and therefore the room was totally dark.

7.1.6.2. 2D digital photography guidelines

Issues surrounding the photography protocol and best practice have been discussed in [2.3.4](#). With that in mind, the wound digital photography was done considering the following:

1. Camera type

A DSLR camera, Nikon D70 with a sensor of 6.24-megapixel and focal length ranged from 18-70 mm was used. The sensor was APS-C (Advanced Photo System type-C), and the crop factor (focal length multiplier) was 1.5.

2. Camera sitting

Manual mode was used to choose an appropriate aperture size (f-stop), shutter speed and ISO. The f-stop used was between f4 to f6.3, shutter speed was around 1/30 sec and ISO was 400.

3. Lens

A Hoya (+4) close-up was screwed over the primary lens of the camera. The close-up lens was used to reduce the minimum focusing distance of the camera lens and allow it to focus more closely on the subject (Canon, 2017). This was used to achieve an element of magnification (hence, element of detail) in the 2D results. Although a ring light flash is preferable with close-up photography, it was not used because it had been tested before and it was found to produce pale-coloured results. Therefore, the aperture (f-stop) was the key setting to compensate for the element of light loss (light block) in the close-up photography. An ISO of more than 400 was not used to avoid grainy results as the sensor of the Nikon D70 was cropped. The shutter speed was around 1/30 sec; a slower shutter speed of less than 1/30 sec was not used to avoid blurred results since the camera was hand-held and the subjects were not static. Therefore, opening the aperture was the main setting to have better exposure. The f-stop used was between f/4 – f/6.3; two injuries were captured with f/9 and f/20.

In this work, as the close-up lens was used, and the recorded wounds had variable sizes, focal lengths were variable. Therefore, for each injury one focal length of around 24-35 mm was used, followed by a second of around 40-50 mm. Treuillet et al. (2009, p. 754) proposed that “no zooming value is fixed, to leave the operator free to choose the best centering for a large variety of wound sizes”.

4. Camera position

In this work, injuries were located on different areas of the body, so it was impossible to fix the camera on a tripod. Therefore, it was hand-held parallel to the wound.

5. Photographic scale

A straight rigid scale with matte finish was used. The scale was placed on the surface of the skin on the same plane as the injury to avoid scale distortions. The scale was

not used to estimate the wounds sizes, it used only to calibrate the ImageJ software; for that reason, the straight scale was used with all different types of the injuries.

6. Participant position

The digital photography, 3D scanning and the manual wound measurements were all obtained in the same posture.

7.2 Results

The results below are displayed in two main sections: a comparison between 3D and 2D documentation results and a comparison between 3D and conventional wound measurements.

7.2.1 Comparison between 3D and 2D documentation results

The structured light 3D scanner was generally able to reconstruct wounds from living subjects. The recording wounds were closed traumatic injuries, such as abrasion, bruise and stitched wounds. Therefore, the comparison below centred on evaluation of 3D documentation results of the 3D scanner compared to the 2D results of the digital photography. The comparison, which was visually on screen, it was an overall comparison to observe the differences between both documents.

Although at first glance, the overall presentation of both results was similar, the 3D models of the scanner had extra features over the 2D photographs. These features are presented below:

7.2.1.1 Final 3D models represented the 3D surface geometry of the wounded areas

The active 3D surface scanning computed 3D coordinates (x, y, z) of the object's surface points and represented the 3D surface geometry of the scanned area with colour-textured information; and therefore, the shape of the wounded areas in the 3D results had a high degree of adherence to the original shape. Whereas the digital photography created flat 2D photographs with two dimensions (x & y). Figure 7.1 shows a small ordinary contused wound with moderate swelling in 3D and 2D presentation. The 3D result (3D document) was able to represent the swelling in a more original form. While the 2D result was flat. The same can be seen in Figure 7.2.



Figure 7.1: 3D document (first) and 2D document (second) of small ordinary contused wound with moderate swelling



Figure 7.2: 3D document (first) and 2D document (second) of longitudinal brush abrasion

N.B. Different types of abrasions (blunt force injuries) can be found in [Appendix B](#) in 3D and 2D documents (Figures B.1-B.7).

7.2.1.2 Final 3D models displayed the wounded areas without clutter

The scanner scanned an object between determined distances (minimum and maximum distance). Any object beyond the maximum distance could be acquired as noise with the 3D data; however, this kind of the noise could be controlled by using a black screen ([5.3](#)). Any other unwanted, proximal item (e.g. the stand) was removed manually using the Mephisto process software before the final processing. Therefore, the final 3D results displayed only the wanted area without clutter or extra information. In contrast, the 2D images of standard digital photography could be crowded because the 2D image has a depth of field, i.e. the interested object could be presented with background and foreground clutter. However, using close-up digital photography usually produces an image with little depth of the field especially if a longer focal length is used. In this work, some 2D results presented the interested area with surrounding items and background clutter when the shorter focal length was selected.

7.2.1.3 Final 3D models reflected true scales

The active 3D surface scanning did not require placing a scale around the object as it represented actual size 3D results. Therefore, the 3D results had no scales and that provided extra advantages, such as:

- The 3D results were free from type 2, 3 and 4 scale distortions.
- Important findings in the 3D documents were never obscured by the scale.
- The 3D measurements were achieved quickly and could be repeated more consistently.
- There was no risk of infection.

Generally, 2D results are always presented with scales; these can obscure the trauma and make the wound measurements difficult to obtain.

7.2.1.4 Final 3D models showed the full image of the wanted area

Structured light 3D scanners can record an entire field of view at once instead of one point at a time (Georgopoulos, Ioannidis and Valanis, 2010; Ishii, 2012); for that reason, when the injury was distributed on a larger surface, such as fabricated multiple superficial incised wounds on the back, the 3D surface scanner was able to reconstruct almost the full image of the wounded area. The close-up digital photography, with a longer focal length such as 40 mm, produced a narrower angle of view, and reduced the total recorded area of the fabricated injuries. Another example of 2D restriction was two healed bite marks on the anterior aspect of the right forearm. The 3D scanner reconstructed the full image of both of the marks in one model (Figure 7.3 first), whereas the close-up digital photography, with focal length 31 mm, captured each bite mark in a separate photograph (Figure 7.3 second and third).

It should be mentioned that the size of the reconstructed area presented by the 3D scanner was based on the size of the calibration board. The calibration process was obtained by using the recommended calibration board size (25x18 cm); this size was convenient for the reconstruction of most sizes of wounded areas in this work, apart from smaller size injuries. However, the board size can be increased or decreased based on the size of the scanned area.



Figure 7.3: 3D and 2D documents of two healed bite marks

7.2.1.5 Final 3D models had unique ability to be manipulated on the screen

3D results can be manipulated on the monitor because the results have three axes (x, y, z). This manipulation offers the examiner greater visualization, the option to follow the direction of some injuries, and to pick an exact starting point of the greatest wound dimensions. On the other hand, digital photography generates flat and static images, using two axes (x & y).

7.2.1.6 Clarity of the 3D results

The 3D surface scanning was carried out in the dark room, only the scanner emitted direct white light to illuminate the surface of the wounded area. Exposure were kept within recommended values. The shutter speed (Tv) was set within 0'6 -1/10 to obtain uniform illumination (as the projector had a frame lag). ISO was set between 100-200. The aperture value (Av) was decided during the calibration process to avoid under or over exposure. All these controlled factors contributed to produce clear 3D results. However, in case of human skin, the aperture value should be selected with caution; the reasons will be explained in 7.5.3.1 and 7.5.3.2. The clarity of the 3D documents played an important role in wound interpretation. For example, it was useful for interpretation of the colour change of a bruise. It is well known that the colour change of a bruise is used to estimate the time of an assault. Figure 7.4 clearly shows the colour change of the bruise in the 3D result, which better corresponded to the time of the trauma than the 2D result (aperture and shutter speed were f/6.3 and 1/30 sec). The bruise of this example was recorded 5 days after the attack. The clarity of the 3D document was also useful for recognizing nearly healed bruises when there were multiple bruises from different occasions. With cut wounds that had been stitched, their 3D surface scanning outcomes were clear. The wound edges, margins and angles were all clear and easily interpreted (Figure 7.5 and Figure 7.6). The healing process of stitched cut wounds was also exposed clearly in 3D result (Figure 7.7). Regarding the digital photography, the ISO, shutter speed and aperture values required more considerations; the clarity of the 2D results is based extensively on the photographer's skills and experience. Moreover, the close-up photography can produce darker exposure images as the intensity of light that reaches the sensor can be reduced (Foster and Barker, 1996; Constant, 2000). Using a ring light flash is recommended with the close-up photography (Constant, 2000; Vecellio and Bryant, 2017); however, in this case it was not used, and therefore some 2D digital results had darker exposure and were subsequently adjusted slightly in Photoshop.

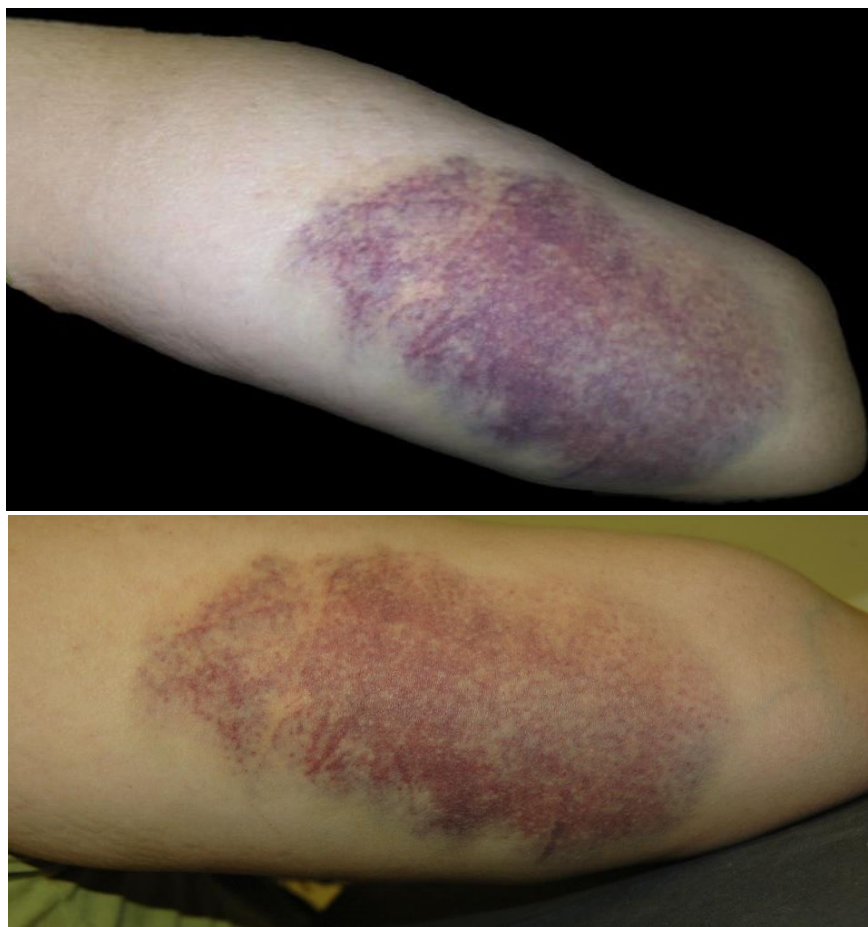


Figure 7.4: 3D document (first) and 2D document (second) of bruise on the posterior aspect of the right arm



Figure 7.5: 3D document (first) and 2D document (second) of stitched defence cut wound



Figure 7.6: 3D document (left) and 2D document (right) of stitched cut wound on the anterior aspect of the left arm



Figure 7.7: 3D document (left) and 2D document (right) of stitched cut wound on the postero-lateral aspect of the left arm

7.2.2 Comparison between 3D and conventional wound measurements

The 3D measurement method is still a novel method; is the reason for the comparison, to know if there is a significant difference between ordinary and 3D measurement methods. Twenty wounds were selected and measured. The recorded dimensions ranged from approximately 10 to 85 mm. Figure 7.8 shows a simple chart of the manual, 2D and 3D wound measurements and their recorded dimensions (lengths). Table 7.4 shows the mean and standard deviation of each method.

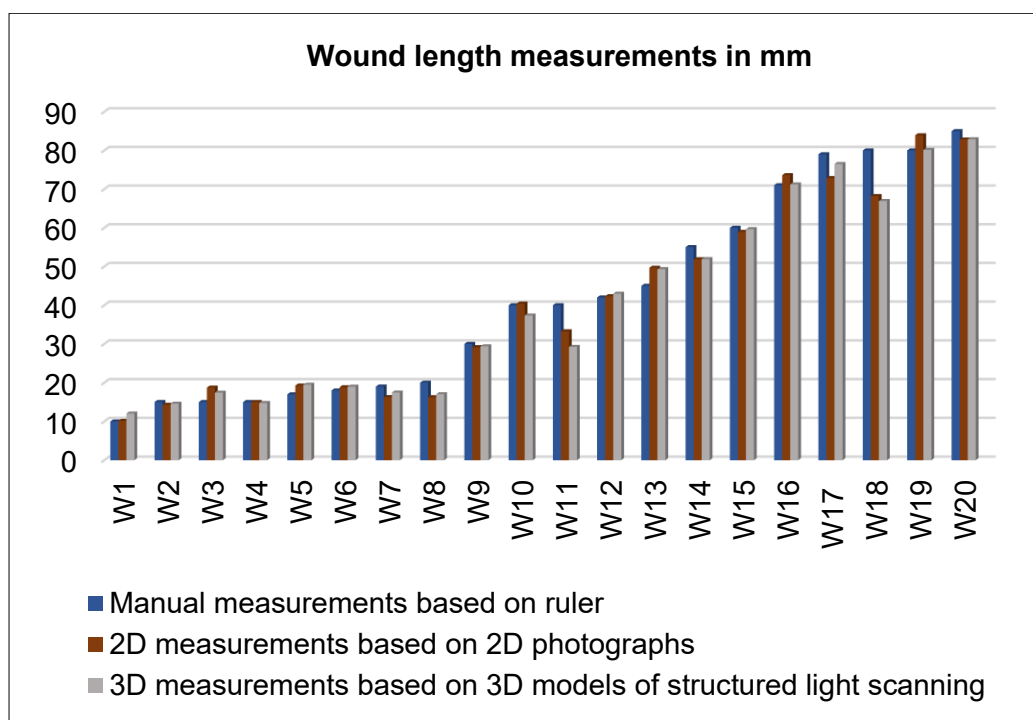


Figure 7.8: Manual, 2D and 3D wound measurements of the recorded dimension

Table 7.4: Descriptive statistics of all measurements

	Manual measurements	2D measurements	3D measurements
N.	20	20	20
Mean	41.80	40.80	40.46
Std. deviation	26.18	25.29	24.93
Minimum	10	10.14	12.90
Maximum	85	83.93	82.90

The Friedman test demonstrated that there was no statistically significant difference between the measurements: $\chi^2(2) = 0.400$, $p = 0.819$.

Spearman's correlation established a strong positive correlation (relation) between the measurements, which were statistically significant (Figure 7.9 and Table 7.5). Spearman's correlation between the manual and 3D measurements was ($r_s(18) = 0.967$, $p = 0.000$) and the magnitude of the relationship was 93.5 %. The correlation

between the 2D and 3D measurements was ($r_s(18) = 0.994, p=0.000$), the magnitude of the relationship being 98.8 %. The overall strong positive correlation between the conventional and 3D measurements supported the first result of the Friedman test. Intra observer reliability of the 3D measurements using the Intra-Class Correlation Coefficient (ICC) produced good reliability (ICC= 0.999) (Figure 7.10). However, the two sets of 2D measurements obtained almost the same results (ICC=0.991) (Figure 7.11).

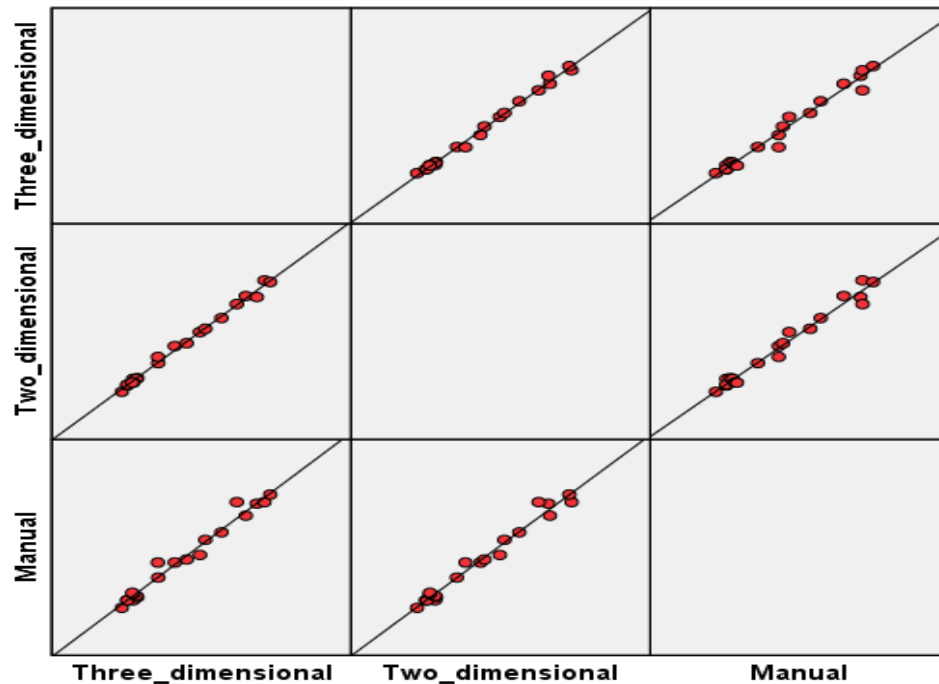


Figure 7.9: Scatterplot matrix of manual, 2D and 3D measurements

Table 7.5: Spearman's correlations between manual, 2D and 3D measurements

Correlations					
			3D	2D	Manual
Spearman's rho	3D	Correlation Coefficient	1.000	.994**	.967**
		Sig. (2-tailed)	.	.000	.000
		N	20	20	20
	2D	Correlation Coefficient	.994**	1.000	.959**
		Sig. (2-tailed)	.000	.	.000
		N	20	20	20
	Manual	Correlation Coefficient	.967**	.959**	1.000
		Sig. (2-tailed)	.000	.000	.
		N	20	20	20

** . Correlation is significant at the 0.01 level (2-tailed).

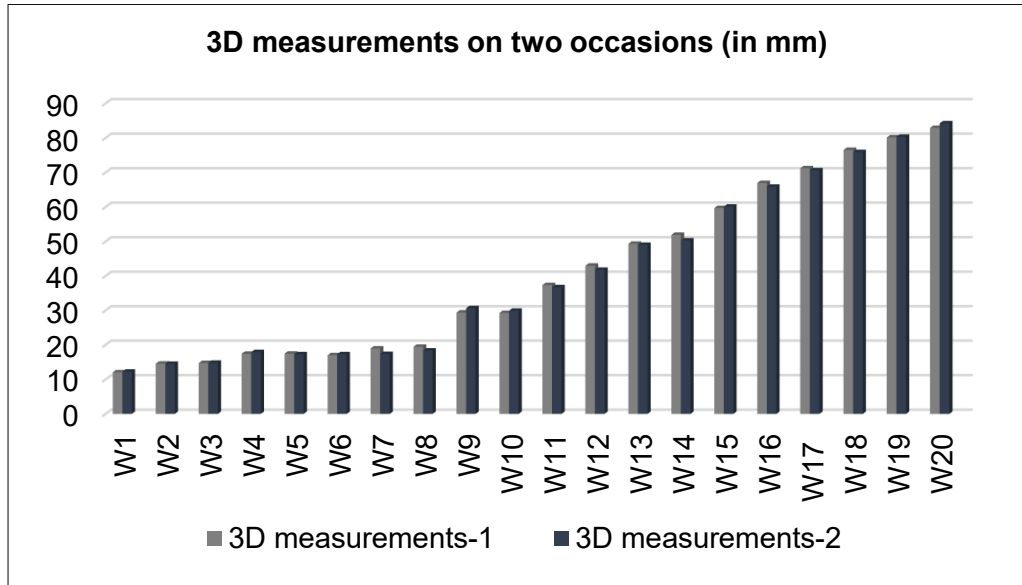


Figure 7.10: Two sets of 3D measurements of the same wound dimensions by the same observer

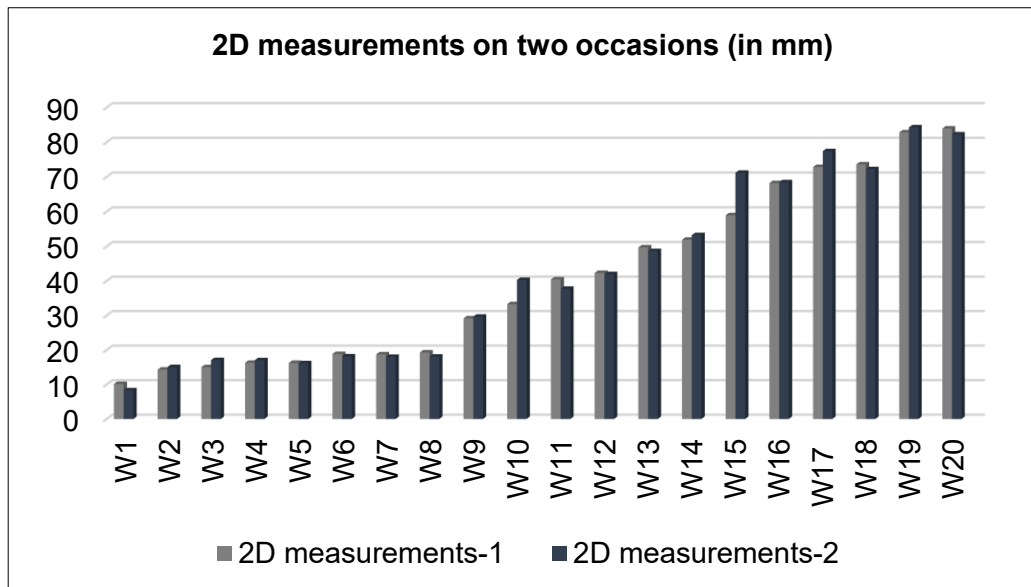


Figure 7.11: Two sets of 2D measurements of the same wound dimensions by the same observer

7.3 Discussion

In clinical forensic medicine, the examiner writes a medico-legal report about the injury explaining the type of injury, the wound dimensions, the expected causative tool, whether or not the injury will cause permanent infirmity, etc. Prosecutors rely on these reports to categorise the crime as a minor crime or criminal offence (1.2). The importance of these reports was the main motivation of second objective of this research, which is: *to assess the method's capability for reconstructing traumas*

(close wounds) from living subjects in clinical forensic medicine, to ascertain how helpful it would be in the recording of these injuries. The method was generally able to reconstruct different types of closed traumas (abrasions, bruises and stitched wounds) from living subjects. The results were visually acceptable final 3D models (geometries and colour-textured). Each of these consisted of two raw point clouds (raw data). However, 3D data deviation analysis using CloudCompare software was used first to evaluate the accepted two raw 3D data of each case in order to detect any surface deviation between them before final post-processing to 3D models. Both selected 3D data were analysed by calculating the cloud to cloud (C2C) absolute distances between them. The 3D data were found to be completely matched with no deviation (0.0 mm deviation), therefore the data processed obtained the final 3D results. The accepted final 3D results of the injuries were then compared to 2D results of the photography and the evaluation was centred mainly on document's features more than wound's features. Although 2D digital photography with a close-up lens was used in this work to capture the injuries, the 3D surface scanner was able to impose its efficiency without using the magnifying lens, and it generated more valued 3D documents. The 3D results represented the 3D surface geometry of the wounded area, for that reason the shape of the wounded areas in the 3D results had a high degree of adherence to the original shape. These results could be manipulated on the monitor, displayed only the wounded area without extra information, displayed almost the full image of the wounded area, and represented the actual scales (for that reason the scanning did not require a scale), according to Komar, Davy-Jow and Decker (2012, p. 188), "3D images are saved as microns, which are a measurement of space, rather than pixels". These advantages were in addition to the clarity of the wounded area in the 3D documents. In comparison, the 2D results were static and flat, i.e. cannot present the topography of the wounded area (Savage and Jeffery, 2013; Campana et al., 2016; Koller, et al., 2019). The 2D results had a photographic scale, an ABFO No.2 scale is usually used as a standard reference scale in forensic photography; however, Ferrucci et al. (2016, p. 509) remarked that "a review of commercially available photography scales shows a lack of consistency in quality and accuracy", implying that they are not accurate enough to be use as standard. The 2D results could include clutter around the wounded area, FFLM, (2017, p. 5) stated that clutter in the images "can provide distraction in a photo by steering the viewer's gaze away from the main focus of the photograph". The 2D results were prone to being under or overexposed. All observed limitations of the 2D results were already presented and discussed before in Chapter 2.

From a technical point of view, it has been shown that the scanning process was operated indoors with no artificial or natural light. This is because the stronger lighting conditions compete with the structured light (Abate et al., 2007; Georgopoulos, Ioannidis and Valanis, 2010; Carew and Errickson, 2019), resulting in poor 3D reconstructed data (Gupta, Yin and Nayar, 2013). Completing the process indoors meant the scanning method was not affected by the lighting condition. Also, the selection of the exposure triangle of the scanner was within recommended values. Whereas the lighting condition is not easy to control during ordinary digital photography (Bianco and Williams, 2002; Green and Schulman, 2010; Casas, Castaneda and Treuillet, 2011; Chang, Dearman and Greenwood, 2011; Marsh, 2011; Shaw and Bell, 2011; Pavlovic et al., 2015) and perfect selection of the exposure triangle requires experience. Moreover, the distance (minimum and maximum distances) had to be determined in the scanning settings of the Pico Scan 3 software. Conversely, the 2D results are susceptible to being negatively affected by improper distance (Verhoff et al., 2012). In this study, as close-up photography was used, the images were captured in the closest distance at which the lens was in focus. Furthermore, three different scanning approaches were followed to access the injuries in different areas of the body; these approaches aimed to make the scanned area face the scanner in a parallel way. However, angulation of the scanner had no impact on the 3D results since the results were generated in three axes. Casas, Castaneda, and Treuillet (2011) stated that “3D methods have been developed to obtain more accurate measurements without the constraint of the view-angle of a device”. This means that the 3D results were not affected by the angular distortion. On the other hand, a slight change in the camera angle can have influences on the 2D results, as well as on the wound measurements (Palmer, Ring and Ledgard, 1989; Rennert et al., 2009; Treuillet, Albouy and Lucas, 2009). Finally, structured light 3D surface scanning was an accurate method because: (a) it projected light patterns with a coding strategy that allowed accurate correspondence between the projected image and the captured image (Salvi, Pages and Batlle, 2004; Salvi et al., 2010; Geng, 2011; Ishii, 2012). (b) The Pico Scan structured light 3D surface scanner was based on Phase Measuring Profilometry (PMP) which is an accurate and robust principle (Salvi, Pages and Batlle, 2004; Wang et al., 2007; Georgopoulos, Ioannidis and Valanis, 2010; Lohry, Chen and Zhang, 2014). (c) The 3D surface scanning was preceded by a geometric calibration process that uses a robust and accurate algorithm to reconstruct accurate 3D results (Errickson, Thompson and Rankin, 2015; Pandy and

Cather, 2016; Errickson et al., 2017; Shamata and Thompson, 2018-a; Shamata and Thompson, 2018-b; Thompson and Norris, 2018). Conversely, the digital photography could easily introduce error or doubt in the photographs (2.3.3).

No statistically significant difference between the 3D and conventional wound measurements was found, which generally agreed with the results of Sivanadan and Lisscio (2017) and Villa (2017-a). However, Villa has compared the ruler and 3D measurements based on photogrammetry, passive 3D surface scanning. No statistically significant difference between the 3D and conventional measurements was primary evidence for the acceptance of 3D measurements based on structured light 3D scanning.

The Spearman's correlation between the 2D and 3D measurements (98.8%) was stronger than the correlation between the ruler and 3D measurements (93.5%) because the manual measurements were taken during the medico-legal examination, while the measurements of 2D and 3D were conducted afterward on a computer screen at the same time.

The 2D and 3D measurements were not influenced by skin elasticity, movements or changes in the subject's position; because of that, the measurements displayed good Intra observer reliability. Moreover, wound measurements held on the computer screen have a higher level of reliability (Anthony, 1985, cited in Majeske, 1992, p. 57).

Depth dimensions were not considered in this application. As mentioned earlier, the work was conducted in the Centre of Clinical Forensic Medicine, the volunteers were wounded live cases, and they had already obtained medical intervention. The cut, stab and contused wounds had been stitched. Thus, almost all recorded injuries were closed having length \pm width dimensions. Therefore, the depth dimensions have been considered in Chapter 8 when the scanning was applied to open injuries.

Finally, Table 7.6 shows some differences between ruler, 2D and 3D measurement methods and exposes the advantages of the 3D measurement method.

Table 7.6 Differences between 3D and conventional measurement methods

Feature	Ruler measurement method	2D measurement method (based on 2D photographs)	3D measurement method (based on 3D models)
Risk of infection	Contact method, has risk of infection	Contact method, has risk of infection	Non-contact method, has no risk of infection

Scale requirements	It requires a scale during photography	It does not require a scale during scanning
Permanent records	It has no permanent records	It provides permanent records with wound appearance & colour	It provides permanent records with 3D surface geometry and colour-textured information
The natural body curvature	It considers the body surface curvature. A tape measure is used instead of a rigid ruler for curved areas	It does not consider the body surface curvature
Measurement information	Linear dimensions (length and width)	Linear dimensions and wound surface areas	It can provide more measurement information, such as depth and volume
Depth measurements	Depth is measured by invasive tools, such as an electronic calibre or a cotton bud	Depth cannot be obtained from 2D flat photographs	Depth or volume can be measured by 3D software
Area measurements	It can overestimate the actual area of the wound by up to 10% to 44%	It can underestimate the actual area of the wound by up to 10% to 34.8%	It is an effective method for measuring the surface area
Impacting factors	Movement and changing the subject position have influences on the measurements	Distance, lighting conditions, angle of acquisition have influences on the measurements	It is developed to be more controlled method. Light conditions, angle of acquisition and distance are under control
Reliability	Subjective method, limited by Inter-observer variability	Has low Inter-observer variation	It has a lowest Inter-observer error
Accuracy	It has a questionable accuracy	It is accurate with smaller and regularly shaped wounds	It has better accuracy when compared to conventional methods

7.5 Difficulties faced with this application

Although the Pico Scan 3D scanner successfully reconstructed different types of real traumatic injuries from living victims, the work faced some difficulties. These difficulties were categorised into: problems related to using a living body, problems related to the 3D scanning method, and problems related to the improper use of the scanner.

7.5.1 Problems related to using a living body

These problems were mainly related to the movement and breathing of the living subject. They were categorised as:

- 7.5.1.1 Change of posture
- 7.5.1.2 Motion effect
- 7.5.1.3 Thoracic and diaphragmatic breathing

7.5.1.1 Change of posture

Changing the posture of a scanned area during the 3D acquisition (Figure 7.12) caused obvious overlapping artefact in the final 3D model, which is indicated with a circle shape in Figure 7.13. Changing the position caused muscle contraction and relaxation, which subsequently caused slight changes in the muscle contour. Therefore, the calculation of 3D coordinates of some previously measured points in the first view (first raw 3D data) were not at the same 3D position in the next data resulting in some points lose their alignment, and overlapping artefacts being the result (5.1).

However, selecting and processing the raw 3D data that had the same posture solved this issue. Selection was based on visual inspection, and the final 3D model was assessed by measurement comparison and raw 3D data deviation analysis and found to be precise (Section 7.6).

N.B. Figures that are presented below were taken (snapped) from 3D models in the 3D MeshLab software, or from 3D raw data in the Mephisto process software.



Figure 7.12: Changing the posture during 3D acquisition

The leg in the left 3D raw data is mostly in the upright position, while in the right data is moved slightly backward



Figure 7.13: Final 3D model of leg with overlapping artefact

7.5.1.2 Motion effect

Although the participants were aware of the need to keep still, some of them moved during the acquisition phase. This movement caused motion artefacts in the form of distorted points in the reconstructed raw 3D data. This artefact was observed mainly in the lower limb scanning. This problem was also the possible cause of the blurred 3D data in some cases.

All 3D non-contact surface scanning methods (active and passive) prefer the object to be static; however, moving objects are expected to be recorded perfectly by structured light 3D method since it is able to measure almost the entire field of view or wide field of view at once (Georgopoulos, 2010; Patil, Kothari and Bhurchandi, 2015). Although the Pico scan structured light 3D scanner is characterized by speedy 3D measurement, some results were affected by participant movement.

7.5.1.3 Thoracic and diaphragmatic breathing

In Chapter 6, it was established that thoracic and diaphragmatic breathing had negative influences on the raw 3D data of chest and abdominal areas when: (1) the volunteer was in a standing position, (2) the scanner was the Pico Scan, and (3) the holding of breath was not requested. The negative impacts of breathing were displayed in the form of (a) distorted points that were explained mostly by the movement of the participant despite their trying to stay still during the scanning time, and (b) horizontal lines that were the result of thoracic and diaphragmatic breathing. Therefore, in this application, these areas were scanned by the same scanner while the participant was in a sitting position. It was noticed that the sitting position was helpful, and reduced the negative impacts of the breathing process (Figure 7.14), if the participant was cooperative. Therefore, the final 3D results (Figure 7.15) were accepted because they were assessed by measurement comparison and raw 3D data deviation analysis and found to be precise (Section 7.6).

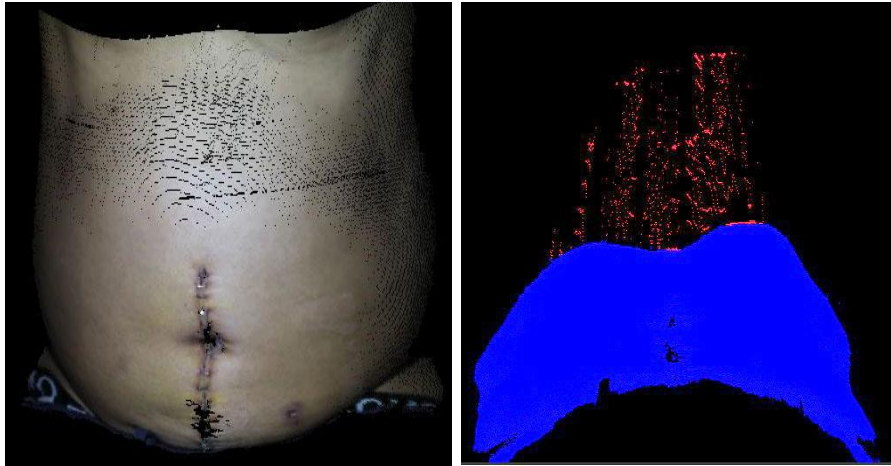


Figure 7.14: 3D raw data of abdomen

Raw 3D data with slight horizontal lines around the epigastric area (left). The same data manipulated to show few distorted points highlighted in red colour (right)

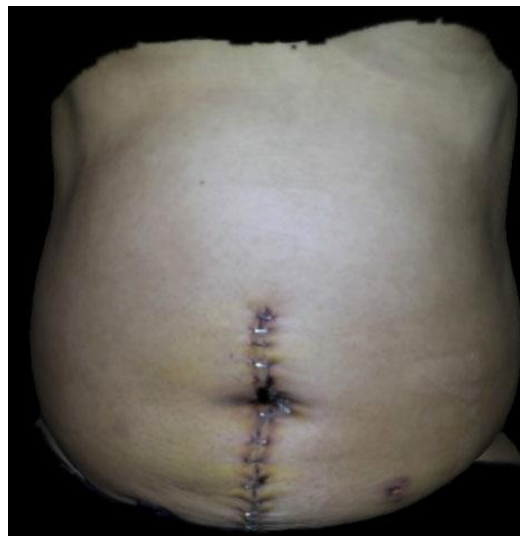


Figure 7.15: Final 3D model of abdomen

The model is resulting from processing two raw 3D data in the same inspiratory phase

7.5.2 Problems related to 3D scanning method

These issues were mainly about the failure of the scanner to scan injuries in some situations, such as:

- 7.5.2.1 Extended wounds
- 7.5.2.2 Smaller injuries
- 7.5.2.3 Wounds on dark (black) skin
- 7.5.2.4 Illumination of unwanted area

7.5.2.1 Extended wounds

Scanning only the injured surface in a stationary manner was used as a standard technique. Therefore, an extended wound that included more than one surface around the limb was not reconstructed completely, such as bruise on the anterior aspect of the arm which was extended to the medial and lateral surfaces. Plassmann and Jones (1998) wrote that an extended wound around the limb may cause problems to photography or techniques that are based on optical methods. Even if the injury is quite visible by the method and acquired successfully, wound measurements will not necessarily be reliable. This is because these methods ignore the surface curvature, and result in imprecise wound measurements.

7.5.2.2 Smaller injuries

The scanning process was preceded by a geometric calibration process, which was achieved with a standard calibration board, with a size of 21x15 squares (25x18 cm). This size was convenient for reconstructing the wounded area (an injury + anatomical area around it). In a medico-legal report, it is vitally important to describe the injury and the location of the injury; therefore, any documentation method should record the injury + the anatomical landmarks. For that reason, the photographer usually takes distance photographs in addition to close-up photographs. However, using this board size was not suitable for smaller size injuries. The scanning results of smaller injuries were not detailed, such as an inlet of a typical firearm injury or stab wound (Figure 7.16). Using a smaller size calibration board could help to reconstruct the details of smaller injuries. However, it will not be a practical solution because the recorded area will be small, representing only the injury without any anatomical landmarks. Moreover, swapping between different board sizes according to the available injury size and re-starting the calibration process would require some time. Participants do not like to wait, and the clinical forensic medicine examination office is usually an overcrowded place, requiring a quick method. For these reasons, the calibration process in this work was prepared with a standard board size in the early morning, each day.



Figure 7.16: 3D result (left) and 2D result (right) of small stitched stab wounds

7.5.2.3 Wounds on dark (black) skin

When dark skin was recorded by the Pico Scan 3D surface scanner, the intensity threshold needed to be reduced or set to zero. Even so, the injuries on dark skin were not reconstructed clearly. The injuries that were recorded were small; therefore, the unclear 3D wounds on the dark skin could be due to the small size of the injury, and not due to the skin colour. Larger wounds on dark skin are required to be reconstructed to decide whether the ambiguity is related to the wound size or the skin colour.

7.5.2.4 Illumination of unwanted area

The issue was noted in two situations in which the injury was not fully facing the scanner resulting in most of the projected light illuminating the bare, unwanted area of the body. These situations are:

1. When the injury was located on an unreachable body site, it was not easily accessed by the scanner. An example such as a site was the postero-medial of the arm (Figure 7.17 first images).
2. When the injury was located on the periphery of the expected scanned area³², i.e. when the injury was located more laterally (Figure 7.17 second images).

In these two situations, a professional hand-held scanner is a solution. It can easily access and scan unreachable wound sites.

³²The expected scanned area is an area illuminated by the light and its size corresponded to the calibration board size.

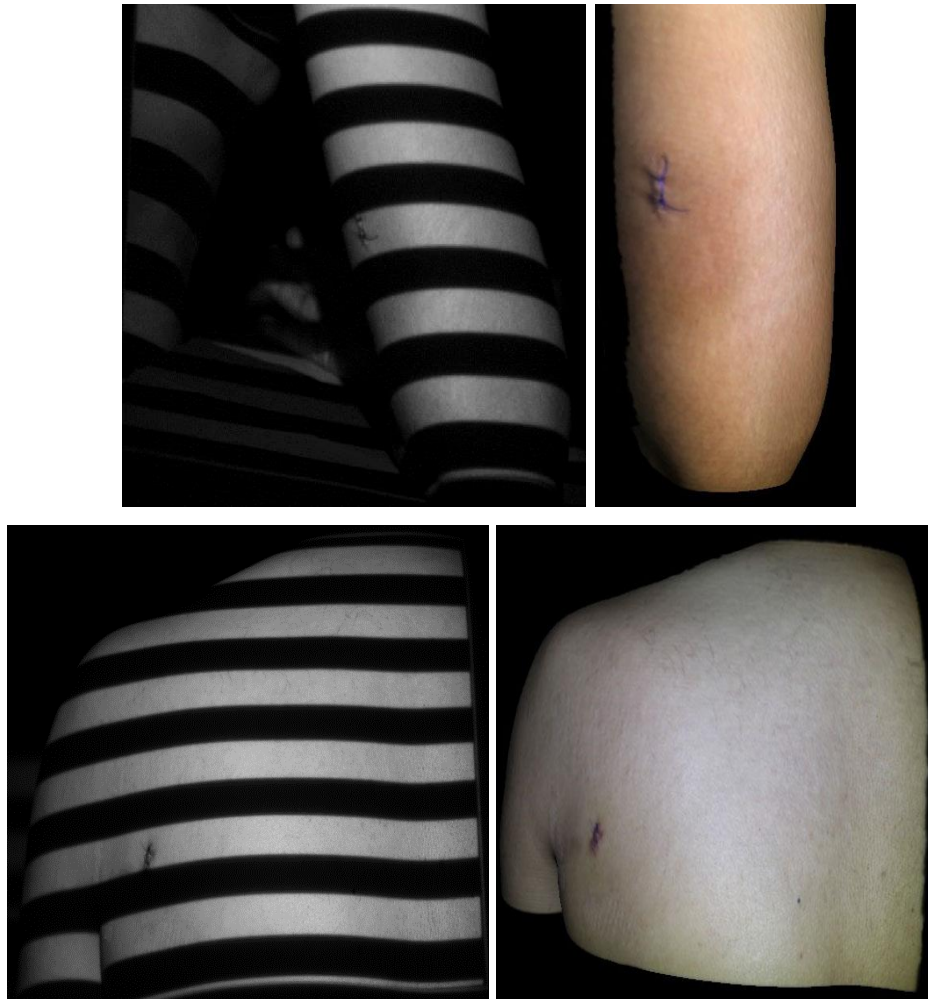


Figure 7.17: Illumination of unwanted area

First images: Stitched surgical wound located on the postero-medial aspect of the right arm, second images small stitched stab wound on the postero-lateral aspect of the left shoulder (left images are recorded with light stripes, right images are final 3D models).

7.5.3 Problems related to improper use of the scanner

The scanning of human skin required the perfect selection of exposure settings and the maintaining the exact scanning distance. Therefore, the following problems appeared when these two crucial steps were not properly applied:

- 7.5.3.1 Reconstruction inconsistent degree of skin colour
- 7.5.3.2 Reconstruction over or underexposed data
- 7.5.3.3 Reconstruction unfocused 3D data

7.5.3.1 Reconstruction inconsistent degree of skin colour

Although the participants had the same nationality, they had variable degrees of skin colour; thus, each participant required different values of aperture to represent the natural colour of the scanned area. However, it was noticed that with some participants, the skin colour reconstructed to an inconsistent degree (Figure 7.18).

Although the aperture of the camera of the Pico Scan 3D scanner had a wide range of values (from f/4 to f/25), the suitable range for the skin scanning was limited to between f/4 and f/6.3. This limited range; in addition to the projection of direct white light, could have explained this issue.



Figure 7.18: 3D result (first) with inconsistent degree of skin colour and 2D result (second)

First image is 3D model of stitched wound, the injury was reconstructed with f/5 and shutter speed 1/6 sec. Second image is 2D photograph of the same injury (Focal length: 25 mm, aperture: f/6.3, and shutter speed: 1/30 sec).

7.5.3.2 Reconstruction over or underexposed data

Reconstruction overexposed data (Figure 7.19) could take place when the area was illuminated with too much light (using a larger aperture). As explained above (7.5.3.1),

the suitable aperture range with the skin was limited to between $f/4$ and $f/6.3$; therefore, an unsuitable selection by the user within this limited range could have simply caused overexposure with projected direct white light.

Reconstruction underexposed data (Figure 7.20) could be explained by the choice of an inappropriate value of the intensity threshold because the intensity threshold was required to be considered with darker skin colour. The selection of a smaller aperture setting was another explanation.

The issues demonstrated above (7.5.3.1 and 7.5.3.2) imply that the exposure setting is important in the case of human skin digitization.

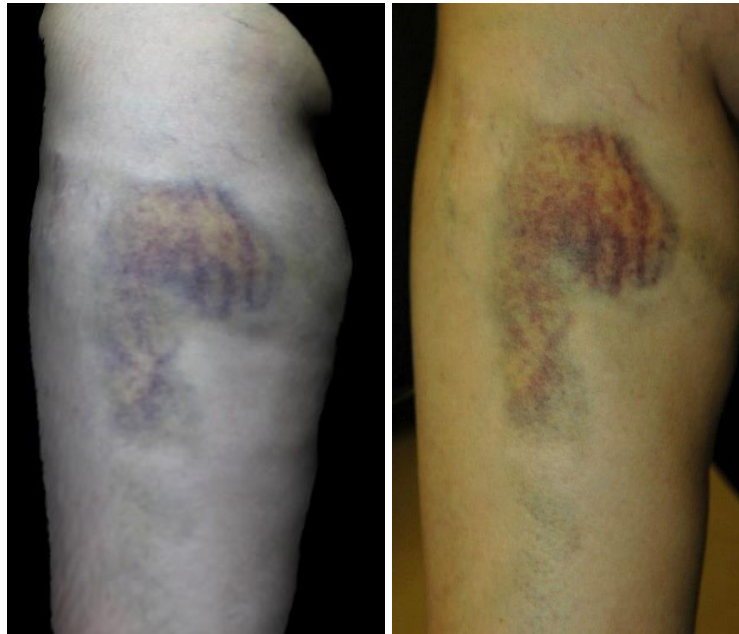


Figure 7.19: Overexposed 3D result

Left image is overexposed 3D model of bruise located on the upper medial aspect of the right leg, the aperture value of the scanner was $f/5$ and shutter speed was $1/5$ sec. Right image is 2D photograph of the same injury (Focal length: 31 mm, aperture: $f/6.3$, and shutter speed: $1/30$ sec)



Figure 7.20: Underexposed 3D result

Left image: Under exposed 3D model of un-healed firearm injury on the lower medial aspect of the left leg, it is also not in focus. The aperture, shutter speed and intensity threshold of the scanner were $f/5.6$, $1/8$, and 5. Right image: 2D photograph of the same injury (Focal length: 29 mm, aperture: $f/4$, and shutter speed: $1/30$ sec)

7.5.3.3 Reconstruction unfocused 3D data

The scanning process was done using the same distance at which the camera and the projector were in focus, i.e. the same distance at which the calibration was obtained. Therefore, changing the distance led to loss of camera and projector focus, and the loss of calibration. The same situation could occur when the scanner was shaken.

In Chapter 6, the scanner was prepared (calibrated) for a particular height to approach a particular area (either areas of upper limb, lower limb or torso). In this way, upward and downward adjustment of the tripod was avoided, and thus shaking of the scanner and loss of the exact distance was avoided. Whereas this application was conducted in a Medico-Legal Centre, and the researcher could not anticipate the location of the injury. Therefore, different wounded areas of the upper limb were usually scanned from the exact distance because the wanted area could be rested on the ordinary stand using the pre-set distance mark. Scanning the wounded areas of the lower limb involved the use of a chair as some participants preferred to support their raised foot or leg. Injuries of the thigh were scanned while the participants were in a sitting position, as were scans of wounded areas on the torso. Scanning while the participants were sitting on a chair or had raised their leg onto a chair required

adjustment of the tripod in order to move the scanner down, which both could lead to the loss of the exact distance and obtaining out of focus 3D data. In addition to this, movement was another factor explaining blurred, out of focus results. Figure 7.21 shows out of focus recent 3D firearm injuries.



Figure 7.21: Out of focus 3D result

Left image is 3D model of three inlets of firearm injury on the upper lateral aspect of the right leg, the 3D result is not satisfactory because of lacking the exact distance during scanning. Right image is 2D photograph of the same injury (Focal length: 35 mm, aperture: f/6.3, and shutter speed: 1/30 sec).

Finally, carrying out research work in an active and overcrowded area was not easy and not completely comfortable for the researcher. However, there is a need to test research methods in the field. The Medico-Legal Centre, which was the working area where this research was located, was a busy place. A further consideration is that when the participants (who had originally come for a medico-legal examination) agreed to take part in the research, they usually asked it to be done as quickly as possible.

7.6 Assessment of torso and lower limb 3D models

As mentioned earlier in Section 7.5.1.3, scanning the torso faced some difficulties arising from the breathing process; however, scanning this area in the sitting position reduced the negative impacts of breathing. There was also the problem of changing the posture of the lower limb during the 3D acquisition time, which caused obvious overlapping artefacts in the final 3D image (7.5.1.1); nevertheless, selecting and processing data with the same posture solved this issue.

Torso 3D models and lower limb models were evaluated using the following analyses:

7.6.1 Wound measurement comparison

7.6.2 3D data deviation analysis

7.6.1 Wound measurement comparison

3D wound length measurements that had been taken from four 3D models of the torso and a lower limb model were compared to ruler measurements, and the difference was calculated. The differences between the measurements ranged from 0.33 to 2.1 mm. These were small differences, and it suggested that a difference of less than or up to 5 mm (0.5 cm) was not considered significant.

7.6.2 3D data deviation analysis

Two raw 3D data of each example measured above in 7.6.1 were analysed using CloudCompare software to detect any surface change (deviation) between the two 3D point clouds (raw data). The analysis was done before final post-processing. The higher density point cloud was used as a reference cloud and the second one was used for comparison. The analysis was achieved by computing the absolute distances from each point of the compared cloud to the reference cloud (cloud to cloud, C2C, distances). However, before the distances were computed, both sets of data (reference and compared data) were closely aligned. Then the cloud registration was carried out, the registration being based on the Iterative Closest Point (ICP) algorithm to minimize the difference and the distance between the two 3D entities.

The results were displayed in the colour and deviation values. In all examples, the compared data was completely matched to the reference, and therefore the difference between the two entities were in the blue zone (0.0 mm deviation). C2C comparisons and histograms of only two examples are shown below (Figure 7.22 and 7.23).

N.B. This type of analysis was applied to all accepted 3D raw data in this study. In all cases, two selected raw 3D data were compared and found to be completely matched to each other (0.0 mm deviation).

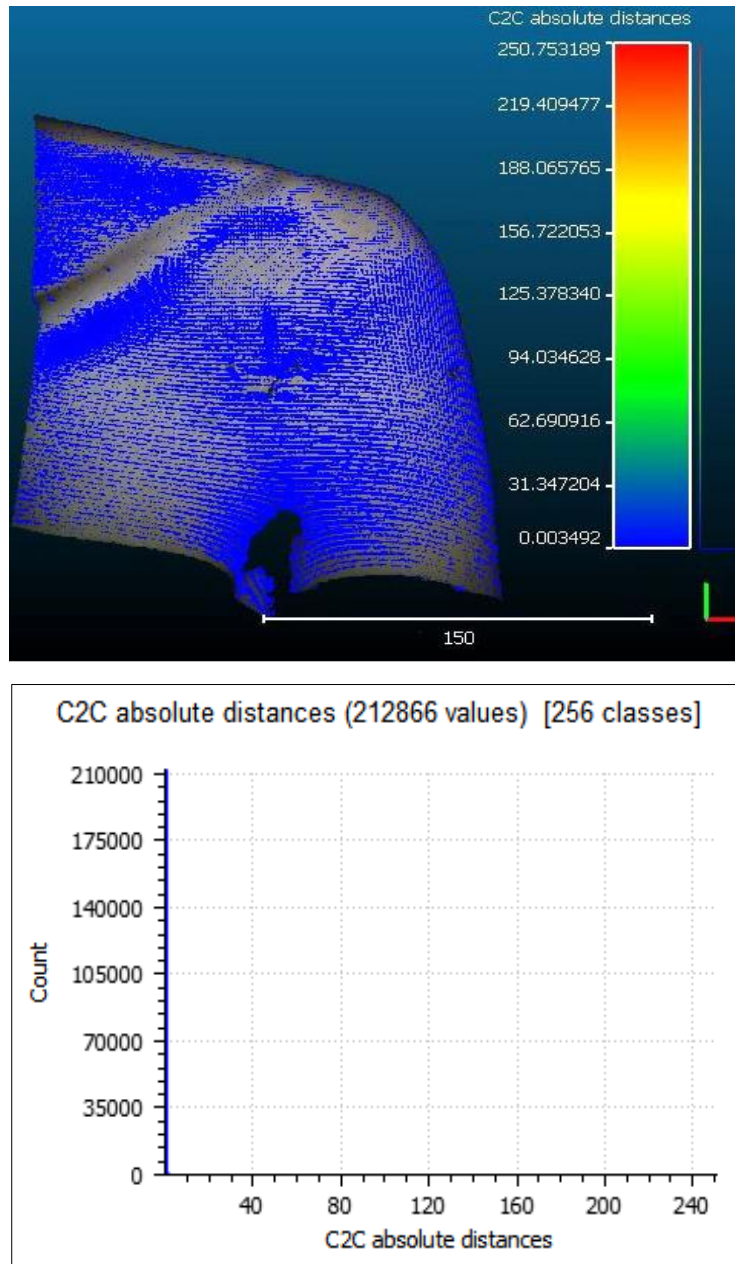


Figure 7.22: C2C comparison between two 3D raw data of the anterior aspect of the left shoulder (first) and its histogram (second)

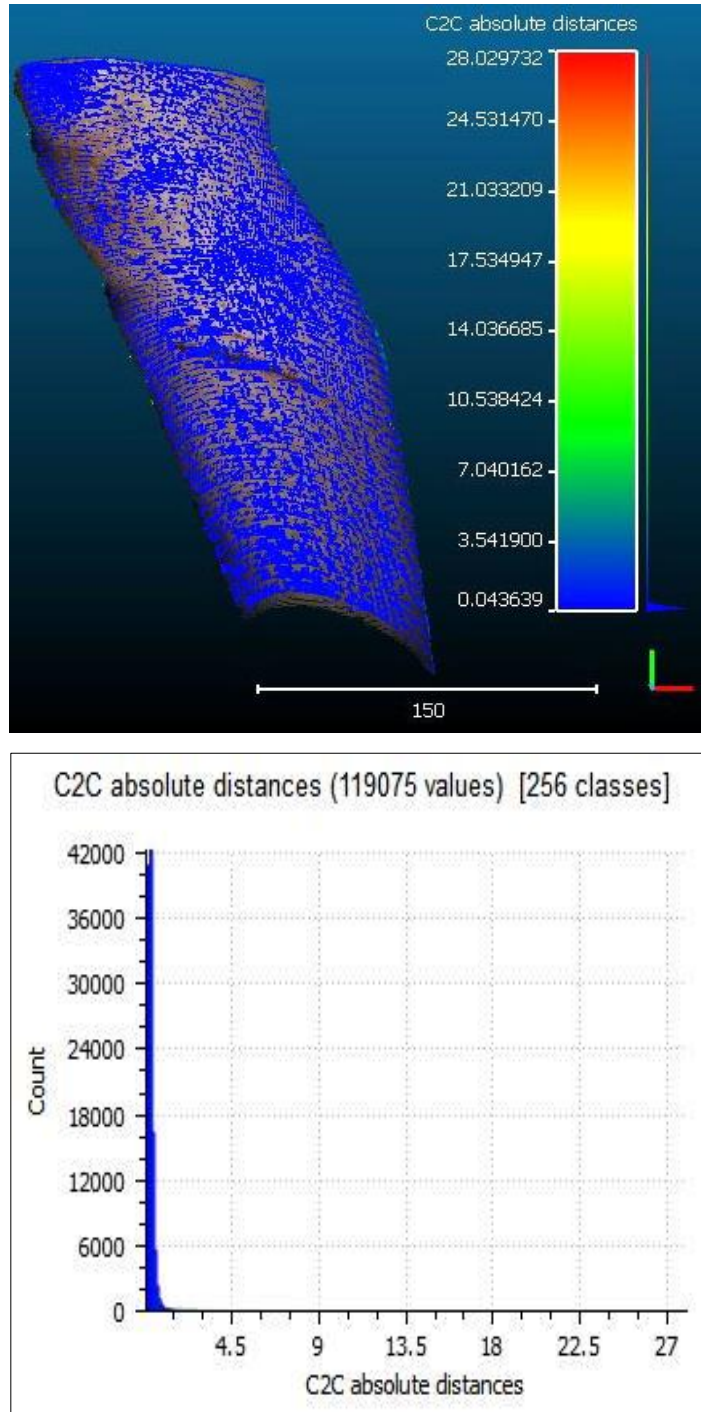


Figure 7.23: C2C comparison between two 3D raw data of the upper lateral aspect of the left leg (first) and its histogram (second)

In conclusion, the assessment that is demonstrated above showed that the difference between the manual and 3D wound measurements using the torso and the lower limb models ranged from 0.3 to 2.1 mm, which is considered not significant. Moreover, the 3D raw data deviation analysis of the same models completely matched, and revealed

zero deviation. Therefore, both assessments means that the tested models were precise.

7.7 Conclusion

Although the application faced some difficulties, the work here demonstrates that a revised 3D method was effective in reconstructing traumatic injuries from living bodies. The results were acceptable 3D models of different types of traumas. When the 3D results of this method were compared to the 2D results of digital photography, they were found to have extra features and advantages over the 2D results. The 3D results represented the 3D surface geometry of the wounded area, could be manipulated on the monitor, displayed only the injured area without extra information, represented the actual size and thus a scale was not required during the scanning, and displayed almost the full image of the injured area. These advantages are in addition to the clarity of the documents. On the other hand, the 2D results were flat and static, had a photographic scale, could include clutter when presenting the wounded area, and were prone to poor exposure. Moreover, the 3D scanning method was able to overcome the main deficiencies of digital photography in relation to the lighting conditions, angle of acquisition and the distance. Furthermore, the 3D surface scanning that was based on structured light was an accurate technique.

Friedman test showed no statistically significant difference between the conventional and 3D wound length measurements, and there was a strong positive correlation between the measurements established by the validity of the 3D measurements based on the Pico Scan 3D surface scanning. Moreover, the intra-observer reliability of the 3D measurements was good (0.999).

In light of the above, the Pico Scan 3D surface scanner can be used as a recording method to record real traumatic wounds of living victims. However, the method still requires some improvements to make it more easily applicable in the field.

Chapter 8: Determining the effectiveness of structured light 3D surface scanning for the assessment of open wounds

In Chapter 7, a range of traumatic injuries on living subjects were scanned by structured light 3D scanning. The wounds included different types of traumatic injuries, such as abrasions, bruises and stitched wounds. The injuries were closed, and the participants were living persons. In this chapter, open injuries having complicated areas and depths located on static mannequins were scanned using the same technique. Therefore, the work here addresses the third objective of the research, which is: *to evaluate the possibility of using structured light 3D surface scanning for digitizing open injuries containing complicated areas and depths*. The 3D results of open injuries were assessed visually, then the results were compared visually to the results that were obtained by digital photography; the comparison mainly focused on the sharpness of the features of the injuries in both 3D and 2D documents. Wound measurement comparisons between the 3D measurements and conventional measurements (manual and 2D methods) were also evaluated to validate the 3D measurements; the measurements included wound length, width, surface area and depth. Moreover, a brief comparison between the complete and limited 3D surface scanning of the injured mannequins was done to ascertain which one would be more practical and applicable to wounded cadavers. Furthermore, the repeatability of the structured light 3D surface scanning was confirmed in two different ways: using CloudCompare software to detect any surface change between the two 3D entities of the same object, and by repeating the wounds scanning and their area measurements.

Therefore, this chapter starts by providing materials and methods, results and a discussion of structured light application to open injuries. Then it presents separately the repeatability assessment of structured light scanning. Finally, the chapter summarises the overall conclusion of the chapter.

8.1 Materials and Methods

8.1.1 Mannequins and Injuries

In forensic medicine, open injuries are usually seen on cadavers; for this research, corpses were not involved due to ethical reasons. Additionally, it is difficult when autopsies are carried out in environments that have little control when relatives are very close to the autopsy room and behave in a disruptive manner. Accordingly, it was supposed that reconstruction of the traumas from dead bodies is similar to

reconstruction of the traumas from mannequins; particularly the wet, moist and hairy surfaces of real open wounds have been tested by structured light 3D surface scanning and their results were satisfactory (6.1.2.4). Therefore, the decision was to use mannequins instead of real bodies.

Eight mannequins were used to mimic the bodies and comprised different parts of the human body. Six mannequins were shaped from forensic cases. They were hand-made by alginate life casting. They comprised: two heads (head A and head B); a leg and foot; a wrist and hand, and two hands (hand A and B). Each mannequin had a traumatic injury, the total number of wounds amounting to six traumatic injuries. The injuries were two explosion injuries at the top of the heads A and B, a cut wound on the leg, a lacerated wound on the dorsal aspect of the hand, a suicidal cut wound on the wrist, and a cut wound on another hand. All of them had interior (depth and volume).

A further two mannequins (A and B) represented the sacral areas and buttocks shaped from a 74-year-old woman, and they had pressure injuries. All of the injuries were good examples to be scanned because most of them had depth, the deepest was around 3 to 5 cm, and they had undermined area and tunnelling. Mannequin A was Seymour II Wound Care Model-0910 and mannequin B was Stant Stage 4 Pressure Injury Model-0970. Mannequin A had four stages of pressure injuries and mannequin B had only stage-4 and stage-3 injuries. The total number of pressure injuries on these two mannequins were nine, some of these were located on the lowermost part of the mannequins and others were located on lateral aspects. The stage-4 injuries in both mannequins were located on highly curved areas. The overall surface of both mannequins was uneven.

All the described injuries above were shaped from real cases to ensure applicable results (scanning and measurement results). Therefore, the injuries had variable shapes and sizes as would be found in reality. The wound shapes were irregular, but some wounds had few well-defined shapes. The wounds were of smaller and larger sizes. The total number of injuries amounted to fifteen injuries: eleven injuries had depth and volume, three injuries had undermined areas and tunnelling, and four injuries were closed. They are summarised in Table 8.1. Each injury was scanned by the structured light 3D scanner and recorded by the professional digital camera. The measurements were taken from all injuries.

Table 8.1: Types and number of recorded injuries on artificial mannequins

Mannequin	No. of injuries	Type of injuries
Mannequin A (sacral area)	7	Stage-1 to stage-4 pressure injuries. Un-stageable pressure injury. Deep tissue pressure injury (DTPI). Long surgical wound.
Mannequin B (sacral area)	2	Stage-3 and stage-4 pressure injuries.
Head A	1	Explosion injury.
Head B	1	Explosion injury.
Leg & foot	1	Cut wound.
Wrist & hand	1	Suicidal cut wound with tentative marks.
Hand A	1	Cut wound.
Hand B	1	Lacerated wound.

8.1.2 Structured light scanning

Structured light 3D surface scanning was conducted using an HP 3D surface scanner Pro S3. The scanner was fully demonstrated in [4.3](#). The scanning was conducted in a dark room (M8.03). The computer was an Alienware (i7 processor and GeForce GTX (770) graphic card). Figure 8.1 shows structured light scanning of mannequin A by the HP 3D surface scanner Pro S3. The camera of the scanner was set to the recommended angle (20 or 22°); the scanning distance was the distance at which the object filled almost the whole of the camera view; it was based on an object size (Figure 8.2), the scanning profile was speed or default profile.

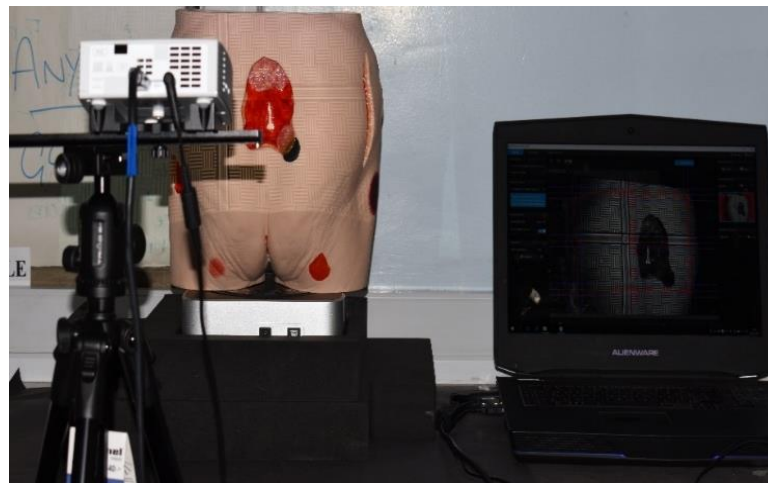


Figure 8.1: Structured light scanning of Mannequin A using the HP scanner

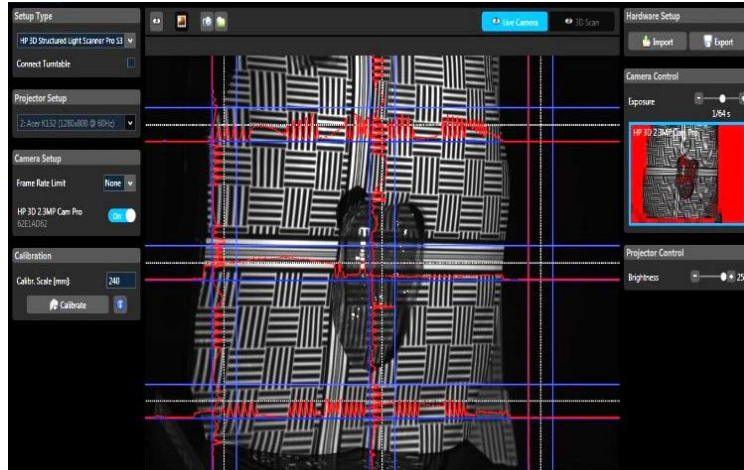


Figure 8.2: Mannequin wrapped with light pattern and filled the camera view

Some mannequins were scanned 360° (a complete 3D surface scanning). These were: mannequin A; mannequin B; head A; head B; leg and foot.

Mannequins A and B were shaped from extremely curved areas (sacral areas and buttocks), and the injuries were distributed on uneven surfaces. When a limited scanning to the injury views was undertaken, the aligned results were unsatisfactory because they were a result of the fusion of different scans with different contours. Therefore, it was decided to scan mannequins A and B using complete 3D surface scanning instead of scanning each injury individually.

It was important to make complete scanning of head A and B because their injuries were located on the top of the head, and they had good facial details. However, limited surface scanning to the injury views was also done for both heads.

The leg injury was on a large mannequin. It comprised of different interesting views, such as the toes area, the sole and the heel; therefore, it was scanned using complete surface scanning, as well as limited scanning to the injury.

Other smaller soft mannequins underwent limited scanning. The scanning was limited to the injury views only (Figure 8.3).



Figure 8.3: Limited 3D surface scanning to the injury

In case of complete surface scanning, the raw scans included the anterior view, right view, left view, back, top, bottom, and overlapping views. Some extra scans were taken of the injuries and of complicated areas, such as the undermined areas, tunnelling, the under-chin area, behind the ear and the toes area. Figure 8.4 shows the different recorded views of the leg. Most of views were scanned in two parts and then fused together. The raw scans were aligned and fused using 1000 resolution, 1 sharpness and 10% close holes.

Both the complete and limited 3D surface scanning were compared to conclude which would be more convenient for practical work. The comparison included: scanning time; cleaning and alignment time; fusion time; total number of scans; total number of fused scans (used scans); number of vertices and faces in final results; file size. The pattern parameter profile of the scanning and the resolution of the fusion were kept the same in both types of the scanning.

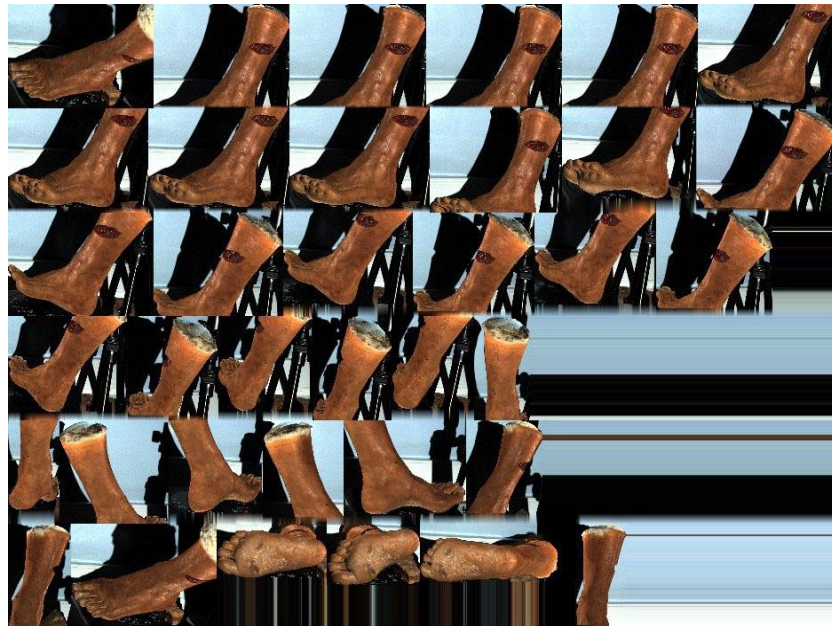


Figure 8.4: Different recorded views of complete 3D surface scanning

8.1.3 Digital photography

The Nikon D3400 with a zoom lens of 18-55 mm focal length was used. The effective megapixels of this camera were 24.2. The manual mode was employed. All injuries were captured by shutter speed 1/200, aperture f/8 and ISO 200. The used focal length was 35 mm with all injuries. A pop-up flash was enough as the working room had good lighting. A scale was placed on the same plane as the injury without bending or tilting.

The scales were Y and straight-scales. The straight scale was used with the two longitudinal wounds. Finally, the injuries were captured at the closest distance at which the injury and the scale filled the camera view and the flash had no effect on the result. According to Wendelken et al. (2011), photographs can be taken at any distance so long as the wound and the scale fill most of the camera view. The injuries were acquired at the right angle as much as possible to obtain photographs free from angular distortion. In order to make sure the photographs had no distortion, two axes of the scale were set to be parallel to the image frame, i.e. the photograph was framed squarely (Wendelken et al., 2011). Each captured photo was displayed on a large computer-screen to inspect the injury, the scale, and the rounded circle references of the scale, which were supposed to be all rounded, not oval (Green and Schulman, 2010).

8.1.4 Wound measurements

Measurements of the injuries were taken to compare the ordinary measurement methods (manual and 2D methods) to the 3D measurement method. The measurements included wound length, width, surface areas and depth. The measurements were taken in cm. Most of the measurements were taken on two occasions to assess intra-observer reliability.

8.1.4.1 Length and width measurements

The length and width measurements of all wounds were taken using three different methods: the manual, 2D and 3D methods. The measurements were taken with care to obtain more consistent statistical results. The following points were considered during the measurements:

- All measurements were taken at the same time so that the exact starting points of the linear dimensions could apply in all methods.
- The measurements of each wound were taken three times and average values were recorded.

- Width dimensions were measured to be perpendicular to the length.

The exact starting points of the measured dimensions were marked on copy-photographs to record them for the second measurement event and to reduce the memory bias. The interval between the two measurement sessions was 7 days.

Direct manual measurements were taken using a tape measure. The tape measure was better than a rigid ruler on the uneven anatomical surfaces; the tape can bend with the body's surface curvature. The measurement technique was to record the longest length and widest width perpendicular to one another, regardless of head-to-toe orientation (Langemo et al., 2008).

2D measurements were based on 2D digital photographs. The 2D photo of each injury was opened in Image J software; length and width dimensions were taken after scale setting; the known distance was 1 and the unit of length was cm.

3D measurements were based on structured light 3D models. The 3D model of each injury was imported to the MeshLab software in an OBJ file, and then the length and width were measured digitally on screen.

All measurements (length and width) were tabulated (Table 8.2). The length and width dimensions were recorded again after seven days for reliability assessment.

Table 8.2: Wound length and width dimensions using tape, 2D and 3D methods

	Recorded dimensions	Manual measurements	2D measurements	3D measurements
Wound 1	Length	5.9	4.69	5.14
	Width	0.7	0.57	0.74
Wound 2	Length	4.1	3.45	3.64
	Width	1.6	1.57	1.69
Wound 3	Length	6.7	5.38	6.12
	Width	2.5	2.43	2.61
Wound 4	Length	3	2.87	3.17
	Width	3	2.88	3.00
Wound 5	Length	4	3.49	3.98
	Width	3	2.68	2.92
Wound 6	Length	3.6	3.41	3.79
	Width	3	3.13	3.30
Wound 7	Length	6.5	5.62	5.77
	Width	5.2	5.26	5.15
Wound 8	Length	5.2	4.98	5.11
	Width	4.4	3.37	3.98
Wound 9	Length	5.1	4.71	5.10
	Width	5	4.83	4.92
Wound 10	Length	5.1	4.71	5.10
	Width	5	4.62	4.88
Wound 11	Length	11.2	10.52	11.78
	Width	8.9	8.4	8.69
Wound 12	Length	11.2	10.19	11.36
	Width	8.8	7.92	8.76
Wound 13	Length	10.8	9.86	10.14
	Width	9.2	8.80	8.93
Wound 14	Length	11	10.02	10.09
	Width	9.6	8.87	9.02
Wound 15	Length	12.9	11.82	12.72
	Width	2	1.78	2.04

8.1.4.2 Surface area measurements using 2D and 3D methods

As noted in Section [8.1.1](#), the injuries were shaped from real cases to ensure applicable results; therefore, they had variable shapes and sizes. From a research's point of view, the analysis of wound samples which had sizes and shapes similar to the real wounds would be better than an analysis of data similar to textbook examples. However, measuring such wound raised two issues. First, there was no available ruler-based formula to calculate manually the area of the irregularly shaped wounds. Second, the measurement of larger wounds required more attention since the reliability of the results decreases when the wound areas are increased (Wendelken et al., 2011; Oien et al., 2002, cited in Shaw and Bell, 2011, p. 75).

Concerning the first issue, measurements of the wound areas using available ruler-based formulas were tried, the tested formulas were:

- Multiplying length x width (L X W).
- Multiplying length x width x 0.785 (L X W X 0.785).
- Elliptical method (length x width perpendicular to each other x 3.1416/4).

It was noted that wound areas resulting from second and third formulas were almost the same ([Table A.2](#) in Appendix A). However, the results of these formulas were not used in comparison and interpretation. This is because previous research had already confirmed that these formulas overestimate the dimensions of the wound areas, particularly in case of larger and irregularly shaped wounds. The first formula assumes the wound shapes are a rectangular or square, and the results are overestimated by 10-40%. The second formula underestimates the larger or irregular wounds. The last equation overestimates the wound areas and is not recommended in fields where the measurement of the wound areas is significant ([2.4.3](#)). Therefore, measurement of the wound areas by using the linear wound dimensions and applying a formula was not included, and a decision was taken to calculate the wound areas digitally using the 2D method and the 3D method.

Regarding the second issue, after the overall analysis of the wound area, the sample was divided and the smaller wounds were analysed separately.

Therefore, surface area measurements were collected using 2D and 3D methods. ImageJ software and 2D digital photographs were used for the 2D area measurements. Geomagic Studio software and 3D models were used for the 3D area measurements. The wound areas were calculated by outlining the border of the wounds on-screen. The borders were marked with attention to obtain only the traumatized area without intact skin inside the selection. With the Geomagic Studio software, the 3D models in OBJ files were used because these files had colour-

texture information over the geometry, which was helpful in recognizing and marking the wound boundary; STL files were not helpful (Figure 8.5 first). Since these methods were achieved by tracing the wound boundary with human intervention, each wound was imported to the software three times. On each time, the scale (for Image J software) was re-set to record three areas with different setting. The average value of the three measurements of each wound was recorded. All measurements were tabulated and are shown in Table 8.3. The measurements were taken again using the same method after seven days.

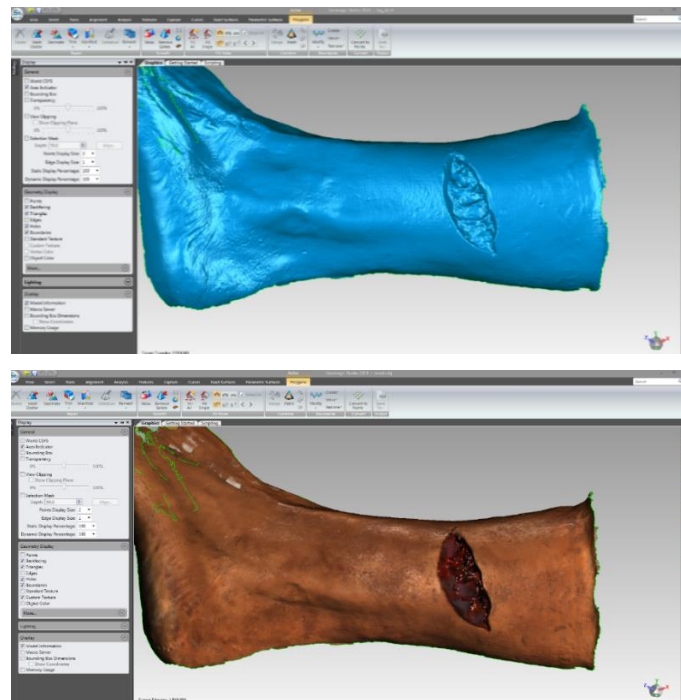


Figure 8.5: 3D result of STL and OBJ file format

Table 8.3: Wound areas using 2D and 3D methods

Wound	2D measurements	3D measurements
Wound 1	2.13	3.63
Wound 2	3.71	5.58
Wound 3	9.92	17.72
Wound 4	6.88	7.43
Wound 5	8.19	12.39
Wound 6	7.91	8.97
Wound 7	22.5	30.74
Wound 8	13.07	17.38
Wound 9	21.17	21.82
Wound 10	18.38	30.26
Wound 11	64.20	96.56
Wound 12	61.19	95.44
Wound 13	43.44	55.48

Wound 14	39.17	58.62
Wound 15	16.69	44.29

8.1.4.3 Depth measurements

A cotton bud (Q-tip), an electronic calibre or a probe is used to measure wound depth manually (Ozturk et al., 1996; Savage and Jeffery, 2013; Shah, Wollak and Shah, 2015). Whereas 3D software is used to measure wound depth three-dimensional using 3D models on screen. The depth is measured as the maximum distance between the bed of the wound and the approximated healthy skin (Plassmann and Jones, 1998; Callieri et al., 2003).

In this work, the depth of the wounds was collected manually and three-dimensional. It was measured from a deep point in the injured surface to the border of the intact skin in an oblique way using a rigid ruler. It was measured obliquely to match the same on the screen of the CloudCompare and Geomagic Studio 3D software (Figure 8.6 left). Sansoni et al. (2009) measured the wound depth from 3D models in the same oblique manner (Figure 8.6 right).

The depth of each wound was measured three times and the average values were tabulated (Table 8.4).

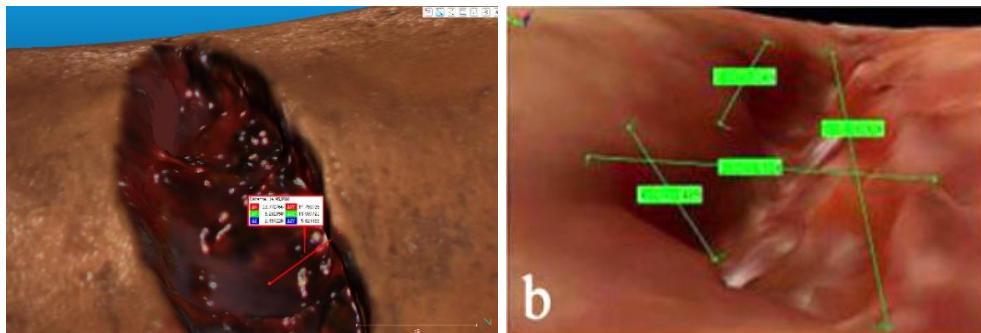


Figure 8.6: 3D depth measurement using HP scanner (left) and Konica Minolta scanner (right)²⁶

Table 8.4: Wound depths using manual and 3D methods

Wound	Manual measurements	CloudCompare 3D measurements	Geomagic 3D measurements
Wound 1	0.5	0.43	0.46
Wound 2	0.8	0.74	0.81
Wound 3	1.4	1.49	1.47
Wound 5	1	0.90	0.86
Wound 7	2.5	2.54	2.47
Wound 10	2.7	2.59	2.46
Wound 11	4.9	4.82	4.83
Wound 12	5	4.91	4.70
Wound 13	2.4	2.43	2.45
Wound 14	2.5	2.52	2.52
Wound 15	2.8	2.45	2.56

8.1.5 Wound measurement analyses

The following analyses were considered to investigate the collected 3D and conventional measurements:

8.1.5.1 Visual assessment

Excel 2016 was used to display all the measurements in bar charts for visual assessment. Moreover, some types of descriptive statistics, such as mean and standard deviation were also considered for each set of measurement and between the measurements.

8.5.1.2 Differences between the measurements

The differences between the measurements of each wound using the different methods were calculated ([Table A.3](#), [Table A.4](#) and [Table A.5](#) in Appendix A). It was achieved by making a direct subtraction and ignoring the negative sign (i.e. absolute difference). Then mean, minimum and maximum differences of each set of differences were considered and displayed in the results.

In the area measurements, the difference between the 2D and 3D measurements of each wound were reported in the results since the differences were larger in some wounds and smaller in others. Based on the results, the wounds were categorised into smaller and larger wounds. Subsequently, the measurements of smaller wounds were analysed separately.

Moreover, wound area measurements using the 3D method underwent to additional analysis.

8.5.1.3 Statistical significance tests

The appropriate significance tests were applied to the measurements to assess if there was statistically significant difference between the 3D and the other measurements. The tests were applied by using IBM SPSS Statistics 23 software. The sample size was fifteen cases, which was an appropriate sample for application of these tests and to obtain consistent outcomes. The following testes were used:

1. Friedman test for length and width measurements

The Friedman test was applied to the length and width measurements that had been taken from the same injuries using the three different approaches (manual, 2D and 3D method). The test is a non-parametric test. It was used as an alternative to the one-way ANOVA with repeated measures since the data violated an important normality assumption of one-way ANOVA with repeated measures. The assessment of the normality was based mainly on the Shapiro-Wilk test (SW) (Laerd Statistics, 2018). The data of the lengths and widths of all the measurement methods were not normally distributed as the sig. values of the SW test were less than 0.05 except in the case of the width dimensions using the manual and 2D methods (Table 8.5). The normality could not be assumed, and so the Friedman test was applied to the data instead of using the ANOVA test.

The outcome of Friedman test showed an overall statistically significant difference between the mean ranks of all related groups, it did not identify which groups in particular different from each other. Therefore, sign test was used.

2. Sign test for length and width measurements

In order to know where the differences occurred, the Wilcoxon signed rank test was required to be applied to each pair of related groups; it was applied to the manual and 2D measurements; the manual and 3D measurements; and the 2D and 3D measurements for both dimensions (length and width). However, the distribution of the differences between each paired related group was not symmetrical in shape (Box plots shape); therefore, the sign test was applied to each paired related groups instead of the Wilcoxon test.

3. Sign test for area measurements

The test was applied to the 2D and 3D area measurements to confirm that the differences between them were statistically significant. This test was used because the distribution of the differences between two related groups were neither normal nor

symmetrical, i.e. the differences were not normally distributed for a Dependent T-Test (Table 8.5), and had no symmetrical shape for the Wilcoxon Signed-Rank Test.

4. Dependent T-Test for depth measurements

The test was applied to the manual and 3D depth measurements to assess the difference between them. This test was used since the distribution of the differences between two related groups were normally distributed (Table 8.5).

Table 8.5: Significance values of SW test of all measurements

Length measurements using:	Sample size	Sig.
Manual (tape)	15	0.03
2D (Image J)	15	0.01
3D (MeshLab)	15	0.01
Width measurements using:	Sample size	Sig.
Manual (tape)	15	0.06
2D (Image J)	15	0.08
3D (MeshLab)	15	0.04
Area measurements using:	Sample size	Sig.
2D (ImageJ) & 3D (Geomagic)	15	0.008
Depth measurements using:	Sample size	Sig.
Manual & 3D (CloudCompre)	11	0.057
Manual & 3D (Geomagic)	11	0.218

8.5.1.4 Intra-observer reliability

According to Koo and Li (2016, p. 155), “before any measurement instrument or assessment tools can be used for research or clinical applications, their reliability must be established”. This is because most measurements in science contain measurement error and it is important to assess the amount of such error by measuring using a reliability index (Shrout and Fleiss, 1979). Intra- observer reliability was used in this research: “it reflects the variation of data measured by one observer across two or more trials” (Koo and Li, 2016, p. 156). In this work, reliability was determined by taking two sets of measurements using the same method, taken from the same wounds, by the same examiner on two occasions (a seven day interval) and analysing the two sets using Interclass Correlation Coefficient (ICC) test. The reliability assessment was done to the different types of wound measurements: length and width measurements using the manual, 2D and 3D methods, and surface area measurements using the 2D and 3D methods. The model selection of the ICC was a two-way mixed effect, the type selection was absolute agreement, and the confidence interval was 95%.

8.2 Result

8.2.1 Structured light 3D surface scanning of open wounds

Although the 3D surface scanner scans the surface objects, the light patterns of the structured light scanner were able to reach the floors of the injuries and deformed by the shape of the inner wounds. The 3D results of the open wounds exhibited detailed and intact geometry without holes or defects, combined with evident colour-texture information (Figures 8.7 and 8.8). The maximum depth of these scanned wound was 3 to 5 cm.

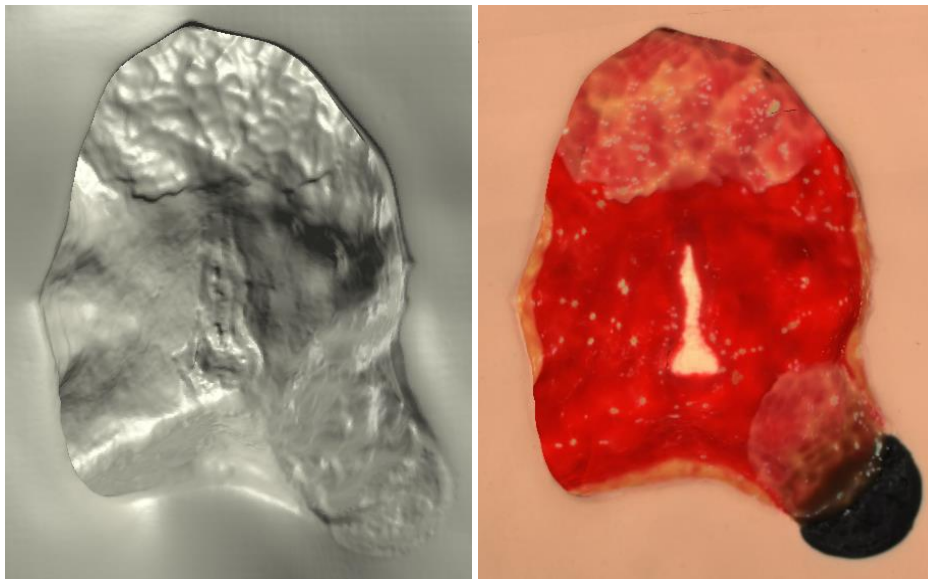


Figure 8.7: Detailed geometry and colour texture of stage-4 pressure injury

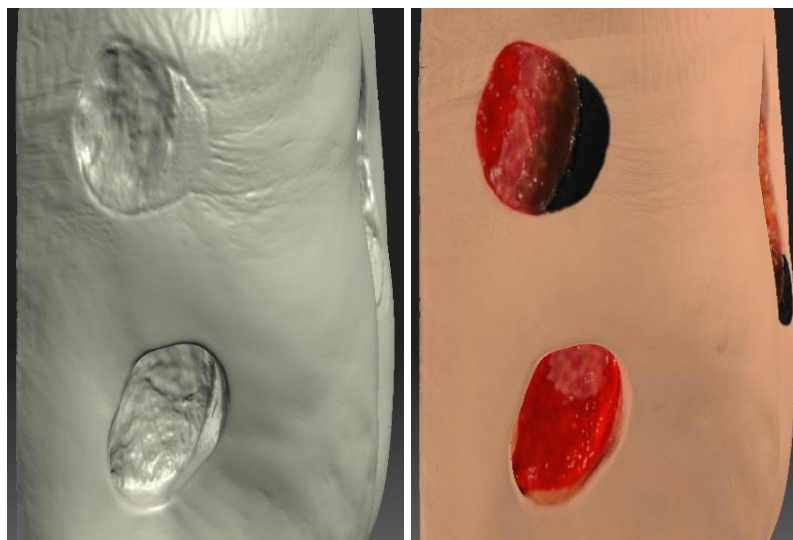


Figure 8.8: Detailed geometry and colour texture of unstageable pressure injury and stage-3 pressure injury

8.2.2 Features of open wound in 3D and 2D results

The wound features, such as the wound border, angles, margin, interior and undermined areas were compared in the 3D models and ordinary 2D photographs to decide which document had recorded clearer wound features. The overall sharpness of the wound features was almost the same in both documents. This is because a professional camera model was used to capture the 2D photographs. However, some wound characteristics were still clearer in the 3D wounds. These features were:

1. Colour-texture resolution

Colour-textured resolution of the 3D results was evident and useful, especially in the case of the bruise. The resolution of the bruise in a 3D result was better than the resolution of the bruise in a 2D result (Figure 8.9). The faint periphery of the bruise was displayed clearly by zooming-in the 3D model on the screen. Usually there is a colour difference between the margin and the centre of the bruise. This is because the bruise tends to heal from the periphery towards the centre (Madea, 2013). The same bruise in the 2D photo was also clear, but it was not as sharp as in the 3D result. The difference between the 3D and 2D surface area measurements of this bruise was around 4.31 cm² because the calculation of the area was based on an outline of the border of the bruise, which was sharper in the 3D result. However, the difference was also related to the ignorance of the surface curvature of the 2D method.

Note that the recorded injuries in this study had no traumatic bruises, the injury in Figure 8.9 is deep tissue pressure injury, has the same features of the traumatic bruise.



Figure 8.9: 3D and 2D results of deep tissue pressure injury

2. Wound edges

The edges of the wounds in the 3D results were represented with a high degree of similarity to the original edges. They were better than the edges of the wounds in the 2D results (Figures 8.10 and 8.11).

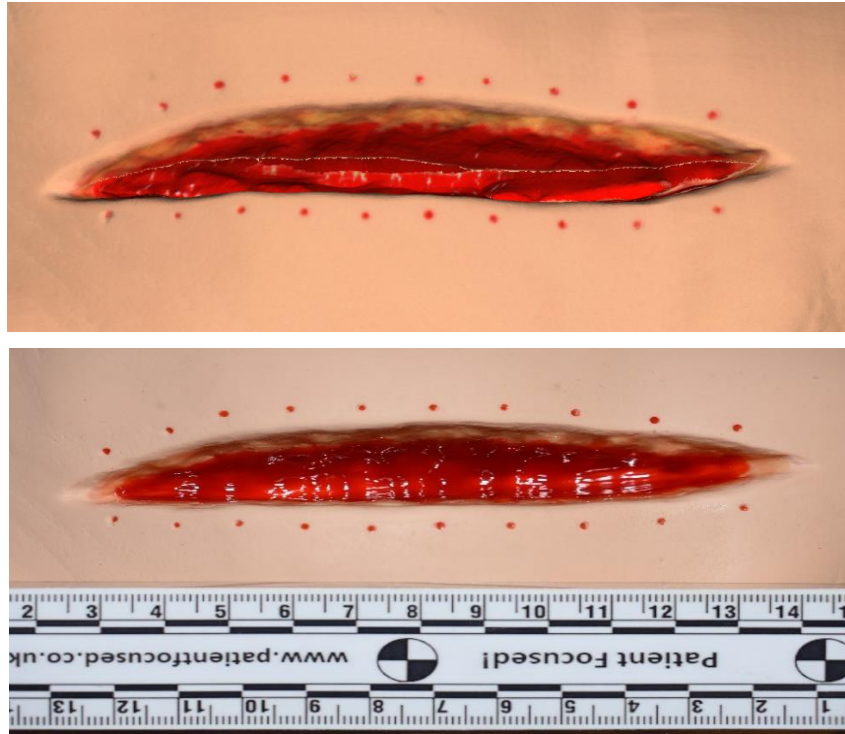


Figure 8.10: 3D and 2D results of long surgical wound



Figure 8.11: 3D and 2D results of explosion injury at the top of the head

3. Undermined areas

The undermined areas of some injuries were complicated and concealed; however, they were exposed to the light and scanned by the structured light scanner after some manipulation of the mannequins and angulation of the scanner. Figure 8.12 shows 3D result of undermined area (indicated with arrows) of stage-4 pressure ulcer. The angulation of the scanner during the scanning time had no impact on the 3D results. Conversely, the digital photography captured these concealed areas with angulation, but this introduced angular distortion in the 2D results.

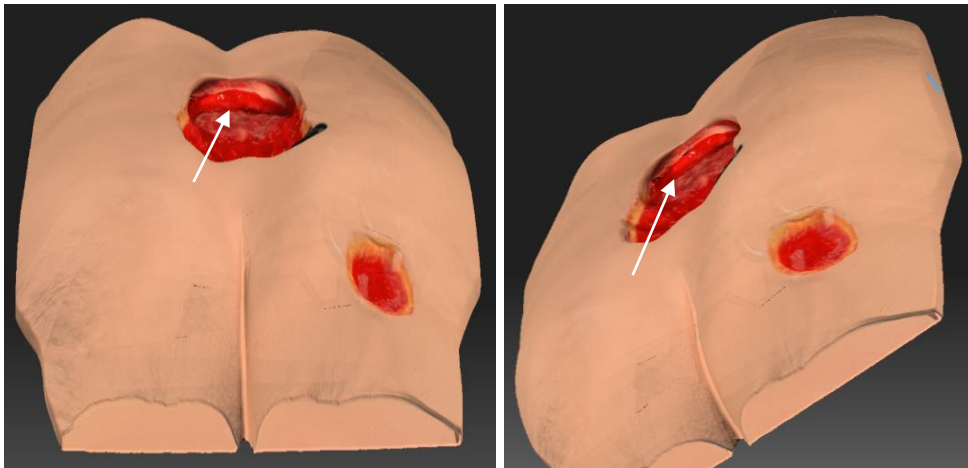


Figure 8.12: 3D result of mannequin B shows undermined area

On the other hand, representation of the white slough tissue of pressure injuries was clearer in the 2D results than in the 3D results (Figures 8.13). Additionally, the yellow subcutaneous tissue in interior of wounds (indicated with an arrows in Figure 8.14) was clearer in the 2D photographs than 3D the models. The mannequins were scanned many times; (1) at different closer distances, (2) with a smaller calibration scale size and (3) using different exposures, but the results remained the same. This was possibly due to the composition of the material used to create the wounds on these mannequins.

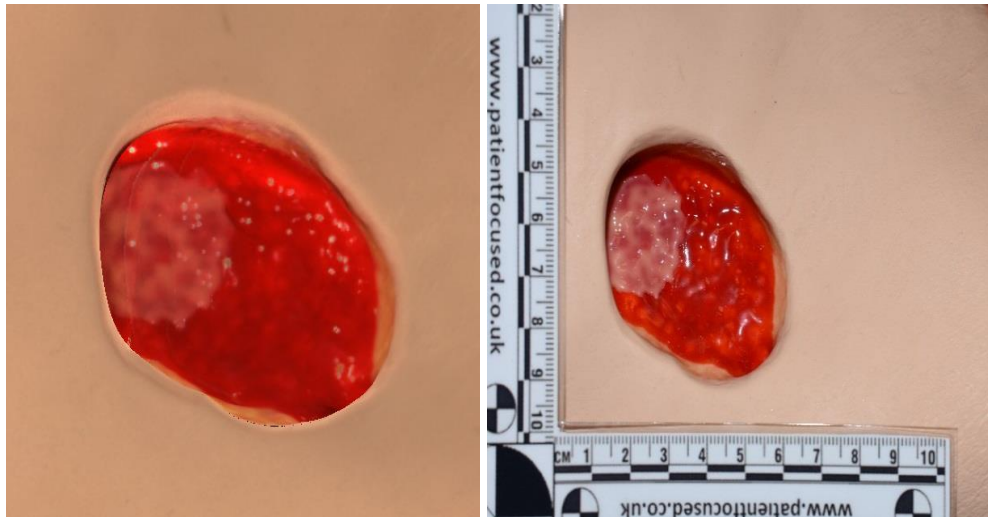


Figure 8.13: 3D and 2D results of stage-3 pressure injury

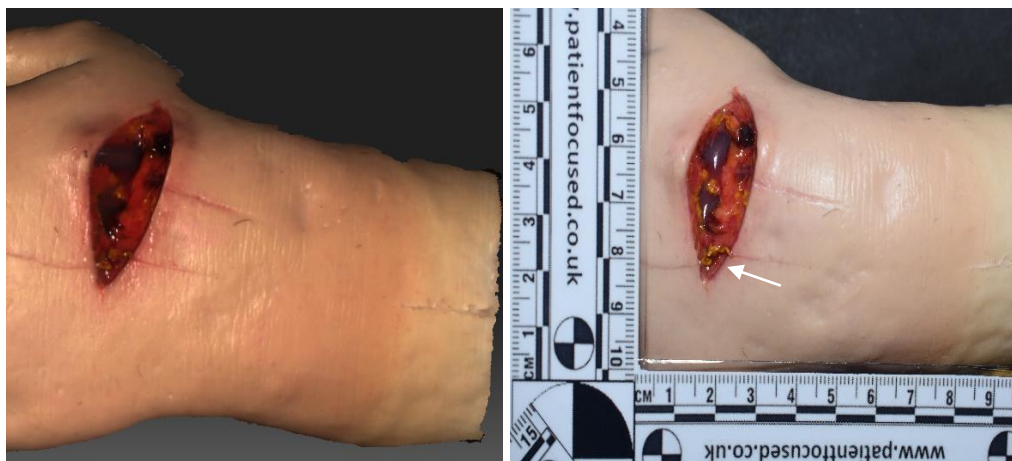


Figure 8.14: 3D and 2D results of cut wound on the dorsal aspect of the hand

8.2.3 Complete versus limited structured light 3D surface scanning

Some mannequins were recorded using two types of scanning. In the complete scanning, the entire mannequins were scanned (360° scanning), whereas in the limited scanning, only the injury views were scanned. The results show that the sharpness of the injuries recorded using both methods were the same; however, each type of scanning had its advantages and disadvantages. Table 8.6 summarises some scanning parameters used during the complete 3D scanning, Table 8.7 summarises the same parameters of the limited scanning.

Table 8.6: Scanning parameters of complete 3D surface scanning

Scanning parameters	Mannequin A	Mannequin B	Head A	Head B	Leg & foot
Calibration scale (mm)	240	240	120	240	120
Camera angle	22°	22°	20°	20°	22°
Scanning time ³³ (min: sec)	35:13	-----	33:31	26:44	41
Total scans	63	63	49	48	85
Cleaning & alignment time (hrs: min: sec)	> 3 hrs	> 3 hrs	3:52	3:33	5:1:34
Fusion time (min: sec)	19: 52	11: 40	12: 48	12: 14	11: 52
Used scans	33	39	26	27	39
N. of vertices in final result	3126592	512544	2474146	2355006	920932
N. of faces in final result	6253192	1025080	4948268	4707352	1840155
File size of obj. (MB)	466	71.8	365	348	129

Table 8.7: Scanning parameters of limited 3D surface scanning

Scanning parameters	Leg & foot	Wrist	Hand A	Hand B	Head A	Head B
Calibration scale (mm)	120	120	120	120	240	240
Camera angle	22°	20°	22°	22°	22°	20°
Scanning time (min: sec)	4: 52	1: 36	1: 9	4: 26	2: 57	1: 56
Total scans	10	4	4	11	7	6
Cleaning & Alignment time (min :sec)	12: 54	5: 51	4: 21	17: 59	12: 11	7: 34
Fusion time (min: sec)	2: 25	1: 31	2: 8	2: 42	2: 38	4: 39
Used scans	6	4	4	10	7	6
N. of vertices in final result	765179	638899	655282	375009	1575098	1048033
N. of faces in final result	151888 1	1264795	1302352	744293	3140994	2086009
File size of obj. (MB)	106	88.6	89.9	420	226	146

³³ Scanning time was 15 sec or 18 sec x total no. of scans + time that required to turn and manipulate the mannequin.

The 3D results of the complete surface scanning obtained overall mannequin details, injury details and the actual skin colour. The main advantage of the complete 3D surface scanning was that it allowed the operator to display the mannequins on the screen from different views (anterior, back, top, bottom and injured view). Figures 8.15 to Figure 8.17 show the complete 3D surface scanning results of mannequin A, head B, and leg and foot. However, complete 3D surface scanning had some drawbacks, which were:

1. It was time-consuming, particularly the alignment step. As can be seen from a highlighted row in Table 8.6, this step took about three hours or more, sometimes taking as much as a whole day.
2. More storage space was required.



Figure 8.15: Detailed geometry and colour-textured information of the complete 3D surface scanning of the head

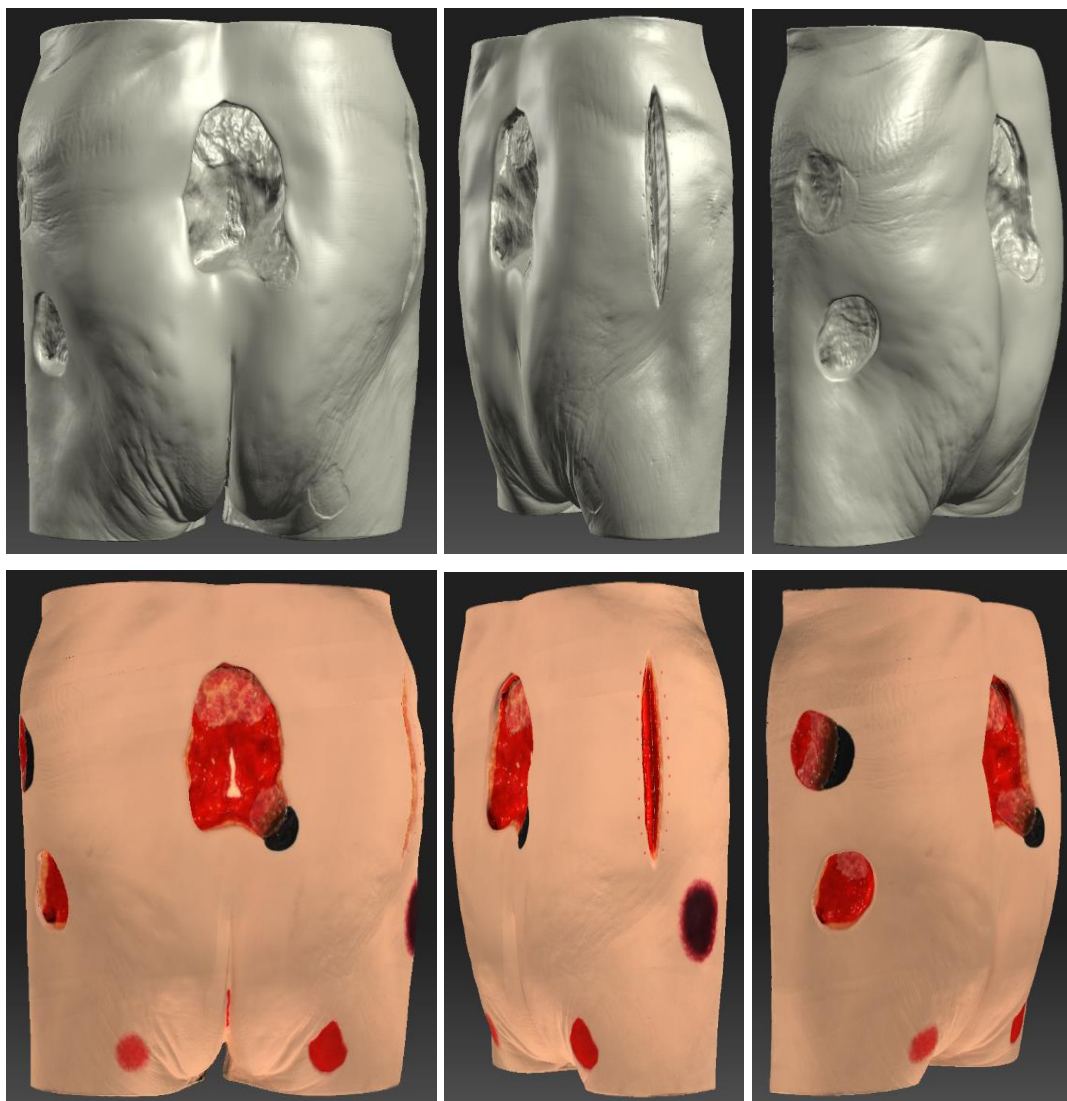


Figure 8.16: Complete 3D surface scanning of Mannequin A



Figure 8.17: Complete 3D surface scanning of Leg and foot

On the other hand, the limited 3D scanning of the views of interest was more practical and time-saving. Moreover, their 3D results were opened more rapidly in the 3D software for visualization, analysis or measurement. Additionally, they were smaller regarding desk space. Figure 8.18 shows a 3D result of the limited scanning.

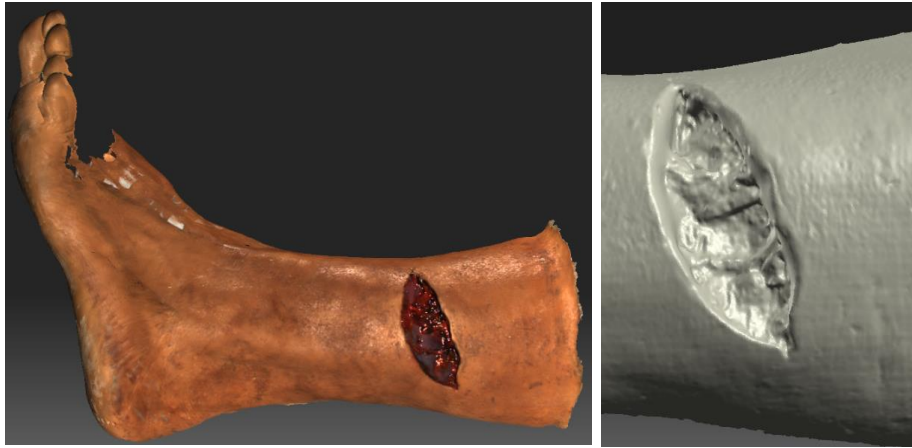


Figure 8.18: 3D result of limited scanning of cut wound (left), the wound magnified to show detailed geometry (right)

8.2.4 Wound measurements analysis

This section show the results of the comparison between 3D and conventional wound measurements. The comparison includes wound lengths, widths, depths and surface areas. The results of further analysis concerning the accuracy and precision of 3D area measurements are also presented in this section. Finally, the intra-observer-reliability of all collected measurements are displayed.

8.2.4.1 Comparison between 3D and conventional wound measurements

Measurements of fifteen wounds were taken manually and digitally by 2D and 3D methods. This was done to compare the 3D measurement method that was based on structured light scanning method with conventional methods, and to see if there were any differences between them. Length, width, surface area and depth were all compared.

8.2.4.1.1 Length and width measurements

The tape, Image J and MeshLab software were used to measure the length and width manually, two dimensionally and three-dimensionally respectively ([8.1.4.1](#)). The length and width measurements were compared by interpretation of bar charts and descriptive statistics; calculation of the differences between the measurements; and application of statistical significance test.

8.2.4.1.1.1 Bar chart and descriptive statistics of length and width measurements

Figure 8.19 and Figure 8.20 show bar charts of the length and width measurements that were measured by the manual, 2D and 3D methods.

It was clear that all the manual and 3D measurements were closer to each other in both dimensions. The mean and standard deviation of both sets of measurements were almost the same (Table 8.8 and 8.9). The same was noted in the measurements taken on the second occasion, after seven days.

Conversely, all 2D length and width measurements were smaller than the other measurements in both dimensions.

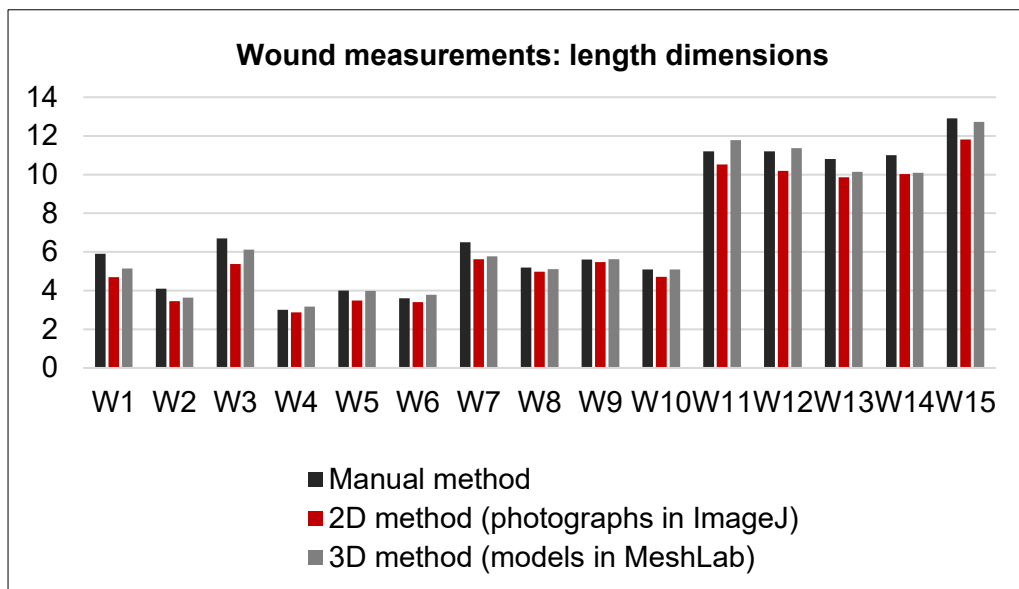


Figure 8.19: Wound length measurements in cm

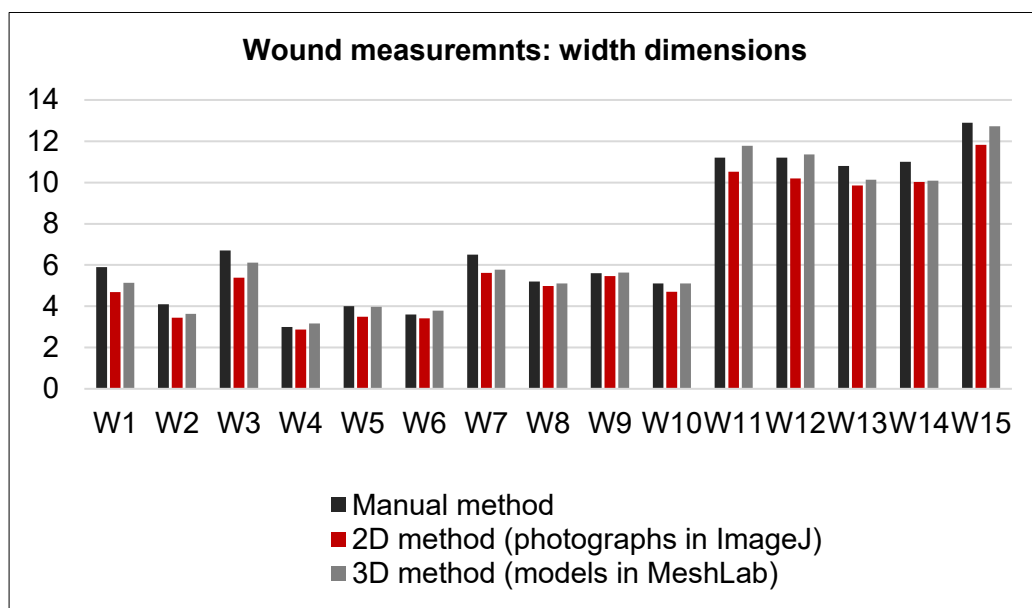


Figure 8.20: Wound width measurements in cm

Table 8.8: Descriptive statistics of length measurements

	Manual method	2D method	3D method
N.	15	15	15
Mean	7.12	6.43	6.90
Std. deviation	3.33	3.10	3.32
Min.	3	2.87	3.17
Max.	12.90	11.82	12.72

Table 8.9: Descriptive statistics of width measurements

	Manual method	2D method	3D method
N.	15	15	15
Mean	4.79	4.47	4.71
Std. deviation	2.99	2.80	2.85
Min.	0.70	0.57	0.74
Max.	9.60	8.87	9.02

8.2.4.1.1.2 Differences between the measurements

The differences between the length measurements of each wound using the manual and 2D method; manual and 3D method; and 2D and 3D method were calculated ([Tables A.3](#) in Appendix A). The mean, minimum and maximum difference of each set of differences are presented below in Table 8.10. The same has been done with the width measurements ([Table A.4](#) in appendix A). The mean of the differences between the manual and 3D measurements of both dimensions was smaller than other differences.

Table 8.10: Differences between wound measurements of linear dimensions

Diff. between length measurements	Mean diff.	Min. diff	Max. diff.
Diff. between manual & 2D	0.69	0.13	1.32
Diff. between manual & 3D	0.37	0.00	0.91
Diff. between 2D & 3D	0.47	0.07	1.26
Diff. between width measurements	Mean diff.	Min. diff	Max. diff.
Diff. between manual & 2D	0.34	0.03	1.03
Diff. between manual & 3D	0.16	0.00	0.58
Diff. between 2D & 3D	0.25	0.09	0.84

8.2.4.1.1.3 Statistical significance test

In order to assess statistically significant difference between the three groups of measurements (manual, 2D and 3D measurements) of both measured dimensions (length and width), the Friedman test was used. The test revealed an overall statistically significant difference in the length measurements ($\chi^2 (2) = 23.42$, $p=0.000$), and in width measurements ($\chi^2 (2) = 14.95$, $p=0.001$).

In order to know which groups exactly differed from each other, a sign test was used. The test displayed no statistically significant difference between the manual and 3D measurements of both measured dimensions. However, there was a statistically significant difference between the 2D and other measurements of both measured dimensions (Table 8.11). Based on the frequencies tables of the test, the wound measurements were reduced in both dimensions when the 2D method was applied.

Table 8.11: Significance values of Sign test between wound measurements of linear dimensions

Methods	Manual vs 2D measurements	Manual vs 3D measurements	2D vs 3D measurements
Exact Sig. (length)	0.000	0.424	0.000
Exact Sig. (width)	0.007	0.424	0.001

Because, no statistically significant difference was observed between the manual and 3D measurements of both measured dimensions (length and width), spearman's correlation test was applied to these measurements to measure the strength of the relationship between them, and the results established a strong positive correlation between them (Figure 8.21). The correlation between the manual and 3D length measurements was ($r_s (13) = 0.981$, $p=0.000$), the magnitude of the relationship was 96.2 %. The correlation between the manual and 3D width measurements was ($r_s (13) = 0.992$, $p=0.000$), the magnitude of the relationship was 98.4 %.

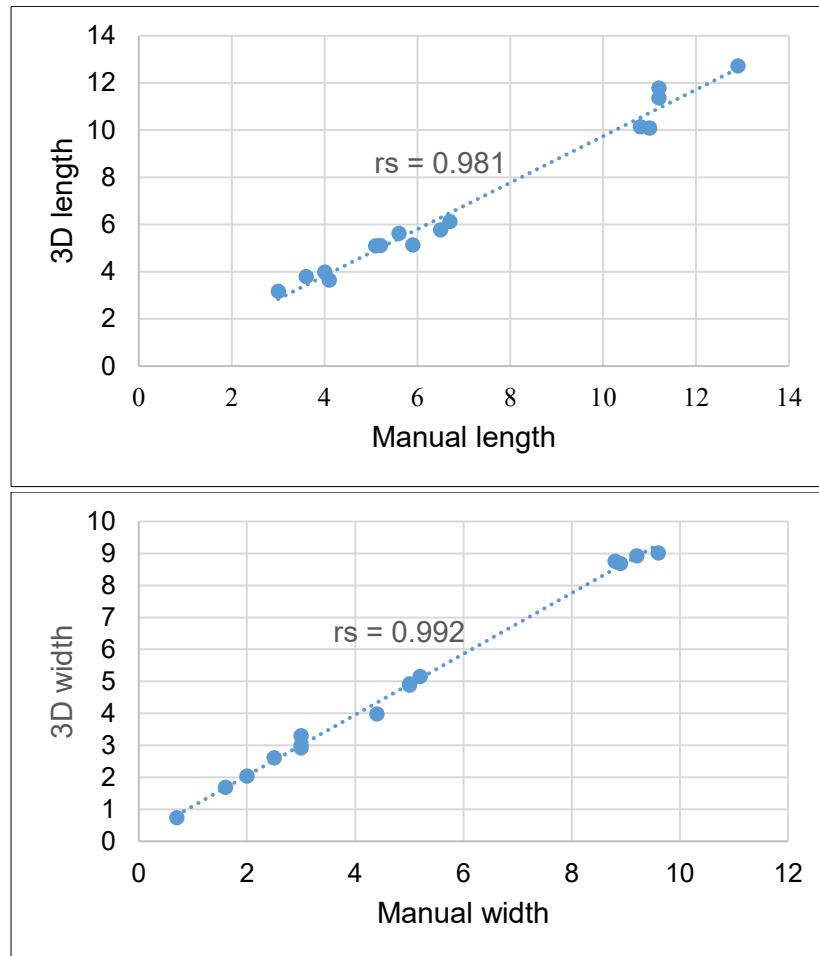


Figure 8.21: Correlation between direct manual and 3D measurements (in cm).

8.2.4.1.2 Surface area measurements

Wound areas were measured on the screen using Image J software with 2D plane photographs, and measured in Geomagic Studio software using actual-size 3D models (8.1.4.2). The measurements were compared by interpretation of the bar chart and descriptive statistics; calculation of the differences between 2D and 3D measurements; and application of statistical significance test.

8.2.4.1.2.1 Bar chart and descriptive statistics of area measurements

Figure 8.22 displays the wound areas measured using both methods. It was clear that the overall 2D measurements were less than the 3D measurements. This was noticeable in wound nos. 11 to 15, which were larger and irregular-shaped wounds. The same was observed in the measurements recorded seven days later.

Table 8.12 presents descriptive statistics of both measurements. Significant standard deviation of each data set was expected since the sample had smaller and larger size

wounds, and nothing was indicated for either set. However, the clear difference between the mean and standard deviation of 2D and 3D sets was more important and required more analysis.

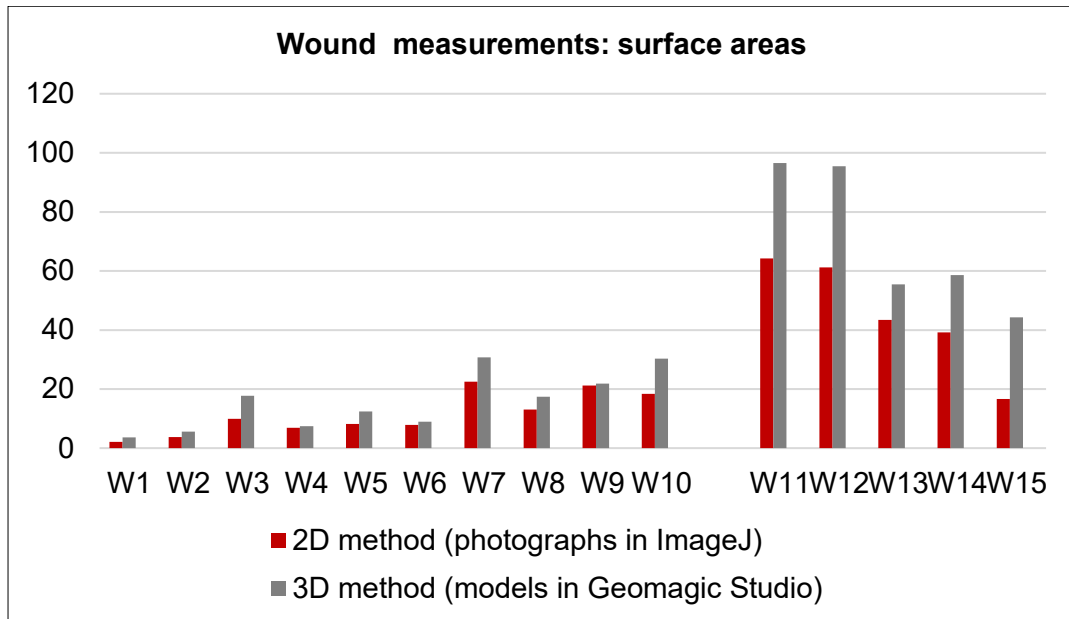


Figure 8.22: Wound area measurements in seq. cm

Table 8.12: Descriptive statistics of area measurements

Methods	2D method	3D method
N	15	15
Mean	22.57	33.75
Std. deviation	20.14	30.60
Minimum	2.13	3.63
Maximum	64.20	96.56

8.2.4.1.2.2 Differences between 2D and 3D measurements

The differences between the surface area measurements of the 2D method and 3D method of measuring each wound, the means of all the differences, along with the minimum and maximum differences are all displayed in Table 8.13. The mean of all the differences was 11.18 cm².

However, some smaller differences were noted in seven wounds (wounds no.1, 2, 4, 5, 6, 8 and 9): these are highlighted in Table 8.13. These wounds all had the same following features:

- They were of a smaller area (around 20 cm² areas or less).
- They had a more regular shape.

- They were located on less curved surfaces such as wound no. 9, which was located on an almost flat surface, and revealed 0.6 cm² difference between the methods. Wound no. 3 had an area of less than 20 cm², but the difference was around 7.80 cm², which was possibly because the wound was located on the leg, which had a higher surface curvature. According to Shetty et al. (2012, p. 428), “wounds on curved surfaces like the limbs where it has been shown to underestimate the size of the wounds”. The same was noted in wounds no.7 and wound no.10.

Table 8.13: Differences between 2D and 3D measurements of surface areas

Wound	2D measurements	3D measurements	Diff. between both measurements
Wound 1	2.13	3.63	1.50
Wound 2	3.71	5.58	1.87
Wound 3	9.92	17.72	7.80
Wound 4	6.88	7.43	0.55
Wound 5	8.19	12.39	4.20
Wound 6	7.91	8.97	1.06
Wound 7	22.5	30.74	8.24
Wound 8	13.07	17.38	4.31
Wound 9	21.17	21.82	0.65
Wound 10	18.38	30.26	11.88
Wound 11	64.20	96.56	32.36
Wound 12	61.19	95.44	34.25
Wound 13	43.44	55.48	12.04
Wound 14	39.17	58.62	19.45
Wound 15	16.69	44.29	27.60
Mean of all differences			11.18
Min. diff.			0.55
Max. diff.			34.25

Highlighted wounds show smaller differences between 2D and 3D areas

8.2.4.1.2.3 Statistical significance test

The exact sign test was applied to the two sets of measurements (2D and 3D area measurements) to confirm the difference between them was statistically significant. The Exact Sig. was 0.000.

8.2.4.1.2.4 Smaller size wounds

The seven wounds that showed smaller differences between the 2D and 3D wound area measurements were separated from the whole sample and presented in a

separate chart (Figure 8.23). The mean of all the differences was smaller (2.02 cm²). The standard deviation of both sets of measurements narrowed, being 6.41 and 6.59 respectively for the 2D and 3D measurements (Table 8.14). Distribution of the differences between two related groups of the smaller wounds were normally distributed; therefore, they were analysed using the Dependent t-test. However, before applying this to the smaller sample size, the power of the test was calculated first in the G-power software and found to be 79.6%.

The results of the t-test showed a statistically significant difference: ($t(6) = -3.352, p = 0.015$), the mean of the areas increased from 9 to 11 cm² when the 3D method was applied. Therefore, the statistically significant difference between both of the measurements was still observed.

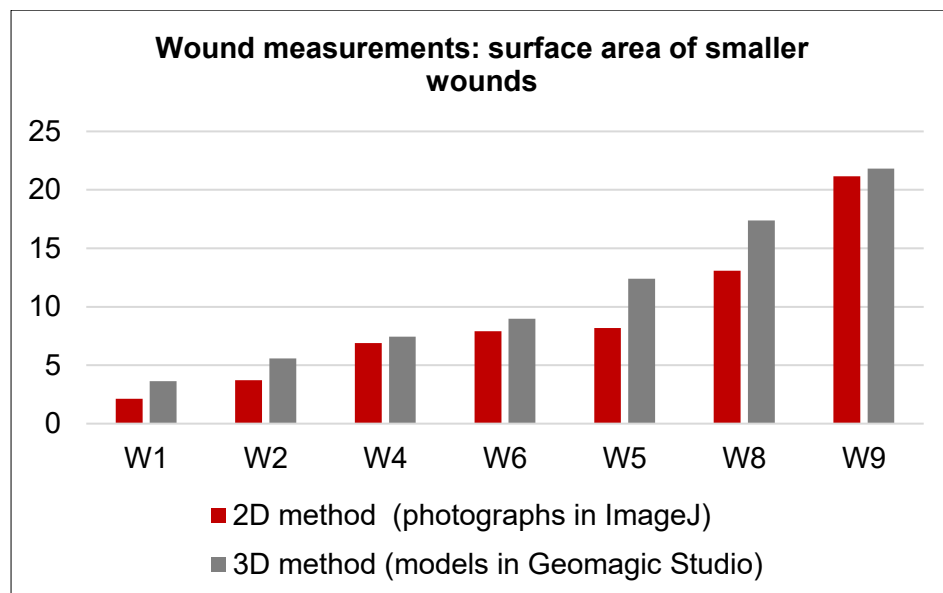


Figure 8.23: Area measurements of smaller wounds in seq. cm

Table 8.14: Descriptive statistics of area measurements of smaller wounds

Methods	2D method (Image J)	3D method (Geomagic Studio)
N	7	7
Mean	9.01	11.03
Std. deviation	6.41	6.59

Based on the all results reported above, the difference between both methods was obvious, particularly with larger size and irregularly shaped wounds. When the smaller wounds were analysed separately, the results became closer to each other. However, a statistically significant difference between both methods was still obtained, even with smaller wounds.

8.2.4.1.3 Depth measurements

The wound depth was measured manually using a rigid ruler, and on screen of the 3D software: Cloud Compare and Geomagic Studio (8.1.4.3). The depth measurements were compared by interpretation of the bar chart and descriptive statistics; calculation of the differences between the manual and 3D measurements; and application of statistical significance test.

8.2.4.1.3.1 Bar chart and descriptive statistics of depth measurements

With all depth measurements, the manual and 3D measurements were close to each other (Figure 8.24). The mean and standard deviation of each set of measurements were almost the same (Table 8.15).

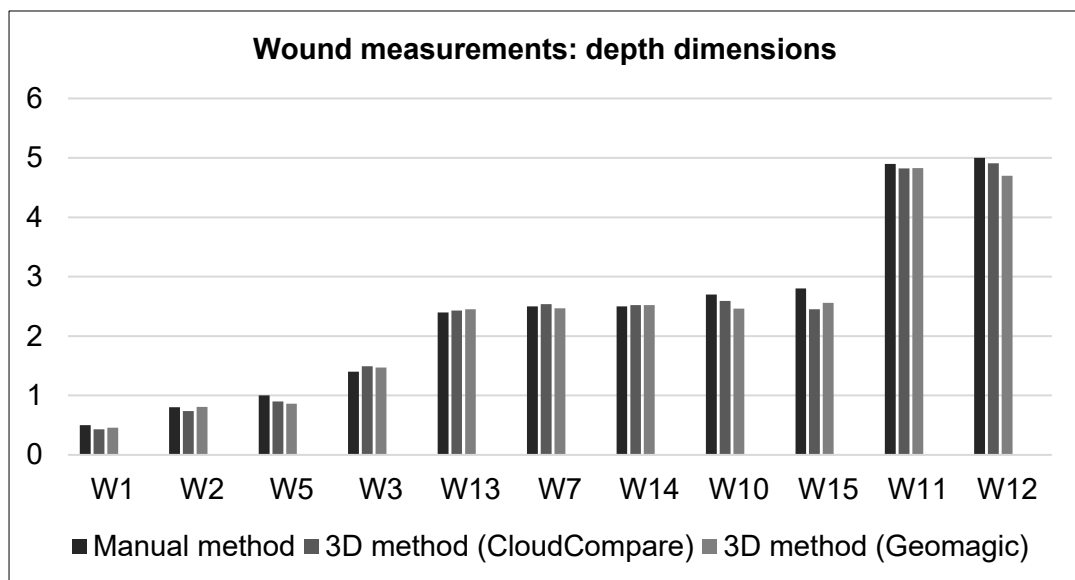


Figure 8.24: Wound depth measurements in cm

Table 8.15: Descriptive statistics of depth measurements

Methods	Manual method	3D method (CloudCompare)	3D method (Geomagic)
N	11	11	11
Mean	2.41	2.35	2.33
Std. deviation	1.50	1.48	1.44
Minimum	0.50	0.43	0.46
Maximum	5	4.91	4.83

8.2.4.1.3.2 Differences between the measurements

The difference between the depth measurements of each wound using the manual and 3D CloudCompare method, and using the manual and 3D Geomagic methods

were calculated ([Table A5](#) in appendix A). Table 8.16 displays only the mean of all the differences.

Table 8.16: Differences between manual and 3D depth measurements

Diff. between depth measurements	Mean diff.	Min. diff	Max. diff.
Diff. between manual & 3D (CloudCompare)	0.09	0.02	0.35
Diff. between manual & 3D (Geomagic)	0.11	0.01	0.30

8.2.4.1.3.3 Statistical significance test

Because the distribution of the differences between two related groups were normally distributed, the T-test was applied. The result of the test revealed no statistically significant difference between the manual and 3D (CloudCompare) depth measurements: $t(10) = 1.754$, $p=0.11$. The difference between the manual and 3D (Geomagic) depth measurements was almost not statistically significant: $t(10) = 2.137$, $p=0.058$.

The strength of the relationship between the manual and 3D depth measurements was a strong and positive correlation ($r(9) = 0.997$, $p=0.000$), the magnitude of the relationship was 99.4 % (Figure 8. 25).

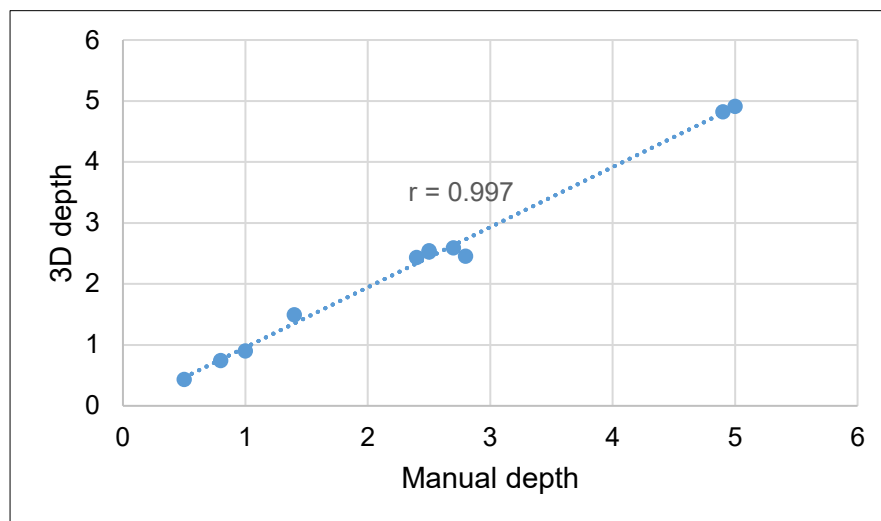


Figure 8.25: Correlation between direct manual and 3D measurements (in cm).

8.2.4.2 Further analysis around 3D surface area measurements

Since 3D wound measurements are novel measurements, the accuracy and precision of collected 3D surface areas were considered in the following two sections: 8.2.4.2.1 and 8.2.4.2.2.

8.2.4.2.1 Accuracy of 3D surface area measurements

Based on the underlying techniques of the 3D scanning, it was known that the 3D models were of actual measurable size of the original; however, there were no available control measurements to prove the 3D results were accurate. Bowling et al. (2009, p. 94) cited that “with no known gold standard approach to the accurate measurements of wounds, direct analysis of accuracy is impossible”.

However, some mathematical formulas based on the shape of the wound can be used to calculate more accurate wound areas (Johnson, 1995). Therefore, six wounds were selected as they had a less irregular shape; they were closer to being circular or elliptical. Their areas were approximated by applying circle and ellipse formulas: ($\pi \times r^2$) and ($\pi \times a \times b$). Then the manually approximated areas were compared to the 2D and 3D areas. The closest approximated areas were with the 3D areas (Table 8.17). However, the shapes of these wounds were not perfectly circular and elliptical; therefore, this application was not rigorous enough to propose that the 3D areas were more accurate than the 2D areas.

Table 8.17: Manual areas of six selected wounds against 3D and 2D areas

Wound	Shape	Manual area using circle or ellipse formulas	3D area using Geomagic	2D area Using ImageJ
W 4	Circle	7.07	7.43	6.88
W 5	Almost circle	12.56	12.39	8.19
W 7	Almost circle	33.27	30.74	22.5
W 8	Ellipse	17.96	17.38	13.07
W 9	Almost circle	20.42	21.82	21.17
W 10	Almost ellipse	20.02	30.26	18.38

8.2.4.2.2 Precision of 3D surface area measurements

Due to the 3D measurement method still being novel, more analysis is needed when using these measurements. Therefore, two small applications were completed (1) the 3D wound areas were calculated from the same models in a different 3D software and compared to the first set of measurements, and (2) the 3D surface scanning of the wounds was repeated to generate new 3D models and to replicate the measurements which were then compared to the first set. The applications are demonstrated below:

1. The 3D areas of 12 wounds out of a total 15 wounds were calculated in another 3D software: MeshLab software. The 3D results (areas) in MeshLab software were

almost equal to the first set of measurements that were calculated using Geomagic Studio software (Table 8.18).

In order to measure the areas in the MeshLab software, each wound was segmented using CloudCompare software (Figure 8.26), saved as OBJ file, then the file was opened in the MeshLab software to calculate the area by using compute geometric measures.

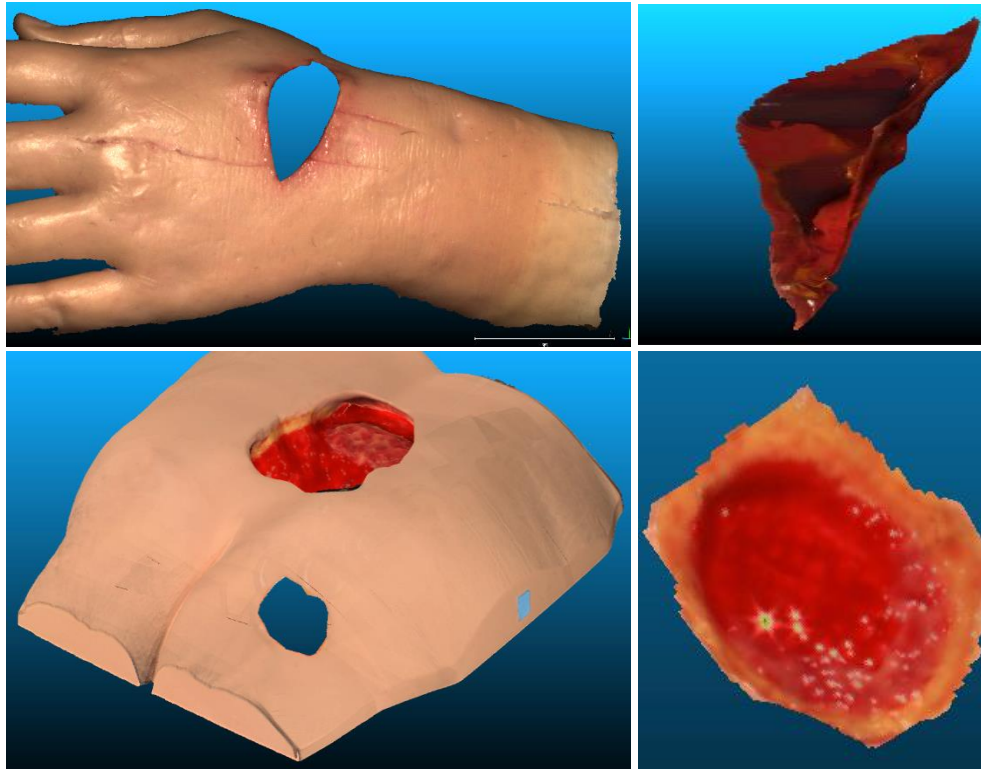


Figure 8.26: Segmented wounds in CloudCompare software

Table 8.18: 3D wound areas in MeshLab and Geomagic software

Wound	3D areas in MeshLab	3D areas in Geomagic
Wound 1	3.80	3.63
Wound 2	5.31	5.58
Wound 3	17.97	17.72
Wound 4	7.03	7.43
Wound 5	11.58	12.39
Wound 6	8.38	8.97
Wound 7	31.17	30.74
Wound 8	16.29	17.38
Wound 9	21.28	21.82
Wound 10	----	30.26
Wound 11	----	96.56
Wound 12	----	95.44
Wound 13	55.99	55.48
Wound 14	62.06	58.62
Wound 15	56.47	44.29

2. The wounds were scanned again at a different time. Some scanning parameters were changed deliberately, such as the camera angle (although it remained within the recommended range), distance, and \pm calibration scale. Some mannequins were scanned with the same scanning conditions. Then the area of each wound was calculated again in the same way (using Geomagic studio software). The 3D areas of the second scanning (Table 8.19) were almost the same as the previous 3D areas of the first scanning (the first set of measurements).

Therefore, in both applications, the 3D area measurements were consistent.

Table 8.19: 3D wound areas based on twice scanning of the same wounds

Wound	3D area measurements of 1 st scanning	3D area measurements of 2 nd scanning
Wound 1	3.63	3.70
Wound 2	5.58	5.55
Wound 3	17.72	17.72
Wound 4	7.43	7.30
Wound 5	12.39	12.45
Wound 6	8.97	8.77
Wound 7	30.74	31.86
Wound 8	17.38	17.21
Wound 9	21.82	22.89
Wound 10	30.26	31.51
Wound 11	96.56	97.21
Wound 12	95.44	95.12
Wound 13	55.48	56.61
Wound 14	58.62	58.17
Wound 15	44.29	38.33
Mean	33.75	33.63
Std. Deviation	30.60	30.55
Min. value	3.63	3.70
Max. value	96.56	97.21

Measurements of each wound were taken three times in Geomagic Studio software and average values were used in seq. cm

8.2.4.3 Intra-observer reliability

Intra-observer reliability of all measurements using different methods was determined using the ICC test on two sets of measurements. The measurements were taken from the same injuries by the same observer after seven days, using the same measurement method. The results are displayed in Table 8.20. According to Koo and Li (2016), ICC values (correlation coefficient) between 0.75 and 0.9 indicates good reliability and more than 0.90 indicates excellent reliability. In this study, the reliability was good (0.9) with all measurement methods except the reliability of the 3D measurement method, which was excellent (1.000) in width dimensions and surface areas.

Table 8.20: Single measures of ICC

	Measured dimensions	Manual	2D	3D
ICC Single measures	Length	0.999	0.997	0.998
	Width	0.999	0.998	1.000
	Area	0.999	1.000

Confidence interval was 95%

8.3 Discussion

The 3D surface scanner is used to scan the surface objects; therefore, in this study scanning the open wounds to depths of 3 to 5 cm caused some concern. However, the light pattern of the scanner reached the floor of the injuries and was deformed by the form of the inner wounds: the 3D results were detailed, exhibiting intact geometry without holes or defects, and integrated with colour-texture information. In some publications from forensic literature, active and passive 3D scanning methods are used successfully to scan open injuries on cadavers; however, the authors did not state the maximum depth of the recorded injuries (Sansoni et al., 2009; Villa, 2017-a). Some wounds had complicated and concealed areas, such as the undermined and tunnelling areas. Therefore, the mannequins were physically manipulated while the scanner was angulated to expose these areas to the light for optimal working of the camera. The areas were almost 100 % scanned by structured light, and the angulation of the scanner during the scanning had no impact on the 3D results (Casas, Castaneda, Treuillet, 2011). However, in the literature review, Plassmann and Jones (1998) stated that the MAVIS 3D structured light system was unable to calculate wounds which have undermined areas, but the system is no longer in use and has been replaced by the MAVIS II (Abdul-Rani et al., 2011).

Some important wound features were clearer in structured light 3D documents than in the photographs, such as the colour-textured resolution of a faint margin bruise. Sharpness of the periphery of the bruise was helpful in surface area measurements as they were calculated by outlining of the bruise margin. However, not all types of 3D surface scanning can generate high-resolution results. It has been noted in the study of Villa (2017-a) that the Photogrammetry is not able to produce a clear margin of the bruise because the passive 3D methods cannot generate high-resolution 3D models when they are compared to active scanners (Bruschweiler et al., 2003; Lohry, Chen and Zhang, 2014). Moreover, the wound edges of the 3D results represented with a high degree of similarity to the original edges. Wound border interpretation is important analysis during medico-legal examination of open wounds and required careful examination in case of overlapping between lacerated and incised wounds, which can take place in some situations in forensic medicine (see [2.2.2.1](#)).

The overall documentation of the open injuries by the structured light 3D surface scanner was easier than using digital photography. This was decided based on (1) the simplicity of the technique, and (2) time required for wound documentation. During the photography, the angle of acquisition, scale, room illumination, reflection and shadow in photographs, and the flash and exposure triangle were considered.

Capturing one wound using the camera was repeated several times in order to decide whether the photograph was sharp enough, the scale was right, and the image had no angular distortion. On the other hand, the structured light 3D surface scanning was a more controlled process. The scanning was carried out in the dark room, the exposure values were within the recommended range and the angulation of the scanner had no impact on the results. Moreover, Once the perfect calibration had been achieved (within 44 sec), the scanning was completed rapidly (within 15 sec.) and the results were acceptable.

Although the results of the complete scanning of the static mannequins comprised valuable complete 3D models, displayed on the screen from different angles with detailed geometry and colour-textured information, collection was time-consuming, particularly regarding the alignment of the scans. Additionally, with some areas, there were some difficulties. For example, the leg and foot mannequin had different sides (anterior of the foot, toes, heel and sole) which all required detailed scanning. The 3D results showed that the areas between the toes (Figure 8.27) were not perfect and the imaging was not sharp, which was possibly due to the complexity of the area. Agisoft software faced the same difficulty in calculating the area between the fingers and legs, Michienzi et al. (2018) claimed that this is due to the adverse position of the mannequin; they cannot adjust a wider stance like living people. Reconstruction of other views of the same mannequin were adequate (see [Figure 8.17](#)). Moreover, the complete 3D surface scanning is suitable only for static objects. To best achieve a complete scanning of an injured area of a real cadaver, the body should be in the rigor mortis phase and the scanning should be completed using a hand-held scanner. Thus, scanning the injury views was more practical, time-saving and would be applicable and highly recommended as standard technique to scan the injured areas of the dead bodies.



Figure 8.27: 3D result of toes area of leg and foot mannequin

In live body, this type of scanning (360°-scanning) has already been tested in [5.1](#), and the results were found to have been impacted by the physiology of movement. The results presented overlapping artefacts due to the changing of the surface contour when the area was turned from one view to another. Therefore, scanning only an injured surface in a stationary manner was more efficient and was used as a standard scanning technique. Supporting this, Ebert et al. (2016) stated that scanning is generally limited to the injury to reduce the total effort required, and to avoid the movement effect which can cause difficulty in a scan fusion. Moreover, Urbanova, Hejna and Jurda (2015) cited that in forensic examinations, a small to medium area of the body surface scanning is useful. However, from a researcher's point of view, if the area could be kept constant by a fixation, and the hand-held 3D structured light scanner used, the complete scanning of live areas could be achieved without artefacts.

The statistical analysis of the wound length and width measurements of the three different methods: manual-tape method, 2D method and 3D method revealed no statistically significant difference in both dimensions between the manual and 3D measurements. The same was observed in the depth measurements. The strength of the relationship between the manual and 3D measurements was strong, positive correlations. The result was generally supported by some publications (Sivanadan and Lisscio, 2017; Villa, 2017-a; Bowling et al., 2009). Sivanadan and Lisscio (2017) applied Student t-tests to eleven linear measurements collected using the manual-tape method and the 3D methods based on hand-held structured light (the Artec Eva) and laser (the FARO Scan Arm) scanning. Measurements based on the FARO Edge Scan Arm laser scanning were used as a control. They found no difference between the manual and structured light measurements; the p-value was equal for both manual and Artec Eva measurements in comparison to the control measurements. Meanwhile, Villa (2017-a) applied the Wilcoxon signed-rank test to manual and 3D linear measurements based on single camera photogrammetry, and she also found no statistically significant difference between the manual and 3D measurements. Bowling et al. (2009) found a strong correlation between manual measurements (length, width and area with median size 9.4 cm²) and 3D measurements of foot ulcers. However, there was a statistically significant difference in the length and width measurements between the 2D and the other methods (the manual and 3D methods). The 2D method, which was based on the flat photographs, did not consider the normal surface curvature, particularly if the wounds were located on highly curved areas. On the other hand, the manual measurements were direct measurements, taken by the

tape, which was deformed (bent) by the anatomical shape of the surface, and considered up and down areas. Moreover, the linear dimensions of the manual method were direct measurements and meant to be actual measurements. The 3D measurements were based on the 3D models that were constructed in actual size. Because of this, there was no significant difference between the direct manual measurements and 3D measurements. Also, the mean of the differences between the manual and 3D measurements of both dimensions (length and width) was also smaller than other differences. The same result was established by Michienzi, et al. (2018) when they compared ruler, photographic, and 3D measurements using multi-camera photogrammetry.

A difference was expected to be obtained between the wound areas calculated by the 2D and 3D methods since it was known that the 2D method ignored the surface curvature. However, the overall mean of differences was large (11.18 cm²). The difference was proportionate to the larger wound size and irregularly shaped wounds. When the smaller wounds and less irregularly shaped wounds were analysed separately, the mean of differences between the measurements were reduced (2.02 cm²), as well as the mean and standard deviation became closer. This possibly means that the algorithm of the 2D software (ImageJ) was not suitable for measuring the larger sized wounds and the irregularly shaped wounds, which consequently means that the algorithm was precise only for smaller and regular traced areas. This explanation was supported by some publications in the clinical literature. Oien et al. (2002), cited in Shaw and Bell (2011, p. 75) compared wound areas using four measurement methods: L x W; acetate tracing; digital and mechanical planimetry, and established that the agreement between the measurements is high with smaller wounds of less than 10 cm²; the difference appears when the wound size is increased. Moreover, Thomas and Wysocki (1990) compared three measurement methods based on film photographs, acetate tracing and the kundin method, and concluded that the wound area measurements are similar when the wounds are smaller and close to being ellipses or circles. However, ignorance of the surface curvature, especially highly curved surfaces, was another important factor which could cause underestimation of the 2D area measurements, and subsequently differences between the measurements of both methods (2D and 3D). This explanation is also supported by some publications in the clinical literature review (Palmer, Ring and Ledgard, 1989; Plassmann and Jones, 1998; Bianco and Williams, 2002; Little et al., 2009; Treuillet, Albouy and Lucas, 2009; Casas, Castaneda and Treuillet, 2011). Finally, Shetty et al. (2012) used photographs and Image J software to calculate

wound areas and they obtained remarkable underestimation when the wounds were located on the curved surfaces.

On the other hand, when Kecelj-Leskovec et al. (2007) compared 2D wound area measurement using digital photography and 3D areas using laser 3D scanning of 15 leg ulcers applying Student's t test, they found no statistically significant difference between the methods (2D and 3D); however, the size of these measured ulcers were < 10 cm in diameter.

In order to assess the performance of the image J software with regularly shaped areas, three regularly shaped objects (a rounded plate, a small rectangular eraser and a larger rectangular planed surface) were scanned and photographed by the same scanner and camera. The 2D and 3D results were opened in the same software (Image J and Geomagic). In each software, the circle and rectangular areas were measured three times and the average values were used. The areas were also measured manually by applying the formulas for circular and rectangular areas. The results are shown in Table 8.21. As can be seen, with regularly shaped areas, all the results were close to each other.

Table 8.21: Area measurements of regularly shaped objects

Object no.		Manual area	2D area in Image J	3D area in Geomagic
1	Small rectangular area	12.42	11.24	12.15
2	Larger rectangular area	264.67	266.25	265.10
3	Small circular area	23.76	23.71	24.03

Two serious reasons were considered as possible causes of the overall obvious difference between the 2D and 3D wound areas. These reasons were the possibility of angular distortion in the 2D documents or incorrect 3D surface scanning.

When 2D photographs have angular distortion, the 2D measurements are assumed to be underestimated (Palmer, Ring and Ledgard, 1989; Rennert et al., 2009; Treuillet, Albouy and Lucas, 2009). However, this reason was excluded in this research because the photographs were recorded with care in order to obtain the 2D images with as little angular distortion as possible. The two axes of the scale were set to be parallel to the image frame; then the photographs were opened on a large computer-screen to inspect the rounded circle references of the scale, which were supposed to be round, not oval. Concerning incorrect 3D surface scanning, the wounds had already been scanned at different times. The wound area measurements were repeated and the later results were almost the same as those of the first set of measurements ([Table 8.19](#)).

In general, the 2D measurement method based on 2D photographs was a problematic method. It required placing a scale on the same injury plane and required photographs free from angular distortion. Setting a scale in the 2D software is a necessary, which consequently could impact the measurements because of the imprecision of the scale itself. According to Ferrucci et al. (2016, p. 509), “a review of commercially available photo scales shows a lack of consistency in quality and accuracy”. Even if all of these conditions were considered, the method still ignored the surface curvature. The impact of the surface curvature on the measurements was increased when the curving of the surface was increased. Moreover, the algorithm of the 2D methods seemed to be precise only with smaller sizes and regularly shaped wounds. On the other hand, the scale and angle of acquisition had no impact on the 3D scanning. Setting a scale was not required in the 3D software measurements since the 3D models were of actual size. Therefore, the 3D surface scanning and the 3D measurements were a more controlled process than when using 2D photography and gathering the 2D measurements.

8.4 Repeatability of structured light 3D surface scanning

Although the structured light 3D surface scanning method is known to be an accurate method and is based on an underlying robust algorithm, the repeatability of the technique was assessed in the CloudCompare software to detect any surface change or deviation between two 3D results of the same object (Forensic Animation, 2012; Lague, Brodu and Leroux, 2013; Bourke, 2015; CloudCompare, 2015).

The same mannequin was scanned twice at different times, but with the same scanning conditions (calibration scale, camera angle and the distance). Both results (3D models) were compared in the CloudCompare software. The first 3D result was used as a reference model since the reference should have the highest possible density, the second result was used as a compared cloud (Figure 8.28 left). The comparison was achieved by computing cloud to mesh (C2M) signed distances between the reference and the comparison model, the result being presented in colour with the actual values of deviation. However, before the distance computation was made, both models were manipulated close to each other, superimposed and aligned. Clouds registration was done, and the final RMS was 0.5 computed on 53539 points. Then, the distance computation was executed while the octree level was on auto.

In the results, the entire colour of the compared model was yellow to green, and the actual value of the deviation of this colour on the scale was around 0.318406 mm (Figure 8.28 right). However, the mean signed distance was 0.135750 and standard deviation was 0.516729. Since the mean deviation value was around zero, structured light 3D surface scanning was considered as highly repeatable.

N.B. The same assessment was applied to all mannequins which means they were scanned twice at different times and their two 3D models were compared. The mean and standard deviation of C2M signed distances between two 3D models of each object were found to be around zero.

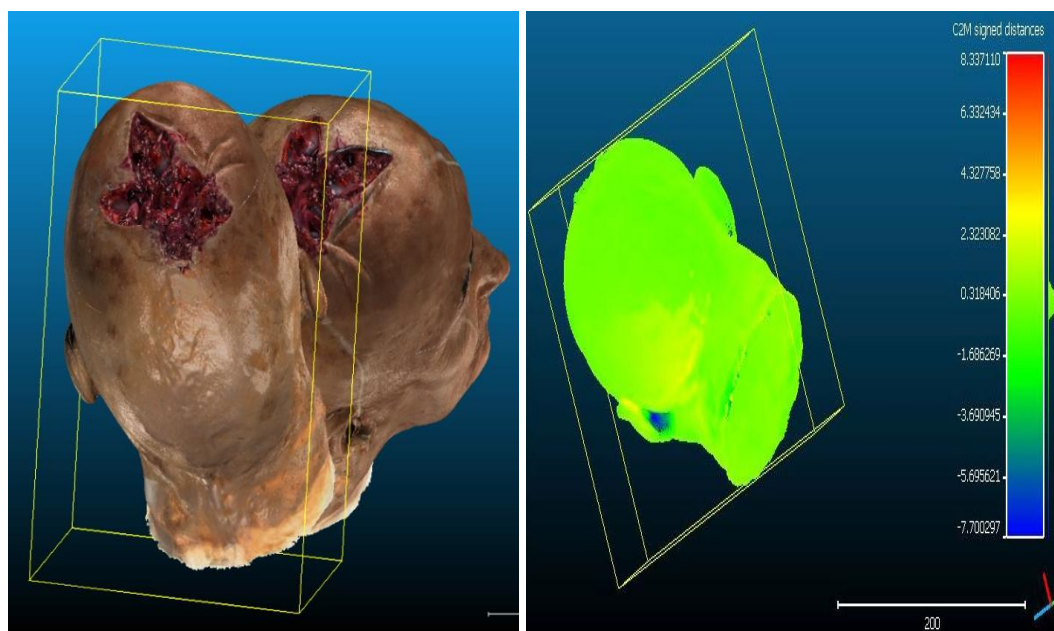


Figure 8.28: 3D models of the same object resulting from different scanning (left), C2M comparison result of these models (right)

Additionally, twice scanning of all injuries at different times that was conducted in [8.2.4.2.2](#), alongside the wound areas being measured from the 3D results of each scanning, was another indication of the repeatability of structured light 3D surface scanning as the results were almost the same ([see Table 8.19](#)).

8.5 Conclusion

Following consideration of the above, the subsequent conclusions can be made:

1. The work confirmed the ability of the structured light 3D surface scanning method to record open injuries to a depth of up to 3 to 5 cm. The light pattern reached the base of the wound and was deformed by the form of the inner wounds. The 3D results of the open wounds had intact geometry without any holes or defects.
2. Based on a visual comparison between the 3D and 2D wound features, the overall sharpness of the wounds in both documents was almost the same; however, some wound features were clearer in the 3D models, such as the undermined areas and wound edges. Moreover, the colour-textured resolution of the 3D injuries was evident and better in the case of the bruise. Magnifying the faint margin of the bruise on the screen was clearer.
3. Complete and limited 3D surface scanning of the injured mannequins revealed that limited scanning to the injury views was time-saving, practical and would be applicable.

4. A comparison of wound length, width and depth measurements between the 3D method and conventional methods showed no statistically significant difference between the manual-tape measurement method and the 3D method and the strength of the relationship between them was strong positive correlation. This is because both sets of measurements were actual measurements. On the other hand, there were statistically significant differences between the length and width of the 2D measurement method and the other methods (manual and 3D). This is because the 2D measurements were based on 2D flat digital photographs and the 2D method did not consider the surface curvature, particularly the highly curved surfaces.

A comparison of 2D and 3D wound area measurements also revealed significant differences, particularly with the larger and irregularly shaped wounds. This is possibly related to the weak performance of the software algorithm of the 2D method when it tried to measure larger and irregular areas. However, the statistically significant difference was also observed in the measurements of smaller sized wounds, which was due to the ignorance of the surface curvature by the 2D method.

Therefore, the wound measurement analysis highlighted two important points:

- The 3D method could be used in the field as an alternative method to the traditional manual approach as it was more effective, contact-less, quick and repeatable.
- The 2D measurement method is a weak method if the photographs captured from highly curved areas, or if it is used to measure larger or irregularly shaped wounds.

5. Scanning all injuries twice at different times alongside the wound areas being measured from the 3D results of each scanning confirmed that 3D measurements results were consistent: mean, standard deviation, minimum and maximum values were almost identical.

6. Intra-observer reliability of length, width and surface areas of all measurement methods was determined using the ICC test on two sets of measurements. Reliability was graded as good (0.9) with all measurement methods other than the 3D measurement method, which was graded as excellent (1.000) in width dimensions and areas.

7. The repeatability of the structured light 3D scanning technique was achieved in the CloudCompare software to detect any surface change between the two 3D results that were obtained by twice scanning of the same mannequin at different times under identical scanning conditions. Both results (3D models) were compared by computing the cloud to mesh (C2M) signed distances between both of them. The comparison

established that the mean signed distance and standard deviation were measured around zero deviation, which indicated that the repeatability of the scanning is high.

8. The overall documentation by the structured light scanning was easier than using the digital photography. This was decided based on the simplicity of the technique, and time required for wound documentations.

Chapter 9: Overall discussion

This chapter is an overall discussion which focusses on the main results of the three experimental applications of Chapters 6, 7 and 8. Studies in these chapters were completed to achieve the three main objectives of this doctoral research (1.5), and to answer the research question (1.4). Therefore, the following sections in this chapter represent a concise overall discussion focussing on the main results relating to the research question and in conjunction with other literature.

9.1 Structured light 3D surface scanning of intact body areas

9.2 Structured light 3D surface scanning of wounded areas

9.3 Structured light 3D surface scanning versus 2D digital photography

9.4 3D wound measurements versus conventional measurements

9.1 Structured light 3D surface scanning of intact body areas

Different intact, uninjured areas of live subjects were scanned. The outcomes were 3D geometric reproductions with colour-textured information in actual-size. The scanning was achieved after setting simple 3D scanning principles (Chapter 5). Different upper and lower limb areas were accessed and scanned. Some known challenging body surfaces, such as dark (black) skin (Errickson, Thompson and Rankin, 2015), hairy and moist surfaces (Urbanova, Hejna and Jurda, 2015; Ebert et al., 2016; Villa, 2017-a) were scanned successfully by a structured light 3D technique. The main difficulty in recording the live subjects was that of breathing (Jones and Rioux, 1997). In this study, the scanning of the torso was challenging due to the impact of the breathing process on the results when the volunteers were in a standing position and their breath was unrestricted (6.1.2.3). The same result was observed by Urbanova, Hejna and Jurda (2015) when the full-body surface of a subject was scanned using two different passive methods, namely a VH1 scanner and a single camera photogrammetry, in the standing as well as in the lying position. However, in the case of using the Pico Scan structured light scanner in this research, scanning the torso areas improved when the volunteer was in the sitting position and quite cooperative. In the case of using the HP structured light scanner, the torso areas scan results also improved when the volunteer was in the sitting position and was requested to hold breath as the acquisition time of this scanner was only 15 sec/scan. Torso scanning in these two situations was determined to be successful because the raw 3D data that were selected to form the final models were assessed and found suitable to be processed as they had no deviations. The data were assessed using

the colour bar comparison of the HP 3D scan software ([6.1.5.2.1](#)), and using CloudCompare software ([7.6.2](#)).

It is difficult to record some areas of the body using a standard digital camera. Such areas are either difficult to see properly through the camera, or it is difficult to place a scale on the same injury plane (Patient Focused, 2018) since the injury is located on an uneven surface. The same problems have been noted when a single camera or multi-camera photogrammetry are used (Villa, 2017-a; Michienzi et al., 2018). Some such areas were scanned using a single camera HP structured light scanner ([6.2](#)) to ascertain if the 3D system could cope. The scanner accessed these areas, and the results were acceptable apart from the left margin of the scanned areas. This was not recorded completely due to a technical problem, which was related to the angle of the single camera of the scanner. When the angle was set to the recommended (20-25°), the camera was pointed more towards the right margin of the scanned area than to the left ([6.2.3](#)). This is called an 'occlusion problem', and it is found with 3D surface scanning systems that are based on a triangulation principle (Morimoto and Fujii, 2005; Lau, 2012). However, it can be solved by using a dual-camera HP structured light scanner.

3D Facial scanning was also achieved using the single camera HP structured light scanner ([6.3](#)). A simple manual face-turning technique was employed ([6.3.2.3](#)) to scan the right and left views of the face in addition to the frontal view. Then, all three views were fused together. The face was turned to the right and left because: (1) the scanner had a single camera mounted on the left side of the projector, and the scanner was not originally designed to scan the face, unlike the Vectra 3D facial scanner (Urbanova, 2016) or the 3dMD face scanner (Goodwin, Evison and Schofield, 2010; Aynechi et al., 2011; Ort et al., 2012); and (2) the facial scanning was done while the participants were sitting on an ordinary chair, not a revolving chair. The fused result of all three views was homogeneous, uniform and had no overlapping artefacts. The facial details of the 3D geometries resulting from the structured light pattern HP 3D scanner were good and, according to Buck et al. (2018), the details of facial geometries resulting from the structured light pattern-stripes scanner are better than the details resulting from a hand-held structured light scanner and single camera photogrammetry. Moreover, when the 3D raw scan deviation analysis between the frontal face view (a reference scan) and the right and left face views (test scans) was done before the scan fusion, the deviation values

were around 0 or 0.1 mm, if the participants had remained still. The deviation analysis was accomplished using the colour bar comparison of the HP 3D scan software ([6.3.2.4](#)).

9.2 Structured light 3D surface scanning of wounded areas

Different types of closed traumatic injuries (abrasion, bruise and stitched cut wounds) were reconstructed successfully from the living victims. The reconstructed traumas had 3D geometries and colour-texture resolution (Chapter 7). This was expected because, in some previous publications from the forensic literature, injuries had already been reconstructed from living cases as well as deceased bodies using structured light scanning (Thal, Braun and Dirnhofer, 2013-a; Thali et al., 2005; Buck et al., 2013; Ebert et al., 2016; Sivanandan and Liscio, 2017; Buck et al., 2018). However, most of these applications focussed on introducing the 3D surface scanning techniques and combined them with the techniques of the internal 3D documentation techniques (MRI /CT). They had used an ATOS structured light 3D scanner to scan the injuries, which is a demanding scanner: using it is time-consuming as the software requires reference marks be attached to the surface of the body. Additional colour texture photographs also need to be applied over the geometrical results. According to Urbanova, Hejna and Jurda (2015), ATOS scanners require more controlled conditions, and Villa (2017-a) stated that the preparation of the body prior to scanning by the ATOS is time-consuming. On the other hand, the Pico Scan and HP structured light 3D scanners that were used in this research were more flexible concerning the reference marks and colour-texture information. Both scanners did not require markers to be placed on the surface of the body, and the colour-textured information was mapped automatically over the geometry. However, because (1) the research scanners were not originally designed for the human body, and (2) the research was conducted in the active Medico-Legal Centre in order to reconstruct a wide range of traumas from living victims, the work experienced some problems ([7.5](#)). These problems could be categorised into three types: problems related to movement and breathing caused by using a living body, problems related to the 3D scanning method, and problems related to the improper use of the scanner. Solutions were found to overcome some of them.

Different types of simulated open wounds having complicated areas and depths of up to 3 to 5 cm located on static mannequins were also recorded successfully in this study (Chapter 8). The structured light patterns reached the base of these wounds

and deformed by the form of the inner wounds. The outcomes were detailed, and intact geometries without holes or defects were gathered.

9.3 Structured light 3D surface scanning versus 2D digital photography

A comparison between the two methods was achieved by evaluating both techniques, their outcomes, and the wound features in their results.

It was noted that the sharpness of the wound features in both documents were almost the same on the screen since the digital camera, which was used for photography, was a professional model and had 24.2 megapixels. However, the wound edges, undermined areas, colour-texture resolutions, especially the resolution of the faint margin of the bruise ([8.2.2](#)), and the overall colour change of the bruises were better in the 3D wounds. Moreover, with cut wounds that had been stitched, their 3D results were clear. The wound edges, margins and angles were all clear and easily interpreted. The healing process of stitched cut wounds was also exposed clearly in 3D results ([7.2.1.6](#)).

The 3D documents themselves were observed to have extra features over 2D photographs ([7.2.1](#)), for example, they contained actual scale and represented the wounded areas adhered strongly to the original scanned areas due to the 3D surface scanning technique representing the 3D geometry of the surface. Additionally, the documents had the unique ability to be manipulated on the screen from different angles and represented only the specific area without clutter. Conversely, the 2D photographs were flat, static (Savage and Jeffery, 2013; Campana et al., 2016; Koller, et al., 2019), reduced 3D injuries to 2D level (Thali, Braun and Dirnhofer, 2003-a), and a scale was required for the photography since the images were saved as pixels rather than microns (Komar, Davy-Jow and Decker, 2012). However, commercially available scales are not accurate enough to use as standard references in photographs (Ferrucci et al., 2016). Additionally, the 2D documents could easily include clutter which can provide distractions in the image by directing the examiner's or audience's gaze away from the main finding.

Regarding the techniques, both of the structured light 3D scanners which were used were accurate. Both scanners had undergone a calibration process that used a robust and accurate algorithm (Errickson, Thompson and Rankin, 2015; Pandy and Cather, 2016; Errickson et al., 2017; Shamata and Thompson, 2018-a; Shamata and Thompson, 2018-b; Thompson and Norris, 2018). The recording technique was also precise, being based on projection-encoded structured light patterns which allowed accurate correspondence between the projected image and the recorded image

(Salvi, Pages, Batlle, 2004; Salvi et al., 2010; Geng, 2011; Ishii, 2012). Moreover, the underlying algorithms, such as the PMP or triangulation algorithm, were accurate, fast and robust (Chen et al., 2009; Yalla and Hassebrook, 2005; Wang et al., 2007; Lohry, Chen and Zhang, 2014). On top of this, the structured light scanning method was under control since it was conducted in a darkroom, the angulation of the scanner during scanning had no impact on its results (Castaneda, and Treuillet, 2011) and the distance was pre-determined. In contrast, the digital photography could be affected easily by the light, the distance and the angle of acquisition. All of which could introduce errors and doubt into the 2D documents ([2.3.3](#)).

9.3.1 Implications of the 3D results and 3D technique

As mentioned before in [2.1](#), the medico-legal examination of the wounds relies on the interpretation of their features to identify the medico-legal significance of the injuries. In some cases, the important features of the wounds are not clear either because of their smaller size, the healing process or overlapping between two types of the wounds ([2.2.2](#)). In these situations, visual examinations alongside the current method of the recording traumas (digital photography) are inadequate for clearly visualizing the wound features. However, because 3D documents have higher levels of resolution and presented some wound features more clearly, they could address these problems more adequately. For example, the type of wound that overlaps between cut and lacerated injuries will be more easily identified from clear wound edges, angles or margins in the high detailed 3D documents. Additionally, the direction of the abrasion can be known from a smaller skin tag (Thali, Braun and Dirnhofer, 2003-a). Furthermore, the colour change of a bruise or a nearly healed trauma will be more easily interpreted. Therefore, clear wound features in the 3D documents will be supportive for wounds interpretation and writing medico-legal reports.

Moreover, it can be said that the extra features of the 3D documents will be favourable during wounds examination and during wounds presentation in court. This is because (1) the 3D actual wound measurements can be repeated any time on screen or reproduced during the presentation of the case inside the court room. (2) The anatomical shape of the wounded or swollen areas could be presented in 3D geometry reflecting the original shape. (3) The examiner can explore and move the traumatic area easily from different angles to show extensive traumas or any associated significant findings in any viewpoint. (4) 3D documents represent only the

area of interest without extra information or clutter, which means that the examiner's or audience's gaze focus on the main finding without interruptions.

Finally, because the structured light scanning technique was faster (15 to 20 sec/scan), more controlled and accurate, it overcame the main deficiencies of digital photography mainly related to angle of acquisition, distance and lighting conditions that discussed in [2.3.3](#).

9.4 3D wound measurements versus conventional measurements

All linear 3D measurements (lengths, widths and depths) taken from the 3D models of living subjects ([7.2.2](#)) and static mannequins ([8.2.4.1.1](#) and [8.2.4.1.3](#)) were close to the manual-tape measurements. Therefore, no statistically significant differences were observed, and the strength of the relationship between them were strong positive correlations. This result was similar to some previous results (Bowling et al., 2009; Sivanadan and Lisscio, 2017; Villa, 2017-a). On the other hand, the 2D measurements that were based on flat photographs were significantly different from the manual and 3D measurements ([8.2.4.1.1](#)) when the wounds were located on uneven surfaces or highly curved areas. This is because the 2D measurement method did not consider the surface curvature. However, when the wounds were located on almost flat surfaces, no statistically significant difference was observed between the 2D, manual and 3D methods ([7.2.2](#)). For that reason, Chang, Dearman and Greenwood (2011) recorded wounds that were located on the flat surfaces of the experimental pigs in order to avoid the impact of the surface curvature, and they obtained no significant difference between the photograph measurements and the Visitrak measurements.

Wound area measurements were also collected from actual-size structured light 3D models and compared to the 2D measurements. The results revealed a difference between the measurements, which was obvious when the wounds were larger and irregularly shaped ([8.2.4.1.2](#)). The reason for this was most likely due to the performance of the algorithm of the ImageJ software that was used to measure the areas in the 2D photographs. The algorithm became imprecise when the areas were larger and irregularly shaped. When the smaller wounds were analysed separately ([8.2.4.1.2.4](#)), the measurements became closer. Some previous publications from the clinical literature confirmed that the results of area measurements based on conventional methods are similar when the measured areas are smaller and regular (Thomas and Wysocki, 1990; Oien et al., 2002, cited in Shaw and Bell, 2011, p.75).

Moreover, the area measurements based on the photographs were clearly impacted by the natural curvature of the human body (Palmer, Ring and Ledgard, 1989; Plassmann and Jones, 1998; Little et al., 2009; Treuillet, Albouy and Lucas, 2009; Bianco and Williams, 2002; Casas, Castaneda and Treuillet, 2011).

9.4.1 Implications of the 3D wound measurement results

According to the results of the wound measurement analysis, the 3D measurements were valid and can be used as an alternative method to the current measurement methods to overcome their limitations and inaccuracies ([2.4.3](#) and [2.4.5](#)). Particularly, the 3D measurement method is a non-contact, quicker and based on accurate and more controlled technique. It also provides permanent records and more measurement information, such as wound depths.

Chapter 10: Conclusion and implications of the study

10.1 Conclusion

This research has assessed the efficiency of the structured light 3D surface scanning technique for recording and analysing different types of traumatic wounds, while involving living subjects and considering current recording methods. The aim of this assessment was to answer the main research question, which is: *can the above-mentioned method be used to reconstruct and analyse the different types of traumatic injuries in forensic medicine?* The assessment has been completed by accomplishing the three following research objectives, which are:

1. To evaluate the ability of structured light 3D surface scanning for recording different intact uninjured areas of living subjects in order to consider the overall feasibility of the method on the human body.
2. To assess the method's capability for reconstructing traumas from living subjects in clinical forensic medicine.
3. To evaluate the possibility of using structured light 3D surface scanning for digitizing open injuries containing complicated areas and depths.

Accordingly, the study has established that with regards to objective 1, the structured light 3D surface scanning method was able to access and record different intact body areas of living persons; including the areas of the extremities, torso areas, challenging surfaces (such as dark skin and hairy surfaces), facial scanning and complicated anatomical areas, for example, the neck and the axillary area. The recorded areas came in the form of 3D geometric reproductions with colour-textured information. For objective 2, the method was capable of reconstructing different types of closed traumas from living subjects in the Medico-Legal Centre. These reconstructed traumas were abrasions, bruises and stitched wounds which were visually acceptable 3D models (geometries and colour-textured). Importantly, the 3D results had some useful features that made them more effective than conventional 2D documents. For example, the 3D models had true scales and displayed 3D geometry of the wounded areas while they could be manipulated from different observable angles. Moreover, it was shown that applying this technique was faster and more controlled than the photographic method. This technique was practised in dark rooms while the exposure values were within the recommended range and the angulation of the scanner had no impact on the result. Following this, the scanning distance was defined, and once the calibration was completed and the scanning settings were selected, the scanning process was achieved rapidly within 15 to 20 sec/scan and therefore, it overcame the

main disadvantages of digital photography related to distance, impact of the lighting condition and angular distortion. Regarding objective 3, this method was able to digitize extensive injuries having complicated areas and depths up to 3 to 5 cm. The 3D results of the open wounds presented detailed and intact geometries without holes or defects, combined with evident colour-textured information. Additionally, some important wound features were better in the 3D wounds than the 2D wounds, for example, undermined areas, wound edges and colour-textured resolution especially the resolution of the faint margin of the bruise and the overall colour change of the bruises.

Additionally, this study has validated 3D wound measurements of structured light 3D models. No statistically significant differences were shown between the direct manual measurements and 3D measurements of length, width and depths. The Spearman's (r_s) and Pearson correlation (r) tests established strong positive correlations between the measurements, which were statistically significant. This validation of the 3D wound measurements in the study is a novel finding and a positive development in wound measurement as the 3D measurement method is a non-contact method, based on a faster, more controlled and accurate technique while providing permanent records with 3D surface geometry and coloured-textured information. On the other hand, deficiencies of the 2D wound measurement method was exposed within this study. The method underestimated the measurements, particularly when used for larger and irregular shaped wounds located on uneven surfaces.

Therefore, it can be said that the structured light 3D scanning technique can be used for wound documentation and measurements in forensic medicine. However, for now, the method should be limited to wounds that have complicated scenarios in conjunction with digital photography as more studies are still needed in this area.

10.2 Implications of the study

The implications of this study are presented below in three sections: a contribution to the knowledge; the implications for practice, the implications for future research.

10.2.1 Contribution to knowledge

1. Most of the studies in the literature review focused on introducing active and passive 3D surface scanning techniques or combine these external methods with the techniques of the internal 3D documentation (MRI /CT). Researchers previously scanned traumatic injuries or subject full bodies while they were introducing these techniques; however, they did not concentrate on analysing the 3D results or compare them to current 2D results. In this study, 3D results of different types of traumatic injuries were analysed while considering the results of current documentation methods. By doing this, it was easy to highlight the advantages of 3D surface scanning while exposing disadvantages of the existing recording method. Additionally, it was easy to show how 3D results of the recorded injuries could address the current issues in medico-legal centres surrounding wound interpretation, documentation and measurements ([9.3.1](#) and [9.4.1](#)). Moreover, most of the studies in the literature review used the ATOS structured light 3D scanner, which is difficult to apply for routine works in forensic medicine. In addition, the equipment is expensive (costing up to € 50.000). However, this research has demonstrated two more applicable and affordable structured light scanners, which were accurate, fast and produced high resolution results. This means that they can be easily attained and used in many medico-legal centres for practical applications, or research works.

2. This study has considered some deficiencies in the literature review, such as, shortage in the 3D reconstruction of the traumas from living persons. Additionally, there is no written standard procedure for scanning injured live subjects and no study has yet validated structured light 3D wound measurements, particularly depths and surface areas. Therefore, (a) this study involved scanning injured live subjects in the Medico-Legal Centre and provided much information about 3D reconstruction of injuries from living subjects. For example, how different areas of the living body could be accessed and scanned, what are the limitations that could be faced during scanning and how these could be addressed. This information will increase the understanding of other researchers and allow them to be aware of the limitations and to overcome them easily in future applications. (b) This study set up useful and simple guidelines to access and scan different body areas of living subjects. (c) The research

validated 3D wound measurements collected from structured light models, including length, width and depth dimensions of the wounds.

10.2.2 Implications for medico-legal practice

It has been explained in [9.3.1](#) and [9.4.1](#) how the research findings are able to address current challenges in practice surrounding traumatic wound analysis alongside wound recoding and measurements. Briefly, this demonstrates that some important wound features are better recorded in 3D results while the 3D documents have extra features compared to the 2D documents. Additionally, the 3D technique was faster, more controlled and accurate method that overcame the main weaknesses of the digital photography relating to lighting conditions, angle of acquisition and distances. Furthermore, validated 3D wound measurements can be used to address the serious disadvantages of the current measurement methods as the 3D versions are actual sizes and based on accurate recording. Therefore, the structured light technique can be used in actual practice (medico-legal centres) to overcome the current recording deficiencies. However, because the 3D surface scanning method in forensic medicine is still a novel method and still requires more research, it was recommended to use alongside digital photography in some cases associated with difficult scenarios. These situations, for example, severe trauma alongside any injuries that will cause permanent infirmity or facial deformity, or, a crime that involve multiple assailants. By this way, the new 3D technique will be gradually introduced, and become dominant in the practical field.

10.2.3 Implications for future research

Some suggested future works are summarised below for forensic practitioners who wish to explore this approach further. The first two recommendations are around the same research topic that expand the 3D wound reconstruction, analysis and measurements, and that provide more validation of the concept. The next three recommendations are more advanced applications, but are still in relation to the traumatic wound reconstruction and analysis in forensic medicine. The last recommendation is about establishing of a wide-ranging protocol of structured light 3D surface scanning of traumatic injuries in order to apply it in all medico-legal centres and to be accepted in court. These six recommendations are:

1. Three separate structured light scanning applications are required to apply to three different types of trauma separately: blunt force injuries, sharp force injuries and

firearm injuries. Analysis of the 3D results of each type of trauma individually will expand and strengthen any wider 3D wound analysis.

2. The accuracy of structured light 3D wound measurements should be confirmed in comparison to control measurements.

3. Application of structured light 3D surface scanning to scan traumatic injuries and their suspected causative tools for matching and find correspondence is highly recommended.

4. Application of this technique during the autopsy to record injured organs, such as a heart with a penetrating wound, or any other traumatised solid organs, is an area of interest. During the conventional autopsy, the body cavities are dissected and their organs are removed and examined outside the body. Therefore, these traumatized organs can be scanned three-dimensionally inside the autopsy room. The 3D results of this application would be useful, especially if the traumas were the cause of death.

5. It is also recommended to combine structured light 3D surface scanning results of deadly penetrating injuries with 3D documentations results of CT/MRI (virtual autopsy) of the same injuries to obtain complete recording images from external to internal.

6. Within this study, simple scanning guidelines were set up to scan different body areas of living subjects (5.5). These guidelines included using an appropriate 3D scanning technique to scan different body areas, optimal numbers of scan for each scanned area, scanning approaches to access different body areas and the elimination of background noise from the scans. However, a comprehensive scanning protocol should be established. It should include court requirements of (1) admissible 3D documents, such as the minimum number of vertices, and (2) used scanner, such as the level of resolution and accuracy of the scanner. It should also consider scanning approach to access different areas of deceased bodies.

References

1. Abate, AF., Nappi M., Riccio, D. and Sabatino, G. (2007) '2D and 3D Face recognition: a survey', *Pattern Recognition Letters*, 28(24), pp. 1885-1906. DOI: [10.1016/j.patrec.2006.12.018](https://doi.org/10.1016/j.patrec.2006.12.018).
2. Abdul-Rani, M., Chong, KK., Hani, AFM., Yap, YB. and Jamil, A. (2011) 'Analytical studies on volume determination of leg ulcer using structured light and laser triangulation data acquisition techniques', 18th *Iranian Conference of Biomedical Engineering*, Tehran, Iran, 14-16 December 2011, pp. 119-122. DOI: [10.1109/ICBME.2011.6168536](https://doi.org/10.1109/ICBME.2011.6168536).
3. Adams, LP. and Spirakis, A. (1997) 'Stereo-photogrammetry', in Shelton, JC and Orr, JF. (eds.) *Optical Measurement Methods in Biomechanics*. London: Chapman and Hall, pp. 17-37. DOI: [10.1007/978-0-585-35228-2_2](https://doi.org/10.1007/978-0-585-35228-2_2).
4. Akca, D. (2012) '3D Modeling of culture heritage objects with a structured light system', *Mediterranean Archaeology and Archaeometry*, 12(1), pp. 139-152.
5. Al Ali, A., Richmond, S., Popat, H., Toma, AM., Playle, R., Zhurov, AI., Marshall, D., Rosin, P. and Henderson, J. (2014) 'The influence of asthma on face shape: a three-dimensional study', *European Journal of Orthodontics*, 36(4), pp. 373-380. DOI: [10.1093/ejo/cjs067](https://doi.org/10.1093/ejo/cjs067).
6. Al Ali, A., Richmond, S., Popat, H., Playle, R., Pickles, T., Zhurov, A., Marshall, D., Rosin, P., Henderson, J. and Bonuck, K. (2015) 'The influence of snoring, mouth breathing and apnoea on facial morphology in late childhood: a three-dimensional study', *British Medical Journal*, 5(9), pp. 1-9. DOI: [10.1136/bmjopen-2015-009027](https://doi.org/10.1136/bmjopen-2015-009027).
7. Al-Khatib, AR. (2010) 'Facial three dimensional surface imaging: an overview', *Archives of Orofacial Sciences*, 5(1), pp. 1-8.
8. Archaeology data service (2009) *Introduction to the laser scanning guide*. Available at: http://guides.archaeologydataservice.ac.uk/g2qp/LaserScan_1-2 (Accessed: 30 March 2016).

9. Arias-Sánchez, P., Armesto, J., Rodríguez-Pérez, JR. and Sanz-Ablanedo, E. (2009) 'Metric potential of a 3D measurement system based on digital compact cameras', *Sensors*, 9(6), pp. 4178-4194. DOI: [10.3390/s90604178](https://doi.org/10.3390/s90604178).
10. Artec3D (2018) *Artec Eva*. Available at: <https://www.artec3d.com/portable-3d-scanners/artec-eva> (Accessed: 2 June 2018).
11. Aung, SC., Ngim, RCK. and Lee, ST. (1995) 'Evaluation of the laser scanner as a surface measuring tool and its accuracy compared with direct facial anthropometric measurements', *British Journal of Plastic Surgery*, 48(8). pp. 551-558. DOI: [10.1016/0007-1226\(95\)90043-8](https://doi.org/10.1016/0007-1226(95)90043-8).
12. Avon, SL., Victor, C., Mayhall, JT. and Wood, RE. (2010) 'Error rates in bite mark analysis in an in vivo animal model', *Forensic Science International Journal*, 201(1), pp. 45–55. DOI: [10.1016/j.forsciint.2010.04.016](https://doi.org/10.1016/j.forsciint.2010.04.016).
13. Aynechi, N., Larson, B., Leon, V. and Beiraghi, S. (2011) 'Accuracy and precision of a 3D anthropometric facial analysis with and without landmark labelling before image acquisition', *An International Journal of Orthodontics and Dentofacial Orthopedics*, 81(2), pp. 245-252. DOI: [10.2319/041810-210.1](https://doi.org/10.2319/041810-210.1).
14. Baker, HC., Marsh, N. and Quinones, I. (2013) 'Photography of faded or concealed bruises on human skin', *Journal of Forensic Identification*, 63(1), pp. 103-125.
15. Battle, J., Mouaddib, E. and Salvi, J. (1998) 'Recent progress in coded structured light as a technique to solve the correspondence problem: a survey', *Pattern Recognition*, 31(7), pp. 963-982. DOI: [10.1016/S0031-3203\(97\)00074-5](https://doi.org/10.1016/S0031-3203(97)00074-5).
16. Bianco, M. and Williams, C. (2002) 'Using photography in wound assessment', *Practice Nurses*, 13(11), pp. 505-508. DOI: [10.12968/pnur.2002.13.11.10844](https://doi.org/10.12968/pnur.2002.13.11.10844).
17. Bhullar, DS. and Aggarwal, KK. (2007) 'Medicolegal diagnosis and pattern of injuries with sharp weapons', *Journal of Indian Academy of Forensic Medicine*, 29(4), pp. 112-114.

18. Blais, F. (2004) 'Review of 20 years of range sensor development', *Journal of Electronic Imaging*, 13(1), pp. 231-240. DOI: [10.1117/1.1631921](https://doi.org/10.1117/1.1631921).
19. Bland, JM. and Altman, DG. (2010) 'Statistical methods for assessing agreement between two methods of clinical measurements', *International Journal of Nursing Studies*, 47, pp. 931-936. DOI: [10.1016/s0140-6736\(86\)90837-8](https://doi.org/10.1016/s0140-6736(86)90837-8).
20. Bloemen, EM., Rosen, T., Cline, JA., LoFaso, V., Clark, S., Mulcare, MR., Stern, ME., Mysliwiec, R., Flomenbaum, N., Lachs, MS. and Hargarten, S. (2012) *Comprehensive photography protocol general & specific guidelines for photographing injuries in older adults*. Available at: <http://nyceac.com/wp-content/uploads/2012/02/Photography-Protocol.pdf> (Accessed: 7 November 2016).
21. Bouguet, J-Y. and Perona, P. (1998) '3D Photography on your desk', *Sixth International Conference on Computer Vision*, Bombay, India, 7-7 January 1998, pp. 43-50. DOI: [10.1109/ICCV.1998.710699](https://doi.org/10.1109/ICCV.1998.710699).
22. Bourke, P. (2015) *Workflow for comparing two photogrammetrically reconstructed mesh*. Available at: <http://paulbourke.net/miscellaneous/cloudcompare/> (Accessed: 1 August 2018).
23. Buchon-Moragues, F., Bravo, JM., Ferri, M. and Redondo, J. (2016) 'Application of structured light system technique for authentication of wooden panel painting', *sensors*, 16(6), pp. 881. DOI: [10.3390/s16060881](https://doi.org/10.3390/s16060881).
24. Bruschiweiler, W., Braun, M., Dirnhofer, R. and Thali, MJ. (2003) 'Analysis of patterned injuries and injury-causing instruments with forensic 3D/CAD supported photogrammetry (FPHG): an instruction manual for the documentation processes', *Forensic Science International Journal*, 132(2), pp. 130–138. DOI: [10.1016/S0379-0738\(03\)00006-9](https://doi.org/10.1016/S0379-0738(03)00006-9).
25. Bryant, JL., Brooks, TL., Schmidt, B. and Mostow, EN. (2001) 'Reliability of wound measuring techniques in an outpatient wound centre', *Ostomy Wound Management*, 47(4), pp. 44-51.

26. Boersma, SM., Van den Heuvel, FA., Cohen, AF., Scholtens, REM. (2000) 'Photogrammetric wound measurement with a three-camera vision system', *International Archives of Photogrammetry and Remote Sensing and Spatial Information Sciences*, 33, pp. 84-91.
27. Bowling, FL., King, L., Fadavit, H., Paterson, JA., Preece, K., Daniel, RW., Matthews, DJ. and Boulton, AJ. (2009) 'An assessment of the accuracy and usability of a novel optical wound measurement system', *Diabetic Medicine*, 26(1), pp. 93-96. DOI: [10.1111/j.1464-5491.2008.02611.x](https://doi.org/10.1111/j.1464-5491.2008.02611.x).
28. Bowling, FL., King, L., Paterson, JA., Hu, J., Lipsky, BA., Matthews, DR. and Boulton, AJM. (2011) 'Remote assessment of diabetic foot ulcers using a novel wound imaging system' *Wound Repair and Regeneration*, 19(1), pp. 25-30. DOI: [10.1111/j.1524-475X.2010.00645.x](https://doi.org/10.1111/j.1524-475X.2010.00645.x).
29. Boyat, AK. and Joshi, BK. (2015) 'A review paper: noise models in digital image processing', *Signal and Image Processing: An International Journal*, 6(2), pp. 63- 75. DOI: [10.5121/sipij.2015.6206](https://doi.org/10.5121/sipij.2015.6206).
30. Breitbeck, R., Ptacek, W., Ebert, L., Furst, M., Kronreif, G. and Thali, M. (2013) 'Virtobot-A robot system for optical 3D scanning in forensic medicine', *Proceedings of 4th International Conference on 3D Body Scanning Technologies*. Long Beach CA, USA, 19-20 November 2013, pp. 84-91. DOI: <http://dx.doi.org/10.15221/13.084>.
31. Brennan, PAW. (2006) 'The medical and ethical aspects of photography in the sexual assault examination: why does it offend?', *Journal of Clinical Forensic Medicine*, 13(4), pp. 194-202. DOI: [10.1016/j.jcfm.2006.02.004](https://doi.org/10.1016/j.jcfm.2006.02.004).
32. Bruno, F., Bianco, G., Muzzupappa, M., Barone, S. and Razionale, AV. (2011) 'Experimentation of structured light and stereo vision for underwater 3D reconstruction', *ISPRS Journal of Photogrammetry and Remote Sensing*, 66(4), pp. 508–518. DOI: [10.1016/j.isprsjprs.2011.02.009](https://doi.org/10.1016/j.isprsjprs.2011.02.009).
33. Buck, U., Nather, S., Braun, M. and Thali, MJ. (2009) 'External Body Documentation', in Thali, MJ, Dirnhofer, R. and Vock, P. (eds.) *The Virtopsy Approach*

3D Optical and Radiological Scanning and Reconstruction in Forensic Medicine. Boca Raton: CRC Press, pp. 151-156.

34. Buck, U., Naether, S., Rass, B., Jackowski, C. and Thali, M.J. (2013) 'Accident or homicide- virtual crime scene reconstruction using 3D methods', *Forensic Science International Journal*, 225(1-3), pp. 75-84. DOI: [10.1016/j.forsciint.2012.05.015](https://doi.org/10.1016/j.forsciint.2012.05.015).

35. Buck, U., BuBe, K., Campana, L. and Schyma, C. (2018) 'Validation and evaluation of measuring methods for the 3D documentation of external injuries in the field of forensic medicine', *International Journal of Legal Medicine*, 132, pp. 551-561. DOI: [10.1007/s00414-017-1756-6](https://doi.org/10.1007/s00414-017-1756-6).

36. Callieri, M., Cignoni, P., Pingi, P. and Scopingno, R. (2003) 'Derma: monitoring the evolution of skin lesions with a 3D system', *Proceedings of the Vision, Modeling, and Visualization Conference*, München, Germany, 19-21 November 2003.

37. Campana, L., Breitbeck, R., Bauer-Kreuz, R. and Buck, U. (2016) '3D Documentation and visualization of external injury findings by integration of simple photography in CT/MRI data sets (IprojeCT)', *International Journal of Legal Medicine*, 130(3), pp. 787-797. DOI: [10.1007/s00414-015-1274-3](https://doi.org/10.1007/s00414-015-1274-3).

38. Canon (2017) *Lenses: Close-up lenses*. Available at: http://cpn.canon-europe.com/content/education/infobank/lenses/close-up_lenses.do?page=2 (Accessed: 6 July 2017).

39. Carew, RM. and Errickson, D. (2019) 'Imaging in forensic science: five years on', *Journal of Forensic Radiology and Imaging*, 16, pp. 24-33. DOI: [10.1016/j.jofri.2019.01.002](https://doi.org/10.1016/j.jofri.2019.01.002).

40. Casas, L., Castaneda, B. and Treuillet, S. (2011) 'Imaging technology applied to chronic wounds: a survey', *Proceedings of the 4th International Symposium on Applied Sciences in Biomedical and Communication Technologies*. Barcelona, Spain, 26-29 October 2011, pp. 1-5. DOI: [10.1145/2093698.2093865](https://doi.org/10.1145/2093698.2093865).

41. Chang, AC., Dearman, B and Greenwood, JE. (2011) 'A comparison of wound area measurement techniques: visitrak versus photography', *Eplasty Journal*, 11, pp. 158-166.
42. Chen, X., Xi, J., Jin, Y. and Sun, J. (2009) 'Accurate calibration for a camera-projector measurement system based on structured light projection', *Optics and Laser in Engineering*, 47(3), pp. 310-319. DOI: [10.1016/j.optlaseng.2007.12.001](https://doi.org/10.1016/j.optlaseng.2007.12.001).
43. Chulhyun, A. and Richard, S. (2008) 'Advanced in wound photography and assessment methods', *Advanced in Skin and Wound Care*, 21(2), pp. 85-93. DOI: [10.1097/01.ASW.0000305411.58350.7d](https://doi.org/10.1097/01.ASW.0000305411.58350.7d).
44. Clemson University (2018) *Photogrammetry*. Available at: <https://www.clemson.edu/centersinstitutes/conservation/equipment/photogrammetry.html> (Accessed: 29 March 2016).
45. CloudCompare (2015) *How to compare two 3D entities*. Available at: [https://www.cloudcompare.org/doc/wiki/index.php?title=How to compare two 3D entities](https://www.cloudcompare.org/doc/wiki/index.php?title=How_to_compare_two_3D_entities) (Accessed: 1 August 2018).
46. Conrad, E. (1957) 'Colour photography, an Instrumentality of proof', *Journal of Criminal Law, Criminology*, 48(3), pp. 321-332. DOI: [10.2307/1139597](https://doi.org/10.2307/1139597).
47. Cox-Brinkman, J., Vedder, A., Hollak, C., Richfield, L., Mehta, A., Orteu, K., Wijburg, F., Hammond, P. (2007) 'Three-dimensional face shape in Fabry disease', *European Journal of Human Genetics*, 15 (5), pp. 535-542. DOI: 10.1038/sj.ejhg.5201798.
48. Cohen, N. and Maclennan-Brown, K. (2007) *Digital imaging procedure*. Version 2.1. Available: https://assets.publishing.service.gov.uk/government/uploads/system/uploads/attachment_data/file/378451/DIP_2.1_16-Apr-08_v2.3_Web_2835.pdf (Accessed: 4 April 2018).
49. Constant AR. (2000) *Close-up photography*. Boston Oxford: Focal press.

50. Corsarca, C., Jocea, A. and Savu, A. (2009) *Analysis of error sources in Terrestrial Laser Scanning*. Available at: http://revcad.uab.ro/upload/18_144_Paper11_RevCAD09_2009.pdf (Accessed: 24 June 2016).
51. Crane, J. (2009) 'Injury', in McLay, WDS. (ed.) *Clinical Forensic Medicine*. Cambridge University Press, pp. 99-113.
52. D'Apuzzo, N. and Gruen, A. (2009) 'Recent advances in 3D full body scanning with applications to fashion and apparel', in Gruen, A. and Kahmen, H. (eds.) *Optical 3-D Measurement Techniques*. Vienna, Austria.
53. Darlene, H., Diane, L., Julie, A., Susan, H. and Patricia, T. (2007) 'Measuring wounds', *Nursing*, 37(2), pp. 18-21. DOI: [10.1097/00152193-200702000-00012](https://doi.org/10.1097/00152193-200702000-00012).
54. Davy-Jow, SL., Less, DMB. and Russel, S. (2013) 'Virtual forensic anthropology: novel applications of anthropometry and technology in a child death case', *Forensic Science International*, 224(1-3), pp. e7-e10. DOI: [10.1016/j.forsciint.2012.11.002](https://doi.org/10.1016/j.forsciint.2012.11.002).
55. Denton, JS., Segovia, A. and Filkins, JA. (2006) 'Practical pathology of gunshot wounds', *Archives of Pathology and Laboratory Medicine*, 130(9), pp. 1283-9.
56. De Sainte Croix, MM., Gauld, D., Forgie, AH. and Lowe, R. (2016) 'Three-dimensional imaging of human cutaneous forearm bite marks in human volunteers over a 4-day period', *Journal of Forensic and Legal Medicine*, 40, pp. 34-39. DOI: [10.1016/j.jflm.2016.02.003](https://doi.org/10.1016/j.jflm.2016.02.003).
57. Diane, L., Darlene, H. Julie, A., Patricia, T. and Susan, H. (2006) 'Digital wound photography: points to practice', *Advances in Skin and Wound Care Journal*, 19(7), pp. 386 – 387. DOI: [10.1097/00129334-200609000-00015](https://doi.org/10.1097/00129334-200609000-00015).
58. Diane, L., Julie, A., Darlene, H., Susan, H. and Patricia, T. (2008) 'Measuring wound length, width, and area: which technique?', *Advances in Skin & Wound Care*, 21(1), pp. 42 – 45. DOI: [10.1097/01.ASW.0000284967.69863.2f](https://doi.org/10.1097/01.ASW.0000284967.69863.2f).

59. Ebert, LC., Flach, P., Schweitzer, W., Leipner, A., Kottner, S., Gascho, D., Thali, M.J. and Breitbeck, R. (2016) 'Forensic 3D surface documentation at the Institute of Forensic Medicine in Zurich-workflow and communication pipeline', *Journal of Forensic Radiology and Imaging*, 5, pp. 1-7. DOI: [10.1016/j.jofri.2015.11.007](https://doi.org/10.1016/j.jofri.2015.11.007).
60. Edwards, J. and Rogers, T. (2018) 'The accuracy and applicability of 3D modeling and printing blunt force cranial injuries', *Journal of Forensic Science*, 63(3), pp. 683-691. DOI: [10.1111/1556-4029.13627](https://doi.org/10.1111/1556-4029.13627).
61. Ehlert, A., Salah, Z. and Bartz, D. (2006) 'Data reconstruction and visualization techniques for forensic pathology', *Proceedings of the Eighth Joint Eurographics/IEEE-VGTC conference on Visualization*, Switzerland, 8-10 May 2006, pp. 323-330. DOI: [10.2312/VisSym/EuroVis06/323-330](https://doi.org/10.2312/VisSym/EuroVis06/323-330).
62. Eriksson, G., Eklund, A., Torlegard, K. and Dauphin, E. (1979) 'Evaluation of leg ulcer treatment with stereo-photogrammetry', *British Journal of Dermatology*, 101(2), pp. 123-131. DOI: [10.1111/j.1365-2133.1979.tb05596.x](https://doi.org/10.1111/j.1365-2133.1979.tb05596.x).
63. Errickson, D., Thompson, TJU. and Rankin, BWJ. (2014) 'The application of 3D visualization of osteological trauma for the courtroom: a critical review', *Journal of Forensic Pathology and Imaging*, 2(3), pp. 132-137. DOI: [10.1016/j.jofri.2014.04.002](https://doi.org/10.1016/j.jofri.2014.04.002).
64. Errickson, D., Thompson, TJU. and Rankin, BWJ. (2015) *An optimum guide for the reduction of noise using a surface scanner for digitising human osteological remains*. Available at: http://guides.archaeologydataservice.ac.uk/q2gp/CS_StructuredLight (Accessed: 19 April 2016).
65. Errickson, D., Grueso, I., Griffith, SJ., Setchell, JM., Thompson, TJU., Thompson, CEL. and Gowland, RL. (2017) 'Towards a best practice for the use of active non-contact surface scanning to record human skeletal remains from archaeological contexts', *International Journal of Osteoarchaeology*, 27, pp. 650-661. DOI: [10.1002/oa.2587](https://doi.org/10.1002/oa.2587).

66. Evans, TS., Jones, C. and Plassmann, P. (2013) '3D imaging for bite mark analysis', *Imaging Science Journal*, 61(4), pp. 351-360. DOI: [10.1179/1743131X11Y.00000000054](https://doi.org/10.1179/1743131X11Y.00000000054).
67. Evans, S., Baylis, S., Carabott., Jones, M., Kelson, Z., Marsh, N., Payne-James, J., Ramadani, J., Vanezis, P. and Kemp, A. (2014) 'Guidelines for photography of cutaneous marks and injuries: a multi-professional perspective', *Journal of Visual Communication in Medicine*, 37(1-2), pp. 3-12. DOI: [10.3109/17453054.2014.911152](https://doi.org/10.3109/17453054.2014.911152).
68. Faculty of Forensic and Legal Medicine (FFLM) (2017) *PICS working group guidelines on photography*. Available at: <https://fflm.ac.uk/wp-content/uploads/2018/01/PICS-Working-Group-Guidelines-on-Photography-Dr-Will-Anderson-May-2017.pdf> (Accessed: 3 March 2018).
69. Fernando, B., José María, B., Marcelino, F., Javier, R. and Juan Vicente, S. (2016) 'Application of structured light system technique for authentication of wooden panel paintings', *Sensors Journal*, 16(6), pp. 881-890. DOI: [10.3390/s16060881](https://doi.org/10.3390/s16060881).
70. Ferrucci, M., Doiron, TD., Thompson, RM., Jones, JP., Freeman, AJ., Neiman, JA. (2016) 'Dimensional review of scales for forensic photography' *Journal of Forensic Sciences*, 61(2), pp. 509-519. DOI: [10.1111/1556-4029.12976](https://doi.org/10.1111/1556-4029.12976).
71. Fette, AM. (2006) *A clinimetric analysis of wound measurement tools*. Available at: <http://www.worldwidewounds.com/2006/january/Fette/Clinimetric-Analysis-Wound-Measurement-Tools.html> (Accessed: 30 January 2017).
72. Foltynski, P., Ladyzynski, P., Sabalinska, S. and Wojcicki, JM. (2013) 'Accuracy and precision of selected wound area measurement in diabetic foot ulceration', *Diabetic Technology and Therapeutics*, 15(8), pp. 711-720. DOI: [10.1089/dia.2013.0026](https://doi.org/10.1089/dia.2013.0026).
73. Foltynski, P., Ladyzynski, P., Ciechanowska, A., Migalska-Musial, K., Judzewicz, G. and Sabalinska, S. (2015), 'Wound Area Measurement with digital planimetry: improved accuracy and precision with calibration based on 2 rulers', *PLOS ONE*. 10(8), pp. 1-13. DOI: [10.1371/journal.pone.0134622](https://doi.org/10.1371/journal.pone.0134622).

74. Forensic Animation (2012) *Introductory video on CloudCompare*. Available at: <https://www.youtube.com/watch?v=MQiD4HjhpAU> (Accessed: 1 August 2018).
75. Forensic Medicine for Medical Students (FMMS) (2015-a) *Bite marks*. Available at: <http://www.forensicmed.co.uk/wounds/bitemarks/>(Accessed: 12 December 2015).
76. Forensic Medicine for Medical Students (FMMS) (2015-b) *Wound photography*. Available at: <http://www.forensicmed.co.uk/wounds/wound-documentation/wound-imaging/> (Accessed: 17 November 2016).
77. Foster, GV. and Barker, NJ. (1996) 'Close-up photography of archaeological objects', *Journal of Field Archaeology*, 23(3), pp. 369–375. DOI: [10.1179/009346996791973864](https://doi.org/10.1179/009346996791973864).
78. Geng, J. (2011) 'Structured-light 3D surface imaging: a tutorial', *Advance in Optics and Photonics Journal*, 3(2), pp. 128-160. DOI: [10.1364/AOP.3.000128](https://doi.org/10.1364/AOP.3.000128).
79. Georgopoulos, A., Ioannidis, CH. and Valanis, A. (2010) 'Assessing the performance of a structured light scanner', *International Archives of Photogrammetry, Remote Sensing and Spatial Information Sciences*, Vol, XXXVIII, Part 5, pp. 250-255.
80. Ghasemi, A. and Zahediasl, S. (2012), 'Normality tests for statistical analysis: a guide for non-statisticians' *International Journal of Endocrinology and Metabolism*, 10(2), pp. 486-489. DOI: [10.5812/ijem.3505](https://doi.org/10.5812/ijem.3505).
81. Goldman, RJ. and Salcido, R. (2002) 'More than one way to measure a wound: an overview of tools and techniques', *Advances in Skin & Wound Care Journal*, 15(5), pp. 236-243. DOI:[10.1097/00129334-200209000-00011](https://doi.org/10.1097/00129334-200209000-00011).
82. Goodwin, L., Evison, MP. and Schofield, D. (2010) 'Image quality and accuracy in three 3D scanners, in Evison, M. and Bruegge, RV. (eds.) *Computer-Aided Forensic Facial Comparison*. New York: Taylor and Francis, pp. 11-34.

83. Goos, MIM., Alberink, IB. and Ruifrok, ACC (2006) '2D/3D Image (facial) comparison using camera matching', *Forensic Science International*, 163 (1), pp. 10-17. DOI: [10.1016/j.forsciint.2005.11.004](https://doi.org/10.1016/j.forsciint.2005.11.004).
84. Gorthi, SS. and Rastogi, P. (2010) 'Fringe projection techniques', *Optics and Laser in Engineering Journal*, 48(2), pp. 133-140.
85. Green, WM. and Schulman, E. (2010) 'Forensic photography', in Riviello RJ. (ed.) *Manual of Forensic Emergency Medicine: A guide for Clinicians*. Jones and Bartlett Publisher, pp. 44-58.
86. Gupta, M., Yin, Q. and Nayar, S.K. (2013) 'Structured light in sunlight', *International Conference on Computer Vision*, Sydney, NSW, Australia, 1-8 December, 2013, pp. 545-552. DOI: [10.1109/ICCV.2013.73](https://doi.org/10.1109/ICCV.2013.73).
87. Haghpanah, S., Bogie, K., Wang, X., Banks, PG., Ho, CH. (2006) 'Reliability of electronic versus manual wound measurement techniques', *Archives of Physical Medicine and Rehabilitation*, 87(10), pp. 1396 – 1402. DOI: [10.1016/j.apmr.2006.06.014](https://doi.org/10.1016/j.apmr.2006.06.014).
89. Hanlon, KL. (2017) 'Cross-polarized and parallel-polarized light: viewing and photography for examination and documentation of biological materials in medicine and forensics', *Journal of Visual Communication in Medicine*, 41(1), pp. 3-8. DOI: [10.1080/17453054.2018.1420418](https://doi.org/10.1080/17453054.2018.1420418).
90. Hettrick, H. and Hardigan, P. (2017) 'Early detection of pressure injury using a forensic alternate light source', *Wounds: Compendium of Clinical Research and Practice*, 29(8), pp. 222-228.
91. HP customer support (2019) *HP 3D Scan Software Pro v5 online instructions*. Available at: <https://support.hp.com/us-en/product/hp-3d-structured-light-scanner/14169438/document/c05286558> (accessed: 27 October 2018).
92. Hyzer, WG. and Krauss, TC. (1988) 'Bite mark standard reference scale- ABFO No. 2', *Journal of Forensic Sciences*, 33(2), pp. 498-506. DOI: [10.1520/JFS11963J](https://doi.org/10.1520/JFS11963J).

93. Ishii I. (2012) *A coded structured light projection method for high-frame-rate 3D image acquisition*. Available at: <http://cdn.intechopen.com/pdfs-wm/32185.pdf> (Accessed: 27 October 2016).
94. Jecic, S. and Drvar, N. (2003) 'The assessment of structured light and laser scanning methods in 3D shape measurements', *4th International Congress of Croatian Society of Mechanic*, Bizovac, Croatia, September 18-20 2003, pp. 237-244.
95. John Tzou, C., Artner, NM., Pona, I., Hold, A., Placheta, E., Kropatsch, WG. and Frey, M. (2014) 'Comparison of three-dimensional surface-imaging systems', *Journal of Plastic, Reconstructive and Aesthetic Surgery*, 67(4), pp. 489-497. DOI: [10.1016/j.bjps.2014.01.003](https://doi.org/10.1016/j.bjps.2014.01.003).
96. Johnson, JD. (1995) 'Using ulcer surface area and volume to document wound size', *Journal of the American Podiatric Medical Association*, 85(2), pp. 91-95. DOI: [10.7547/87507315-85-2-91](https://doi.org/10.7547/87507315-85-2-91).
97. Johnson, OR., Lyall, M. and Johnson, CP. (2015) 'The use of dental putty in the assessment of hard surfaces within paved urban areas that may leave defined or patterned marks on bodies', *Medicine, Science and the Law*, 55(2), pp. 129-132. DOI: [10.1177/0025802414527078](https://doi.org/10.1177/0025802414527078).
98. Jones, PRM. and Rioux, M. (1997) 'Three-dimensional surface anthropometry: Applications to the human body', *Optics and Laser in Engineering*, 28(2), pp. 89-117. DOI: [10.1016/S0143-8166\(97\)00006-7](https://doi.org/10.1016/S0143-8166(97)00006-7).
99. Jones, BF. and Plassmann, P. (1995) 'An instrument to measure the dimensions of skin wounds', *IEEE Transactions on Biomedical Engineering*, 42(5), pp. 464-470. DOI: [10.1109/10.376150](https://doi.org/10.1109/10.376150).
100. Jones, R. and Karch, SB. (2003) *Simpson's Forensic Medicine*. 12th edition. London: CRP Press. DOI: [10.1201/b13639](https://doi.org/10.1201/b13639).
101. Kalisperakis, I., Grammatikopoulos, L., Petsa, E. and Karras, G. (2011) 'A structured light approach for the reconstruction of complex objects', *Geoinformatics CTU FCE*, 6, pp. 259 – 266. DOI: [10.14311/gi.6.32](https://doi.org/10.14311/gi.6.32).

102. Karpoor, S. and Arlikatti, PS. (2012) 'Wound photography: a step towards reality', *Indian Journal of Forensic Medicine and Toxicology*, 6(1), pp. 102 – 103.
103. Keast, DH., Bowering, CK., Evans, AW., Mackean, GL., Burrows, C. and D'Souza, L. (2004) 'Measure: a proposed assessment framework for developing best practice recommendations for wound assessment', *Wound Repair and Regeneration*, 12(S1), pp. S1 - S17. DOI: [10.1111/j.1067-1927.2004.0123S1.x](https://doi.org/10.1111/j.1067-1927.2004.0123S1.x).
104. Kecelj-Leskovec, N., Jezersek, M., Mozina, J., Pavlovic, M. and Lunder, T. (2007) 'Measurement of venous leg ulcers with a laser-based three-dimensional method: comparison to computer planimetry with photography', *Wound Repair and Regeneration*, 15(5), pp. 767-771. DOI: [10.1111/j.1524-475X.2007.00300.x](https://doi.org/10.1111/j.1524-475X.2007.00300.x).
105. Kim, H. (2013), 'Statistical notes for clinical researchers: assessing normal distribution (2) using skewness and kurtosis', *Restorative Density and Endodontics*, 38(1), pp. 52–54. DOI: [10.5395/rde.2013.38.1.52](https://doi.org/10.5395/rde.2013.38.1.52).
106. Klaas, E. (2012) *What light colour should a white light scanner use?*. Available at: http://8-tree.com/wp-content/uploads/2012/11/CMSC-2012-What-light-color-should-a-White-Light-Scanner-use_v5-final.pdf (Accessed: 20 July 2016).
107. Klinge, C. and Reiter K. (2008) *UV/IR Injury photography*. Available at: http://www.evidencemagazine.com/index.php?option=com_content&task=view&id=106 (Accessed: 17 November 2016).
108. Koller, S., Ebert, LC., Martinez, RM., Sieberth, T. (2019) 'Using virtual reality for forensic examination of injuries', *Forensic Science International*, 295, pp. 30-35. DOI: [10.1016/j.forsciint.2018.11.006](https://doi.org/10.1016/j.forsciint.2018.11.006).
109. Komar, DA., Davy-Jow, S. and Decker, SJ. (2012) 'The use of a 3D laser scanner to document ephemeral evidence at crime scenes and post-mortem examinations', *Journal of Forensic Science*, 57(1), pp. 188–191. DOI: [10.1111/j.1556-4029.2011.01915.x](https://doi.org/10.1111/j.1556-4029.2011.01915.x).

110. Konica Minolta (2002) *VIVID 910 non-contact 3D digitizer*. Available at: http://www.dirdim.com/pdfs/DDI_Konica_Minolta_Vivid_910.pdf (Accessed: 12 February 2019).
111. Koo, TK. and Li, MY. (2016) 'A guideline of selecting and reporting Intraclass correlation coefficients for reliability research', *Journal of Chiropractic Medicine*, 15(2), pp. 155-163. DOI: [10.1016/j.jcm.2016.02.012](https://doi.org/10.1016/j.jcm.2016.02.012).
112. Koronfel, A. (2014) *Koronfel's forensic medicine*. Available at: <http://koronfel forensic medicine.blogspot.co.uk/2014/12/wounds-stab-wounds.html?view=snapshot> (Accessed: 17 November 2016).
113. Kottner, S., Schaerli, S., Fürst, M., Ptacek, W., Thali, M. and Gascho, D. (2019) 'VirtoScan-on-Rails – an automated 3D imaging system for fast post-mortem whole-body surface documentation at autopsy tables', *Forensic Science, Medicine and Pathology*, pp. 1-15. DOI: [10.1007/s12024-019-00095-5](https://doi.org/10.1007/s12024-019-00095-5).
114. Kovacs, L., Zimmermann, A., Brockmann, G., Gühring, M., Baurecht, H., Papadopoulos, NA., Schwenger-Zimmerer, K., Sader, R., Biemer, E. and Zeilhofer, HF. (2006-a) 'Three-dimensional recording of the human face with a 3D laser scanner', *Journal of Plastic, Reconstructive and Aesthetic Surgery*, 59(11), pp. 1193-1202. DOI: [10.1016/j.bjps.2005.10.025](https://doi.org/10.1016/j.bjps.2005.10.025).
115. Kovacs, L., Zimmermann, A., Brockmann, G., Baurecht, H., Schwenger-Zimmerer, K., Papadopoulos, NA., Papadopoulos, MA., Sader, R., Biemer, E. and Zeilhofer, HF. (2006-b) 'Accuracy and precision of the three-dimensional assessment of the facial surface using a 3D laser scanner', *IEEE Transaction on Medical Imaging*, 25(6), pp. 742-754. DOI: [10.1109/TMI.2006.873624](https://doi.org/10.1109/TMI.2006.873624).
116. Krouskop, TA. Baker, R. and Wilson, MS. (2002) 'A noncontact wound measurement system', *Journal of Rehabilitation Research and Development*, 39(3), pp. 337-346.
117. Laerd Statistics (2018) *ANOVA with repeated measures using SPSS statistics*. Available at: <https://statistics.laerd.com/spss-tutorials/one-way-anova-repeated-measures-using-spss-statistics.php> (Accessed: 12 October 2018).

118. Lague, D., Brodu, N. and Leroux, J. (2013) 'Accurate 3D comparison of complex topography with terrestrial laser scanner: application to the Rangitikei canyon (N-Z)', *ISPRS Journal of Photogrammetry and Remote Sensing*, 82, pp. 10-26. DOI: [10.1016/j.isprsjprs.2013.04.009](https://doi.org/10.1016/j.isprsjprs.2013.04.009).
119. Langemo, D., Anderson, J., Hanson, D., Hunter, S. and Thompson, P. (2008) 'Measuring wound length, width, and area: which technique?', *Advances in Skin and Wound Care*, 21(1), pp. 42-47. DOI: [10.1097/01.ASW.0000284967.69863.2f](https://doi.org/10.1097/01.ASW.0000284967.69863.2f).
120. Lane, C. and Harrell, W. (2008) 'Completing the 3-dimensional picture', *American Journal of Orthodontics and Dentofacial Orthopedics*, 133(4), pp. 612-620. DOI: [10.1016/j.ajodo.2007.03.023](https://doi.org/10.1016/j.ajodo.2007.03.023).
121. Lau, D. (2012) *3D Imaging advances capabilities of machine vision: part III*. Available at: <https://www.vision-systems.com/articles/print/volume-17/issue-6/departments/leading-edge-views/3-d-imaging-advances-capabilities-of-machine-vision-part-iii.html> (Accessed: 1 July 2018).
122. Leipner, A., Baumeister, R., Thali, MJ., Braun, M., Dobler, E. (2016) 'Multi-camera system for 3D forensic documentation', *Forensic Science International*, 261, pp. 123-128. DOI: [10.1016/j.forsciint.2016.02.003](https://doi.org/10.1016/j.forsciint.2016.02.003).
123. LeMay, J. (2002) *Using scales in photography*. Available at: <http://www.rmdiai.org/pdf/Library/Scales%20article.pdf> (Accessed: 3 June 2018).
124. Lievendag, N. (2017) *HP 3D structured light scanner Pro S3 (David SLS-3) review*. Available at: <https://3dscanexpert.com/hp-3d-scanner-pro-s3-david-sls-3-review/> (Accessed: 20 June 2018).
125. Limmen, RM., Ceelen, M., Reijnders, UL., Stomp, SJ., de Keijzer, MK. and Das, K. (2012) 'Enhancing the visibility of injuries with narrow-banded beams of light within the visible light spectrum', *Journal of Forensic Sciences*, 58(2), pp. 518-522. DOI: [10.1111/1556-4029.12042](https://doi.org/10.1111/1556-4029.12042).

126. Lohry, WF., Chen, V. and Zhang, S. (2014) 'Absolute three-dimensional shape measurement using coded fringe patterns without phase unwrapping or projector calibration', *Optics Express Journal*, 22(2), pp. 1287-1301. DOI: [10.1364/OE.22.001287](https://doi.org/10.1364/OE.22.001287).
127. Louis, DT. (1992) 'Photographing pressure ulcers to enhance documentation', *Decubitus*, 5(4), pp. 38-40.
- Luhmann, T., Robson, S., Kyle, S. and Harley, I. (2006) *Close range photogrammetry: principles, methods and applications*. Scotland, UK: Whittles Publishing.
128. Madea, P. (2013) *Handbook of forensic medicine*. Chichester: Wiley-Blackwell.
129. Majeske, C. (1992) 'Reliability of wound surface area measurements', *Physical Therapy Journal*, 72(2), pp. 138-141. DOI: [10.1093/ptj/72.2.138](https://doi.org/10.1093/ptj/72.2.138).
130. Marjanovic, D., Dugdale, RE., Vowden, P. and Vowden, R. (1998) 'Measurement of the volume of a leg ulcer using a laser scanner', *Physiological Measurement*, 19(4), pp. 535-543. DOI: [10.1088/0967-3334/19/4/008](https://doi.org/10.1088/0967-3334/19/4/008).
131. Malhotra, A., Gupta, K. and Kant, K. (2011) 'Laser triangulation for 3D profiling of target', *International Journal of Computer Applications*, 35(8), pp. 47-50.
132. Malian, A. and Azizi, A. (2005) 'Development of a robust photogrammetric metrology system for monitoring the healing of bedsores', *The Photogrammetric Record*, 20(111), pp. 241-273. DOI: [10.1111/j.1477-9730.2005.00319.x](https://doi.org/10.1111/j.1477-9730.2005.00319.x).
133. Mansurov, N. (2017) *What is distortion?* Available at: <https://photographylife.com/what-is-distortion> (Accessed: 8 February 2018).
134. Marsh, NP. (2011) 'The photography of injuries', in Gall, J. and Payne-James, J. (eds.) *Current Practice in Forensic Medicine*. John Wiley & Sons, Ltd, pp. 159-192.
135. Mayrovitz, HN., Smith, J. and Ingram, C. (1998) 'Comparisons of venous and diabetic plantar ulcer shape and area', *Advanced in Wound Care*, 11(4), pp. 176-182.

136. McPherron, SP., Gernat, T. and Hublin, JJ. (2009) 'Structured light scanning for high-resolution documentation of in situ archaeological finds', *Journal of Archaeological Science*. 36(1), pp. 19–24. DOI: [10.1016/j.jas.2008.06.028](https://doi.org/10.1016/j.jas.2008.06.028).
137. Michienzi, R., Meier, S., Elert, L.C. and Martinez, R.M. (2018) 'Comparison of forensic photo-documentation to a photogrammetric solution using the multi-camera system "Botscan"', *Forensic Science International Journal*, 288, pp. 46-52. DOI: [10.1016/j.forsciint.2018.04.012](https://doi.org/10.1016/j.forsciint.2018.04.012).
138. Meek, CM. (2017) *Cross-polarized reflective light dental photography: the silver bullet of tooth shade selection*. Available at: <https://www.dentistryiq.com/articles/2017/03/cross-polarized-reflective-light-dental-photography-the-silver-bullet-of-tooth-shade-selection.html> (Accessed: 15 January 2019).
139. Mohite, PM., Mohite, DP., Dixit, PG., Anjankar, AJ. And Keche, AS. (2013) 'Autopsy evaluation of defence wounds in homicidal death in Central India', *Journal of Forensic Research*, 4(05), pp. 1-4. DOI: [10.4172/2157-7145.1000205](https://doi.org/10.4172/2157-7145.1000205).
140. Morimoto, M. and Fujii, K. (2005) 'A portable 3D scanner based on structured light and stereo camera', *IEEE International Symposium on Communication and Information Technology*, Beijing, China, 12-14 October 2005. DOI: [10.1109/ISCIT.2005.1566919](https://doi.org/10.1109/ISCIT.2005.1566919).
141. Naeem, M., Qureshi, I. and Azam, F. (2015) 'Face recognition techniques and approaches: a survey', *Science International Journal*, 27(1), pp. 301-305.
142. Ohshima, T. (2000) 'Forensic wound examination', *Forensic Science International*, 113(1), pp. 153-164. DOI: [10.1016/S0379-0738\(00\)00269-3](https://doi.org/10.1016/S0379-0738(00)00269-3).
143. Ort, R., Metzler, P., Gujer, AK., Matthews, F., Zemmann, W., Gratz, K. and Lubbers, H. (2012) 'The reliability of a three-dimensional photo system- (3dMDface-) based evaluation of the face in cleft lip infants', *Plastic Surgery International*, 2012, pp. 1-8. DOI: [10.1155/2012/138090](https://doi.org/10.1155/2012/138090).

144. Ozkalipci, O. and Volpellier, M. (2010) 'Photographic documentation, a practical guide for non-professional forensic photography', *Torture Journal*, 20 (1), pp. 45-52.
145. Ozturk, C., Dubin, S., Schafer, ME., Wen-Yao, S. and Min-Chih C. (1996) 'A new structured light method for 3-D wound measurement', *Proceedings of the IEEE 22nd Annual Northeast Bioengineering Conference*, New Brunswick, NJ, USA, 14-15 March 1996, pp. 70-71. DOI: [10.1109/NEBC.1996.503222](https://doi.org/10.1109/NEBC.1996.503222).
146. Palmer, RM., Ring, EFJ. and Ledgard, L. (1989) 'A digital video technique for radiographs and monitoring ulcers', *Journal of Photographic Science*, 37(3-4), pp. 65-67. DOI: [10.1080/00223638.1989.11737014](https://doi.org/10.1080/00223638.1989.11737014).
147. Pandey, SC. and Cather, S. (2016) *Close-range 3D imaging for documentation and monitoring dynamic deterioration process in wall painting*. Available at: http://network.icom.museum/fileadmin/user_upload/minisites/cidoc/BoardMeetings/Satish_Pandey.pdf (Accessed: 15 July 2016).
148. Pastorious, W. (2015) *Structured light vs. laser triangulation for 3D scanning and inspection*. Available at: <http://lmi3d.com/blog/structured-light-vs-laser-triangulation-3d-scanning-and-inspection> (Accessed: 29 March 2016).
149. Patidar, P. and Srivastava, S. (2010) 'Image de-noising by various filters for different noise' *International Journal of Computer Applications*, 9(4), pp. 45-50. DOI: [10.5120/1370-1846](https://doi.org/10.5120/1370-1846).
150. Patient Focused (2018) *Recent courses*. Available at: <https://www.patientfocused.co.uk/external-courses/> (accessed: 17 June 2018).
151. Patil, H., Kothari, A. and Bhurchandi, KM. (2015) '3D face recognition: features, databases, algorithms and challenges', *Artificial Intelligence Review, An International Science and Engineering Journal*, 44(3), pp. 393-441. DOI: [10.1007/s10462-015-9431-0](https://doi.org/10.1007/s10462-015-9431-0).
152. Pavlovic, P., Diaci, J., Mozina, J. and Jezersek, M., (2015) 'Wound perimeter, area, and volume measurement based on laser 3D and colour acquisition',

BioMedical Engineering OnLine, 14(1), pp. 39-53. DOI: [10.1186/s12938-015-0031-7](https://doi.org/10.1186/s12938-015-0031-7).

153. Payne-James, J. (2003) 'Assault and injury in the living', in Payne-James, J., Busuttil, A. and Smock, W., (eds) *Forensic Medicine: Clinical and Pathological Aspects*. London: Greenwich Medical Media, pp. 543–563.

154. Payne-James, J., Crane, J. and Hinchliffe, JA. (2005) 'Injury assessment, documentation and interpretation', in Stark, MM. (ed.) *Clinical Forensic Medicine: A Physician's Guide*. Totowa: Humana Press Inc., pp. 127-158.

155. Payne-James, JJ. (2012) 'Rules and scales used in measurement in the forensic setting: measured-and found wanting', *Forensic Science Medicine Pathology*, 8(4), pp. 482-483. DOI: [10.1007/s12024-012-9320-7](https://doi.org/10.1007/s12024-012-9320-7).

156. Perreault, A. (2016) *What you need to know about 3D scanning*. Available at: <http://3dscanningservices.net/blog/need-know-3d-scanning/> (Accessed: 20 June 2018).

157. Plassmann, P. (1995) 'Measuring wounds', *Journal of Wound Care*, 4(6), pp. 269-272. DOI: [10.12968/jowc.1995.4.6.269](https://doi.org/10.12968/jowc.1995.4.6.269)

158. Plassmann, P. and Jones, TD. (1998) 'MAVIS: a non-invasive instrument to measure area and volume of wounds', *Medical Engineering and Physics Journal*, 20(5), pp. 332-338. DOI: [10.1016/S1350-4533\(98\)00034-4](https://doi.org/10.1016/S1350-4533(98)00034-4).

159. Plassmann, P. and Peter, M. (2001) 'Recording wound care effectiveness', *Journal of Tissue Viability*, 12(1), pp. 24-28. DOI: [10.1016/S0965-206X\(02\)80006-7](https://doi.org/10.1016/S0965-206X(02)80006-7).

160. Pounder, D. (1993) *Lecture notes in forensic medicine*. Available at: <http://www.chymist.com/Forensic%20Medicine%20Notes.pdf> (Accessed: 22 November 2015).

161. Rajbhandari, SM., Harris, ND., Sutton, M., Lockett, C., Eaton, S., Gadour, M., Tesfasye, S. and Ward, JD. (1999) 'Digital imaging: an accurate and easy method of

measuring foot ulcers', *Diabetic Medicine*, 16(4), pp. 339-342. DOI: [10.1046/j.1464-5491.1999.00053.x](https://doi.org/10.1046/j.1464-5491.1999.00053.x)

162. Rajshekar, M., Kruger, E. and Tennant, M. (2012) 'Photographic imaging distortion and its effects on forensic bite mark analysis', *Journal of Advanced Oral Research*, 3 (3), pp. 1-6. DOI: [10.1177/2229411220120301](https://doi.org/10.1177/2229411220120301).

163. Rennert, R., Golinko, M., Kaplan, D., Flattau, A. and Brem, H. (2009) 'Standardization of wound photography using the wound electronic medical record', *Advances in Skin and Wound Care*, 22(1), pp. 32-38. DOI: [10.1097/01.asw.0000343718.30567.cb](https://doi.org/10.1097/01.asw.0000343718.30567.cb).

164. Riviello, RJ. (2010). 'Forensic documentation', in Riviello, RJ. (ed.) *Manual of Forensic Emergency Medicine: A guide for Clinicians*. Jones and Bartlett Publisher, pp. 59-64.

165. Rocchini, C., Cignoni, P., Montani, C., Pingi, P. and Scopigno, R. (2001) 'A low cost 3D scanner based on structured light', *Computer Graphics Forum*, 20(30), pp. 1-11. DOI: [10.1111/1467-8659.00522](https://doi.org/10.1111/1467-8659.00522).

166. Rogers, LC., Bevilacqua, NJ., Armstrong, DG. and Andros, G. (2010) 'Digital planimetry results in more accurate wound measurements: a comparison to standard ruler measurements', *Journal of Diabetes Science and technology*, 4(4), pp. 799-802. DOI: [10.1177/193229681000400405](https://doi.org/10.1177/193229681000400405).

167. Rowan, P., Hill, M., Gresham, GA., Goodall, E. and Moore, T. (2010) 'The use of infrared aided photography in identification of sites of bruises after evidence of the bruise is absent to the naked eye', *Journal of Forensic and Legal Medicine*, 17(6), pp. 293–297. DOI: [10.1016/j.jflm.2010.04.007](https://doi.org/10.1016/j.jflm.2010.04.007).

168. Sadlo, F., Weyrich, T., Peikert, R. and Gross, M. (2005) 'A practical structured light acquisition system for point-based geometry and texture', *Proceedings Eurographics/IEEE VGTC Symposium Point-Based Graphics*, Stony Brook, NY, USA, 21-22 June 2005. DOI: [10.1109/PBG.2005.194069](https://doi.org/10.1109/PBG.2005.194069).
169. Salvi, J., Pages, J. and Battle, J. (2004) 'Pattern codification strategy in structured light systems', *Pattern Recognition Journal*, 37(4), pp. 827-849. DOI: [10.1016/j.patcog.2003.10.002](https://doi.org/10.1016/j.patcog.2003.10.002).
170. Salvi, J., Fernandez, S., Pribanic, T. and Llado, X. (2010) 'A state of the art in structured light patterns for surface profilometry', *Pattern Recognition Journal*, 43(8), pp. 2666-2680. DOI: [10.1016/j.patcog.2010.03.004](https://doi.org/10.1016/j.patcog.2010.03.004).
171. Samad, A., Hayes, S., French, I., Dodds, S. (2002) 'Digital imaging versus conventional contact tracing for the objective measurement of venous leg ulcers', *Journal of Wound Care*, 11(4), pp. 137-140. DOI: [10.12968/jowc.2002.11.4.26385](https://doi.org/10.12968/jowc.2002.11.4.26385).
172. Samadder, S. (2016) *Post-mortem artefact*. Available at: <http://www.slideshare.net/SujeetSamadder/postmortem-artefacts> (Accessed: 18 November 2016).
173. Sansoni, G., Cattaneo, C., Trebeschi, M., Gibelli, D., Porta, D., and Picozzi, M. (2009-a) 'Feasibility of contactless 3D optical measurement for the analysis of bone and soft tissue lesions: new technologies and perspectives in forensic sciences', *Journal of Forensic Science*, 54(3), pp. 540–545. DOI: [10.1111/j.1556-4029.2009.01041.x](https://doi.org/10.1111/j.1556-4029.2009.01041.x).
174. Sansoni, G., Trebeschi M. and Docchio, F. (2009-b) 'State-of-the-art and applications of 3D imaging sensors in industry, cultural heritage, medicine and criminal investigation', *Sensors*, 9(1), pp. 568-601. DOI: [10.3390/s90100568](https://doi.org/10.3390/s90100568).
175. Saukko, P. and Knight, B. (2004) *Knight's Forensic Pathology*. 3rd edition. London: CRP Press. DOI: [10.1201/b13642](https://doi.org/10.1201/b13642).
176. Saukko, P. and Pollak, S. (2013) 'Self-inflicted injury', in Siegel, J A., Saukka, P.J. and Houcks, MM. (eds.) *Encyclopedia of Forensic Sciences*, pp. 110-115.

Available

at:<http://www.sciencedirect.com/science/referenceworks/9780123821669#ancv0155>

(Downloaded: 27 November 2016).

177. Savage, JM. and Jeffery, SL. (2013) 'Use of 3D photography in complex-wound assessment', *Journal of Wound Care*, 22(3), pp. 158-60. DOI: [10.12968/jowc.2013.22.3.156](https://doi.org/10.12968/jowc.2013.22.3.156).

178. Shah, A., Wollak, C. and Shah, JB. (2015) 'Wound measurement techniques: comparing the use of ruler method, 2D imaging and 3D scanner', *Journal of the American College of Clinical Wound Specialist*, 5(3), pp. 52-57. DOI: [10.1016/j.jccw.2015.02.001](https://doi.org/10.1016/j.jccw.2015.02.001).

179. Shamata, A. and Thompson, TJU. (2018-a) 'Using structured light three-dimensional surface scanning on living individuals: key considerations and best practice for forensic medicine' *Journal of Forensic and Legal Medicine*, 55, pp. 58-64. DOI: [10.1016/j.jflm.2018.02.017](https://doi.org/10.1016/j.jflm.2018.02.017).

180. Shamata, A. and Thompson, TJU. (2018-b) 'Documentation and analysis of traumatic injuries in clinical forensic medicine involving structured light three-dimensional surface scanning versus photography', *Journal of Forensic and Legal Medicine*, 58, pp. 93-100. DOI: [10.1016/j.jflm.2018.05.004](https://doi.org/10.1016/j.jflm.2018.05.004).

181. Sharma, M., Khajja, BS., JHA, S., Mathur, GK. and Mathur, V.N. (2011) 'Forensic wound interpretation of injuries/ wounds found on the human body', *Journal of Punjab Academy of Forensic Medicine and Toxicology*, 11(2), pp. 105-109, <http://medind.nic.in/jbc/t11/i2/jbct11i2p105.pdf>.

182. Shaw, J. and Bell, PM. (2011) *Wound measurement in diabetic foot ulceration*. Available at: <http://cdn.intechweb.org/pdfs/24689.pdf> (Accessed: 8 November 2017).

183. Sheasby, DR. and MacDonald, DG. (2001) 'A forensic classification of distortion in human bite marks', *Forensic Science International Journal*, 122(1), pp. 75-78. DOI: [10.1016/S0379-0738\(01\)00433-9](https://doi.org/10.1016/S0379-0738(01)00433-9).

184. Sherpherd, R. (2003) *Simpson's Forensic Medicine*. 12th edn. London: Arnold. z

185. Shetty, R., Sreekar, H., Lamba, S., Gupta, AK. (2012) 'A novel and accurate technique of photographic wound measurement', *Indian Journal of Plastic Surgery*, 45(2), pp. 425 – 429. DOI: [10.4103/0970-0358.101333](https://doi.org/10.4103/0970-0358.101333).
186. Sholts, SB., Walker, PL., Kuzminsky, SC., Miller, KWP, Warmlander, SKTS (2011) 'Identification of group affinity from cross-sectional contours of the human midfacial skeleton using digital morphometrics and 3D laser scanning technology', *Journal of Forensic Science*, 56(2), pp. 333-338. DOI: [10.1111/j.1556-4029.2011.01701.x](https://doi.org/10.1111/j.1556-4029.2011.01701.x).
187. Shrout, PE. and Fleiss, JL. (1979) 'Intraclass Correlations: uses in assessing rater reliability', *Psychological Bulletin*, 86(2), pp. 420-428. DOI: [10.1037/0033-2909.86.2.420](https://doi.org/10.1037/0033-2909.86.2.420).
188. Sikka, N., Pirri, M., Carlin, KN., Strauss, R., Rahimi, F. and Pines, J. (2012) 'The use of mobile phone cameras in guiding treatment decisions for laceration care', *Telemedicine and e-Health*, 18(7), pp. 554–557. DOI: [10.1089/tmj.2011.0216](https://doi.org/10.1089/tmj.2011.0216).
189. Sivanandan, J. and Liscio, E. (2017) 'Assessing structured light 3D scanning using Artec Eva for injury documentation during autopsy', *Journal of Association for Crime Scene Reconstruction*, 21, pp. 5-14.
190. Slot, L., Larsen, PK. and Lynnerup, N. (2014) 'Photogrammetric documentation of regions of interest at autopsy- a pilot study', *Journal of Forensic Science*, 59(1), pp. 226-30. DOI: [10.1111/1556-4029.12289](https://doi.org/10.1111/1556-4029.12289).
191. Solberg, TD., Kavanagh, B. and Medin, PM (2016) *Image-guided stereotactic radiosurgery and stereotactic body radiation therapy*. Available at: <https://radiologykey.com/image-guided-stereotactic-radiosurgery-and-stereotactic-body-radiation-therapy/> (Accessed: 22 January 2018).
192. Sonkhya, N., Singhal, P. and Srivastava, SP. (2005) 'Civilian firearm injuries in head and neck', *Indian Journal of Otolaryngology and Head and Neck Surgery*, 57(3), pp. 262-265. DOI: [10.1007/BF03008030](https://doi.org/10.1007/BF03008030).

193. Sperring, B. and Baker, R. (2014) 'Ten top tips-taking high-quality digital images of wounds', *Journal of Lymphoedema*, 5(1), pp. 7-8.
194. Spraggs, D. (2007) *How to photograph injuries*. Available at: <http://www.policemag.com/channel/patrol/articles/2007/09/how-to-photograph-injuries.aspx> (Accessed: 27 November 2016).
195. Sprigle, S., Nemeth, M. and Gajjala, A. (2012) 'Iterative design and testing of a hand-held, non-contact wound measurement device', *Journal of Tissue Viability*, 21(1), pp. 17-26. DOI: [10.1016/j.jtv.2011.09.001](https://doi.org/10.1016/j.jtv.2011.09.001).
196. Stella (2017) *Understanding the science behind the magic of 3D scanners*. Available at: <https://matterandform.net/blog/how-do-3d-scanners-work> (Accessed: 8 June 2018).
197. Subke, J., Wehner, HD., Wehner, F. and Szczepaniak, S. (2000) 'Streifenlichttopometrie (SLT): a new method for three-dimensional photorealistic forensic documentation in colour', *Forensic Science International*, 113(1-3), pp. 289-295. DOI: [10.1016/S0379-0738\(00\)00236-X](https://doi.org/10.1016/S0379-0738(00)00236-X).
198. Tehrani, MA., Saghaeian, A. and Mohajerani, OR. (2008) 'A new approach to 3D modeling using structured light patterns', *3rd International Conference on Information and Communication Technologies: From Theory to Applications*, Damascus, Syria, 7-11 April 2008. DOI: [10.1109/ICTTA.2008.4530071](https://doi.org/10.1109/ICTTA.2008.4530071).
199. Tetley, C. (2005) 'The photography of bruises', *Journal of Visual Communication in Medicine*, 28(2), pp. 72-77. DOI: [10.1080/01405110500104043](https://doi.org/10.1080/01405110500104043).
200. Thali, MJ., Braun, M., Brueschweiler, W. and Dirnhofer, R. (2000) 'Matching tire tracks on the head using forensic photogrammetry', *Forensic Science International Journal*, 113(1), pp. 281-287. DOI: [10.1016/S0379-0738\(00\)00234-6](https://doi.org/10.1016/S0379-0738(00)00234-6).
201. Thali, MJ., Braun, M. and Dirnhofer, R. (2003-a) 'Optical 3D surface digitizing in forensic medicine: 3D documentation of skin and bone injuries', *Forensic Science International Journal*, 137(2), pp. 203–208. DOI: [10.1016/j.forsciint.2003.07.009](https://doi.org/10.1016/j.forsciint.2003.07.009).

202. Thali, MJ., Braun, M., Wirth, J. Vock, P. and Dirnhofer, R. (2003-b) '3D surface and body documentation in forensic medicine: 3-D/CAD photogrammetry merged with 3D radiological scanning', *Journal of Forensic Science*, 48(6), pp. 118-486. DOI: [10.1520/jfs2003118](https://doi.org/10.1520/jfs2003118).
203. Thali, MJ., Braun, M., Markwalder, Th.H., Brueschweiler, W., Zollinger, U., Malik, NJ., Yen, K. and Dirnhofer, R. (2003-c) 'Bite mark documentation and analysis: the forensic 3D/CAD supported photogrammetry approach', *Forensic Science International Journal*, 135(2), pp. 115-121. DOI: [10.1016/S0379-0738\(03\)00205-6](https://doi.org/10.1016/S0379-0738(03)00205-6).
204. Thali, MJ., Braun, M., Brueschweiler, W. and Dirnhofer, R. (2003-d) 'Morphology imprint, determination of the injury-causing weapon from the wound morphology using forensic 3D/ CAD- suspected photogrammetry', *Forensic Science International Journal*, 132(3), pp. 177-181. DOI: [10.1016/S0379-0738\(03\)00021-5](https://doi.org/10.1016/S0379-0738(03)00021-5).
205. Thali, MJ., Braun, M., Buck, U., Aghayev, E., Jackowski, C., Vock, P., Sonnenschein, M. and Dirnhofer, R. (2005) 'Virtopsy—scientific documentation, reconstruction and animation in forensic: individual and real 3D data based geometric approach including optical body/object surface and radiological CT/MRI scanning', *Journal Forensic Science*, 50(2), pp. 428–442. DOI: [10.1520/JFS2004290](https://doi.org/10.1520/JFS2004290).
206. Thawer, HA., Houghton, PE., Woodbury, MG., Keast, D. and Campbell, K. (2002) 'A comparison of computer-assisted and manual wound size measurement', *Ostomy Wound Management Journal*, 48(10), pp. 46-53.
207. Thompson, TJU. (2008) 'The role of the photography in the application of forensic anthropology and the Interpretation of clandestine scenes of crime', *Photography and Culture*, 1(2), pp. 165-184. DOI: [10.2752/175145208x373752](https://doi.org/10.2752/175145208x373752).
208. Thompson, TJU. and Norris, P. (2018) 'A new method for the recovery and evidential comparison of footwear impressions using 3D structured light scanning' *Science and Justice*, 58(3), pp. 237-243. DOI: [10.1016/j.scijus.2018.02.001](https://doi.org/10.1016/j.scijus.2018.02.001).
209. Trefan, A., Harris, C., Evans, S., Nuttall, D., Maguire, S. and Kemp, AM., (2018) 'A comparison of four different imaging modalities – conventional, cross polarized,

infra-red and ultra-violet in the assessment of childhood bruising', *Journal of Forensic and Legal Medicine*, 59, pp. 30-35. DOI: [10.1016/j.jflm.2018.07.015](https://doi.org/10.1016/j.jflm.2018.07.015).

210. Treuillet, S., Albouy, B. and Lucas, Y. (2009) 'Three-dimensional assessment of skin wounds using a standard digital camera' *IEEE Transactions on Medical Imaging*, 28(5), pp. 752-762. DOI: [10.1109/TMI.2008.2012025](https://doi.org/10.1109/TMI.2008.2012025).

211. Tong, T. (2011) *3D Scanners: laser versus white Light*. Available at: <https://lmi3d.com/company/digital-hub/blog/3d-scanners-laser-versus-white-light> (Accessed: 29 March 2016).

212. Urbanova, P., Hejna, P. and Jurda, M. (2015) 'Testing photogrammetry- based techniques for three-dimensional surface documentation in forensic pathology', *Forensic Science International Journal*, 250, pp. 77-86. DOI: [10.1016/j.forsciint.2015.03.005](https://doi.org/10.1016/j.forsciint.2015.03.005).

213. Urbanova, P. (2016) 'Performance of distance-based matching algorithms in 3D facial identification', *Egyptian Journal of Forensic Sciences*, 6(2), pp. 135-151. DOI: [10.1016/j.ejfs.2016.04.004](https://doi.org/10.1016/j.ejfs.2016.04.004).

214. Vecellio, ME. and Bryant, EP. (2017) *Pocket guide to crime scene photography*. CRC Press.

215. Verhoff, MV., Kettner, M., Lászik, A. and Ramsthaler, F. (2012) 'Digital Photo documentation of forensically relevant injuries as part of the clinical first response protocol', *Dtsch Arztebl International.*, 109(39), pp. 638–642. DOI: [10.3238/arztebl.2012.0638](https://doi.org/10.3238/arztebl.2012.0638).

216. Verme, R. and Ali, J. (2013) 'A comparative study of various types of image noise and efficient noise removal techniques', *International Journal of Advanced Research in Computer Science and Software Engineering*, 3(10), pp. 617-622.

217. Villa, C. (2017-a) 'Forensic 3D documentation of skin injuries', *International Journal of Legal Medicine*, 131(3), pp. 751-759. DOI: [10.1007/s00414-016-1499-9](https://doi.org/10.1007/s00414-016-1499-9).

218. Villa, C., Hansen, NF., Hansen, KM., Hougen, HP. and Jacobsen, C. (2017-b) '3D Reconstructions of a controlled bus bombing', *Journal of Forensic Radiology and Imaging*, 12, pp. 11-20. DOI: [10.1016/j.jofri.2018.02.004](https://doi.org/10.1016/j.jofri.2018.02.004).
219. Wang, Z., Bovik, AC., Sheikh, HR. and Simoncelli, EP. (2004) 'Image quality assessment: from error visibility to structural similarity' *IEEE transaction on Images Processing*, 13(4), pp. 600-612. DOI: [10.1109/tip.2003.819861](https://doi.org/10.1109/tip.2003.819861).
220. Wang, Y., Liu, K., Hao, Qi., Lau, D. and Hassebrook, L. (2007) 'Multicamera phase measuring profilometry for accurate depth measurement', *Proceeding SPIE 6555, Sensors and Systems for Space Applications*, 03 May 2007. DOI: [10.1117/12.720068](https://doi.org/10.1117/12.720068).
221. Weinmann, M., Schwartz, C., Ruiters, R. and Klein, R. (2011) 'A multi-camera, multi-projector super-resolution framework for structured light', *International Conference on 3D Imaging, Modeling, Processing, Visualization and Transmission*, Hangzhou, China, 16-19 May 2011. DOI: [10.1109/3DIMPVT.2011.57](https://doi.org/10.1109/3DIMPVT.2011.57).
222. Wendelken, ME., Berg, WT., Lichtenstein, P., Markowitz, L., Comfort, C. and Alvarez, OM. (2011) 'Wounds measured from digital photographs using photo digital planimetry software: validation and rater reliability', *WOUNDS: a Compendium of Clinical Research and Practice*, 23(9), pp. 267-275.
223. Whittaker, DK. Brickley, MR. and Evans, L. (1998) 'A comparison of the ability of experts and non-experts to differentiate between adult and child human bite marks using receiver operating characteristic (ROC) analysis', *Forensic Science International Journal*, 92(1), pp. 11–20. DOI: [10.1016/S0379-0738\(97\)00198-9](https://doi.org/10.1016/S0379-0738(97)00198-9).
224. Winkelbach, S., Molkenstruck, S. and Wahl, FM. (2006) 'Low-cost laser range scanner and fast surface registration approach', in Franke, K., Muller, K-R. and Schafer, R. (eds.) *Lecture Notes in Computer Science*, Springer Berlin Heidelberg, pp. 718-728. DOI: [10.1007/11861898_72](https://doi.org/10.1007/11861898_72).
225. Wysocki, A. (1996) 'Wound measurement', *International Journal of Dermatology*, 35, pp. 82-91.

226. Yalla, VG. and Hassebrook, LG. (2005) 'Very high-resolution 3D surface scanning using multi-frequency phase measuring profilometry', *Proceeding SPIE 5798, Spaceborne Sensors II*, 19 May 2005. DOI: [10.1117/12.603832](https://doi.org/10.1117/12.603832).
227. Yetiser, S. and Kahramanyol, M. (1998) 'High-velocity gunshot wounds to the head and neck: a review of wound ballistics', *Military Medicine Journal*, 163(5), pp. 346-351. DOI: [10.1093/milmed/163.5.346](https://doi.org/10.1093/milmed/163.5.346).
228. Zhang, S. and Huang, PS. (2006) 'High resolution, real-time three-dimensional shape measurement', *Optical Engineering Journal*, 45(12), pp.1-8. DOI: [10.1117/1.2402128](https://doi.org/10.1117/1.2402128).
229. Zuckerman, J. (2013) *Pop-up flash: a convenient "taste of light"*. Available at: <https://www.shutterbug.com/content/pop-flash-convenient-%E2%80%9Ctaste-light%E2%80%9D> (Accessed: 1 May 2018).
230. 3D Printer Superstore (2015) *DAVID SLS-3 HD 3D scanner training tutorial 2-setup*. Available at: <https://www.youtube.com/watch?v=1ptq9I-DT3I> (Accessed: 27 October 2018).

Appendices

Appendix A: Tables

Table A.1: Data Collection sheet

Personal questions	Information
Age	
Nationality	
Marital status	
Date of examination	
History	
Time of the violence	
Type of the causative tool	
Examination	
Type of the wound	
Site of the wound	
Wound dimensions	
Type of the causative tool	
Some scanning data	
Calibration result	
Aperture	
Shutter speed	
Intensity threshold	

Table A.2: Wound surface areas (in seq. cm) using ruler-based formulas; in addition to 2D and 3D methods

Wound	L x W	L x W x 0.785	Elliptical method	2D method	3D method
W1	4.13	3.24	3.24	2.13	3.63
W2	6.56	5.15	5.15	3.71	5.58
W3	16.75	13.15	13.16	9.92	17.72
W4	9	7.07	7.07	6.88	7.43
W5	12	9.42	9.42	8.19	12.39
W6	10.8	8.48	8.48	7.91	8.97
W7	33.8	26.53	26.55	22.5	30.74
W8	22.88	17.96	17.97	13.07	17.38
W9	25.5	20.02	20.03	21.17	21.82
W10	25.5	20.02	20.03	18.38	30.26
W11	99.68	78.25	78.29	64.20	96.56
W12	98.56	77.37	77.41	61.19	95.44
W13	99.36	78	78.04	43.44	55.48
W14	105.6	82.896	82.94	39.17	58.62
W15	25.8	20.25	20.26	16.69	44.29

Table A.3: Differences between length measurements of each wound (in cm)

Wound	Diff. between manual & 2D measurements	Diff. between manual & 3D measurements	Diff. between 2D & 3D measurements
W1	1.21	0.76	0.45
W2	0.65	0.46	0.19
W3	1.32	0.58	0.74
W4	0.13	0.17	0.30
W5	0.51	0.02	0.49
W6	0.19	0.19	0.38
W7	0.88	0.73	0.15
W8	0.22	0.09	0.13
W9	0.13	0.03	0.16
W10	0.39	0.00	0.39
W11	0.68	0.58	1.26
W12	1.01	0.16	1.17
W13	0.94	0.66	0.28
W14	0.98	0.91	0.07
W15	1.08	0.18	0.90
Mean diff.	0.69	0.37	0.47
Min. diff.	0.13	0.00	0.07
Max. diff.	1.32	0.91	1.26

Table A.4: Differences between width measurements of each wound (in cm)

Wound	Diff. between manual & 2D measurements	Diff. between manual & 3D measurements	Diff. between 2D & 3D measurements
W1	0.13	0.04	0.17
W2	0.03	0.09	0.12
W3	0.07	0.11	0.18
W4	0.12	0.00	0.12
W5	0.32	0.08	0.24
W6	0.13	0.30	0.17
W7	0.06	0.05	0.11
W8	1.03	0.42	0.61
W9	0.17	0.08	0.09
W10	0.38	0.12	0.26
W11	0.50	0.21	0.29
W12	0.88	0.04	0.84
W13	0.40	0.27	0.13
W14	0.73	0.58	0.15
W15	0.22	0.04	0.26
Mean diff.	0.34	0.16	0.25
Min. diff.	0.03	0.00	0.09
Max. diff.	1.03	0.58	0.84

Table A.5: Differences between depth measurements of each wound (in cm)

Wound	Diff. between manual & 3D measurements (CloudCompare)	Diff. between manual & 3D measurements (Geomagic)
W1	0.07	0.04
W2	0.06	0.01
W3	0.09	0.07
W5	0.10	0.14
W7	0.04	0.03
W10	0.11	0.24
W11	0.08	0.07
W12	0.09	0.30
W13	0.03	0.05
W14	0.02	0.02
W15	0.35	0.24
Mean diff.	0.09	0.11
Min. diff.	0.02	0.01
Max. diff.	0.35	0.30

Appendix B: Figures



Figure B.1: 3D model (left) and 2D photograph (right) of friction abrasion



Figure B.2: 3D model (left) and 2D photograph (right) of tangential longitudinal abrasion



Figure B.3: 3D model (first) and 2D photograph (second) of brush abrasion



Figure B.4: 3D model (first) and 2D photograph (second) of brush abrasion on the lateral aspect of the left elbow

N.B. Dark circles in the 2D results of Figures B.2 and B.4 are possibly Vignetting, which can be seen when the close-up lens is used.



Figure B.5: 3D model (first) and 2D photograph (second) of scratch abrasion on the lower lateral aspect of the right arm





Figure B.6: 3D model (first) and 2D photograph (second) of small healed abrasion, possibly vertical abrasion



Figure B.7: 3D model (first) and 2D photograph (second) of scratch abrasion

Appendix C: Ethical approvals

Appendix C.1: Ethical approval-1

EP Memorandum Approved for student: SHAMATA,
AWATIF Project: SSE - 3D non- contact surface
scanning of trumatic injuries of the soft tissue.

SSE Ethics Online <unity@tees.ac.uk>

To: SHAMATA, AWATIF; Thompson, Tim; Wright, Julie;



SSE
MEMORANDUM

TO: Thompson, Tim

FROM: Taylor, Gillian

STUDENT: SHAMATA, AWATIF

DATE: 25 November 2015

Ethical Approval

Dear Supervisor,

Following your Request for Ethical Approval in relation to the project 3D non- contact surface scanning of trumatic injuries of the soft tissue, please find below the decision that has been made:

Approved

Appendix C.2: Ethical approval-2

EP Memorandum Approved for student: Shamata, Awatif Project: SSE - 3D Non-contact Surface Scanning of Traumatic Injuries to the Soft Tissue.

3 messages

SSE Ethics Online <unity@tees.ac.uk>

Reply-To: "unity@tees.ac.uk" <unity@tees.ac.uk>

To: "Shamata, Awatif" <A.Shamata@tees.ac.uk>, "Thompson, Tim" <T.Thompson@tees.ac.uk>, "Wright, Julie" <Julie.Wright@tees.ac.uk>

SSE

MEMORANDUM

TO: Thompson, Tim

FROM: Taylor, Gillian

STUDENT: Shamata, Awatif

DATE: 14 February 2017

Ethical Release

Dear Supervisor,

Following your Request for Ethical Release in relation to the project 3D Non-contact Surface Scanning of Traumatic Injuries to the Soft Tissue, please find below the decision that has been made:

Approved

Chair Approval Task started by Shamata, Awatif on 13/02/2017 11:26

Comment:

Approved by Taylor, Gillian on 14/02/2017 15:08

Comment: Approved

Appendix C.3: Ethical approval-3


2017

EP Memorandum Approved for student: Shamata, Awatif Project: SSE - Second phase of 3D Non-contact Surface Scanning of Traumatic Injuries to the Soft Tissue.

SSE Ethics Online <unity@tees.ac.uk>

Tue 07/03/2017 11:11

To: Shamata, Awatif <A.Shamata@tees.ac.uk>; Thompson, Tim <T.Thompson@tees.ac.uk>; Wright, Julie <Julie.Wright@tees.ac.uk>;

 Teesside University

SSE
MEMORANDUM

TO: Thompson, Tim
FROM: Taylor, Gillian
STUDENT: Shamata, Awatif
DATE: 07 March 2017

Ethical Approval

Dear Supervisor,

Following your Request for Ethical Approval in relation to the project Second phase of 3D Non-contact Surface Scanning of Traumatic Injuries to the Soft Tissue, please find below the decision that has been made:

Approved

Chair Approval Task started by Shamata, Awatif on 05/12/2016 13:51
Comment:

Approved by Taylor, Gillian on 07/03/2017 11:11
Comment: Approved - Subject to adherence to the University's Fieldwork policy -
Health and safety policy

hi

Appendix C.4: Ethical approval-4

EP Memorandum Approved for student: Shamata, Awatif Project: SSE
- Preliminary work before the third phase of Non-contact 3D Surface
Scanning of Traumatic Forensic Injuries to the Soft Tissue.

SSE Ethics Online <unity@tees.ac.uk>

Wed 21/03/2018 13:04

To: Shamata, Awatif <A.Shamata@tees.ac.uk>; Thompson, Tim <T.Thompson@tees.ac.uk>; Wigham, Vicky <V.Wigham@tees.ac.uk>;



SSE

MEMORANDUM

TO: Thompson, Tim

FROM: Islam, Meez

STUDENT: Shamata, Awatif

DATE: 21 March 2018

Ethical Approval

Dear Supervisor,

Following your Request for Ethical Approval in relation to the project Preliminary work before the third phase of Non-contact 3D Surface Scanning of Traumatic Forensic Injuries to the Soft Tissue, please find below the decision that has been made:

Approved

Chair Approval Task started by Shamata, Awatif on 08/03/2018 14:20
Comment:

Approved by Islam, Meez on 21/03/2018 13:04
Comment: Approved

Appendix C.5: Ethical approval-5

EP Memorandum Approved for student: Shamata, Awatif Project: SSE
- Face Scanning.

SSE Ethics Online <unity@tees.ac.uk>

Mon 20/08/2018 17:17

To: Shamata, Awatif <A.Shamata@tees.ac.uk>; Thompson, Tim <T.Thompson@tees.ac.uk>; Wigham, Vicky <V.Wigham@tees.ac.uk>;



SSE

MEMORANDUM

TO: Thompson, Tim

FROM: Islam, Meez

STUDENT: Shamata, Awatif

DATE: 20 August 2018

Ethical Approval

Dear Supervisor,

Following your Request for Ethical Approval in relation to the project Face Scanning, please find below the decision that has been made:

Approved

Chair Approval Task started by Shamata, Awatif on 20/08/2018 16:17
Comment:

Approved by Islam, Meez on 20/08/2018 17:17
Comment: Approved

Appendix D: Research participant information sheets and consent forms

Appendix D.1: Research participant information sheet and consent form to scan different intact body areas of living subjects

Project title: Using structured light 3D surface scanning on living subjects

This project is a PhD research, undertaking in Forensic Science at Teesside University. We want to invite you to participate in this study. Your participation is voluntary, but it will play an important role to conduct our research. Before your decision, you need to read this information sheet to understand about the study. We provide you with information about:

- General concept and the importance of the project.
- The way of your contribution if you are happy to take part.
- Confidentiality during and after the research work.
- Contact details in case of withdrawal.

If you like more information, you are welcome to ask.

In this project, the researcher is going to scan different parts of the body by a structured light 3D scanner (Pico Scan 3D scanner) to create 3D virtual models of those parts. Body parts, such as bare arms, legs, hands, feet, and trunk (chest and abdomen) will be scanned. The scanning is a safe and non-contact procedure.

Why are we going to scan the body parts and create 3D models?

Because documentation and examination of the body areas in the 3D models will be more useful and accurate than traditional documents used in forensic medicine, such as manual drawing pictures or digital photographs. Moreover, 3D visualization of injuries will be valuable in teaching context for our students in forensic science and forensic medicine, especially when there is no possibility to teach them in a practical area with real injured cases.

The scanning process will be within seconds. The scanning location is Forensic Science Lab (M8. 03) at Teesside University. Volunteers will attend the Lab only once in his and her preferable time by making a convenient arrangement. The volunteers have a choice to tell us what part of the body we can scan it.

Right of withdrawal: If you change your mind after taking part, you have the right to withdrawal, and you do not need to give us a reason for that.

Data confidentiality: All collected data will not be identified; they will be anonymised. Therefore, no personal data will be recorded. The data will be stored in a password

protected university computer and will be accessed only by the researcher and supervisor.

Possible risk: You have to note that although there is a distance between the participant and the scanner, there is also the possibility of minor accidental physical injury.

If you like to take part and help us to conduct our research, we will need your consent below.

Informed consent form:

1. I have read and understand the information sheet for the above project and have had the opportunity to ask questions.
2. I understand my participation is voluntary and that I have the right to withdrawal without giving reasons and without of my rights being affected.
3. I understand that confidentiality will be maintained at all times, that I will not be identified and that my data will be anonymised, unless otherwise explicitly stated.
4. I understand that the data will be accessed only by the research team and stored in a secured place.
5. I agree to take part in this study.

Signature of volunteer.....

Date.....

Telephone No.....

Name of research Awatif Shamata- a PhD researcher at SSE at Teesside University.

Signature of researcher.....

Date.....

Contact details for withdrawal:

E-mail address of supervisor: T.Thompson@tees.ac.uk.
Phone number of supervisor: 01642 352535.

Appendix D.2: Research participant information sheet and consent form for 3D facial scanning

Consent for Participation in Research
 School of Science & Engineering, Teesside University
 PARTICIPANTS COPY
 Project Title

3D facial scanning

Researcher Details

Awatif Shamata: MBCHB / MSc Forensic Medicine

Description of Research

What is the purpose of the study?
 This study is aimed to scan faces and assess final 3D results. This is because 3D documents that are created by the 3D scanner are more accurate than documents obtained by traditional documentation methods such as digital photography.

Why have I been invited?
 A researcher is going to scan the face, and your participation will be important to conduct the work.

Do I have to take part?
 Your participation is voluntary, but it will play an important role to conduct our research.

What will happen if I take part?
 Your face will be scanned by a structured light scanner (HP 3D scanner Pro S3). The scanner will emit white light toward the area, the camera of the scanner will capture images, and the software fuse all images together to create 3D models.

What are the potential disadvantages and risks of taking part in this study?
 Although there is a distance between the participant and scanner, there is also a possibility of minor, accidental physical injury by slipping, if the cables leave messy.

What are the possible benefits of taking part?
 For a researcher, the PhD research study will progress. For the community, analysis of the gathered data will play a role in recommending essential suggestions to improve documentation in the practical work.

What if there is a problem?
 If you change your mind after taking part, you have the right to withdrawal up to 30 December 2018, and you do not need to give us a reason for that.

Will my taking part in the study be kept confidential?

Yes, the collected data will be anonymous. The data will be stored in a password protected university computer and will be accessed only by the researcher and supervisor.

What will happen to the results of the research study?

The results will be analysed by a researcher and will be stored in a password protected university computer.

Who has reviewed the study?

The ethical committee of Teesside University.

Consent:

1. I have read and understand the information sheet for the above project and have had the opportunity to ask questions.
2. I understand my participation is voluntary and that I have the right to withdrawal without giving reasons and without of my rights being affected.
3. I understand that confidentiality will be maintained at all times, that I will not be identified and that my data will be anonymised, unless otherwise explicitly stated
4. I understand that the data will be accessed only by the research team and stored in a secured place.
5. I agree to take part in this study.

.....
Name of participant	Signature	Date
.....
Name of researcher	Signature	Date

Contact details for withdrawal:

E-mail address of supervisor: T.Thompson@tees.ac.uk.
 Phone number of supervisor: 01642 352535.

Personal data including special category data obtained for the purposes of this research project is processed lawfully in the necessary performance of scientific or historical research or for statistical purposes carried out in the public interest. Processing of personal data including special category data is proportionate to the aims pursued, respects the essence of data protection and provides suitable and specific measures to safeguard the rights and interests of the data subject in full compliance with the General Data Protection Regulation and the Data Protection Act 2018.

Consent for Participation in Research
 School of Science & Engineering, Teesside University
 RESEARCHER COPY

Project Title

3D facial scanning

Researcher Details

Awatif Shamata: MBCHB / MSc Forensic Medicine

Description of Research

Scanning of the face will be conducted by a structured light 3D surface scanner. It will be the HP 3D surface scanner Pro S3. Structured light will be projected to the face, and the camera of the scanner will capture the illuminated area. 3D software will process the acquired information to reconstruct 3D models. The results will be considered and analysed.

Consent

- 6. I have read and understand the information sheet for the above project and have had the opportunity to ask questions.
- 7. I understand my participation is voluntary and that I have the right to withdrawal without giving reasons and without of my rights being affected.
- 8. I understand that confidentiality will be maintained at all times, that I will not be identified and that my data will be anonymised, unless otherwise explicitly stated
- 9. I understand that the data will be accessed only by the research team and stored in a secured place.
- 10. I agree to take part in this study.

.....
Name of participant	Signature	Date

.....
Name of researcher	Signature	Date

Contact details for withdrawal

E-mail address of supervisor: T.Thompson@tees.ac.uk
 Phone number of supervisor: 01642 352535

Personal data including special category data obtained for the purposes of this research project is processed lawfully in the necessary performance of scientific or historical research or for statistical purposes carried out in the public interest. Processing of personal data including special category data is proportionate to the aims pursued, respects the essence of data protection and provides suitable and specific measures to safeguard the rights and interests of the data subject in full compliance with the General Data Protection Regulation and the Data Protection Act 2018.

Appendix D.3: Research participant information sheet and consent form to scan injured areas of living subjects

ورقة العمل وبما بخصوص الحثالة المبرحة بـ: مسح سطح حثيث ابعاد ت) اسم الحثالة: د. عواطف محمد شامطة. بلظل ورييس طببشري وماجسوي رطب شرعي. اسم المشرف فستالفسور بيختمون. لفتوراه ئييس قسالمتدري سبجام عقسلي هيبري طليي, زلي باك اي مطلق علمي المعلي, محرر مجله العدله والعلوم.

هذا المشروع علمي درجه لفتوراه في العلوم الطبيه الشرعيه من جامعتسلي هيبري طليي ونرغب في دعوتك لالمشاركه التطوعي وفي هذه الورقة عمل وبما بخصوص الحثال اعليها وقرئها قبل التقويع بل موفقه.

في هذا المشروع سيقوم بتصوير ال جروح بمسح سطح حثيث ابعاد تخراج صورته نبي ابعاد. الطوقه انه, سيرعه وغير مسطح سم ومتشمال جروح في فطحه ارافالعل واللسفاليه والصددر والطن الجذع).

التصوير بالمسح ابعاهي ستمسلي طالضوعلي ال فطحه ال لموتصويره ومن ثم تقوم الكمبريلتق اط للصور وأستخراج صورته نبي ابعاد.

هذا المشروع علمي تطوعي لاجروخي صورته نبي ابعاهي بدل القويثبال تصوي وتلق ليدي أو التوثيق ليارسم.

بعض اطله تصوي رب هذا الماسي ستم تصوي لاجرح جليلك ايها وأخذالي اسات. سريتمسؤولا لعض اسئله نحل ل عمر والجنهيه ويضأسؤلك فطي لاجرح. لهخي جريسيو تامه وش ارتكسنتكون غير متخفه ولن يتم لتعم الهيايتك لخلصه. ييضأ الشارك سبتكون عود لها حث والمشفي نفق طوستفخظ طوقه انه في حله أن غيرت وأك سريكون لي كالتق بانسحاب تخي شمر ييسجل سنه 2017.

وأخيرا. الجهاز ص غير لاجرم ولكن مضاملفي حل سرقو طالجهاز من المكن ارتقيسببفي أحداث أذي بسريط.

أذنترغب بالمشاركه سريكون علي كالتق في رفق فصوله مبرون ميفس أسم الحث أ
شركرا

ال موفقه علي المشاركه التطوعي في اجراء حثبجوان: مسح سطح حثيث ابعاد ت)

1 لوقدأت وفهمت ورقة العمل وبما بخصوص الواصلات المبرهنون أ
 بلخص ووصل اللفوق والمشاركه.

2 لوقد همت بأن مشاركتي تطوعه ولدي لاق بانسحاب.

3 لوقد همت بأن الخي جري سوي تامه وأن مشكلتي ستكون غير مرتعفه ولنيتم أستعمالي ربي
 لا خله.

4 لوقد همت بأن الهيات المشاركة) ستكون عالباحث والمشفي فقط وستفطوقه أنه.

5- لوقد لوي المشاركة.

توقري عال تطوع:.....

رظمتفون:.....

تاريخ المشاركة:.....

اسم الباحث: عواطف محم شمامه.

بحث هكتور في العمل والطي طشرعيه.

التاريخ:.....

في حل مسحب المشاركة هي لمن التوصل من لال هاتف أبليري دالكتورون ييبيل فسور المشرف علي
 البحث.

البريد الإلكتروني: T.Thompson@tees.ac.uk

ال هاتف: 01642352535